ICEA

UNIVERSITÀ DEGLI STUDI DI PADOVA

# SAFE OPERATIONAL BANDWIDTH OF GAS STORAGE RESERVOIRS
# WP3 REPORT

Pietro Teatini
Claudia Zoccarato
Massimiliano Ferronato
Andrea Franceschini
Matteo Frigo
Giovanni Isotton
Carlo Janna

Padova, July 2018

**DIPARTIMENTO DI INGEGNERIA CIVILE, EDILE E AMBIENTALE - I C E A**
*DEPARTMENT OF CIVIL, ENVIRONMENTAL AND ARCHITECTURAL ENGINEERING*

# Contents

# 1. Introduction

The project “Safe operational bandwidth of gas storage reservoirs” is aimed at investigating the geomechanical hazards and risks associated with gas storage in Underground Gas Storage (UGS) reservoirs. In particular, the aim of the research activities is to investigate how possible drivers of fault reactivation can combine in UGS to increase the hazard of (significant) seismic events and/or even induced "un-expected" (micro-) seismicity.

The report summarizes the numerical results obtained by the study. The study discusses the mechanisms of fault reactivation proposed in WP2 using the M3E_GEPS3D code (https://www.m3eweb.it/geomechanical-engineering/). The geomechanical simulations have been carried out on a simplified geologic setting (in terms of both reservoir and fault geometry) and a pressure history representative of the typical UGS reservoirs in The Netherlands. The Norg and Bergermeer UGS fields, which main features have been presented in WP1, represent the “reference” for this modelling application. Faults are simulated using an interface element approach with the hypothesis of “sealing conditions”, i.e., the pore pressure *within* the fault (between the two contact surfaces) does not change with respect to the initial value. This is the most critical condition in relation to fault re-activation. A few preliminary analyses have been carried out also assuming that a portion of the reservoir depletion “enters” the fault material.

The domain geometry, geomechanical parameters, stress regime, pressure history, and range of variability of all these features have been agreed through Skype and face-to-face meetings with SodM personnel. Because of the large number of simulations, also the best way of reporting the modelling outcomes has been agreed between the UniPD and SodM staffs. In particular, apart for the 3D representation of the results for a single “reference” case, it has been decided to summarize the most important outcomes through the criticality index $\chi = \tau/\tau_L$, which represents the ratio between actual tangential stress $\tau$ acting on a fault and the limit tangential stress $\tau_L$ according with the Mohr-Coulomb criterion. When $\chi$=1.0 the fault starts sliding. For each fault, scenario, and loading steps, the following quantities are provided in tabular and/or graphical format:

- activated fault: active thickness $t_a$ (because of the regular geometry of the faults, the thickness is more representative than the area to represents the activated portion of the discontinuity) and maximum sliding $\delta_{max}$;
- inactive fault: maximum value of the criticality factor $\chi_{max}$, and fault thickness with $\chi > 0.8$ ($t_{80}$) and $\chi > 0.5$ ($t_{50}$).

The results presentation is organised as follows. In Section 3 we summarize the outcomes related to the so-called “reference” test case, i.e., a base-case scenario characterized by the simplest parameter configuration, and those obtained through a sensitivity analysis carried out with the reference and varying a single (geometric, geomechanical, stress regime) parameter at a time. Then, the five mechanisms proposed in WP2 are discussed in the sections that follow (Sections 4 to 8).



UNIVERSITÀ DEGLI STUDI DI PADOVA
*Department of Civil, Environmental and Architectural Engineering – ICEA*

## 2. The FE-IE mesh

In this section, the FE-IE mesh is described according to the geometry domain defined during phase WP2. Both tetrahedral and hexahedral meshes are preliminarily developed and tested. For the sake of brevity, only the final mesh is shown in this report, which consists of hexahedron elements for the 3D mesh and 2D elements for the interface elements.

### *2.1 FE mesh*

Based on the typical features of the UGS fields in The Netherlands, the reservoir is made of two adjacent square blocks, 2000 × 2000 m wide and 200 m thick. The reservoir is confined laterally by four sealing faults, namely F1, F2, F4 and F5. Another fault, F3, subdivides the reservoir in two compartments, where the pore pressure change $\Delta p_1$ and $\Delta p_2$ may differ. The original gas in place for each compartment amounts to ~$25\times10^9$ $Sm^3$ assuming p = 200 bar, water saturation = 0, porosity = 0.2, temperature = 373 K, net/gross = 1. The reservoir is embedded in a 30 km wide square domain, such that its size is much larger than the reservoir dimension to minimize the effect of the boundary conditions on the solution in the area of interest.

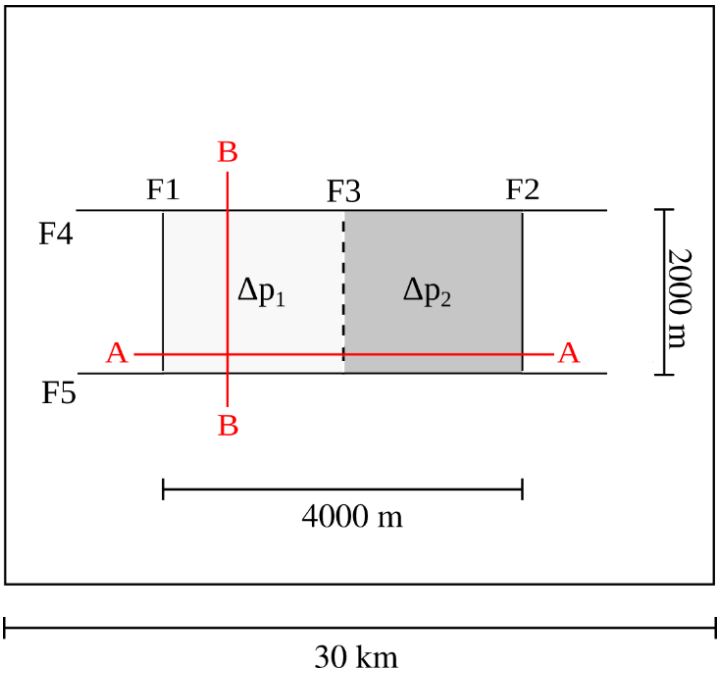


**Figure 1** Plain view of the conceptual model.

According to the geometry shown in Figure 1 and Figure 2, a 3D-FE mesh is developed by using hexahedral elements. These elements are particularly suitable for the symmetric configuration with the faults parallel to the Cartesian axes. Figure 3 shows an axonometric view of the 3D-FE grid used in the geomechanical model. The mesh consists of 253'165 nodes and 236'208 FE elements with a finer discretization in the reservoir layers, i.e., at depth between 1800 and 2200 m. The element size within the reservoir is 100 × 100 × 20 m. The bottom of the model is 5000 m deep and

the land surface is located at the elevation of 0 m. Notice that block 2 can be offset in the vertical direction of 100 m and 200 m, corresponding to half and the entire thickness of the reservoir, respectively. Along the direction orthogonal to the main F1, F2, and F3 faults (i.e., along the B-B direction of Figure 1), the elevation of the reservoir and caprock formations remain constant.

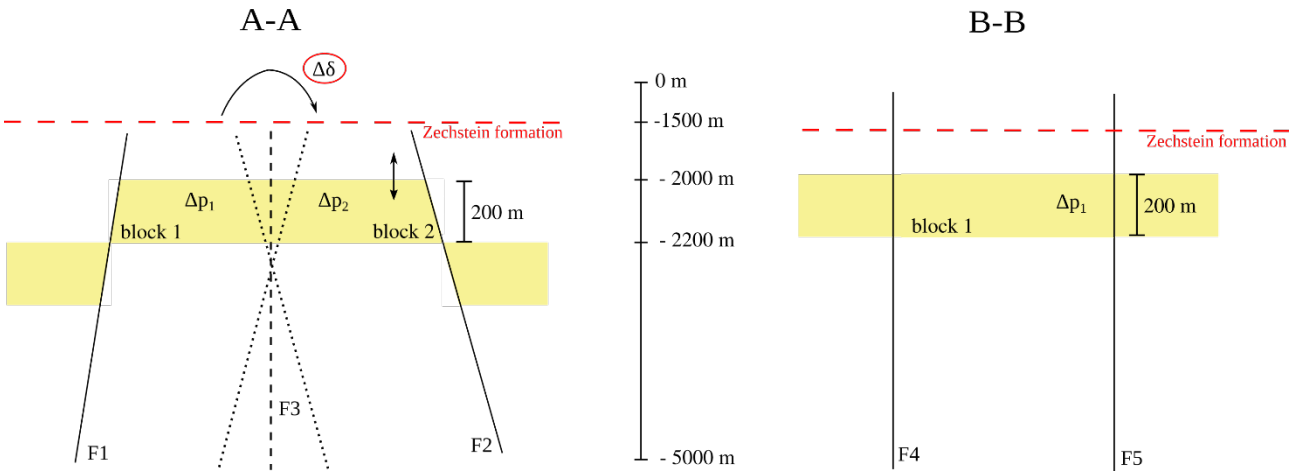


**Figure 2** Vertical sections of the conceptual model along the trace A-A and B-B shown in Figure 1.

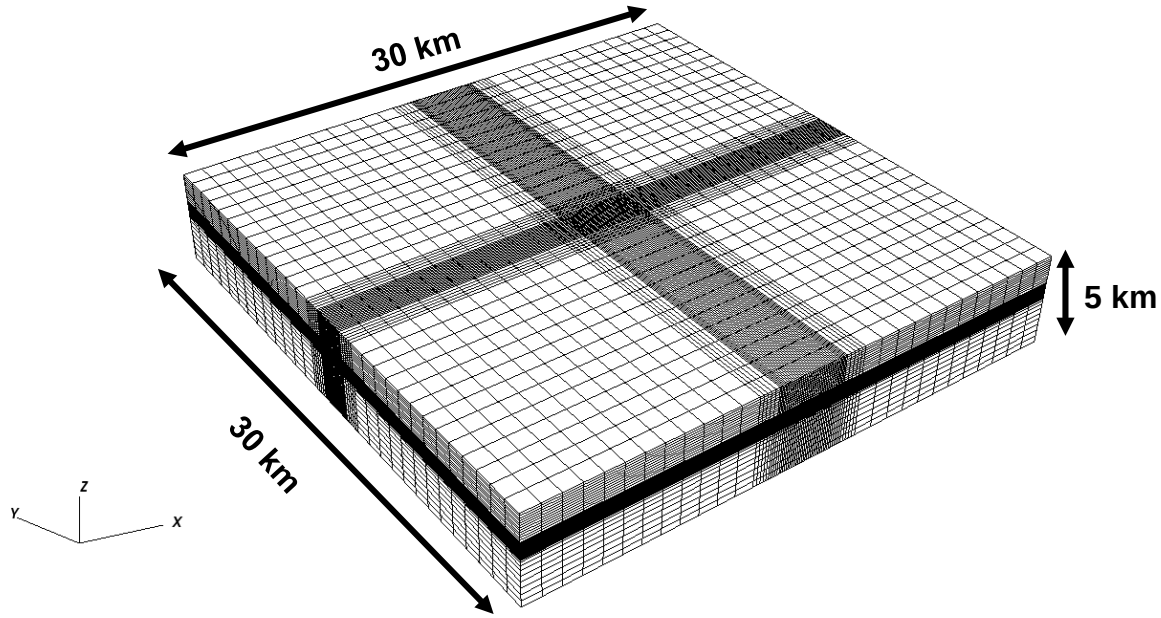


**Figure 3** Axonometric view of the 3D-FE grid used for the geomechanical simulations.

## *2.2 IE mesh*

Based on the novel Lagrangian formulation proposed by Franceschini et al. (2016), interface elements (IE) have been integrated into the 3D geomechanical FE simulator to investigate the mechanical reactivation of faults. A geological fault is a discontinuity in a porous medium, whose

mechanical behaviour is governed by the variation of the stress state in the close surroundings. In the model, the rupture activation is governed by the Mohr-Coulomb failure criterion.

Figure 4 shows the fault system embedded in the continuous 3D grid. Faults F4 and F5 are vertical faults, while F1 and F2 are inclined as shown in Figure 2 with a dip angle equal to ±80°. The dip angle of fault F3 can vary within the range [-65° – +65°]. The faults extend from -3000 m to -1600 m depth, i.e. they terminate within the caprock sealing the reservoir. Figure 5 shows the fault system where F3 is a vertical. This configuration is used for the reference case.

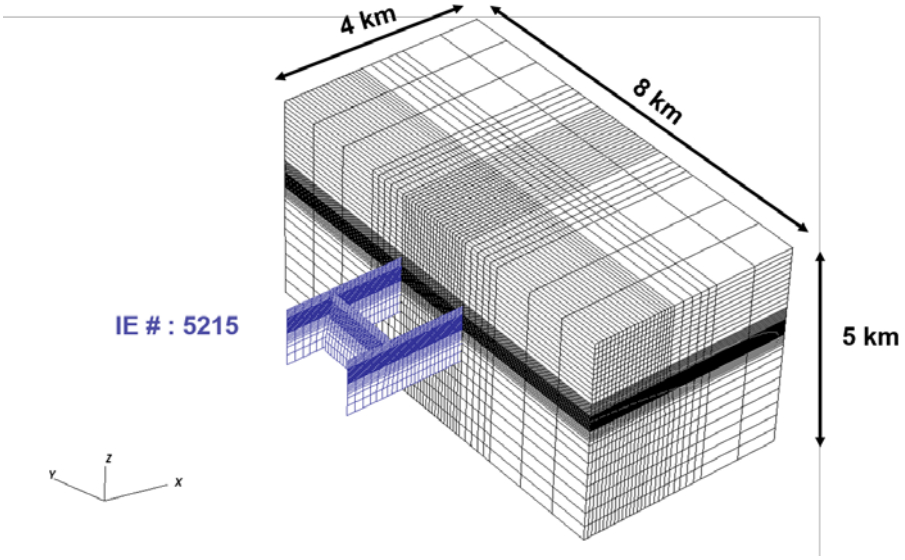


**Figure 4** Axonometric view of the IE grid (blue) embedded in the 3D-FE grid (black).

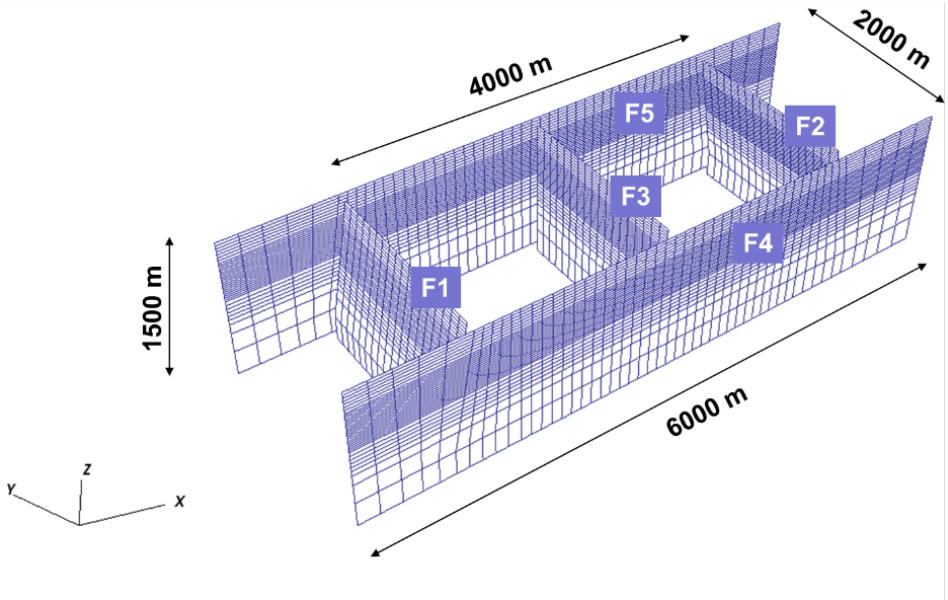


**Figure 5** IE discretization of the fault discontinuities. F1, F2 and F3 are parallel to the y-axis whereas F4 and F5 to the x-axis. F3 is the central fault subdividing the reservoir into two compartments.

## *2.3 Model set-up*

Standard conditions with zero displacement on the outer and bottom boundaries are prescribed, whereas the land surface is a no-stress boundary.

The "reference" case is characterized by the following geological and geomechanical setting:

- the central fault F3 is vertical;
- initial stress regime: the direction of the principal stresses corresponds to the *x*, *y*, and *z* axes of the domain, i.e. $\theta=0°$ (Figure 7). According to the dataset provided by SodM, the gradient for the vertical stress is layer-dependent (Table 1), with $M_1$ and $M_2$ (Table 2) defined by the ratios $M_1=\sigma_h/\sigma_v$ and $M_2=\sigma_H/\sigma_v$ where $\sigma_h$, $\sigma_H$ and $\sigma_v$ are the horizontal and vertical principal components of the *effective* stresses. Figure 6 shows the behaviour of the initial total stresses $\sigma_{TOT,x}$, $\sigma_{TOT,y}$, $\sigma_{TOT,z}$ and the pore pressure P versus depth according to the formation-dependent geomechanical parameters of Table 1, with $M_1$ and $M_2$ values properly modified from Table 2 for total stresses;
- the failure criterion governing the fault reactivation is characterized by the cohesion (*c*) and static friction angle ($\varphi_s$) provided in Table 2;
- the reservoir formation, overburden, and underburden are linear elastic medium; the caprock also behaves as a linear elastic layer. The geomechanical properties are reported in Table 1.

The above parametrization is summarized in Table 2. Note that if the salt caprock is not included in the simulation, we assign the same properties of the overburden formation to the Zechstein formation.

**Table 1** Formation-dependent geomechanical parameters.

| LAYER | DENSITY (kg/m$^3$) | YOUNG MODULUS (GPa) | POISSON RATIO |
|---|---|---|---|
| Overburden | 2200 | 10.0 | 0.25 |
| Zechstein Salt | 2100 | 40.0 | 0.3 |
| Reservoir (Upper Rotliegend) | 2400 | 11.0 | 0.15 |
| Underburden | 2600 | 30 | 0.2 |

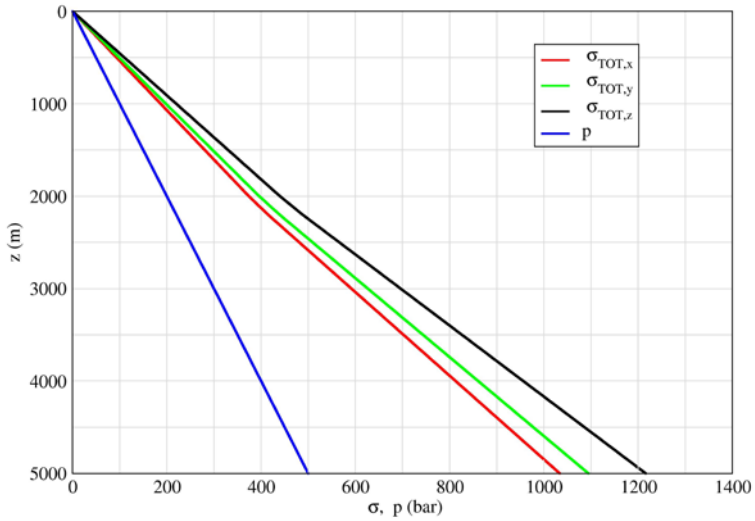


**Figure 6** Initial total stresses $\sigma_{TOT,x}$, $\sigma_{TOT,y}$, $\sigma_{TOT,z}$ and pore pressure p versus depth, according to the formation-dependent geomechanical parameters of Table 1 with $M_1$ and $M_2$ values properly modified from Table 2 for total stresses.

**Table 2** Model parametrization for the "reference" test case.

| PARAMETER | VALUE |
|---|---|
| F3 dip | 90° |
| Offset | 0 m |
| θ | 0° |
| $M_1$ | 0.74 |
| $M_2$ | 0.83 |
| Cohesion | 20 bar |
| Static friction angle | 30° |
| $E_{reservoir}$ | 11 GPa |
| caprock | linear elastic |
| α | 0.86 |
| ν | 0.15 |

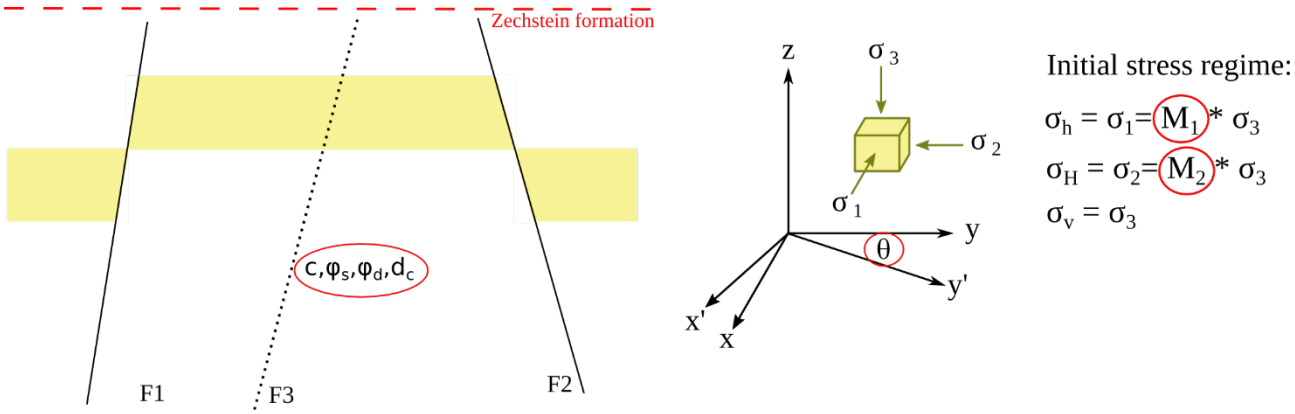


**Figure 7** Main parameters use to characterize the fault behaviour and the initial stress regime.

### *2.4 On the fault stress regime in a 3D setting*

The use of a FE-IE model allows to quantify how the stress regime acting on a fault ($\sigma_n$ normal stress and τ shear stress) changes because of the pressure depletion in the reservoir. Through IEs, a sealing fault can be viewed as an impermeable zero-thickness bound within the continuous body. From a qualitative point of view, the pore pressure decline, which is a volumetric body force, due to hydrocarbon production causes an increase of the effective stress in both the vertical and horizontal direction, yielding a reservoir compaction (along *z*) and contraction (along *x* and *y*). Consequently, a fault bounding or crossing a producing reservoir results unloaded ($\sigma_n$ decreases), generally moving its stress condition toward a more critical state in relation to its possible activation.

In a complex 3D setting as the one addressed in the present study, a quantitative evaluation of the stress rearrangement (within the continuum and on the fault) and the deformation behaviour requires the use of a numerical geomechanical model to solve the global equilibrium in term of stresses and deformations for each loading condition of the system. For a given pressure change ΔP, the system response, and therefore the criticality condition of a fault bounding/crossing the

reservoir, depends mainly on the initial stress regime, the distribution of the mechanical properties within the system (reservoir, underburden, sideburden, overburden), the location and orientation of the fault with respect to the initial stress state and the volume experiencing the depletion.

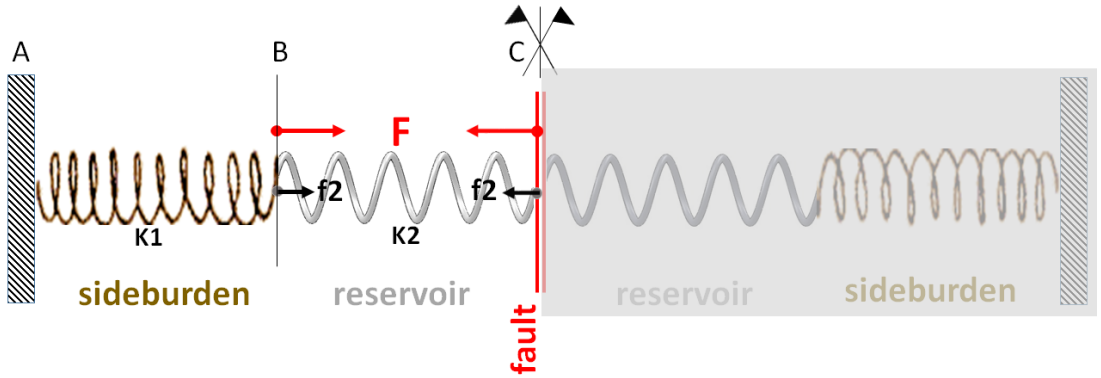


**Figure 8** 1D example used to explain stress redistribution due to an external load F.

Before showing a few specific outcomes obtained by M3E_GEPS3D on the model of interest, it seems useful to explain the concept reported above by the simple 1D system shown in Figure 8. The system is composed by four springs separated by a "fault element" and bounded by two fixed constrains. The central springs, termed "reservoir", are characterised by a stiffness K2 whereas the outer springs, termed "sideburden", by the stiffness K1. Because of system symmetry, only the left part is accounted for. Let load the reservoir by a uniform body force ΔP that correspond to an external load F applied in B and C, i.e. the reservoir boundary. In the following, we compute how F is split between the two springs, i.e. between the fault and the "reservoir".

Because of equilibrium in B:

$$-\Delta l1 \cdot K1 + \Delta l2 \cdot K2 + F = 0$$

where $\Delta l1$ and $\Delta l2$ are the deformation of sideburden and reservoir, respectively. Moreover, for compatibility condition:

$$-\Delta l1 = \Delta l2 = \Delta l$$

and hence:

$$\Delta l = -\frac{F}{K1 + K2}$$

The cumulative force acting on the fault is the sum of the external force F plus the inner force $f2$ absorbed by the reservoir spring. This latter reads:

$$f2 = K2 \cdot \Delta l = -\frac{K2}{K1 + K2} F$$

and therefore:

$$F_{fault} = F + f2 = \frac{K1}{K1 + K2} F$$

which equals the force exerted within the sideburden. The force within the reservoir results:

$$F_{reservoir} = F - F_{fault} = f2$$

Notice that we have a reservoir compaction (the force is negative) and a sideburden extension (the force is positive) in agreement with the arrow orientation shown in Figure 8.

Now, if K1→0, i.e. the reservoir is much stiffer than the sideburden, $F_{fault} = 0$ (the fault is unloaded) and the whole force is kept by the reservoir. Conversely, if the reservoir is much less stiff then the sideburden, i.e. K2 →0, the fault is loaded by the entire force F (as the sideburden) and the reservoir remain unloaded. An intermediate condition results for value of the ratio K1/K2 different from 0 and ∞, with the fault that "feels" different value of the normal stress $\sigma_N$ for the same ΔP value.

The validity of these considerations has been tested also with the 3D model used in this the study. A couple of simulations has been run using the parameters of the reference case (Table 2) except for the values of the Biot coefficient (α = 1), the Poisson ratio (ν = 0.25), the initial stress regime $M_1$=$M_2$=1, and the stiffness distribution, which has been set as follows:

a) $E_{reservoir} / E_{out\_reservoir} = 10^2$;
b) $E_{reservoir} / E_{out+reservoir} = 10^{-2}$.

A ΔP = 100 bar is prescribed within the two compartments. The stress regimes at z = -2100 m in the reservoir and on faults F3 and F4 in undisturbed conditions and after the pressure depletion are shown in Table 3. The values clearly show that, consistently with the 1D case K1→0 described above, in scenario (a) the pressure change caused an increase of the effective stress within the reservoir that is almost equal to ΔP, while $\Delta\sigma_N$ is almost negligible on fault F4 and very small on F3. Conversely, similarly to the case K2→0, in scenario (b) when the reservoir is very compressible the stress change within the reservoir is negligible and the fault unloading is almost equal to ΔP. Therefore, both the faults result much more unloaded (and the criticality index increases significantly more) in scenario (b) than in scenario (a).

**Table 3** Stress regimes obtained by the geomechanical model at z = -2100 m for the two scenarios developed to test the fault unloading when the reservoir is 100 time stiffer or more compressible than the over- side- and underburden.

| **STRESS (bar)** | **$E_{res}/E_{out\_res}=10^2$** | | **$E_{res}/E_{out\_res}=10^{-2}$** | |
|---|---|---|---|---|
| | **initial regime** | **ΔP = 100 bar** | **initial regime** | **ΔP = 100 bar** |
| $\sigma_z$ | -253 | -352 | -253 | -270 |
| $\sigma_x$ | -253 | -345 | -253 | -258 |
| $\sigma_y$ | -253 | -347 | -253 | -258 |
| $\sigma_{N,F3}$ | -253 | -245 | -254 | -160 |
| $\sigma_{N,F4}$ | -253 | -253 | -254 | -160 |

A few simulations have also developed taking into account that a fraction $P_f$ of the reservoir pressure change enters the fault material. In the present preliminary implementation, this corresponds to a Neumann boundary condition imposed on the fault nodes and equal to the product of $P_f$ by the area associated to the grid nodes.

## 3. Sensitivity analysis

In this section, a sensitivity analysis of the model response is reported to clarify the influence of (i) the Biot coefficient, (ii) the model geometry, (iii) the initial stress regime, (iv) the fault and reservoir geomechanical parameters, and (v) the differential pressure in the compartments during UGS. In particular, the analysis aims at identifying those forcing factors that are prone to induced

"un-expected" (micro)-seismicity. Table 4 summarizes the investigated test cases. Prior to the analysis, a section is dedicated to illustrate the model response for the so-called reference test case (parametrization of Table 2) used to compare the results of the sensitivity analysis.

The results are presented in the following subsections. Notice that the values of $t_a$, $t_{80}$, and $t_{50}$ are provided in Annex II.

### *3.1 Reference test case*

The orientation of the horizontal effective principal stresses $\sigma_h$ and $\sigma_H$ is parallel to the Cartesian axes at the onset of the simulation. At reservoir average depth, i.e., z=-2100 m, the vertical effective stresses equals $\sigma_v$ = 25.4 MPa with $\sigma_h = M_1 \cdot \sigma_v$ =18.8 MPa and $\sigma_H = M_2 \cdot \sigma_v$ = 21.1 MPa. The initial normal stress on the faults is shown in Figure 9.

**Table 4** Variability range of the various parameters tested in the sensitivity analysis.

| | **PARAMETER** | **INTERVAL** |
|---|---|---|
| Reservoir and fault geometry | F3 dip | +65°; -65° |
| | compartment offset | 100 m ; 200 m |
| Initial stress regime | $\theta$ | 90° |
| | $M_1$ , $M_2$ | 0.40 ; 0.47 |
| Mohr-Coulomb criterion | c | 0; 100 bar |
| | $\varphi_s$ | 20° |
| | $\varphi_d$ | 10° ; 20° |
| | $d_c$ | 2 mm ; 20 mm |
| Reservoir stiffness | E | 8 GPa; 20 GPa |
| Caprock formation | caprock | viscous |
| Biot coefficient | $\alpha$ | 1.0 |
| UGS pressure change | $\Delta p_1$, $\Delta p_2$ | 100 bar ; 200 bar |

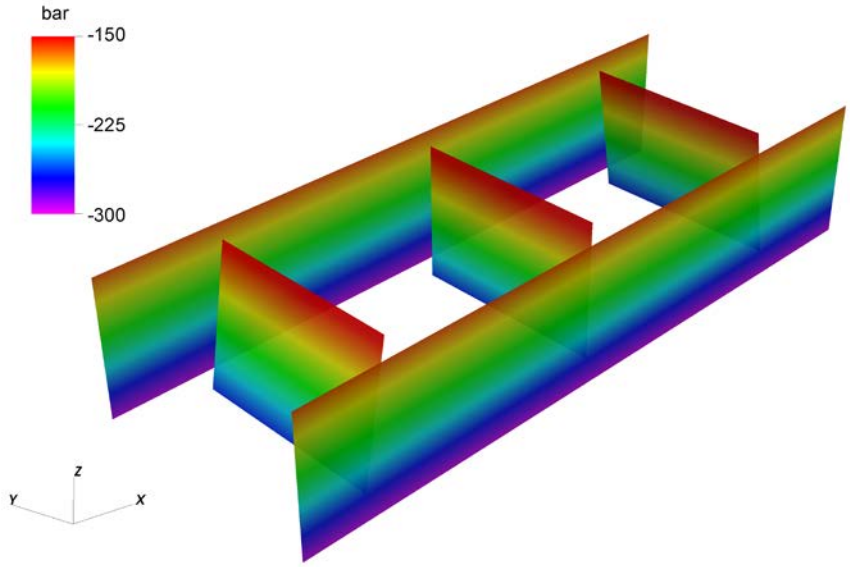


**Figure 9** Initial stress normal to the faults. Negative values mean compression. The principal stresses $\sigma_h$, $\sigma_H$ and $\sigma_v$ are parallel to the Cartesian axes. Faults F4 and F5 are more loaded because of their orthogonality to $\sigma_H$.

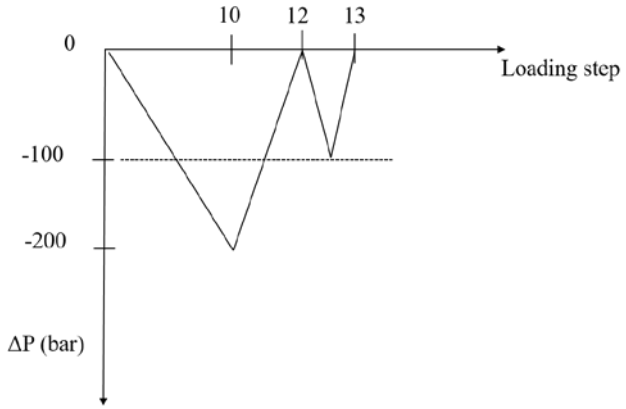


**Figure 10** Pore pressure change in the reservoir compartments 1 and 2.

The pore pressure change, ΔP, is sketched in Figure 10. During a ten-year production phase the reservoir experiences a maximum ΔP = - 200 bar in compartments 1 and 2. Then, the reservoir recovers the initial ΔP in two years during the cushion gas (CG) phase. After that, the UGS phase is simulated where one UGS cycle consists of one year (6-month production and 6-month storage). A 1-year loading step is used during production and CG injection while during UGS the loading step is equal to 0.1 year. Notice that a spatially constant ΔP is prescribed within the reservoir compartments.

Figure 11 provides the time behavior of the maximum sliding computed for the five faults. Fault F1, F2, F4, and F5 activate at loading step = 6. Figure 12a shows the active IE within the IE-mesh. The corresponding IE sliding, δ, are shown in Figure 12b. At loading step 7 (Figure 12c-12d), δ increases and the IEs at the reservoir bottom, i.e., z = -2200 m, start sliding. The maximum δ is reached at loading step = 10 (Figure 12e-12f) with a maximum value of ~1.4 cm at z = -2000 m (reservoir top). Note that fault F3 is inactive because of the symmetry conditions. During CG phase, the faults undergo stabilization and sliding ceases. Moreover, UGS operations do not critically stress the faults in terms of activation.

For inactive faults, it is important to estimate the risk associate with the reservoir exploitation. In Figure 13, the distribution of the criticality factor $\chi$ is shown for a few loading steps between 0 (undisturbed conditions) and 13 (end of UGS cycle). Table 10 (Annex I) provides the $\chi_{max}$ values for the five faults at each simulation loading step. This behavior is the consequence of the normal and shear stress re-distribution occurring on the faults.

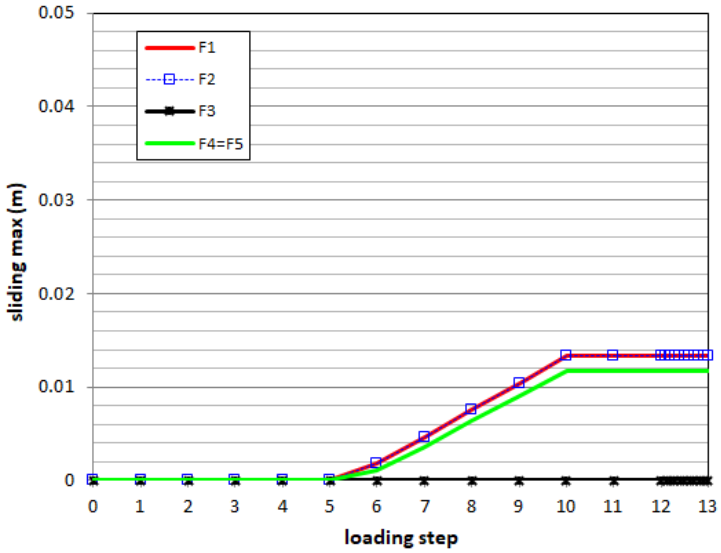


**Figure 11** Maximum sliding $\delta_{max}$ for the reference test case.

It is clear that the most critical condition is reached at loading step 10, i.e. at the end of the production phase ($\Delta P$ = -200 bar). During the CG phase, the faults are primarily stabilized by injection (from loading step 10 to 11). Then, from loading step 11 to 12 (end of CG phase), the top of the reservoir reaches again a highly critical condition with $\chi_{max}$ = 0.89 and $\chi_{max}$ = 0.79 for F1-F2 and F4-F5, respectively. During UGS, $\chi_{max}$ diminishes until loading step = 12.4 and increases again at loading step = 12.5. After that, injection phase starts with the consequence that the faults are stabilized again until loading step = 12.7 with a further destabilization until the end of the UGS cycle.

The shear stress $\tau$ on fault F1 is shown at loading steps 10, 11, 12, 12.5, and 13 in Figure 14a. The initial condition of shear stress slightly differs between top and bottom of the reservoir due to the fault dip (not shown for sake of brevity). The production phase ends at loading step 10 when the higher values of $\tau$ are observed. Note that a positive shear stress characterizes the reservoir bottom and negative the reservoir top. The direction of the shear stress is oriented toward the center of the reservoir. As shown in Figure 12a and Figure 12b, F1 starts sliding at loading step 6 and 7 in correspondence of the reservoir top and bottom, respectively. Thus, the interface elements surrounding the sliding IEs increase their shear stress (Figure 14b) to accommodate the portion in excess to the Mohr-Coulomb limit not supported by the activated elements.

At loading step 11, half of the pore pressure change has been recovered. As the reservoir expands due to pressure recovery, $\tau$ decreases on the reservoir bottom (the orientation remains the same but the absolute value decreases) and an almost null $\tau$ on the previously sliding IEs is obtained at this

step at the reservoir top. On the other hand, τ does not significantly change for the IEs surrounding the activated IEs.

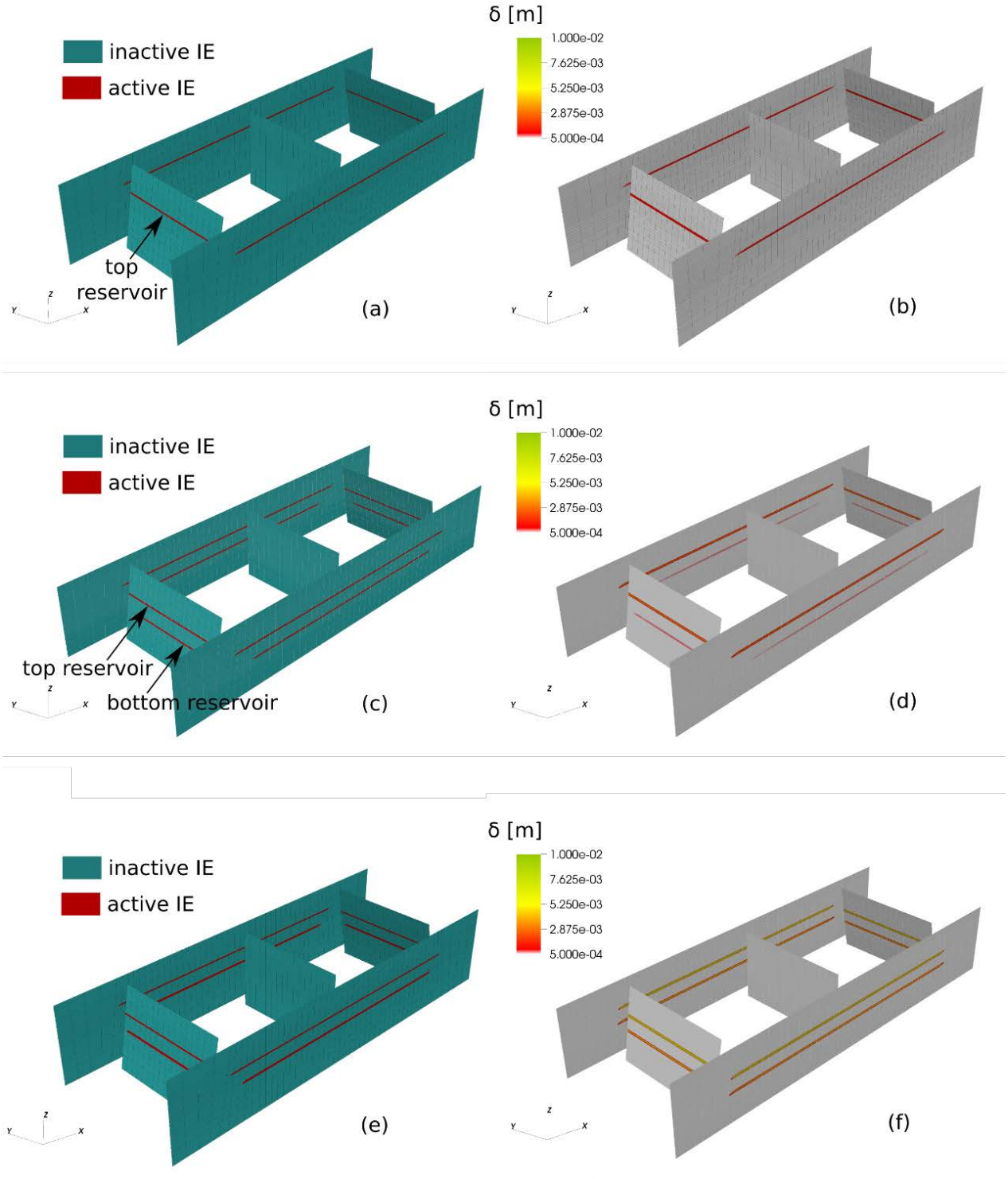


**Figure 12** Reference case: IEs activation and sliding δ on the fault system at (a)-(b) loading step = 6, (c)-(d) loading step = 7, and (e)-(f) loading step = 10. Only the IE at the reservoir top, and secondarily the bottom, are activated. Fault F3 remains inactive.

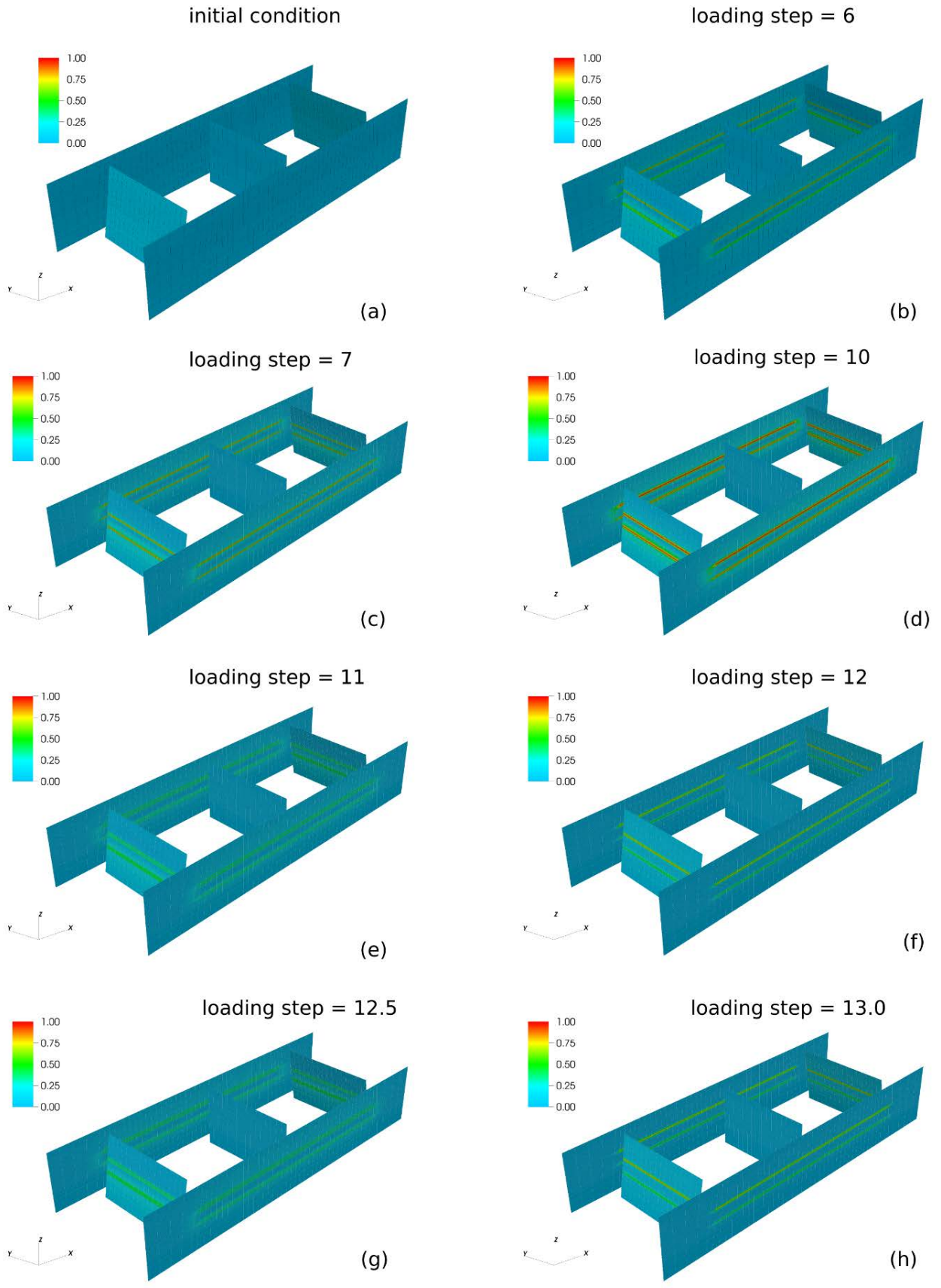


**Figure 13** Reference case: distribution of the criticality factor $\chi$ on the fault system at loading step 0 (initial condition), 6, 7, 10, 11, 12, 12.5, 13.

The reservoir continues to recover pressure and re-expand until loading step 12. During this second part of cushion gas injection shear stress increases, with a sign opposite to that experienced during primary production. A specular behavior occurs for the IEs at the reservoir bottom, although the τ absolute value at the end of CG injection is smaller than that for the top IEs because of the lower sliding experienced during production by the former IEs. Therefore, expansion during CG injection increases the criticality condition of the fault (mainly at the reservoir top) due the stress re-distribution after sliding. During UGS, at the end of the production phase (loading step 12.5), the shear stress almost equals the stress state at loading step 11. Correspondingly, the shear stress at loading step 13 equals the stress state at loading step 12. Indeed, during UGS, sliding does not occur and the porous medium behaves linear elastic.

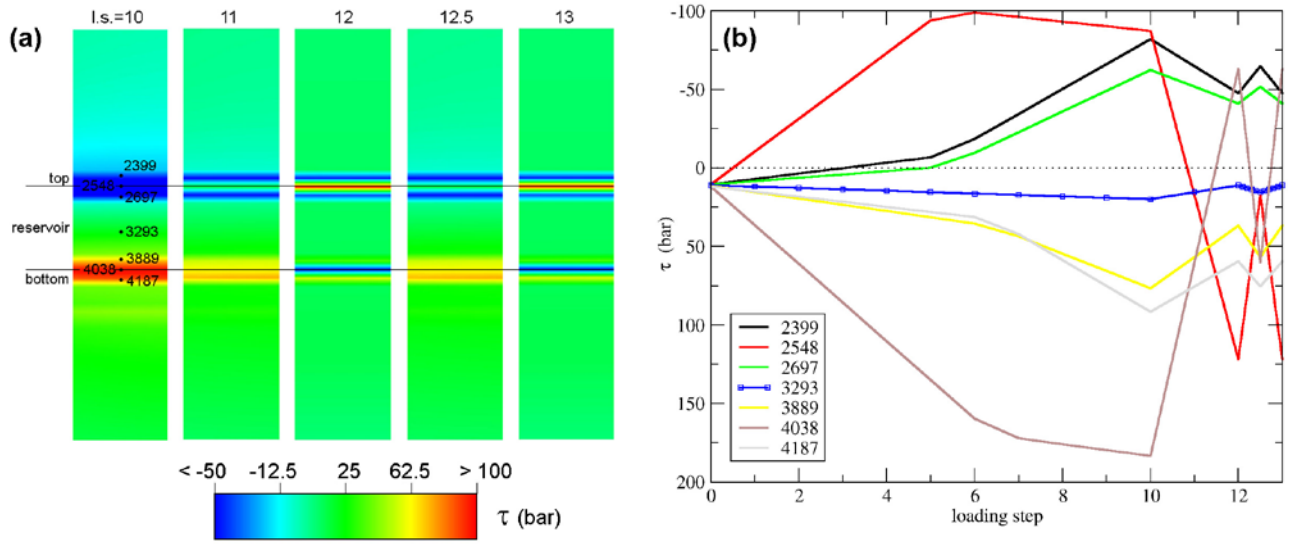


**Figure 14** Reference case: (a) distribution of the shear stress τ for the loading steps (l.s.) 10, 11, 12, 12.5, 13 on fault F1 (dip = 80°). (b) Time behavior of τ for the nodes shown in (a) located at the top, bottom, and center of the reservoir. Positive values mean shear stresses with versus consistent with that of the z-axis.

### *3.2 Biot influence on the model response*

In this section, the influence of the Biot coefficient α on the model response is analysed. In particular, the reference simulation is compared to the case where the grain compressibility is equal to zero, hence α = 1.0. Indeed, α value reads (Geertsma 1973):

$$\alpha = 1 - \frac{c_r}{c_b}$$

where $c_r$ and $c_b$ are the rock matrix and rock bulk compressibility, respectively. The bulk compressibility is related to the vertical uniaxial compressibility by the relationship:

$$c_b = 3 \cdot \frac{(1-\nu)}{(1+\nu)} c_M + c_r$$

with $\nu$ the Poisson ratio and $c_M$ the reservoir compressibility in oedometric conditions. The relationship between $c_M$ and the Young modulus, $E$, reads:

$$c_M = \frac{1}{E}\frac{(1+\nu)(1-2\nu)}{(1-\nu)}$$

Table 5 reports the parametrization characterizing the reservoir layer. By knowledge of $E$, $\nu$ and $c_r$ values, the computation of the compressibility $c_b$ and $\alpha$ is straightforward. The table compares the values obtained with $c_r$ = 3.0E-6 bar$^{-1}$ and $c_r$ = 0.0 bar$^{-1}$.

**Table 5** Variability range of the various parameters tested in the sensitivity analysis.

| Test # | ν | E [Pa] | $c_M$ [bar$^{-1}$] | $c_r$ [bar$^{-1}$] | $c_b$ [bar$^{-1}$] | α |
|---|---|---|---|---|---|---|
| **Reference (α = 0.86)** | 0.15 | 1.10E+10 | 8.65E-06 | 3.00E-06 | 2.22E-05 | 0.86 |
| **α = 1** | 0.15 | 9.47E+09 | 1.00E-05 | 0.0 | 2.22E-05 | 1.00 |

During UGS (ΔP = -100 bar), the change of the reservoir volume amounts to ~1.60 × 10$^6$ m$^3$ and ~1.26 × 10$^6$ m$^3$ with α = 1.0 and α = 0.86, respectively. These values have been obtained by integrating the deformation $\varepsilon_x$, $\varepsilon_y$, and $\varepsilon_z$, which are computed by the model at the element level, over the entire reservoir volume. As an example, Figure 15 shows the behaviour of $\varepsilon_x$, $\varepsilon_y$, and $\varepsilon_z$ obtained with α = 0.86 and α = 1.0 along *x*-*z* cross-sections at *y* = 0m and loading step 12.5 (end of extraction during UGS cycle).

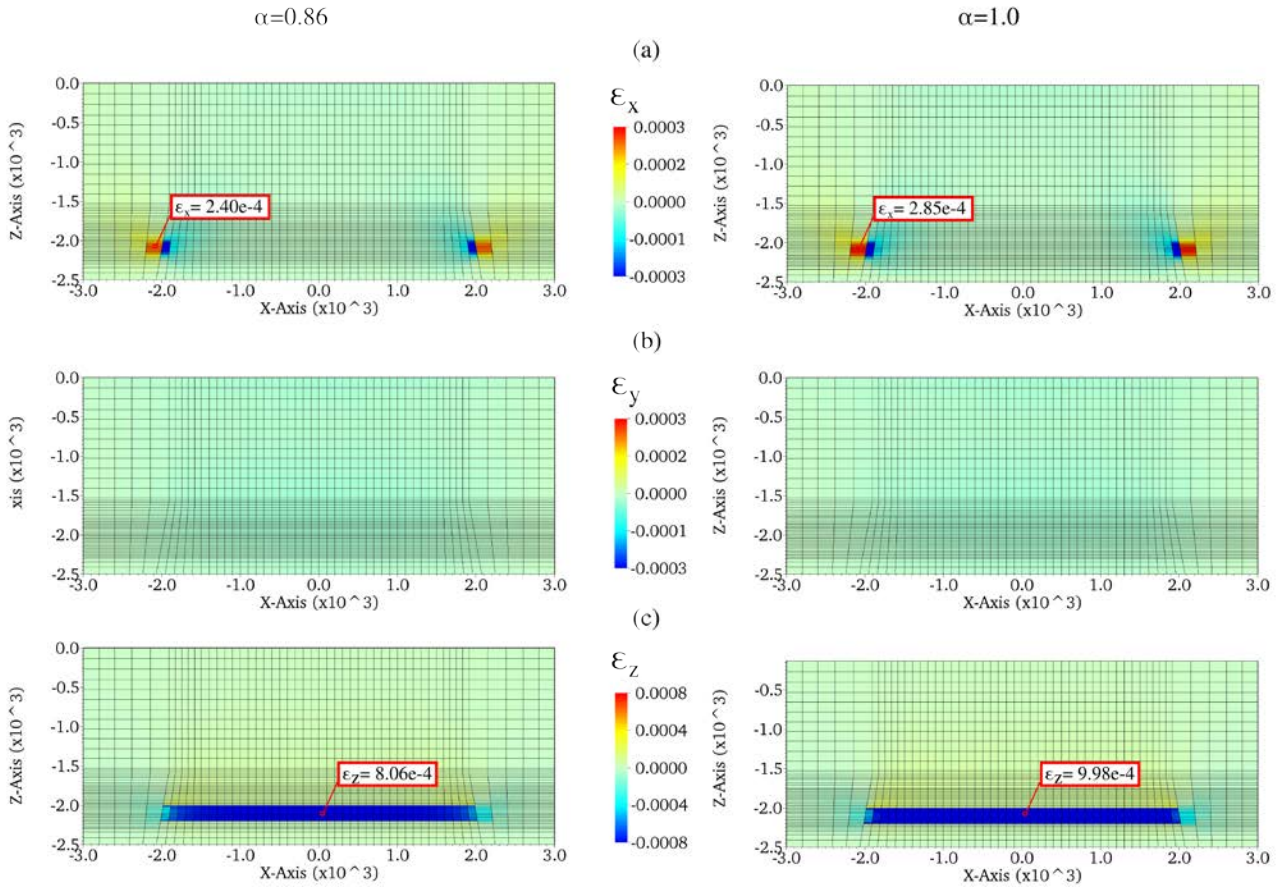


**Figure 15** Deformations (a) $\varepsilon_x$, (b) $\varepsilon_y$, and (c) $\varepsilon_z$ obtained with (left) α =0.86 and (right) α = 1.0. The results are shows for the *x*-*z* cross-section of the domain at loading step 12.5 (end of extraction during UGS cycle).

The results of the geomechanical model are provided in Figure 16 and Figure 17. Figure 16 shows the $\chi_{max}$ behaviour over time and Figure 17 the maximum sliding. The system criticality in term of fault activation is larger when $\alpha$=1.0.

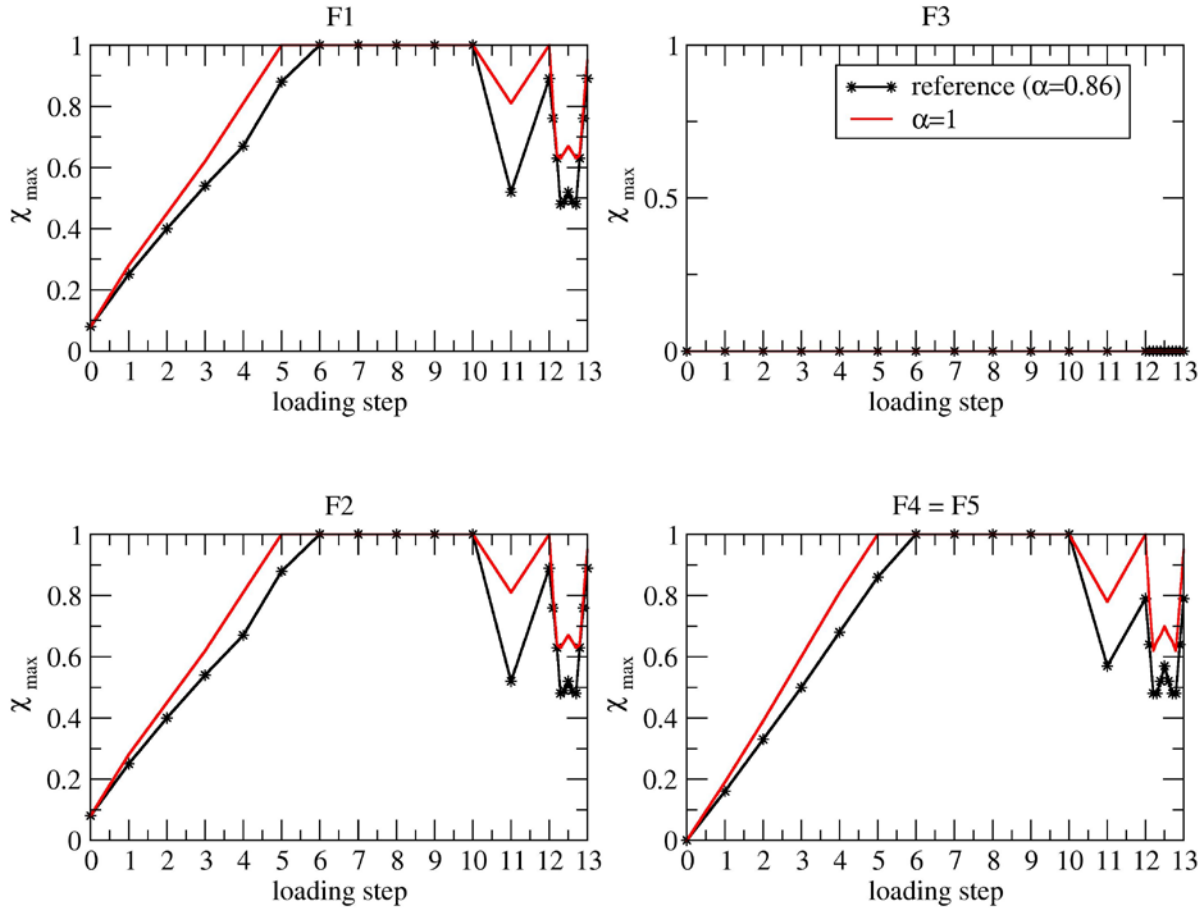


**Figure 16** Effect of the Biot coefficient on the $\chi_{max}$ behavior at increasing loading steps for each fault. Note that due to symmetry F4 and F5 behave identically.

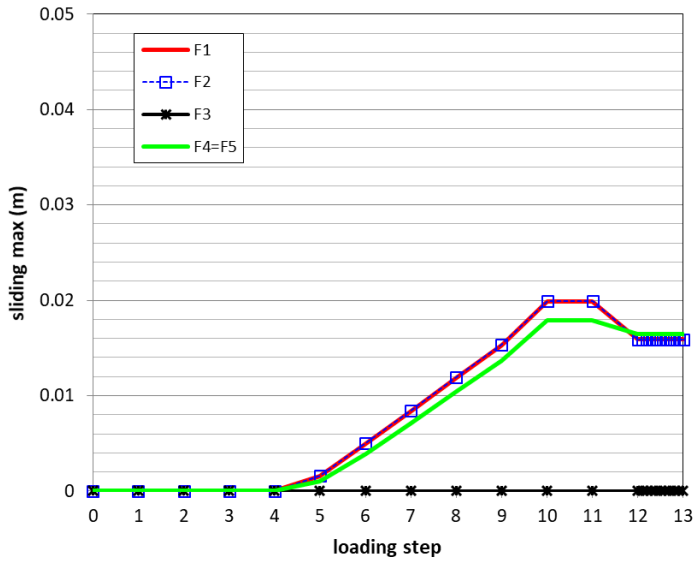


**Figure 17** Maximum sliding $\delta_{max}$ for the test case with $\alpha$=1.

### *3.3 Effect of the reservoir and fault geometry*

In this section, the reservoir and fault geometry are investigated (Table 4). In particular, a dip angle equal to +65° and -65° is assigned to the central fault (F3). Moreover, the compartment offset is investigated with two test cases where block 2 (Figure 2) is displaced of 100 m and 200 m from the original position. The effect on the fault stability is checked using the criticality factor $\chi_{max}$ (Figure 18). The results are compared with the reference test case. The fault geometry is ineffective on fault F1 because the variations do not change the loading conditions on this fault. The major influence on the instability of fault F2 is due to compartment offset. The same behavior is observed for fault F4 and F5. Fault F3 becomes active at loading step = 3 with an offset of 200 m and at loading step = 5 with an offset equal to 100 m. Moreover, the fault re-activates at the end of the cushion gas injection (loading step = 12). During UGS, fault F3 remains inactive but the criticality factory is close to 1.0 for the cases with compartment offset. The fault dip also increases instability, as expected. The values of $\chi_{max}$ are summarized in Table 11 (Annex I).

Figure 19 provides the time behavior of the fault maximum sliding for the various cases addressing reservoir and fault geometry. Notice the value of $\delta_{max}$ = 11 cm obtained for fault F3 for the 200 m offset; this is the maximum value of the sliding obtained in the study.

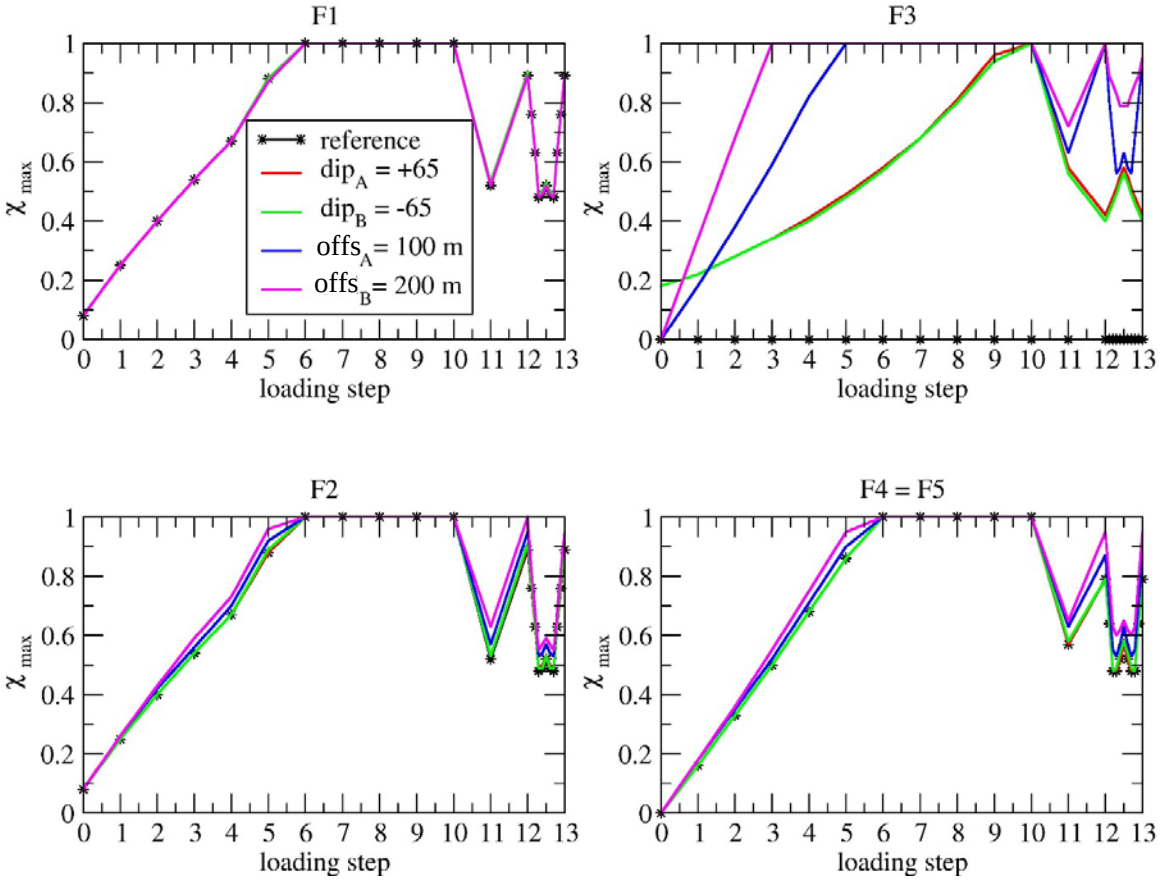


**Figure 18** Effect of the reservoir and fault geometry on the $\chi_{max}$ behavior at increasing loading steps for each fault. Note that due to symmetry F4 and F5 behave identically.

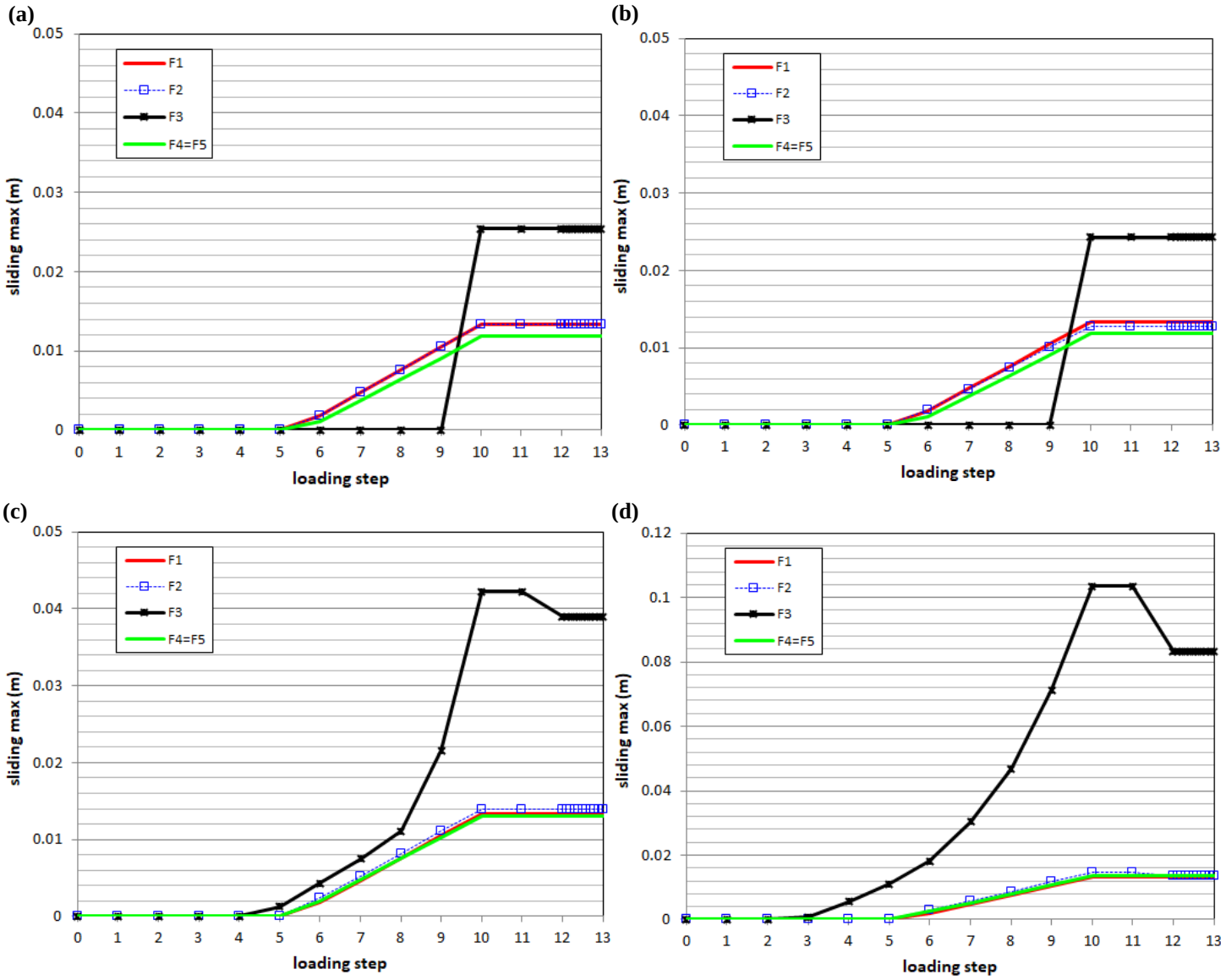


**Figure 19** Maximum sliding $\delta_{max}$ for the various test cases investigating the effect of the reservoir and fault geometry: (a) F3 dip angle equal to +65°, (b) F3 dip angle equal to -65°, (c) compartment offset equal to 100 m, and (d) compartment offset equal to 200 m.

Notice in Figure 18 the $\chi_{max}$ behavior for fault F3 during CG injection (loading steps 11 and 12) and UGS (loading steps from 12.1 to 13). The two investigated geometries (fault dip versus reservoir offset) produce a different trend during these phases, with the criticality index that monotonically decreases during cushion gas when the central fault is characterized by a ±65° slope. The reason for this dissimilarity can be understand by investigating how the shear stress acting of fault F3 varies in the two cases. The comparison is provided in Figure 20.

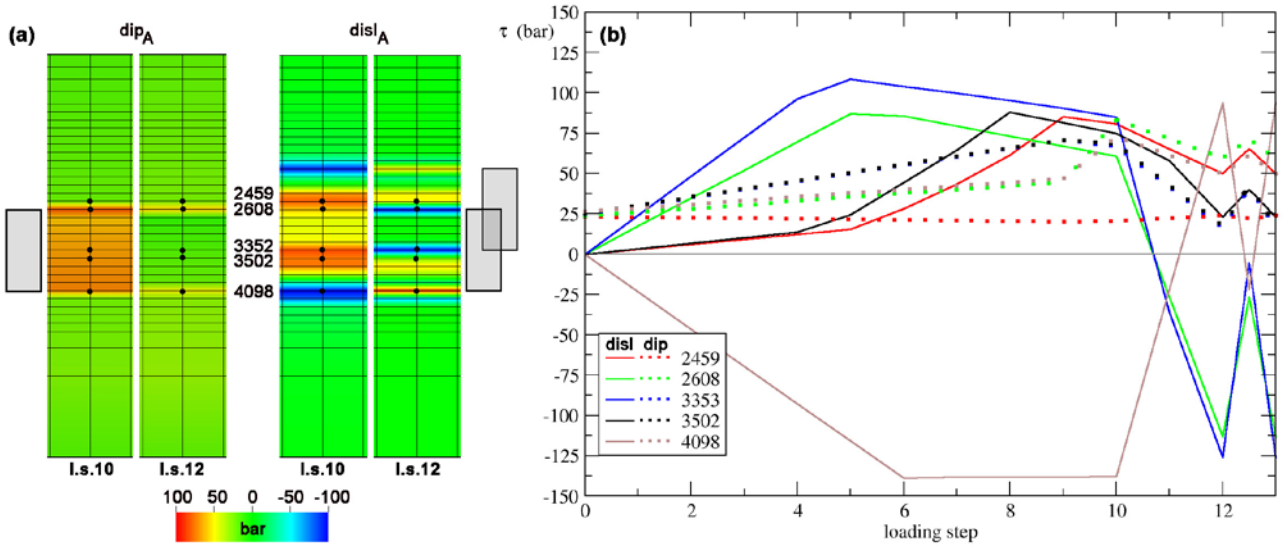


**Figure 20** F3 dip equal to +65° and compartment offset equal to 100 m: (a) distribution of the shear stress τ for the loading steps (l.s.) 10 and 12 on fault F3. The grey boxes highlight the compartment location relative to the stress field. (b) Time behavior of τ for the nodes shown in (a) located at the top, bottom, and center of the reservoir. Positive values mean shear stresses with a versus consistent with that of the z-axis. Continuous and dotted lines refer to the scenarios with a compartment offset equal to 100 m and the F3 dip angle equal to +65°, respectively.

### *3.4 Effect of the initial stress regime*

In this section, the initial stress regime is investigated (Figure 7). A value of θ=90° is considered to simulate an initial stress regime where the principal horizontal stress is aligned parallel to faults F1, F2 and F3, i.e. orthogonal to the reference test case. Moreover, lower values of the factors $M_1$ and $M_2$ are tested according to the indications by SodM. Figure 21 shows the behaviour of the initial total stresses $\sigma_{TOT,x}$, $\sigma_{TOT,y}$, $\sigma_{TOT,z}$ and the pore pressure p versus depth according to the formation-dependent geomechanical parameters of Table 1 with $M_1$ and $M_2$ values properly modified from Table 4 for the total stresses.

The effect on the fault stability is checked using the criticality factor $\chi_{max}$ (Figure 22). The effect of rotating the maximum horizontal stress by 90° is clearly visible on the fact that faults F1 and F2 are more stable while faults F4 and F5 are characterized by a higher instability with respect to the reference. Fault F3 is not affect by this variation. Conversely, F3 is influenced by changing the value of the $M_1$ and $M_2$ parameters, meaning that this new initial stress regime on the fault is much more critical compared to reference. Fault F3 becomes active at loading steps 9 and 10 with this configuration despite the system symmetry; this condition develops because the normal stress acting on the fault vanishes and the fault opens. Similarly, $M_1$ and $M_2$ significantly influence the criticality of faults F1, F2, F4 and F5. Decreasing $M_1$ and $M_2$, i.e. reducing the normal stress on the fault system, might lead to sliding of the lateral faults also at the end of the CG phase. The values of $\chi_{max}$ are reported in Table 12 (Annex I). Figure 23 provides the time behavior of the fault maximum sliding for the various cases addressing the initial stress regime.

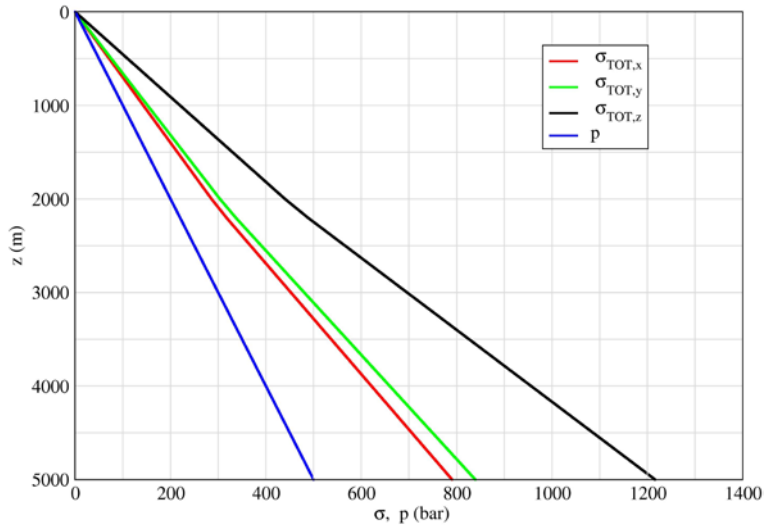


**Figure 21** Initial total stresses $\sigma_{TOT,x}$, $\sigma_{TOT,y}$, $\sigma_{TOT,z}$ and the pore pressure p versus depth according to the formation-dependent geomechanical parameters of Table 1 with $M_1$ and $M_2$ values properly modified from Table 4 for the total stresses.

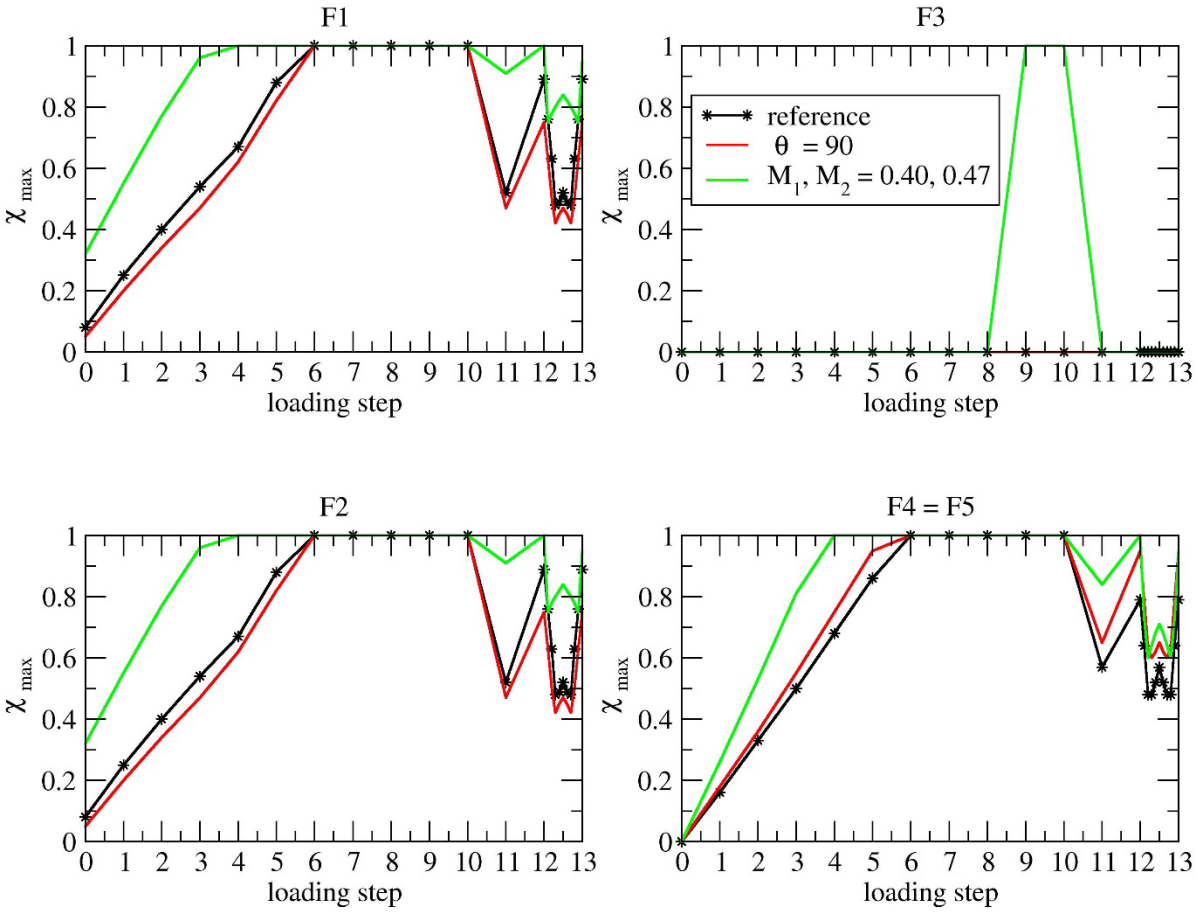


**Figure 22** Effect of the initial stress regime on the $\chi_{max}$ distribution at increasing loading steps for each fault. Note that due to symmetry F4 and F5 behave identically.

In relation to the opening of fault F3, similarly to the explanation provided in section 2.4, we summarize in Table 6 the behaviour of the stress regime at z = -2100 m in the reservoir and on the faults F3 and F4 for a few representative loadings steps. The reference case ($M_1$= 0.74 and $M_2$ =

0.83) and the case with $M_1$= 0.40 and $M_2$ = 0.47 are compared. It clearly appears that, because of the relatively low compression stress in initial condition when $M_1$=0.40, a ΔP = - 180 bar suffices to completely release the normal stress acting on F3. Notice that, in agreement with the theory for a poroelastic reservoir with infinite lateral extension, in the reservoir the variation of stress reads (Table 6):

- $\Delta\sigma_z = -\alpha\Delta p$;
- $\Delta\sigma_x = \Delta\sigma_{xy} = -\alpha\left(1 - \frac{1-2\nu}{1-\nu}\right)\Delta p$.

Moreover, it is interesting to observe that fault F3 is unloaded about twice as much as fault F4 (or the other lateral faults) because of its location between the two depleting compartments.

**Table 6** Stress regimes obtained by the geomechanical model at z = -2100 for the two scenarios addressing different values of the couple $M_1$ and $M_2$ (l.s. = loading step).

| **STRESS (bar)** | **$M_1$= 0.40 , $M_2$ = 0.47** | | | | **$M_1$= 0.74 , $M_2$ = 0.83** | | | |
|---|---|---|---|---|---|---|---|---|
| | **l.s.0** | **l.s.2** | **l.s.6** | **l.s.9** | **l.s.0** | **l.s.2** | **l.s.6** | **l.s.9** |
| ΔP | - | 40 | 120 | 180 | - | 40 | 120 | 180 |
| $\sigma_z$ | -253 | -285 | -350 | -398 | -253 | -285 | -350 | -398 |
| $\sigma_x$ | -101 | -107 | -119 | -130 | -188 | -193 | -207 | -218 |
| $\sigma_y$ | -118 | -125 | -138 | -148 | -209 | -216 | -229 | -239 |
| $\sigma_{N,F3}$ | -101 | -73 | -16 | 0 | -188 | -160 | -103 | -20 |
| $\sigma_{N,F4}$ | -119 | -105 | -77 | -57 | -210 | -196 | -169 | -148 |

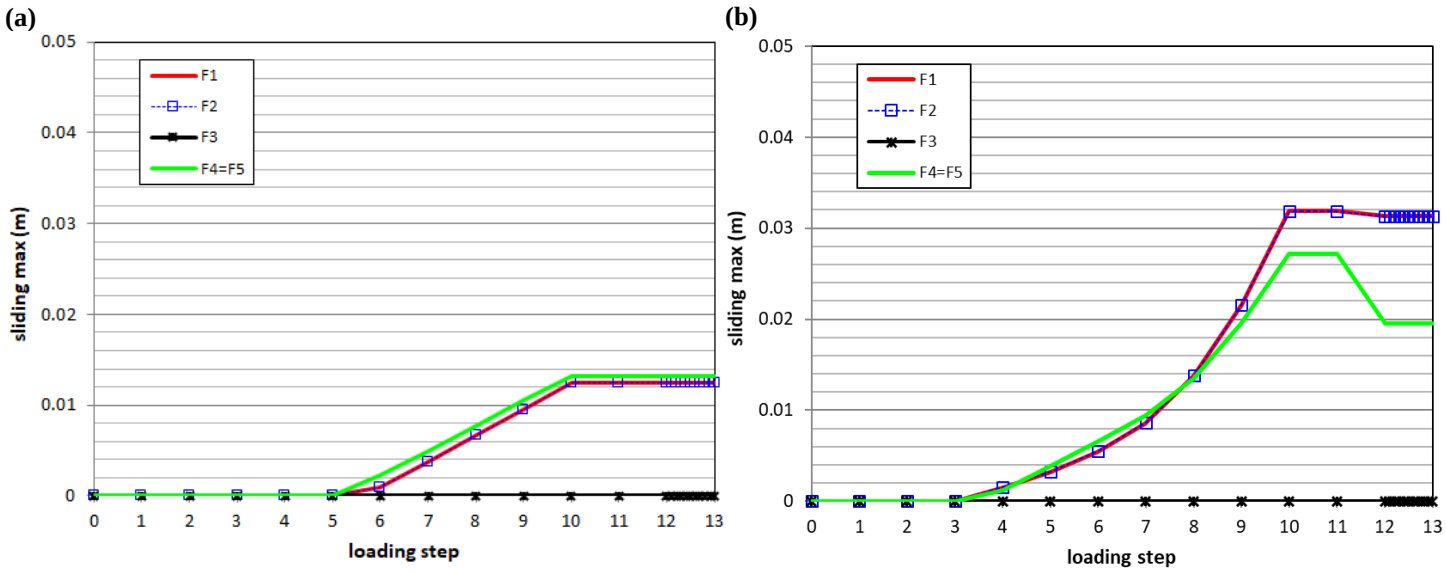


**Figure 23** Maximum sliding $\delta_{max}$ for the various test cases investigating the effect of the initial stress regime: (a) a 90° rotation of the principal horizontal stresses and (b) a ~50% reduction of the principal horizontal stress.

### *3.5 Effect of the Mohr-Coulomb fault parameters*

The Mohr-Coulomb failure criterion is employed and the shear stress limit reads:

$$\tau_{lim} = c - \sigma_n * tan\varphi$$

with $c$ and $\varphi$ the fault cohesion and friction angle, respectively, and $\sigma_n$ the normal effective stress acting on the fault (negative in compression). The sensitivity analysis focuses on the fault cohesion and friction angle. Primarily, the variation of the static friction angle ($\varphi_s$) from the reference case is considered (Table 4). Then, fault weakening is also accounted for (Andrews, 1985; Guatteri and Spudich, 2000), where the friction angle varies according to the relationship $\varphi = \varphi_s + \frac{\varphi_d - \varphi_s}{d_c} \times \delta$ for $\delta < d_c$ and $\varphi = \varphi_d$ for $\delta \geq d_c$ (Figure 24). Therefore, two parameters are necessary to define fault weakening, namely the dynamic friction angle ($\varphi_d$) and the slip weakening distance ($d_c$).

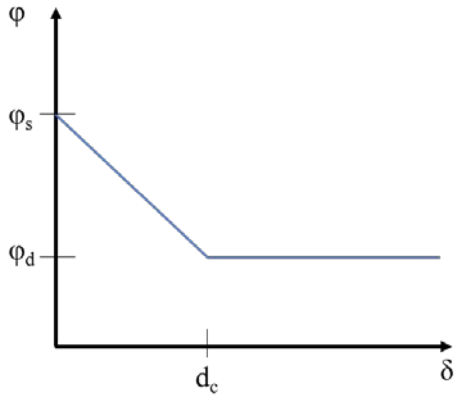


**Figure 24** Fault weakening: behavior of the fault friction angle versus the fault sliding δ.

The results are shown in Figure 25 where the values of the $\chi_{max}$ are plotted at increasing loading steps. As expected, decreasing the fault cohesion or the static friction angle affects the stability of faults F1, F2, F4 and F5 that are less stable. Conversely, fault F3 remains stable ($\chi_{max}$ = 0.0) for the entire simulation because of symmetry conditions. The fault weakening becomes active after sliding begins, reducing the value of the friction angle. The worst case is obtained for $\varphi_d$ = 10° and $d_c$ = 2 mm. This causes faults F1, F2, F4 and F5 to slide also during UGS phase at loading step 12.5, i.e., at the end of the 6-months injection phase. Obviously, an overall stabilizing effect is achieved by enhancing the fault cohesion to 100 bar. For completeness, the values of $\chi_{max}$ are reported in Table 13 (Annex I). Figure 26 provides the time behavior of the fault maximum sliding for the various cases addressing the Mohr-Coulomb parameters.

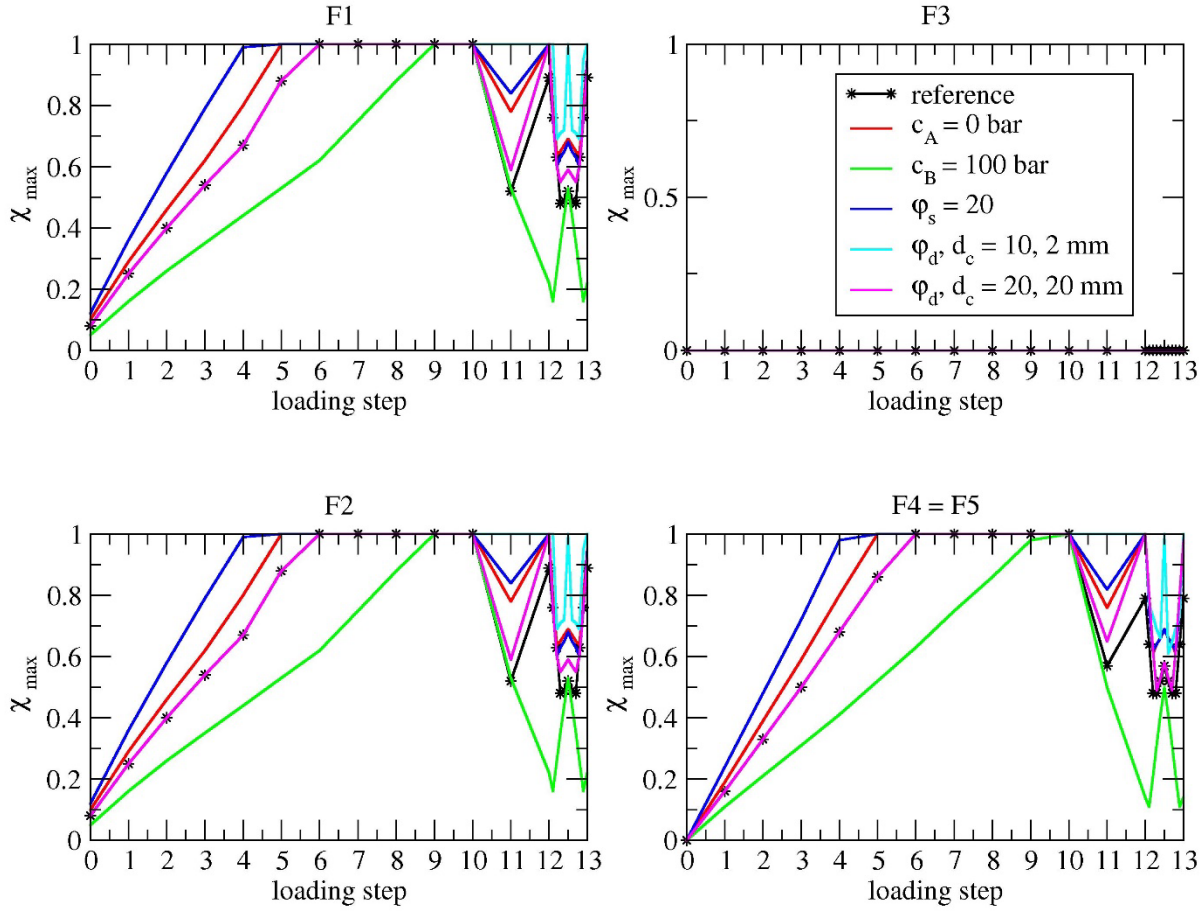


**Figure 25** Effect of the Mohr-Coulomb fault parameters on the $\chi_{max}$ behavior at increasing loading steps for each fault. Note that due to symmetry F4 and F5 behave identically.

The thickness of the active elements and thickness of the elements with $\chi > 0.5$ are plotted for faults F1-F5 in Figure 27 and Figure 28, respectively. The figures compare the behavior provided by the reference simulation and the simulation where a fault weakening with $\varphi_d = 10°$ and a slip weakening distance $d_c = 2$ mm is prescribed. Because of weakening, the fault criticality increases in the latter case yielding a larger activation with respect to the reference, in particular during CG and UGS phases.

**(a)** **(b)**

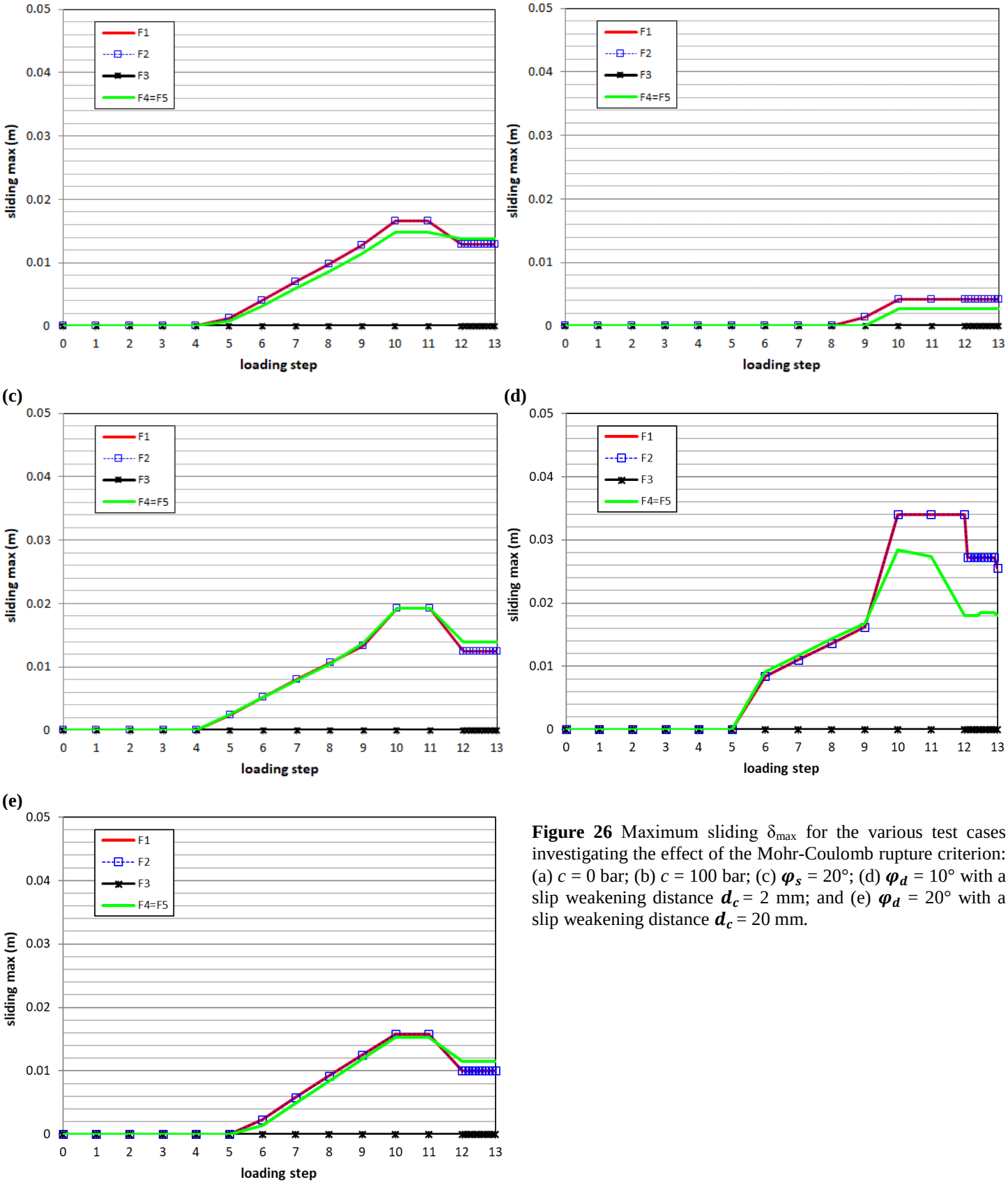


**Figure 26** Maximum sliding $\delta_{max}$ for the various test cases investigating the effect of the Mohr-Coulomb rupture criterion: (a) $c$ = 0 bar; (b) $c$ = 100 bar; (c) $\boldsymbol{\varphi_s}$ = 20°; (d) $\boldsymbol{\varphi_d}$ = 10° with a slip weakening distance $\boldsymbol{d_c}$ = 2 mm; and (e) $\boldsymbol{\varphi_d}$ = 20° with a slip weakening distance $\boldsymbol{d_c}$ = 20 mm.

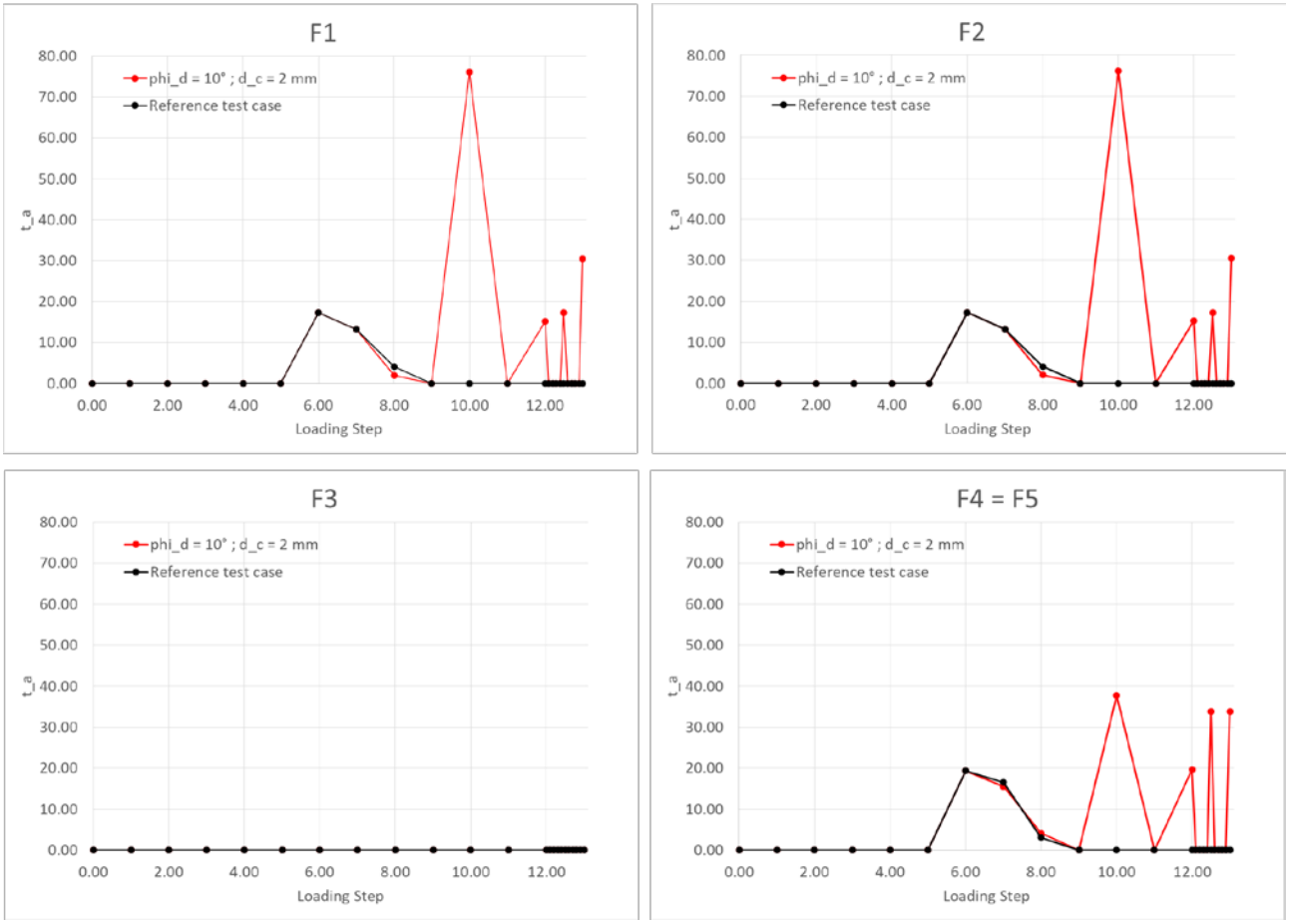


**Figure 27** Thickness of the active elements for faults F1-F5. The reference case is compared with the simulation where weakening is characterized by $\varphi_d = 10°$ and $d_c = 2$ mm.

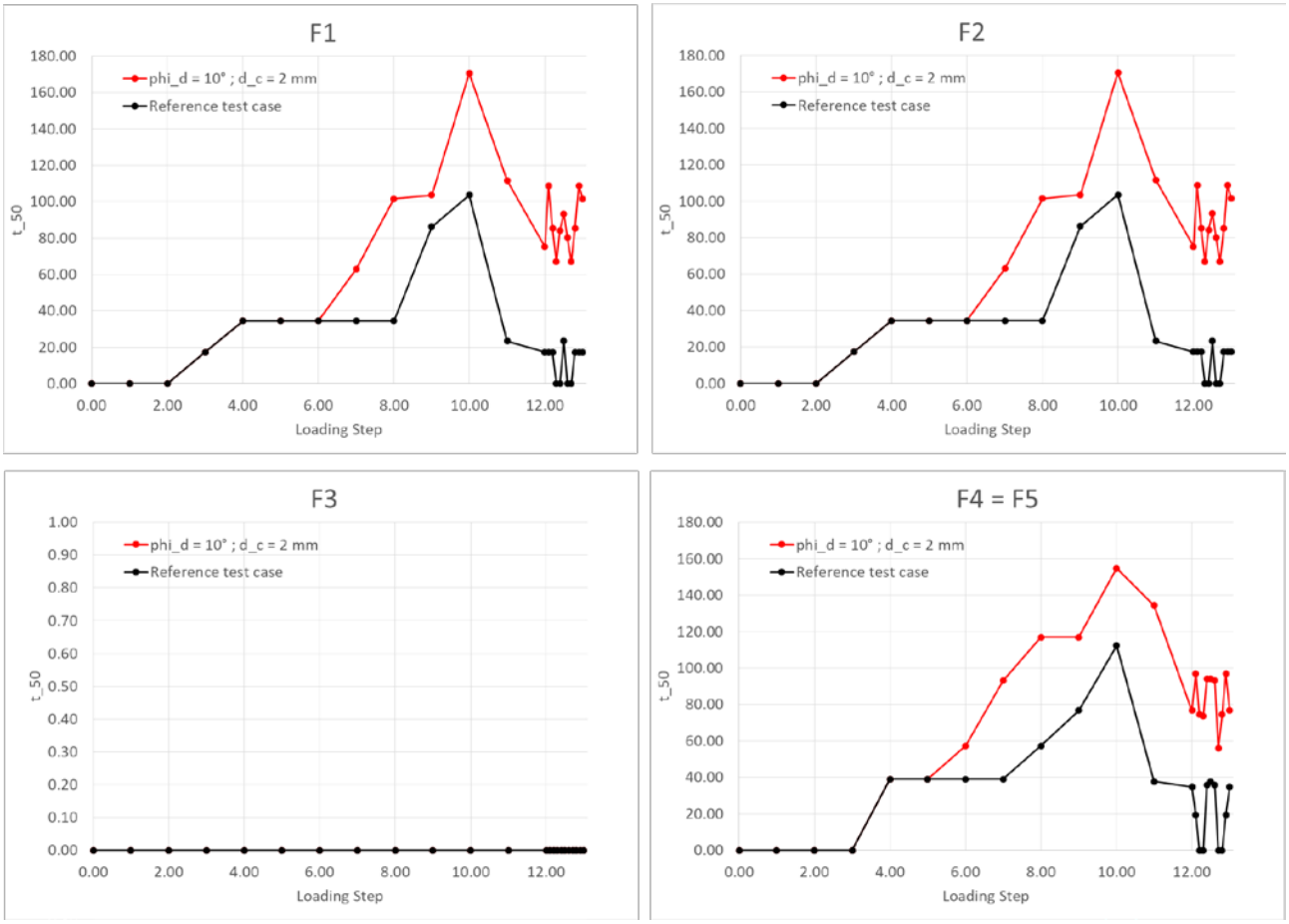


**Figure 28** Thickness of the elements with $\chi > 0.5$ for faults F1-F5. The reference case is compared with the simulation where weakening is characterized by $\varphi_d = 10°$ and $d_c = 2$ mm.

### *3.6 Effect of the reservoir stiffness*

The reservoir stiffness is investigated by using lower and higher values compared to reference where E = 11 GPa. The results are shown in Figure 29 where the values of the $\chi_{max}$ are plotted at increasing loading steps. Decreasing reservoir stiffness enhances fault instability because of the larger compaction and contraction. Fault F3 remains stable during the entire simulation. For completeness, the values of $\chi_{max}$ are reported in Table 14 (Annex I). Figure 30 provides the time behavior of the maximum sliding for the various cases addressing the reservoir stiffness.

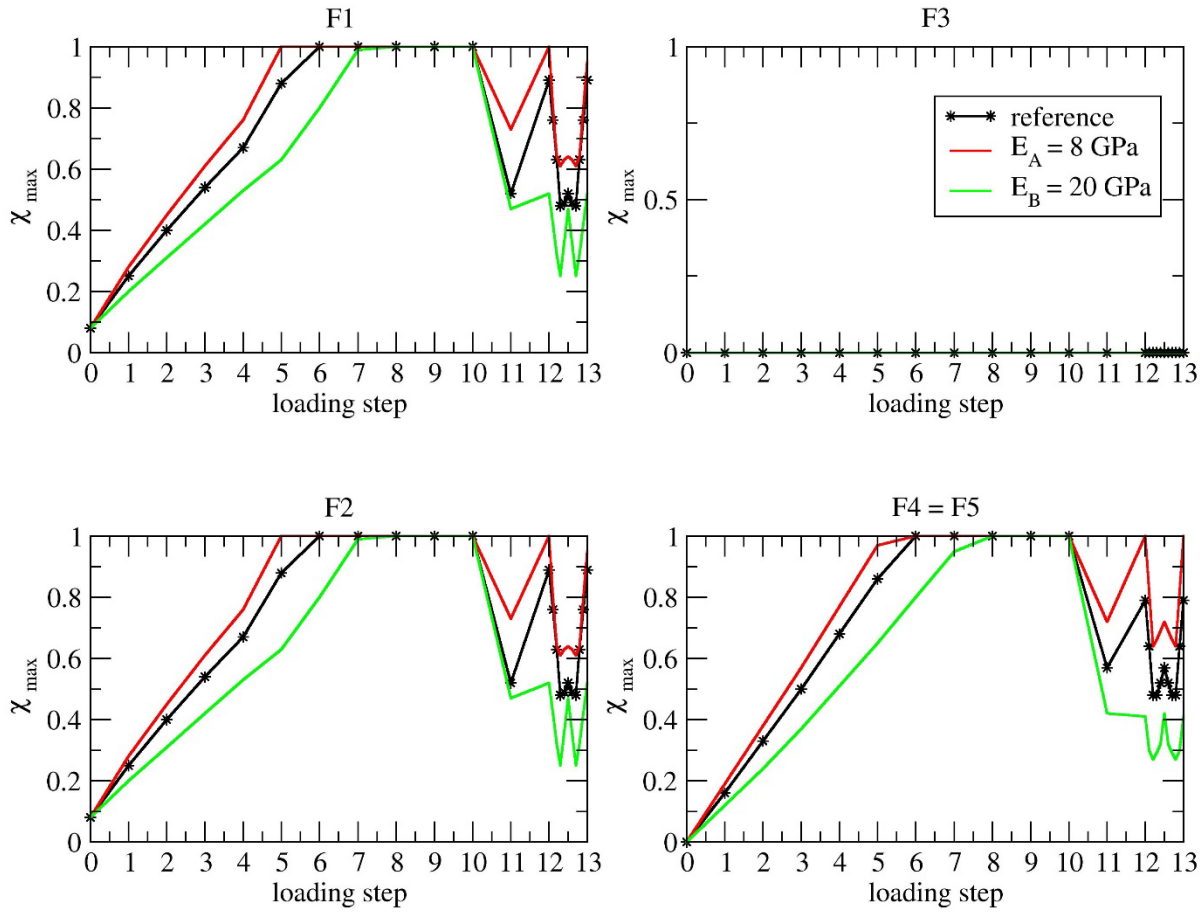


**Figure 29** Effect of the reservoir stiffness on the $\chi_{max}$ behavior at increasing loading steps for each fault. Note that due to symmetry F4 and F5 behave identically.

**Table 7** Stress regimes obtained by the geomechanical model at z = -2100 and ΔP=100 bar for the scenarios addressing different values of the reservoir stiffness.

| **STRESS (bar)** | **$E_{res}$ = 8 GPa** | | **$E_{res}$ = 11 GPa** | | **$E_{res}$ = 20 GPa** | |
|---|---|---|---|---|---|---|
| | **initial stress** | **ΔP=100 bar** | **initial stress** | **ΔP=100 bar** | **initial stress** | **ΔP=100 bar** |
| $\sigma_z$ | -253 | -335 | -253 | -334 | -253 | -330 |
| $\sigma_x$ | -188 | -203 | -188 | -203 | -188 | -203 |
| $\sigma_y$ | -209 | -225 | -209 | -226 | -209 | -227 |
| $\sigma_{N,F3}$ | -188 | -114 | -188 | -117 | -188 | -126 |
| $\sigma_{N,F4}$ | -210 | -170 | -210 | -176 | -210 | -186 |

Similarly to the sensitivity analysis on the initial stress regime, also for this set of simulations characterized by different reservoir stiffness we provide the behaviour of the stress within the reservoir on faults F3 and F4 in Table 7. Consistently with the analyses provided in section 2.4, also in a 3D setting the fault unloading decreases as the reservoir stiffness increases relative to the stiffness of the surrounding medium.

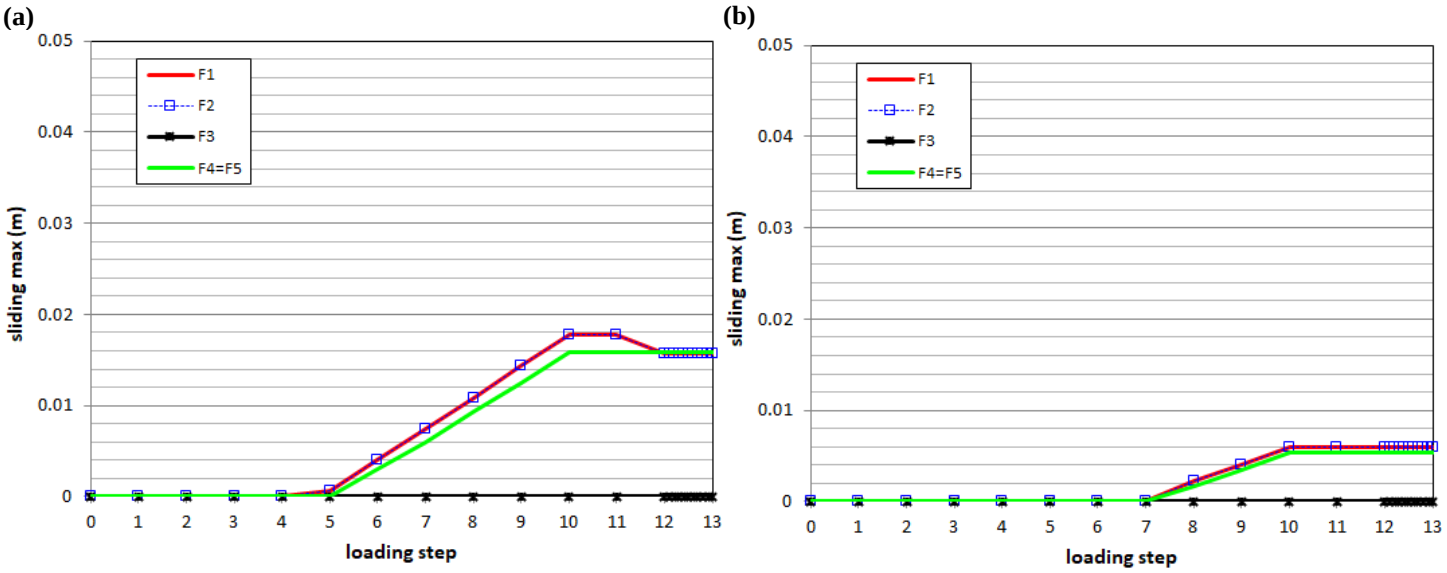


**Figure 30** Maximum sliding $\delta_{max}$ for the various test cases investigating the effect of the reservoir stiffness: (a) E = 8 GPa and (b) E = 20 GPa.

### *3.7 Effect of the differential pore pressure in the reservoir compartments*

In this section, the effect of a different pore pressure change in the two reservoir compartments is investigated. The simulations are identical to the reference until the end of the CG injection phase. During UGS, in block 1 the pore pressure change $\Delta P_1$ is kept equal to reference test case, i.e., minimum $\Delta P_1$= -100 bar (Figure 10), whereas $\Delta P_2$ is 0 bar in simulation 1 for the entire UGS (Figure 31) and $\Delta P_2$ reaches -200 bar in simulation 2 (Figure 31).

Fault F1 is not affected by a different pore pressure compared to the reference and consequently the $\chi_{max}$ behaviour does not change relative to the reference outcome. Conversely, faults F2, F4 and F5 undergo higher instability at loading step = 12.5 when maximum $\Delta P_2$= -200 bar is prescribed within block 2. It is interesting to notice the behavior of fault F3 that is critically stressed by application of differential pore pressure on the two compartments in both simulation 1 and 2. For completeness, the values of $\chi_{max}$ are reported in Table 15 (Annex I).

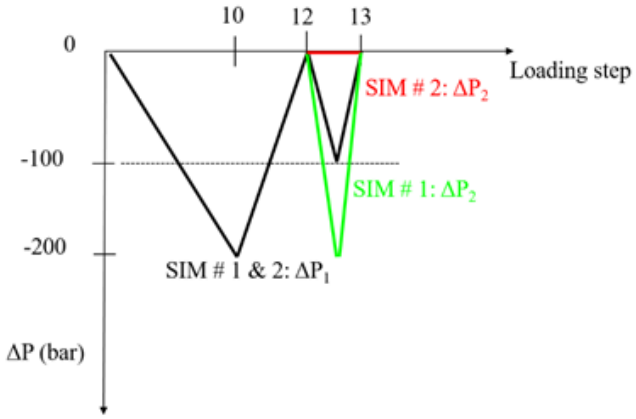


**Figure 31** Pore pressure change $\Delta P_1$ and $\Delta P_2$ in compartments 1 and 2, respectively. Two simulations (SIM 1 & 2) are run to investigate the effect of the differential pore pressure in the reservoir compartments.

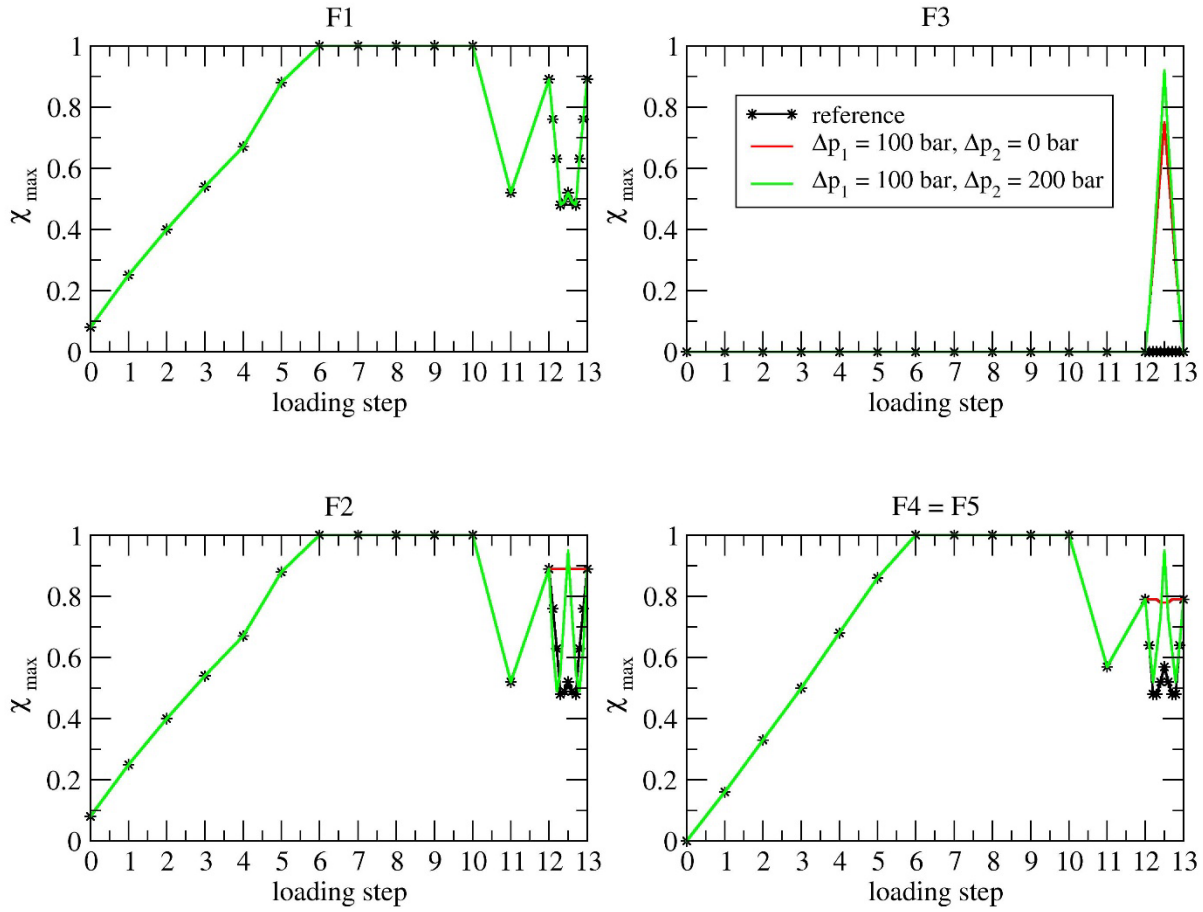


**Figure 32** Effect of the differential pressure on the $\chi_{max}$ behavior at increasing loading steps for each fault. Note that due to symmetry F4 and F5 behave identically.

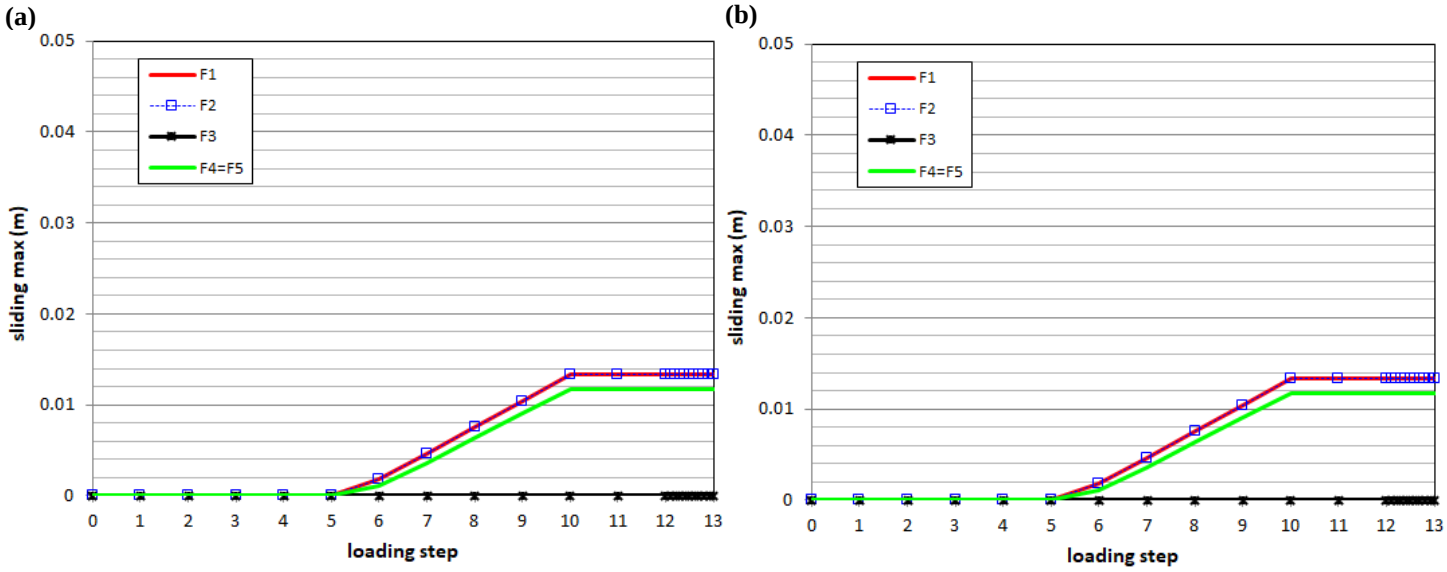


**Figure 33** Maximum sliding $\delta_{max}$ for the test cases investigating the effect of the differential pore pressure in the reservoir compartments: (a) $\Delta P_1$ = -100 bar with $\Delta P_2$ = 0 bar; (b) $\Delta P_1$ = -100 bar with $\Delta P_2$ = -200 bar.

Figure 33 provides the time behaviour of the fault maximum sliding for the various cases addressing the reservoir stiffness. Fault F3 does not slide despite a $\chi_{max}$ larger than in the reference case.

## 4. Mechanism 1: mechanical hysteresis

Because of mechanical hysteresis, during unloading-reloading phases the reservoir becomes stiffer than in loading condition, while the mechanical properties of the surrounding rock remain unaltered. For a same (absolute value of) pressure change, the variation of the stress field within the reservoir can be larger during injection/UGS phase than production because of its larger rigidity in the former condition. Figure 34 shows a sketch of the proposed mechanisms where identical pressure variation is set in compartments 1 and 2. Because of mechanical hysteresis, Young modulus in loading condition ($E_I$) differs from that in the unloading/re-loading phases ($E_{II}$). The effect of changing the ratio $E_{II} / E_I$, with $E_{II} / E_I \geq 1$, during primary production and unloading/re-loading phases is tested.

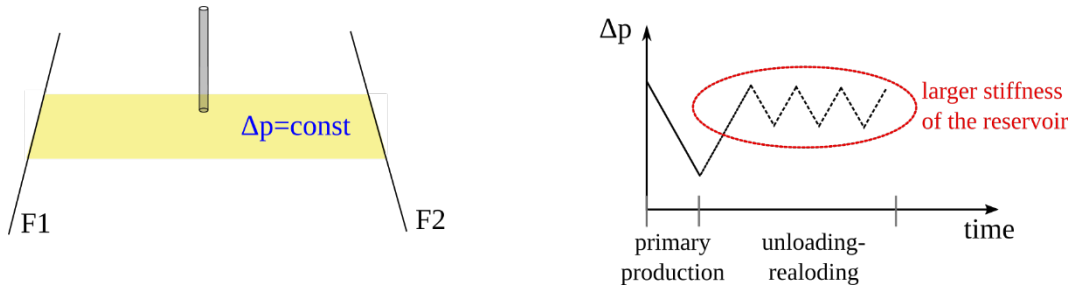


**Figure 34** Mechanism 1: stress redistribution because of a stiffer reservoir during cushion gas injection and UGS cycles.

The reference simulation described in Section 3.1 is used to compare the test case with $E_{II} / E_I = 2.5$. In the Figure 35, the values of the criticality factor $\chi_{max}$ is plotted at increasing loading steps for each fault and compared to the reference test case. F3 is completely inactive during production and UGS phases and the increased stiffness of the reservoir do not threaten the fault stability. The effect of mechanical hysteresis is observable during cushions gas and UGS operations on faults F1, F2, F4 and F5 that are slightly less stable. The values of $\chi_{max}$ are reported in Table 17 (Annex I). The values of $t_a$, $t_{80}$, and $t_{50}$ are provided in Annex II.

Notice that the value of the Biot coefficient varies during unloading or reloading; Table 8 provides the value used in the simulation as obtained starting from the Young modulus value in unloading/reloading condition and the grain compressibility.

**Table 8** Biot coefficient during loading and unloading/reloading conditions.

| Phase | ν | E [Pa] | $c_r$ [bar$^{-1}$] | α |
|---|---|---|---|---|
| **primary production** | 0.15 | 1.10E+10 | 3.00E-06 | 0.86 |
| **UGS** | 0.15 | 2.75E+10 | 3.00E-06 | 0.72 |

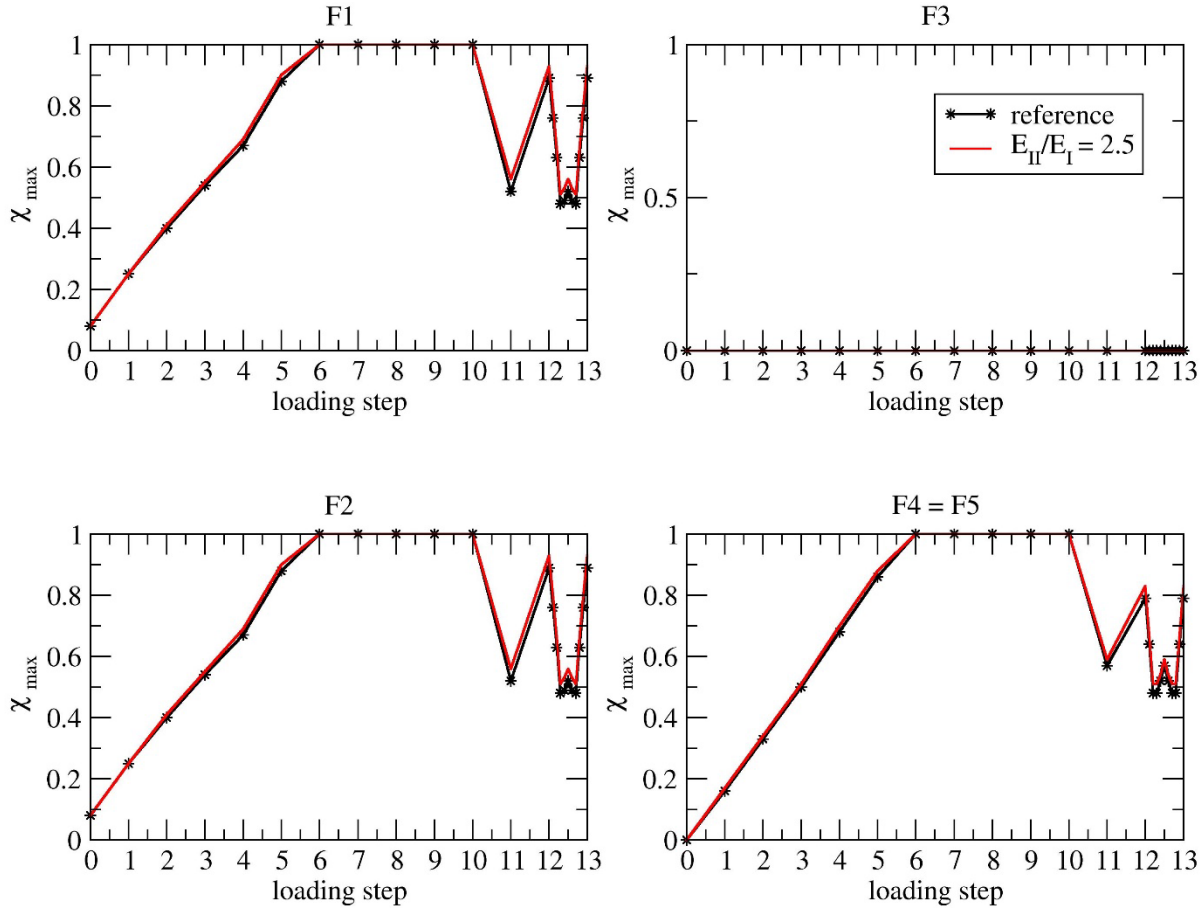


**Figure 35** Mechanism 1: distribution of $\chi_{max}$ at increasing loading steps for each fault. Note that due to symmetry F4 and F5 behave identically.

## 5. Mechanism 2: pore pressure distribution in the reservoir

The spatial gradient of the pore pressure change ΔP within the reservoir blocks can depend significantly on the injection/production rate (Figure 36). Therefore, the effective stress vs total stress distributions at the faults can differ from that within the reservoir compartments, possibly enhancing fault instability.

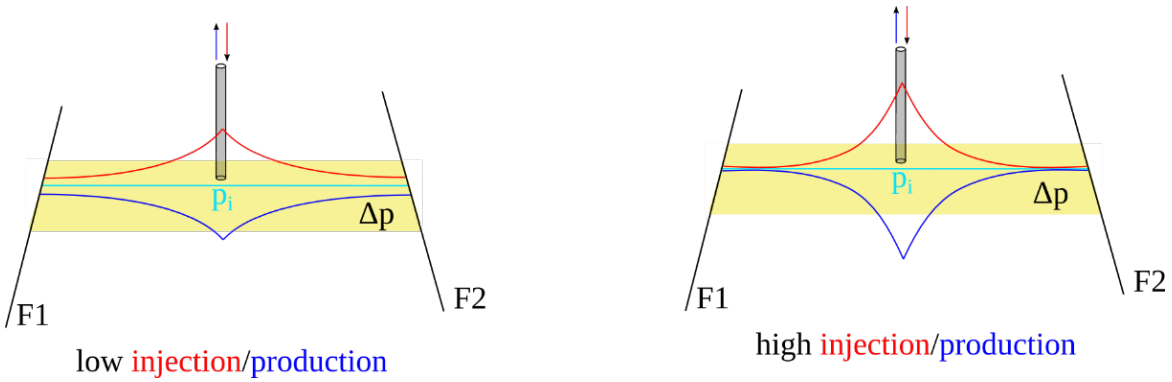


**Figure 36** Mechanism 2: the spatial gradient of the pore pressure change can vary significantly within the reservoir depending on low / high injection or production rates.

The effect of a non-uniform pressure within the reservoir blocks is tested in this section in relation to a single UGS production/injection phase. To this aim, a simplified production model is run in advance of M3E_GEPS3D to compute the pressure distribution within the reservoir block. The free-software Open Porous Media – OPM (https://opm-project.org/) has been used. Figure 37 shows the location of the injection/production wells with respect to the fault system, as agreed with SodM.

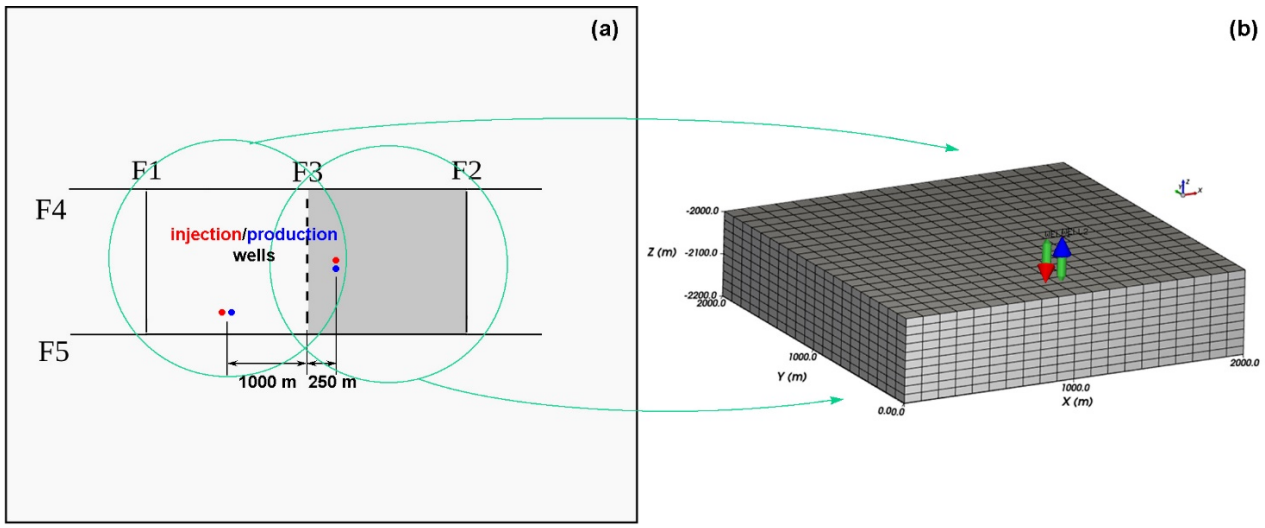


**Figure 37** Mechanism 2: (a) location of the injection/production wells in the two reservoir blocks. (b) 3D finite-difference grid used in OPM to simulate the injection/production phase. The OPM mesh exactly corresponds to the FE grid of a single block within the 3D geomechanical model.

The values of the other main data as planned in the last meeting at SodM headquarters are the following:

- horizontal permeability $k_h$ = 600 mD;
- vertical permeability $k_v$ = 300 mD;
- the time behavior of the production/injection rate shown in Figure 38. The "working gas" volume amounts to $6.5\times10^9$ $Sm^3$ per each compartment.

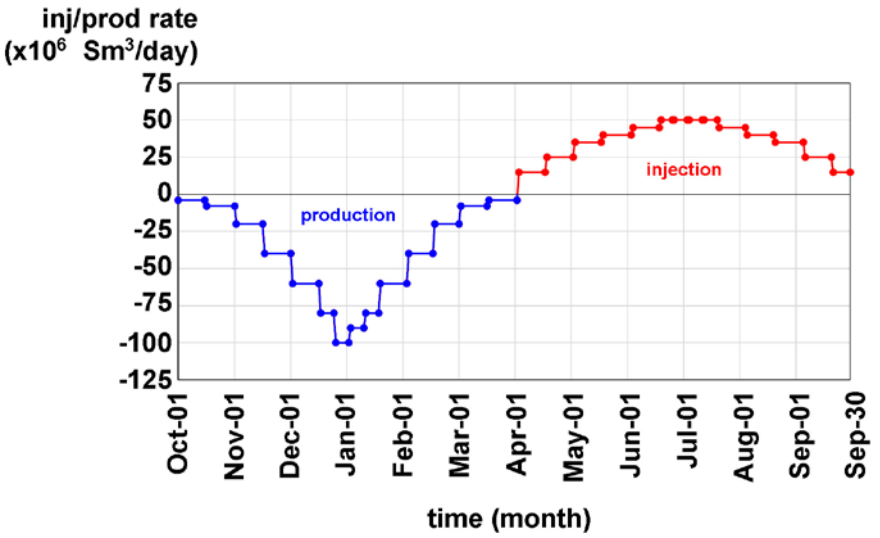


**Figure 38** Mechanism 2: time behavior of the production/injection rate used in the OPM simulation.

The results of the OPM simulation are summarized in Figure 39. The figure shows the depth-averaged pressure behavior along a section passing through the production/injection wells after 3 months (i.e., in correspondence of the maximum production rate), 6 months (i.e., at the end of the production phase), 9 months (i.e., in correspondence of the maximum injection rate), and 12 months at the end of the simulation.

Notice that the pressure change during the entire production (or injection) phase is almost uniform and approximates ±100 bar. Moreover, the stress/strain condition of the system at UGS beginning corresponds to that at the end of the CG in the "reference" case. Therefore, the comparison with the "reference" outcome is straightforward. Figure 40 shows how the OPM pressure changes are combined within the geomechanical simulator; two steps are shown, after 3 and 9 months, i.e. in correspondence of the maximum production and injection rate (Figure 38).

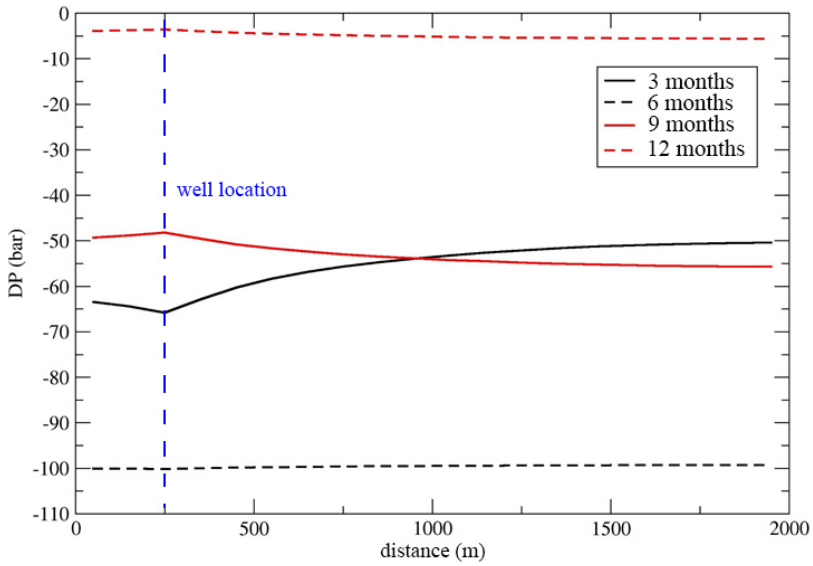


**Figure 39** Mechanism 2: pressure change during a production/injection cycle as obtained by the OPM simulator.

The geomechanical results in term of $\chi_{max}$ are summarized in Figure 41. The uneven pressure distribution within the compartments yield a larger $\chi_{max}$ values in this case with respect to the reference. However, because of the relatively small gradient due to the high reservoir permeability, the difference is relatively small and vanishes at the end of the production and injection phases when the pressure distribution becomes almost uniform (Figure 39) and similar to that used in the reference case. Notice that, due to the pressure difference between the two compartments along fault F3 (Figure 40), in this case also the fault F3 assumes $\chi_{max} > 0$, with an unsymmetrical distribution relative to the symmetry *x*-axis (Figure 42) because the pressure difference between the two blocks along the fault is asymmetrical (Figure 40). For completeness, the values of $\chi_{max}$ are reported in Table 18 (Annex I). The values of $t_a$, $t_{80}$, and $t_{50}$ are provided in Annex II.

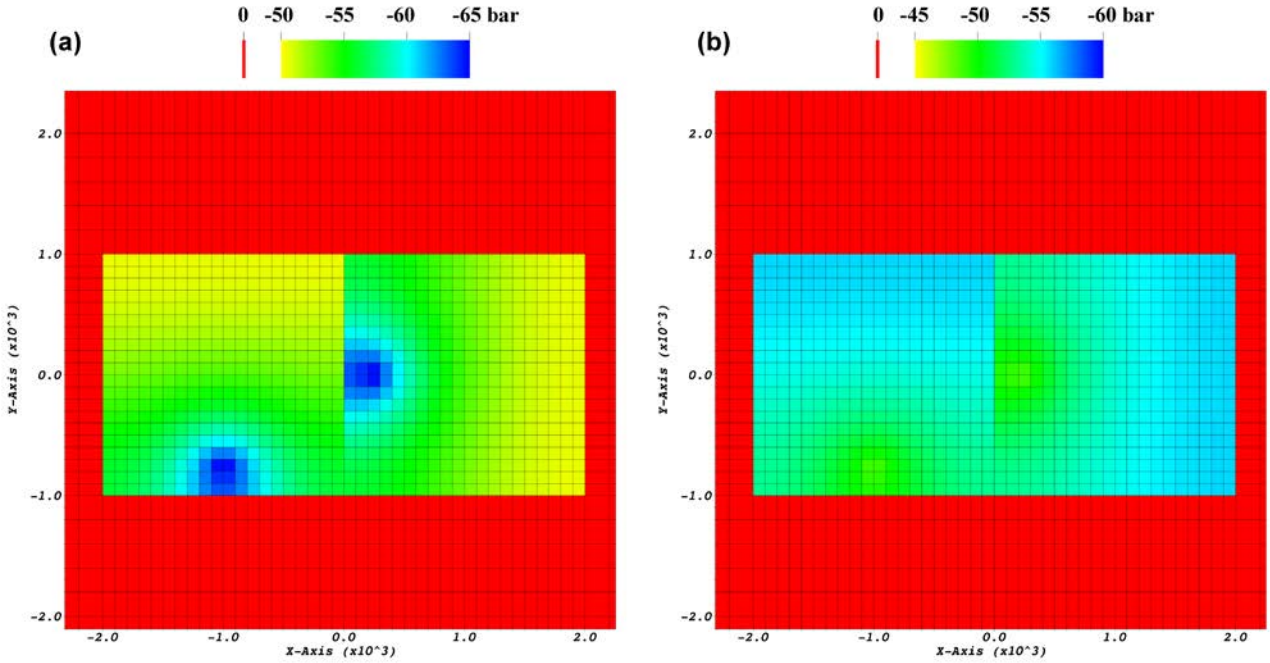


**Figure 40** Mechanism 2: pressure change in (a) January and (b) July, i.e., after 3 and 9 months from the beginning of the UGS cycle and used as forcing factor in the geomechanical simulator.

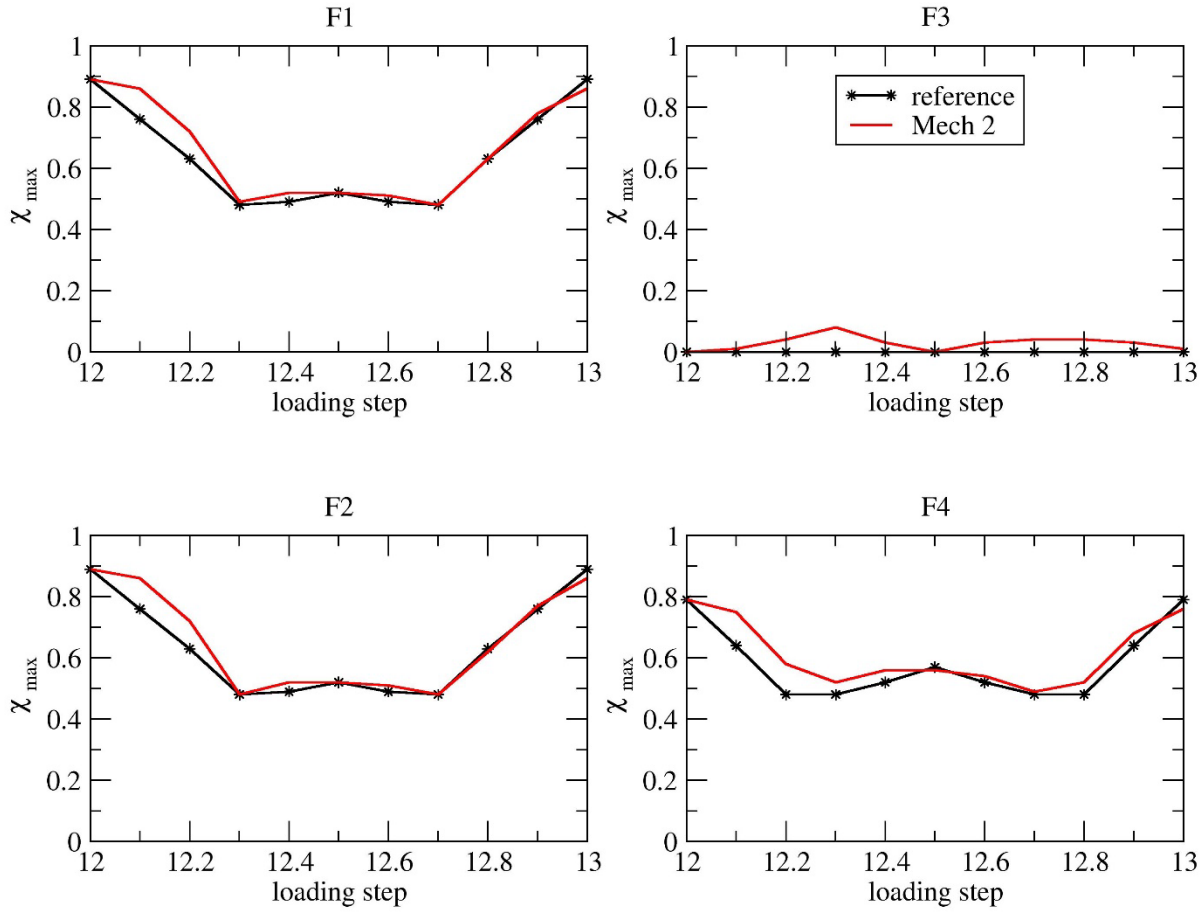


**Figure 41** Mechanism 2: comparison between the time behavior of $\chi_{max}$ over a UGS cycle as obtained with the "reference" case and the space-variable pressure distribution simulated by OPM.

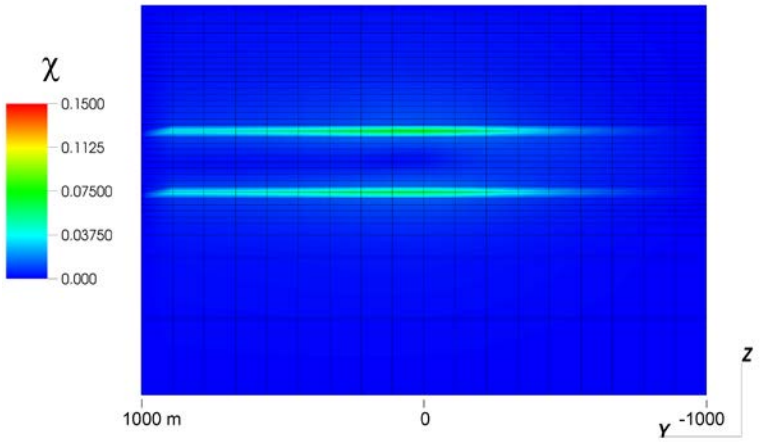


**Figure 42** Mechanism 2: distribution of χ along fault F3 in correspondence of the maximum production rate (month 3).

## 6. Mechanism 3: fault "lubrification" in non-sealing faults

During fluid injection or production from deep reservoirs, pore pressure can propagate within non-sealing faults, changing the effective stress normal to the fault plane and possibly favouring their reactivation (Figure 43). This is a main geomechanical challenge that has been largely addressed in the recent scientific literature dealing with geologic $CO_2$ sequestration (Vilarrasa et al., 2017) and production of unconventional resources through hydraulic fracturing (Schultz et al., 2017), i.e., when the fluid pressure is increased above the natural $p_i$ value. Conversely, in UGS and more specifically for the UGS fields in The Netherlands, pore pressure does not overpass $p_i$. A pressure decrease within the fault acts as a force that increase the stability of the discontinuity.

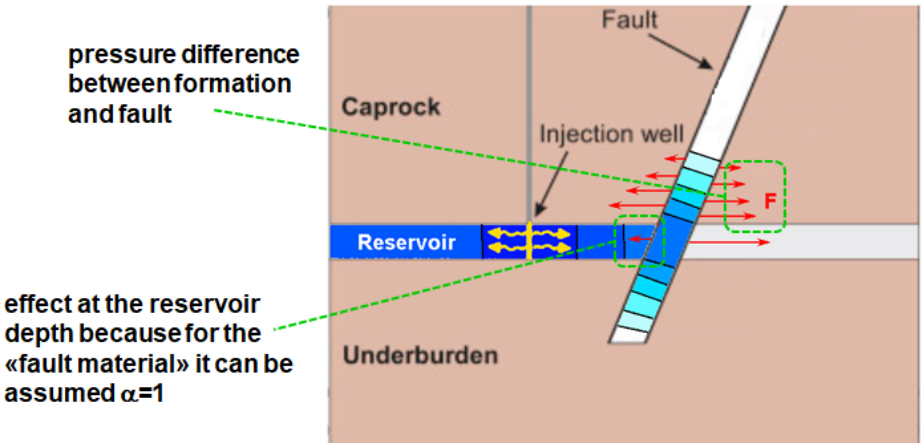


**Figure 43** Mechanism 3: the pore overpressure propagates within a permeable finite-thickness fault zone. The overpressure generates a system of forces that reduces the normal stress acting on the discontinuity surfaces, both in the caprock / underburden (where $\Delta p$=0) and in the reservoir formation if the Biot coefficient (equal to 1) differs from the that of the reservoir formation.

### *6.1 Sensitivity on fault F3*

In the system addressed by the present study, the central fault subdivides two blocks where the pressure change may differ. A number of scenarios has been run where the pressure change $P_f=\Delta p_3$ (Figure 44) in the F3 fault zone, in correspondence of the reservoir depth interval, is alternatively equal to the maximum (-200 bar), minimum (-100 bar), or average (-150 bar) value of the pressure change in the two compartments.

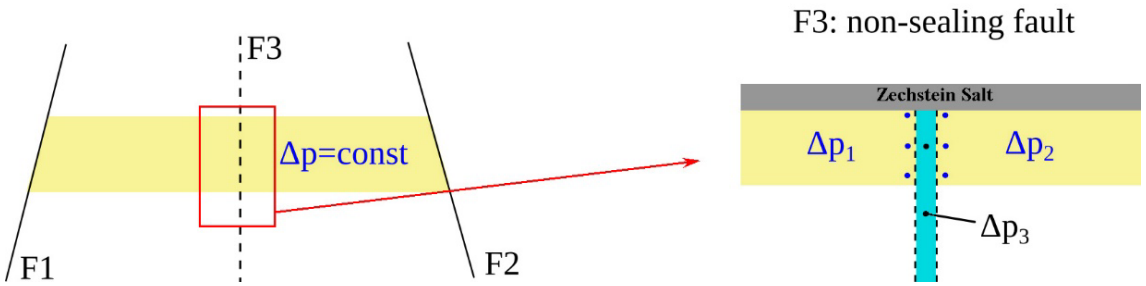


**Figure 44** Mechanism 3: the pore pressure change can propagates in a permeable finite-thickness fault zone.

Moreover, a simple 2D model has been applied to understand the possible $\Delta p_3$ propagation within F3 fault from the reservoir depth downward (Figure 45). Pressure propagation upward has been excluded because of the presence of the Zechstein salt formation. The properties for the fault material and fluid (water) have been derived from the literature:

- F3 fault permeability = $10^{-15}$ $m^2$ (Evans et al., 1997; Zbinden et al., 2017);
- water density $\rho_w$ = 972.3 kg/$m^3$; water viscosity $\mu_w = 4\times10^{-3}$ Pa·s; water compressibility $c_w = 3.73\times10^{-5}$ $bar^{-1}$. These values have been derived after Chierici (1990) and Fine and Millero (1973) assuming a temperature = 100° C, salt concentration = 10%, and pressure = 200 bar.

Table 9 and Figure 46 summarizes the various scenarios that have been simulated. The downward pressure propagation within the fault is addressed in Scenarios A to C. At the reservoir depth, the pressure change in the fault varies linearly in time consistently with the behavior of the reservoir. Scenarios B and C has been introduced to assess the most extreme case (obviously unphysical) where the fault pressure remains unchanged during production ($P_f$ = 0 bar) and suddenly, at the beginning of injection phase, the fault allows propagation of the pressure change. It is therefore assumed that the fault "starts feeling" the pressure change only during the injection phase. In Scenarios D – G the two blocks experience a different pore pressure change, with $\Delta p_3$ assuming alternatively the minimum, maximum, or the average value. Test G is the worst case scenario as the pressure in the fault remains equal to the initial value.

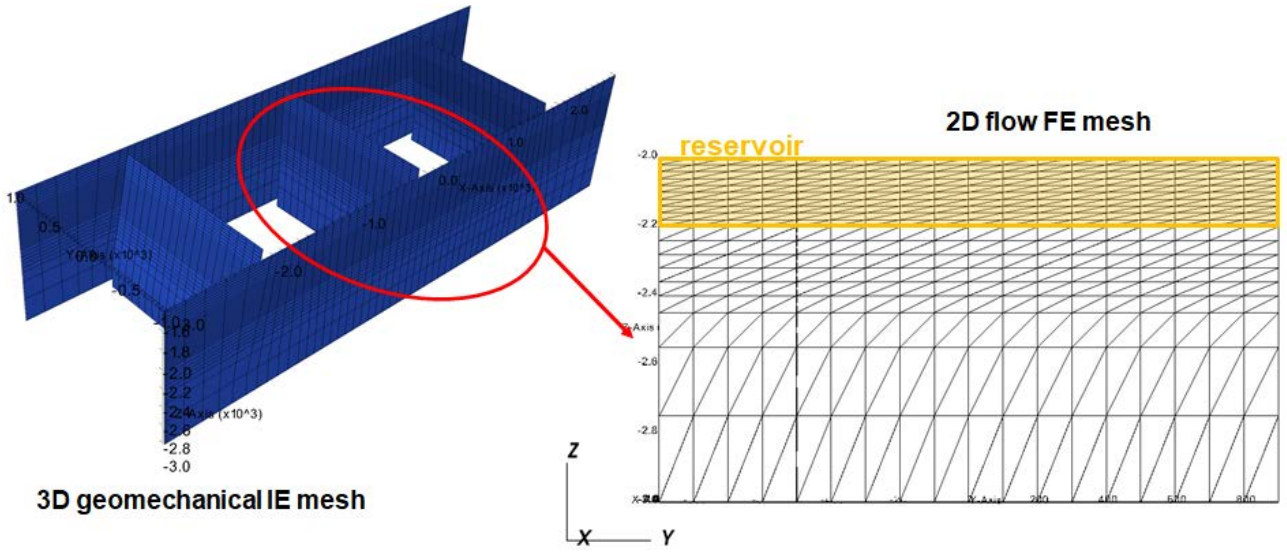


**Figure 45** Mechanism 3: 2D mesh of fault F3 extracted from the geomechanical IE grid.

**Table 9** Mechanism 3: pore pressure changes at the end of the production and injection phases in the various scenarios.

| SCENARIO | BLOCK 1 | | BLOCK 2 | | FAULT F3 | | | |
|---|---|---|---|---|---|---|---|---|
| | prod. | inj. | prod. | inj. | dip | prod. | inj. | depth |
| A | -100 | +100 | -100 | +100 | 0° | -100 | +100 | reservoir + underburden |
| B | -100 | +100 | -100 | +100 | 0° | 0 | +100 | reservoir + underburden |
| C | -100 | +100 | -100 | +100 | +65° | 0 | +100 | reservoir + underburden |
| D | -100 | +100 | -200 | +200 | 0° | -100 | +100 | reservoir |
| E | -100 | +100 | -200 | +200 | 0° | -150 | +150 | reservoir |
| F | -100 | +100 | -200 | +200 | 0° | -200 | +200 | reservoir |
| G | -100 | +100 | -200 | +200 | 0° | 0 | 0 | reservoir |

As an example, Figure 47 shows the results of the flow model along a vertical section; the pore pressure propagates downward for a distance of about 200 m from the reservoir bottom.

The results of the geomechanical model are summarized in Figure 48. Notice that: i) because of the symmetry of the system and the forcing factor, $\chi_{max}$ remains equal to 0 in the reference case and in scenarios A and B; ii) in scenario C, $\chi_{max}$ differs from 0 at loading steps 12 and 13 because of the fault slope; *iii*) the presence of an increasing pressure depletion within the fault (scenarios D, E, and F) increases the stress component normal to the fault plane, thus reducing the risk of fault re-activation; *iv*) the most critical scenario (scenario G) is characterized by a sealing fault. In this latter, the outcome in term of $\chi_{max}$ is consistent with the results shown in Section 3.7.

For completeness, the values of $\chi_{max}$ are reported in Table 19 (Annex I) and those related to $t_a$, $t_{80}$, and $t_{50}$ in Annex II.

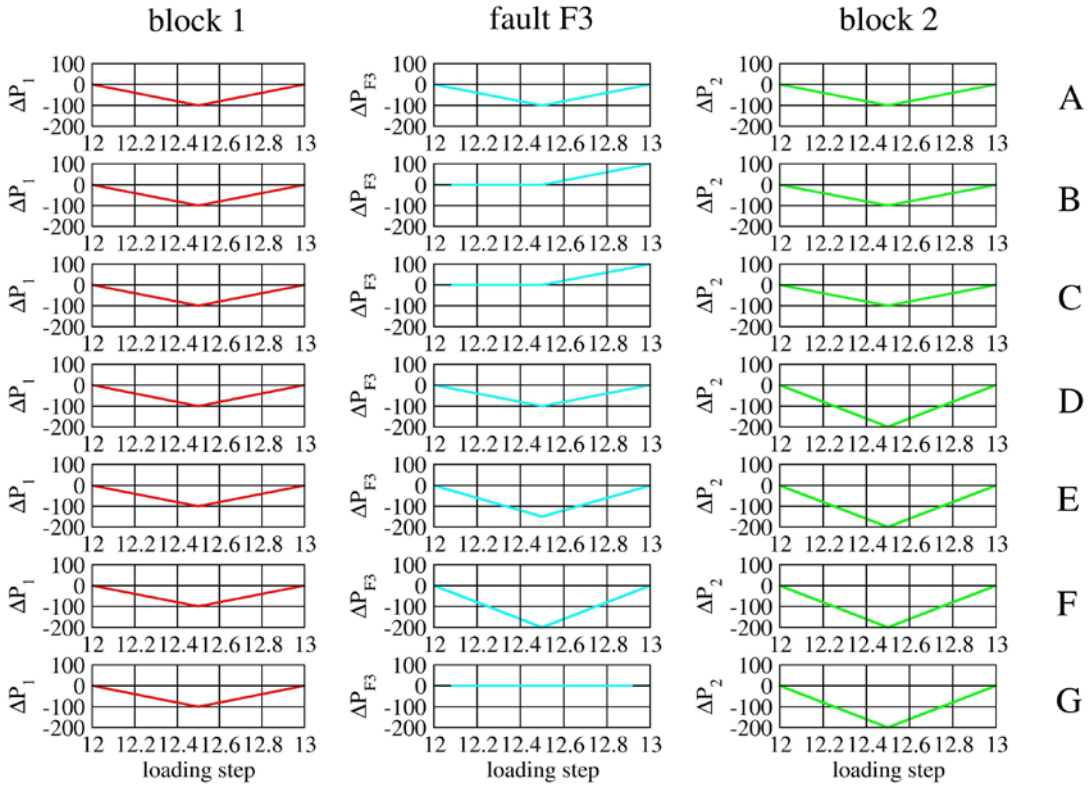


**Figure 46** Pore pressure during UGS phase in the reservoir block 1 ($\Delta P_1$), within the fault F3 ($\Delta p_3$), and in the reservoir block 2 ($\Delta P_2$), according to the scenarios listed in Table 9.

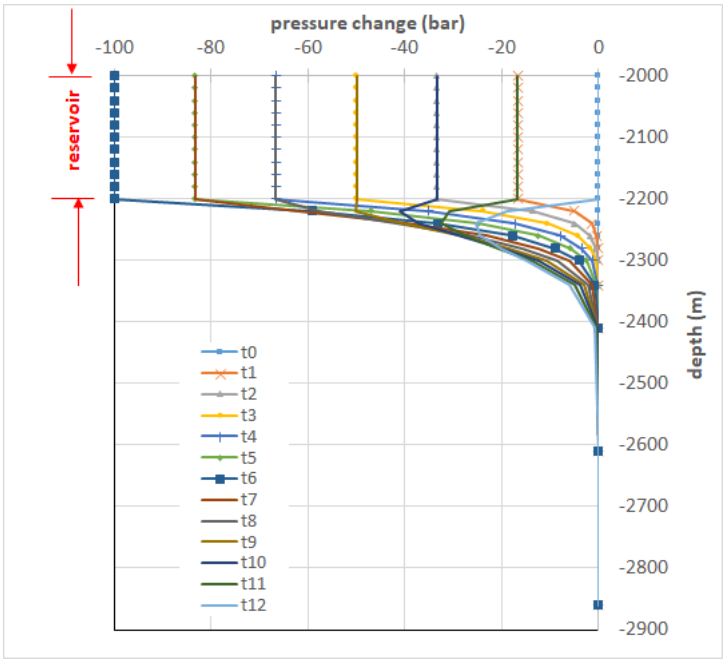


**Figure 47** Mechanism 3, scenario A: evolution of the pore pressure change along a vertical alignment as computed by the 2D flow simulator for a UGS with a pressure decline (production) and recovery (injection) down to 100 bar. Pressure changes extend downward from the reservoir bottom for about 200 m.

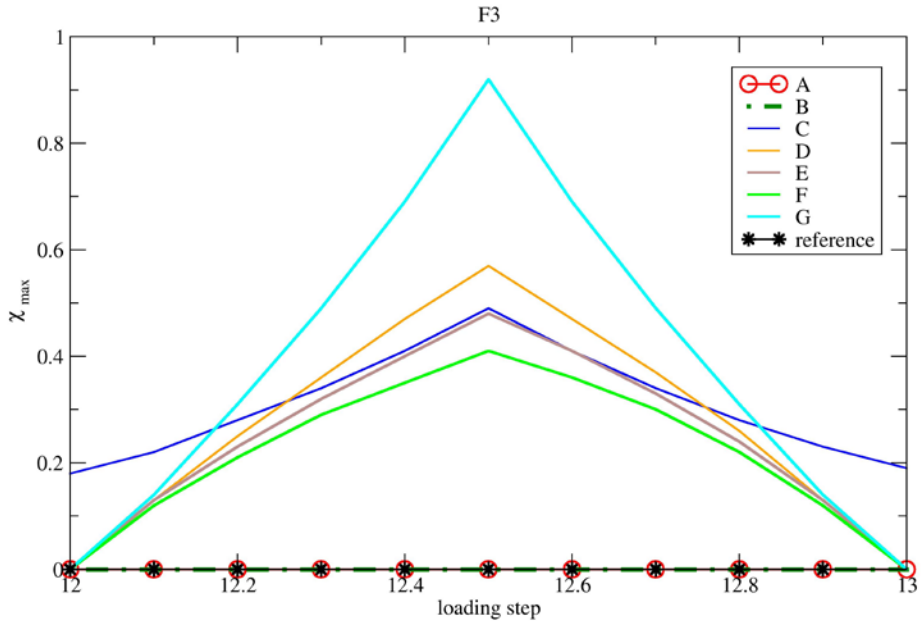


**Figure 48** Mechanism 3: comparison between the time behavior of $\chi_{max}$ over the UGS cycle obtained with the "reference" case and the various scenarios (Table 9) addressing a non-sealing fault with pore pressure depletion (F3).

For test cases A, F, and G, the normal stress $\sigma_n$, the shear stress $\tau$, and the criticality factor $\chi$ on the central fault are shown in Figure 49 at the loading step 12.5. In scenario A, the $\tau$ distribution, thus $\chi$, is constant and equal to zero along the fault due to the symmetry condition. Compared to the initial condition where $\sigma_n$ is within the range -180 ÷ -190 bar (depending on the reservoir depth), at loading step 12.5 $\sigma_n$ slightly increases at the reservoir depth and in the nearby underburden where $\Delta P_3$ propagates. In scenarios F and G, shear stress develops due to the different $\Delta P$ in compartments 1 and 2. Moreover, $\tau$ varies identically in F and G because fault remains inactivate and fault pressure affects only $\sigma_n$. Conversely, $\chi$ differs in these two scenarios because of the different $\sigma_n$ and, consequently, $\tau_L$. A larger $\chi$ develops in scenario G, where $\Delta P_3 = 0$, and $\sigma_n$ decreases because the reservoir shrinkage is not balanced by the pressure depletion within the fault.

## *6.2 Reference test case with fault pressure depletion*

The reference case described in Section 3.1 is here run assuming that the pressure change occurs also within the fault F1 to F5. For each fault, $P_f$ is equal to the average between the pressure between the two sides of the fault. For example, following the history pressure of the reference test, at loading step 10, $P_f$ = -100 bar for the bounding faults F1, F2, F4, F5. A stabilizing effect is obtained compared to the reference case as shown in Figure 50 where $\chi_{max}$ is plotted over the loading steps. For completeness, the values of $\chi_{max}$ are reported in Table 20 (Annex I) and those related to $t_a$, $t_{80}$, and $t_{50}$ in Annex II.

Figure 51 shows the shear stress $|\tau_{actual}|$ at increasing loading steps for a node located on the reservoir top of fault F1. The shear stress increases until loading step 7 when it equals the limit shear stress $\tau_L$, thus the fault starts sliding. The fault slides until loading step 10. During CG and UGS cycle $|\tau_{actual}|$ is always smaller than $\tau_L$.

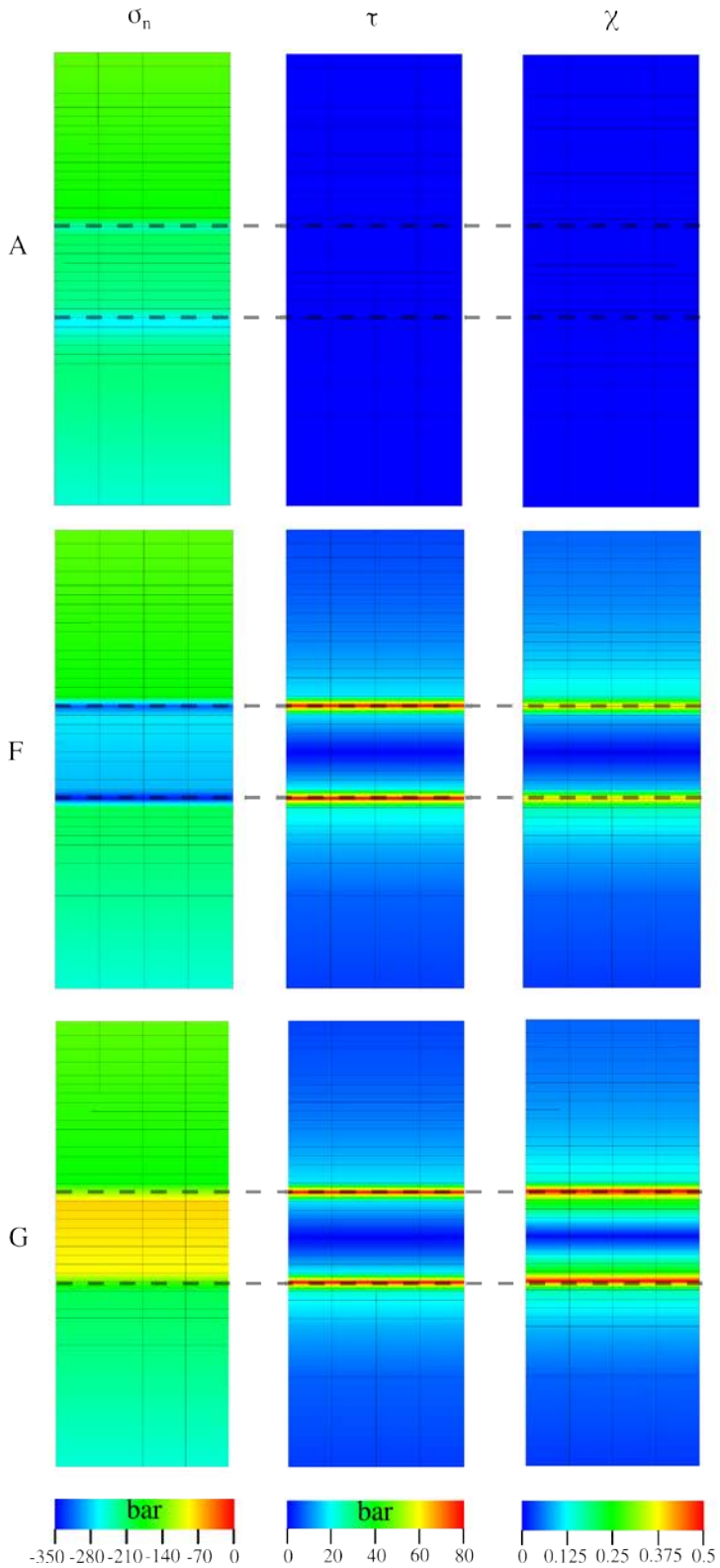


**Figure 49** Normal stress $\sigma_N$, shear stress $\tau$, and criticality factor $\chi$ on the central fault F3 for tests A, F, and G (Table 9) at loading step 12.5. The black-dashed lines represent the reservoir top and bottom placed at z=-2000m and z=-2200m, respectively.

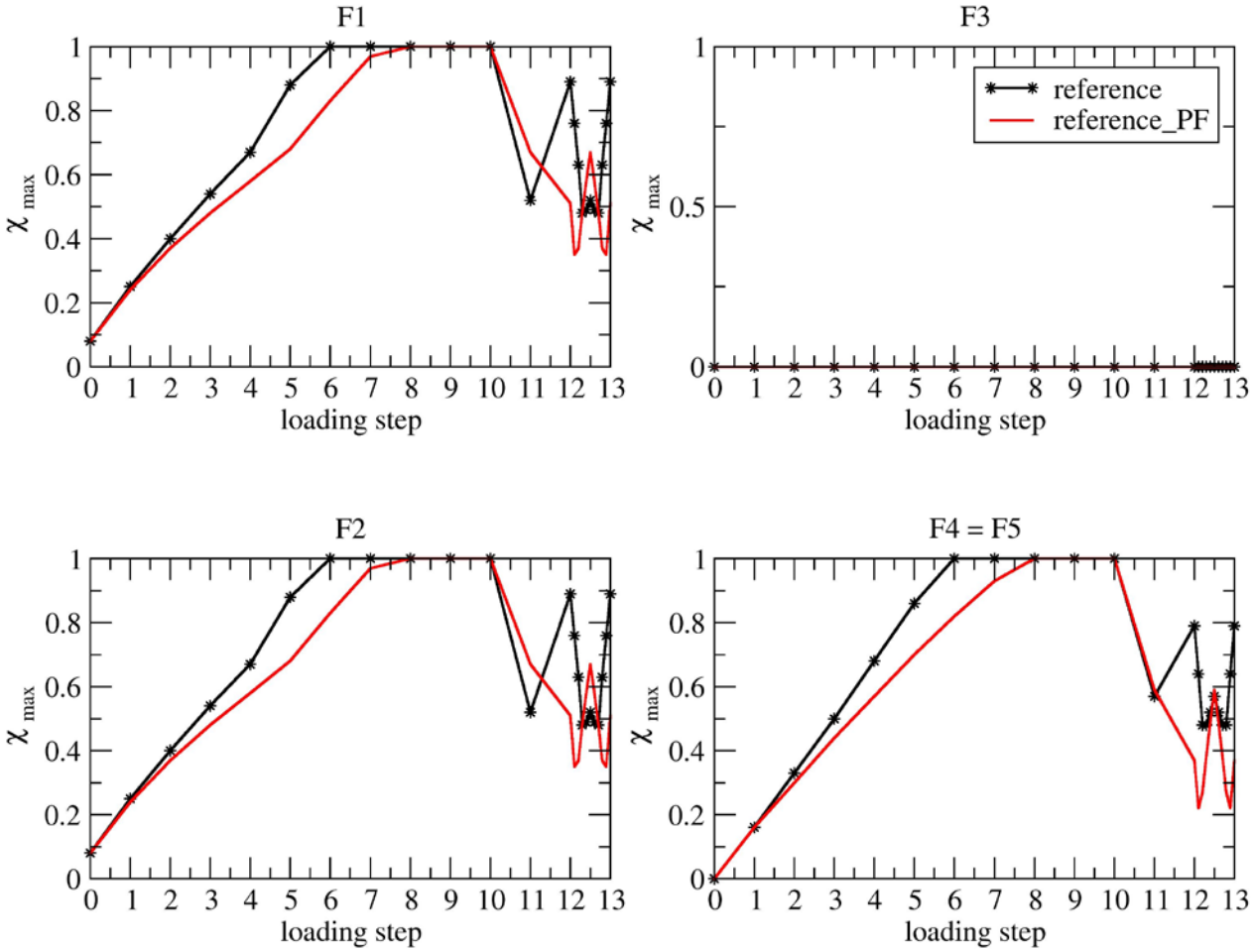


**Figure 50** Comparison between the time behavior of $\chi_{max}$ over the loading steps as obtained with the "reference" case and the "reference" case with fault pressure depletion.

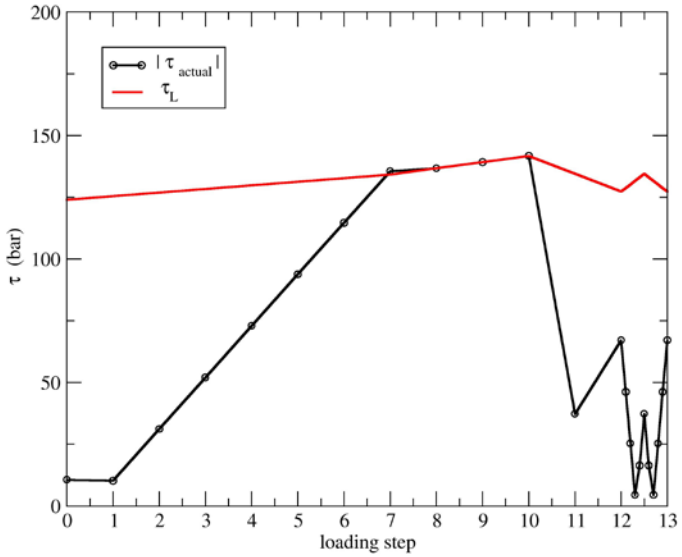


**Figure 51** Time behavior of the actual shear stress (in modulus) versus the limit tangential stress $\tau_L$ for a node located on fault F1 in correspondence of the reservoir top ($x$ = -2000 m, $y$ = 0 m, and $z$ = -2000 m).

## 7. Mechanism 4: pore pressure variation versus time

A larger pressure change during cushion gas injection or a larger pressure fluctuation during a single UGS cycle can produce more significant (micro)-seismic events because a larger fault area can be reactivated.

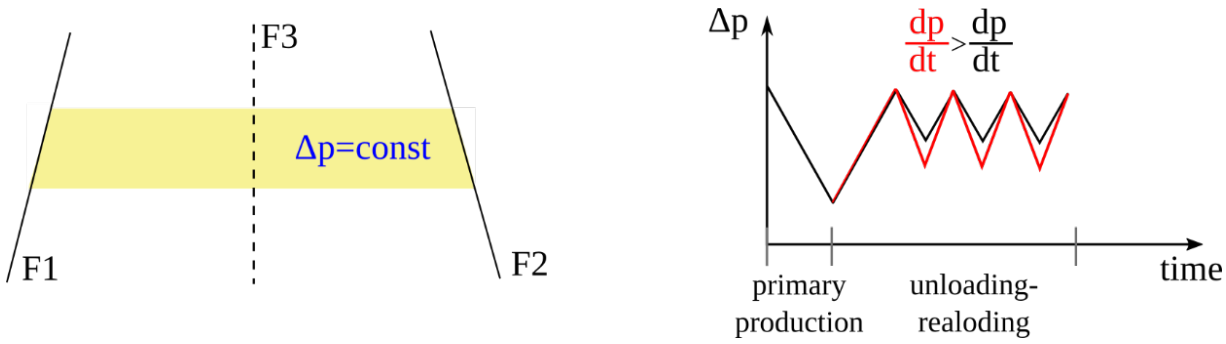


**Figure 52** Mechanism 4: a larger pressure change per loading step during a UGS cycle can activate a larger portion of a fault.

The effect of a larger ΔP change per loading step during a UGS cycle is tested in this case. In particular, the model parametrization described in Section 2.3 (reference test case) is used with the pore pressure change that during the UGS cycle picks to -150 bar (Figure 53) instead of -100 bar as in the reference.

The comparison with the reference test case (Section 3.1) is reported in Figure 54. The distribution of $\chi_{max}$ at increasing loading steps for each fault is identical to the reference until the end of the cushion gas phase (the pore pressure change is the same). During UGS, the larger ΔP change per loading step slightly influences the faults behaviour over the 6-months production phase. The major influence of the investigated mechanism is observed at loading step 12.5 with a certain increase of the criticality factor compared to the reference case. Fault reactivation during UGS is not observed. The values of $\chi_{max}$ are reported in Table 21 (Annex I). The values of $t_a$, $t_{80}$, and $t_{50}$ are provided in Annex II.

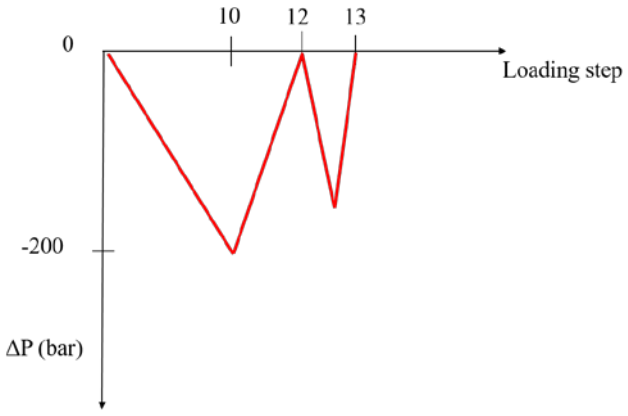


**Figure 53** Pore pressure change in the reservoir compartments 1 and 2.

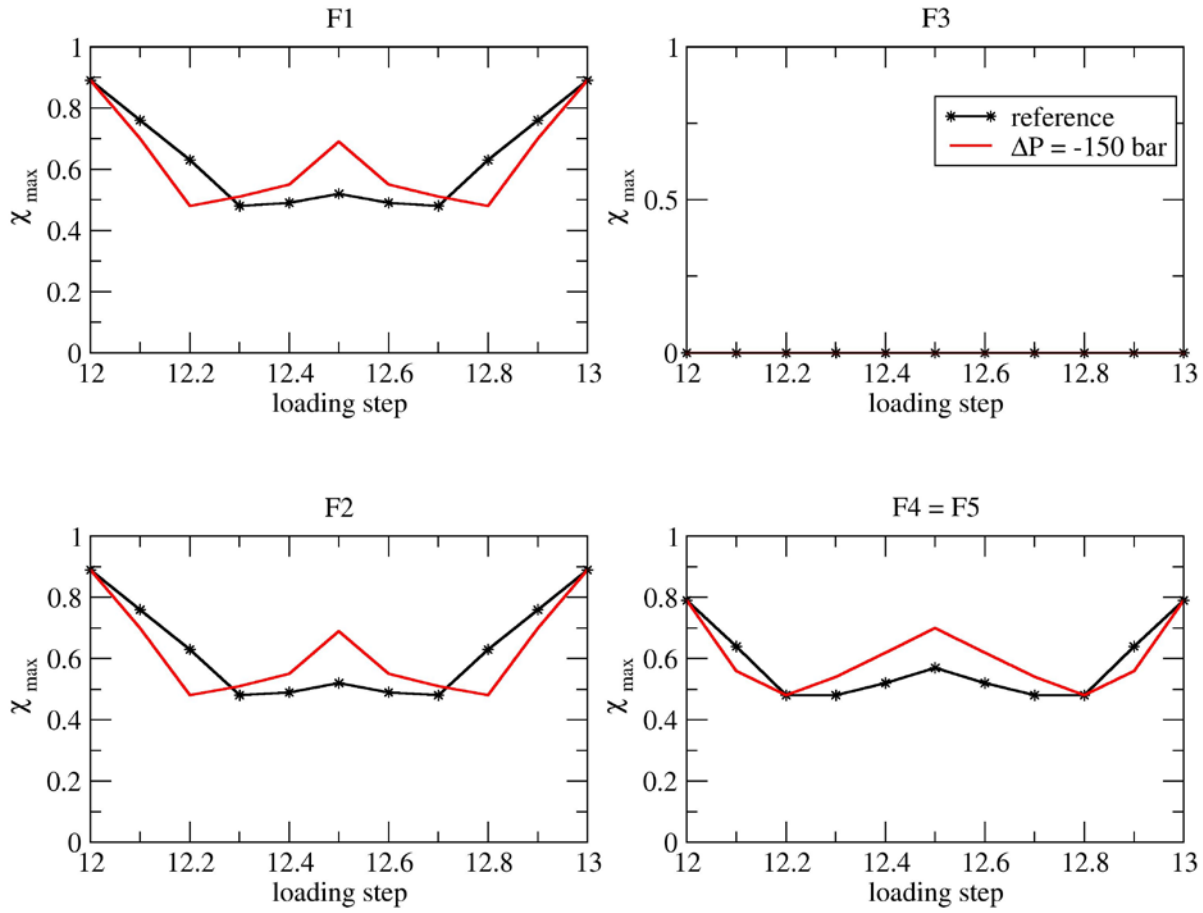


**Figure 54** Mechanism 4: $\chi_{max}$ distribution at increasing loading steps for each fault. Note that due to symmetry F4 and F5 behave identically.

## 8. Mechanism 5: salt caprock

The reference test is based on a linear elastic model for the caprock. Here, the viscous behaviour of the Zechstein formation is introduced to investigate the effect of this mechanism on the model response. In Figure 55, a vertical cross-section of the model domain is shown to illustrate the material distribution. The Zechstein formation overlies the reservoir layer up to z = -1500 m.

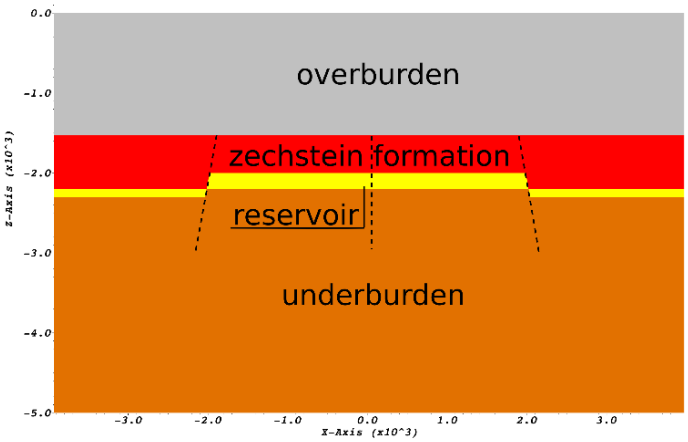


**Figure 55** Stratigraphic distribution of the material properties along a vertical cross-section.

The Maxwell model is implemented in the M3E_GEPS3D geomechanical code to simulate the visco-elastic behavior. The viscous deformation rate reads:

$$\dot{\boldsymbol{\varepsilon}}^{v} = \boldsymbol{V}\,\boldsymbol{\sigma} = \begin{bmatrix} \frac{1}{3\mu} & -\frac{1}{6\mu} & -\frac{1}{6\mu} & 0 & 0 & 0 \\ -\frac{1}{6\mu} & \frac{1}{3\mu} & -\frac{1}{6\mu} & 0 & 0 & 0 \\ -\frac{1}{6\mu} & -\frac{1}{6\mu} & \frac{1}{3\mu} & 0 & 0 & 0 \\ 0 & 0 & 0 & \frac{1}{2\mu} & 0 & 0 \\ 0 & 0 & 0 & 0 & \frac{1}{2\mu} & 0 \\ 0 & 0 & 0 & 0 & 0 & \frac{1}{2\mu} \end{bmatrix} \boldsymbol{\sigma}$$

where μ is the Maxwell parameter that is set equal to $\mu = 10^{17}$ Pa·s (Orlic and Wassing, 2013).

The geomechanical simulations of fault activation described below has been carried out starting from a stress distribution where $M_1 = M_2 = 1$ in the salt layers and $M_1 = 0.74$ and $M_2 = 0.83$ (Table 2) in the other portions of the domain, see Figure 56a. This is obviously an unbalanced stress pattern, which is very simple to assign and use as initial condition but, on the other hand, could provide flawed results. A preliminary long-term analysis has been carried out to check this possibility. Starting from an initial condition where $M_1 = 0.74$ and $M_2 = 0.83$ everywhere (Figure 56b), we let the stress redistributing according to the various properties (viscous and elastic) of the layers. The final equilibrated results is shown in Figure 56c: a smooth transition between $M_1 = M_2 = 1$ in the Zechstein and the elastic stress regime develops within a narrow portion of the reservoir blocks. Therefore, the approximation caused by the unbalance initial stress on the fault behavior is negligible and the stress distribution shown in is warranted to be used in the short-term UGS

simulations. Figure 57 shows that the equilibrated condition needs approximately 300 years to be achieved.

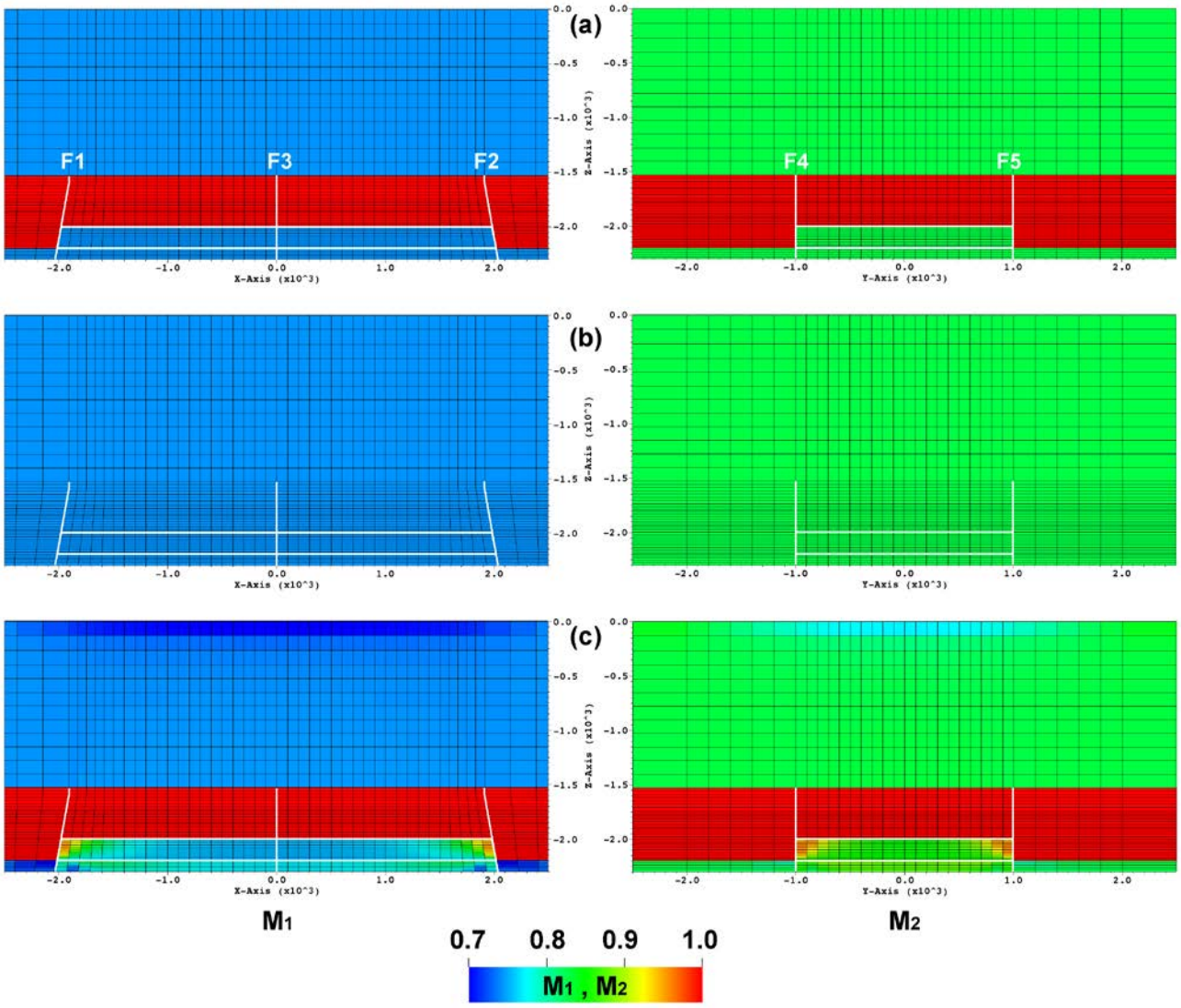


**Figure 56** $M_1$ and $M_2$ distribution along two vertical sections crossing the reservoir center of gravity and aligned along the X and Y direction, respectively. (a) Initial (unbalanced) distribution used in the geomechanical simulations of possible induced seismicity. (b) and (c) Initial and final (after 1000 years) distribution prescribed and computed in the long-term simulation, respectively. The traces of the reservoir compartments and faults are highlighted in white.

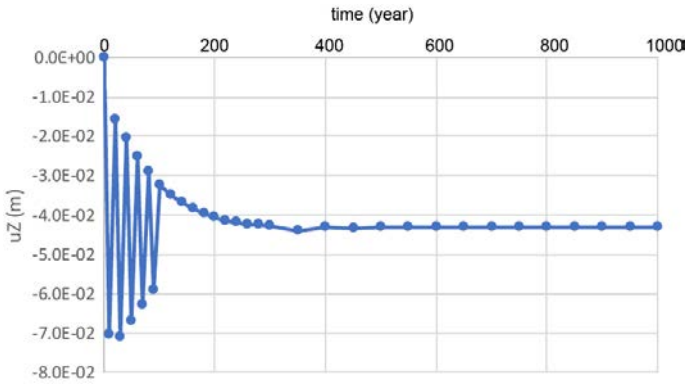

**Figure 57** Long-term evolution of the vertical displacement above the reservoir due to salt flow because of an initial effective stress regime in the whole domain with $M_1$=0.74 and $M_2$=0.83 (Figure 56b).

Figure 58 compares the vertical displacement $d_z$ versus the loading steps as obtained with the elastic (reference) and the viscous (Zechstein formation) caprock. Note that the plot is obtain for the surficial node at location (x, y, z) = (0.0, 0.0, 0.0) m, i.e., above the center of the reservoir.

Figure 59 compares the distribution of the vertical displacements $d_z$ within a vertical cross-section orthogonal to the y-axis at loading step 10 (10 years). As expected, at the end of primary production the subsidence bowl (negative displacements) is more pronounced when the viscous caprock is accounted for. The influence of the Zechstein formation on the fault system is investigated in Figure 60. Faults F1, F2, F4 and F5 undergo a much larger criticality if the salt caprock is considered compared to the reference. Generally, these faults start sliding before the reference case and at the end of the CG phase when $\chi_{max}$ = 1.0 is reached. Notice that the simulation with viscous salt caprock spans 50 years. To appreciate the $\chi_{max}$ behaviour during the UGS cycles, a zoom of Figure 60 is plotted in Figure 61 for loading steps in the range 10-20 years and fault F1. For completeness, the values of $\chi_{max}$ are reported in Table 16 (Annex I) and the values of $t_a$, $t_{80}$, and $t_{50}$ are provided in Annex II. The behaviour of the maximum sliding $\delta_{max}$ is showed in Figure 62.

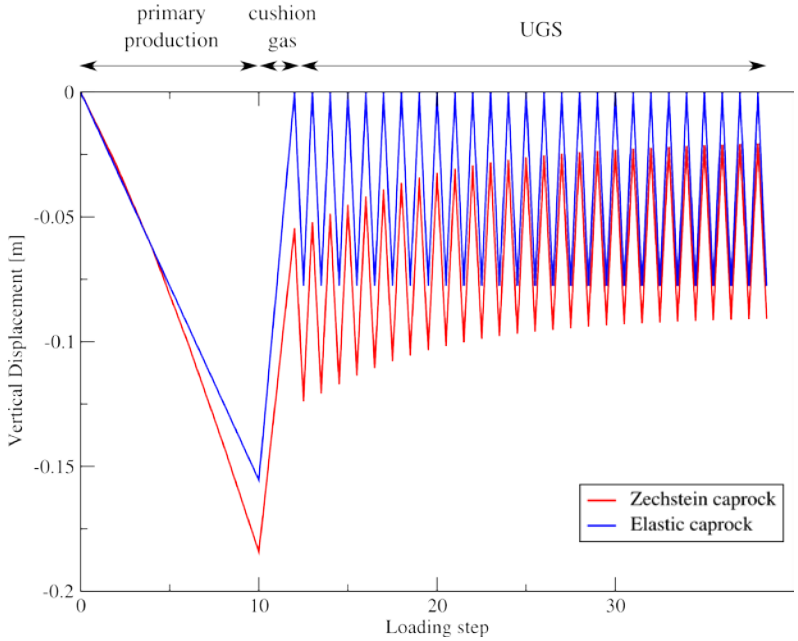


**Figure 58** Vertical displacements over a time window of 40 loading steps (40 years) in case of elastic and viscous caprock. The plot references to the location (x, y, z) = (0.0, 0.0, 0.0) m, i.e., above the center of the reservoir.

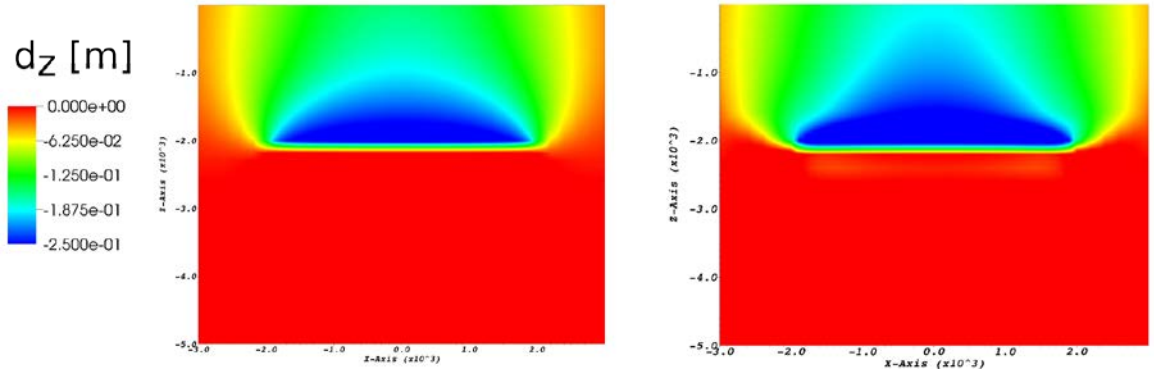


**Figure 59** Distribution of the vertical displacements ($d_z$) on a vertical cross-section normal to the y-axis at loading step 10 (10 years) for (left) elastic and (right) viscous caprock. Negative displacements mean subsidence.

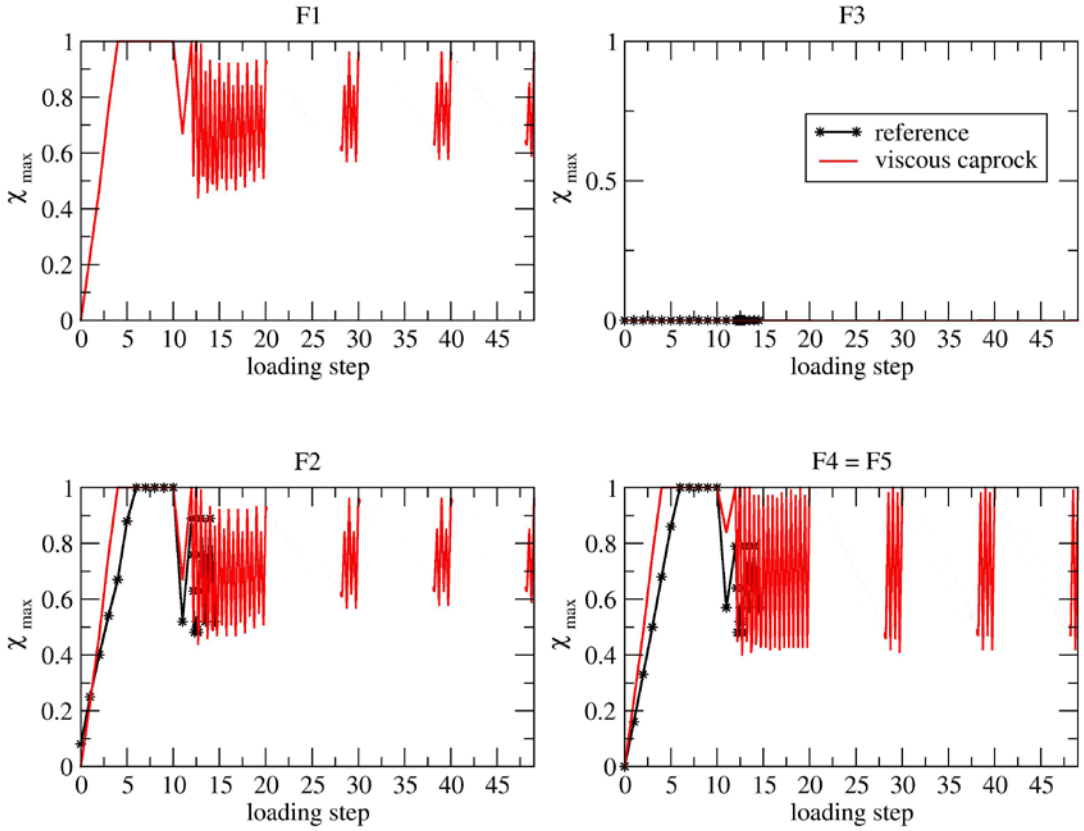


**Figure 60** Effect of the salt Zechstein formation on the $\chi_{max}$ behavior at increasing loading steps for each fault. Notice that due to symmetry F4 and F5 behave identically. Moreover, at the loading step = 0 (initial conditions) $\chi_{max} = 0$ for F1 and F2 although inclined because we set $M_1 = M_2 = 1$ (isotropic initial stress regime) for the salt material.

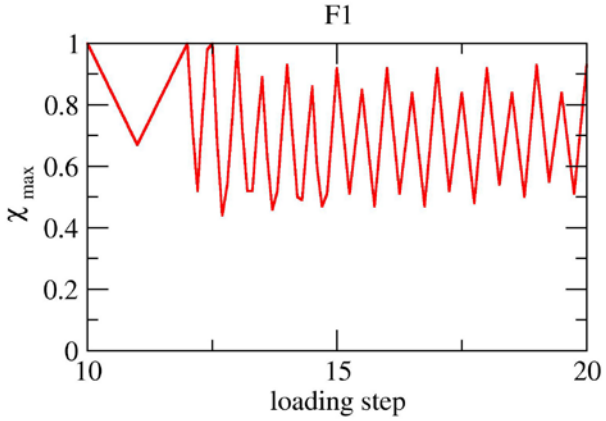


**Figure 61** Mechanism 5, fault F1: zoom of the $\chi_{max}$ behaviour for the loading steps between 10 and 20.

The model output in term of shear stress on the discontinuity surfaces is provided in Figure 63 and Figure 64. With reference to fault F1, Figure 63 shows the $\chi$ and $\tau$ distribution at few representative loading steps: l.s. 4 when the criticality condition picks to 1 and the fault becomes active, l.s. 10 and 12 corresponding to the start and end of cushing gas injection, l.s. 39.25 to l.s. 40 representative of a UGS cycle. Figure 64 compares the time behavior of the shear stress (in modulus) in correspondence of the reservoir top with the limit $\tau_L$. The figure clerly shows when the activation condition occurrs during primary production and cushion gas injection and how the most critical condition ($\chi \rightarrow 1$) during UGS develops at the end of the injection phase.

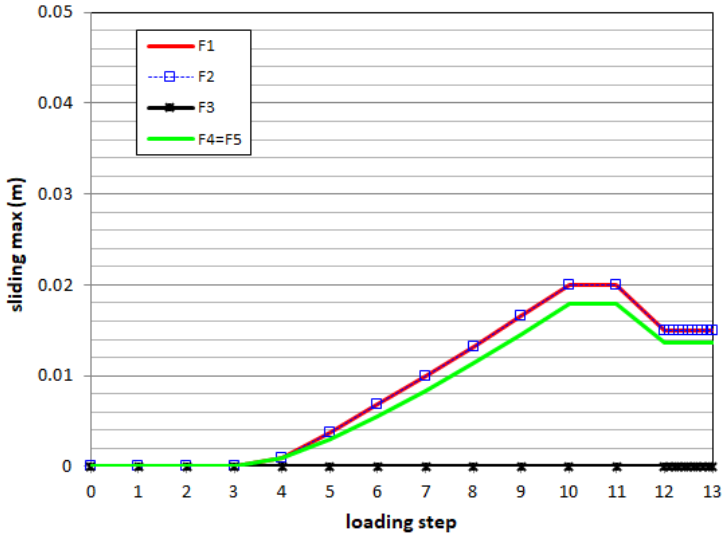


**Figure 62** Maximum sliding $\delta_{max}$ for the case investigating the effect of the viscous behavior of the Zechstein formation. The values remain constant until the end of the simulated time interval (50 years).

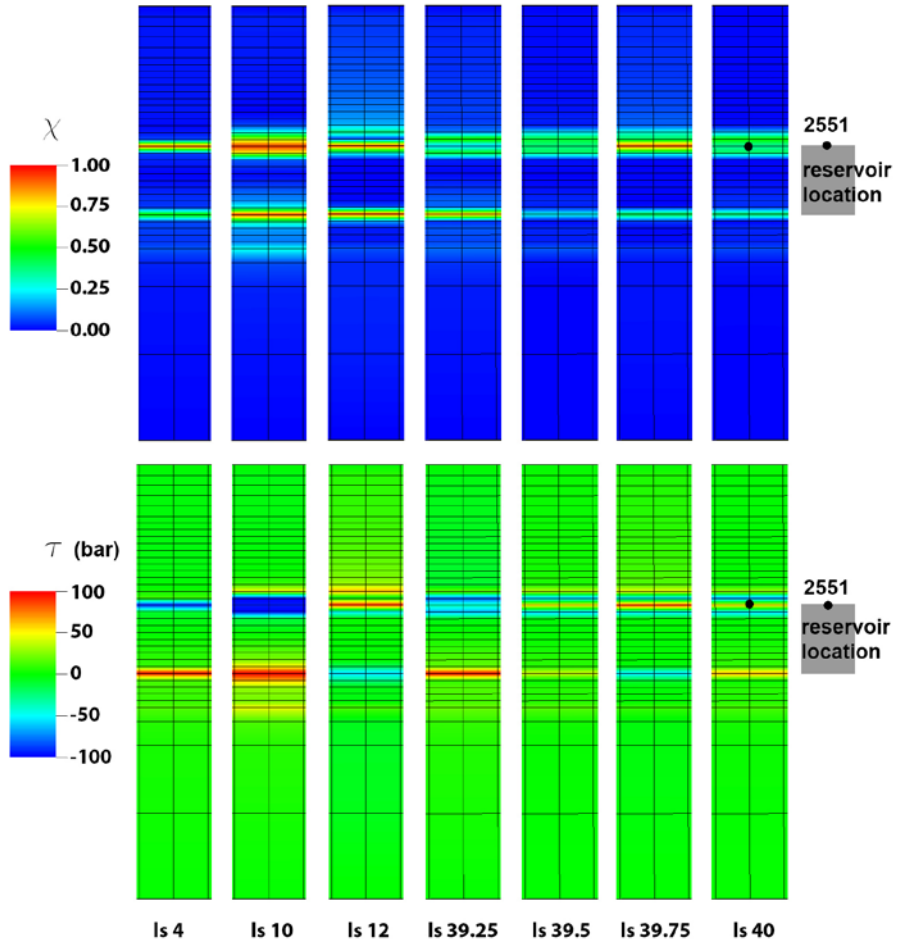


**Figure 63** Fault F1, node 2551 at the reservoir top: χ (above) and shear stress τ (below) for a few representative loading steps (ls). The location of node 2551 is highlighted.

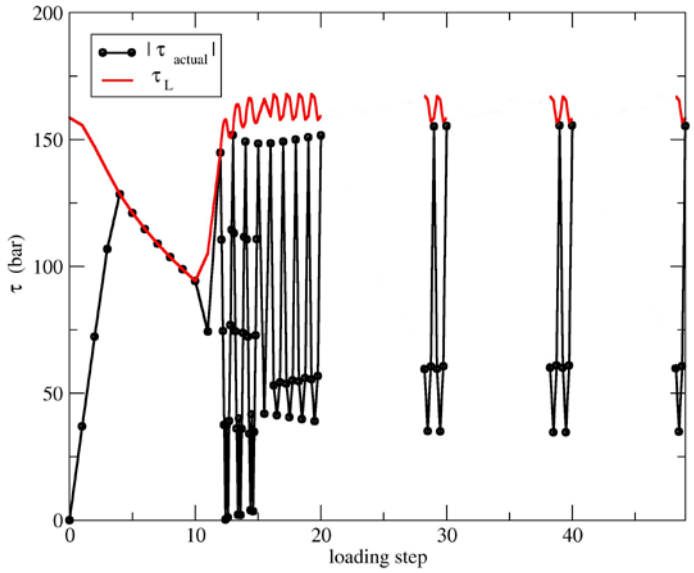


**Figure 64** Fault F1, node 2551 at the reservoir top: behavior versus time of the actual shear stress (in modulus) versus the limit tangential stress $\tau_L$. Notice the slightly different behavior of the cycles for the loading steps > 15 due to the different time step (0.25 yeas vs 0.10 year) used in the time integration.

# 9. Combinations of selected mechanisms and parameters

With the aim of investigating the criticality of the faulting system in more "realistic" conditions and/or "critical" than those investigated above, a set of simulations has been carried where a number of parameters and mechanisms investigated above have been combined.

## *9.1 Combination 1*

A first analysis has been carried out with the following hypotheses:

- $c$ = 0 bar;
- F3 fault dip = +65°;
- compartment offset = 200 m.

For the other parameters, the values adopted in reference test case have been used. Moreover, the same combination has been run by introducing a pore pressure change $P_f$ within each fault with a value equal to the average between the pressures at the two sides of the fault. The simulation outcome in terms of $\chi_{max}$ is shown in Figure 65. The results highlight that, apart for the last period of primary production, other critical conditions for fault reactivation occur during the whole phase of cushion gas injection (fault F3) and, secondarily, at the end of injection phase during UGS (Figure 65). By introducing $P_f$ within the faults, a stabilizing effect is obtained. In Figure 66 and Figure 67 the thickness of the active elements and thickness of the elements with $\chi > 0.8$ are plotted for faults F1-F5. The figures compare the behavior provided by the parameters of combination 1 with and without $P_f$. Because of $P_f$ within the faults, fault activation is delayed and $t_{80}$ is always lower than $t_{80}$ computed without $P_f$.

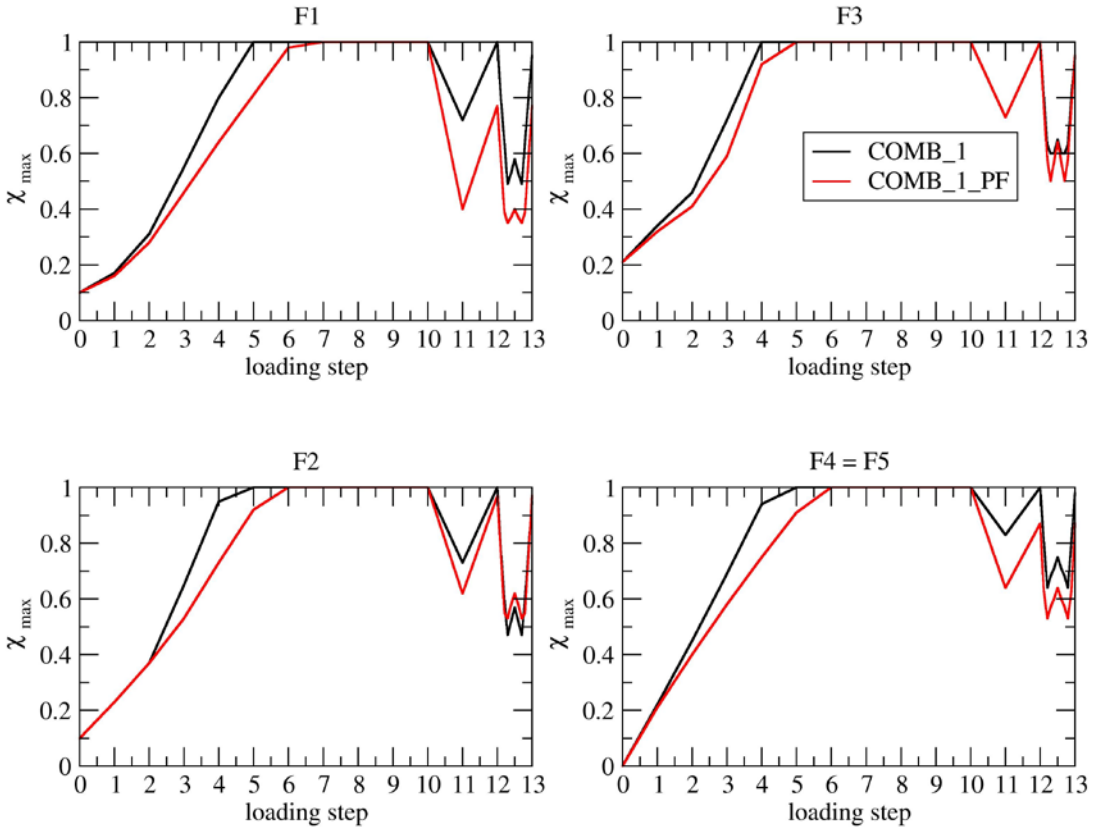


**Figure 65** Combination 1: $\chi_{max}$ versus loading steps for each fault with $P_f = 0$ or $P_f \neq 0$. Note that due to symmetry F4 and F5 behave identically.

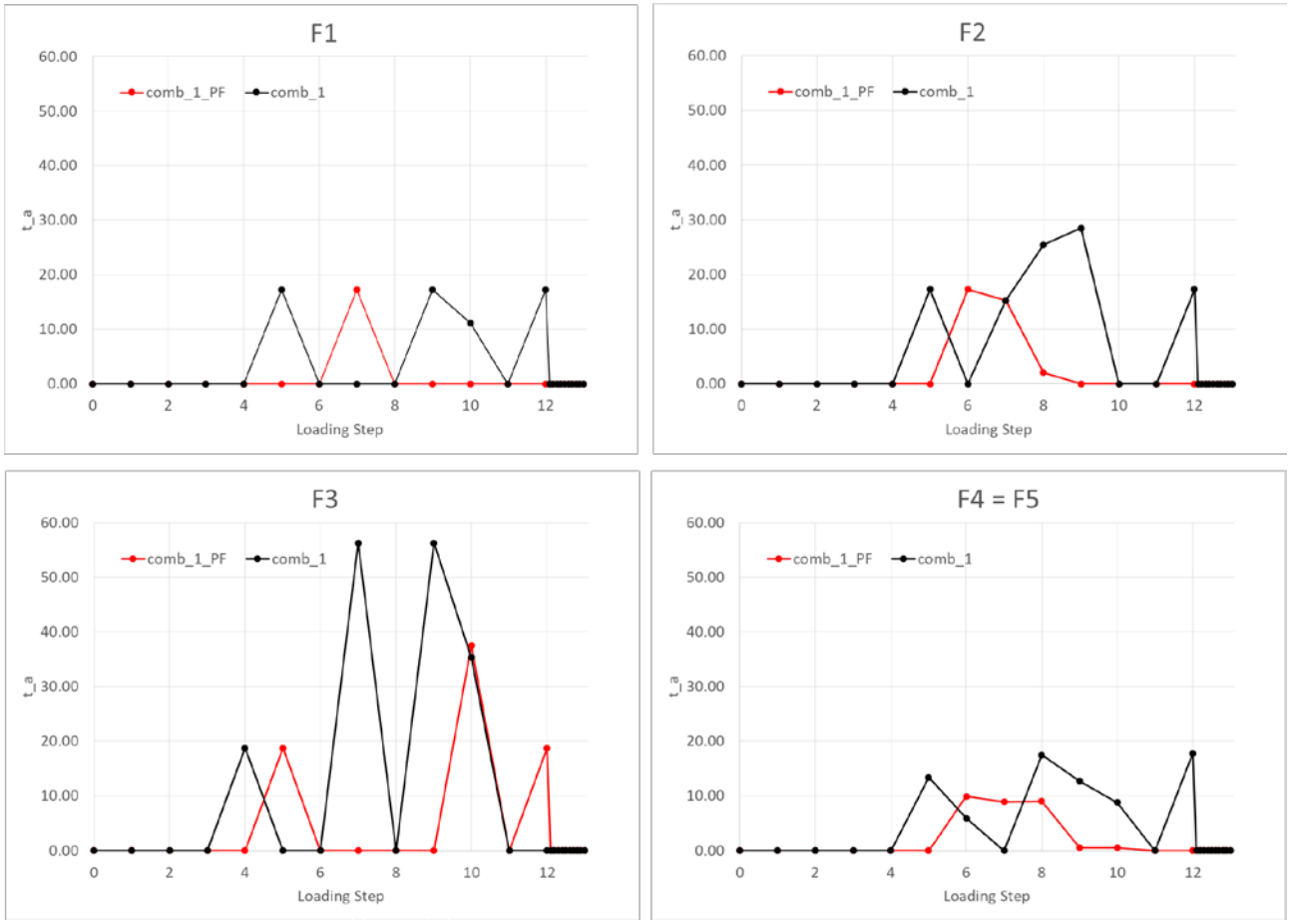


**Figure 66** Thickness of the active elements for faults F1-F5. Combination 1 with $P_f = 0$ or $P_f \neq 0$ are compared.

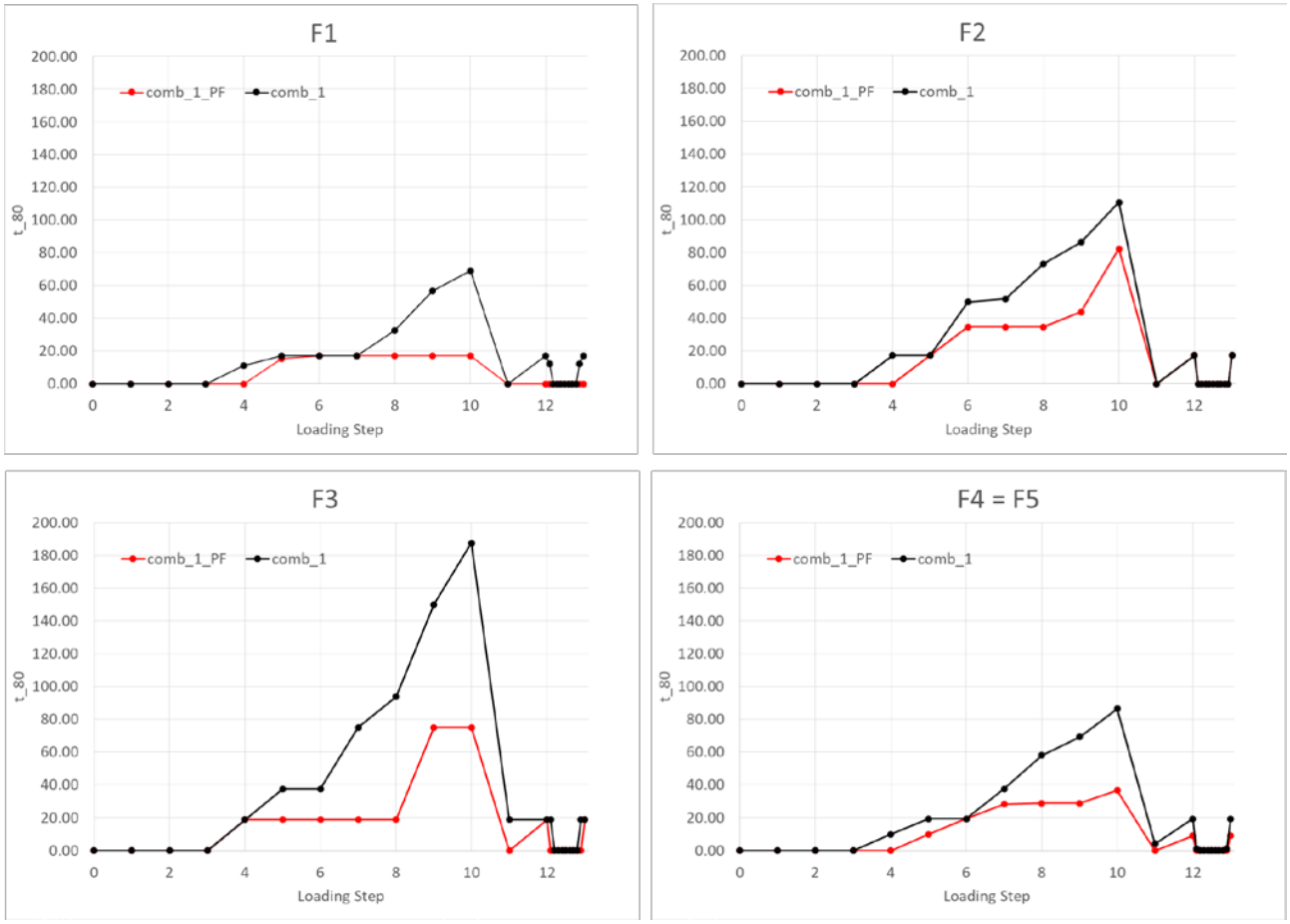


**Figure 67** Thickness $t_{80}$ of the elements with $\chi$>0.8 for faults F1-F5. Combination 1 with $P_f = 0$ or $P_f \neq 0$ are compared.

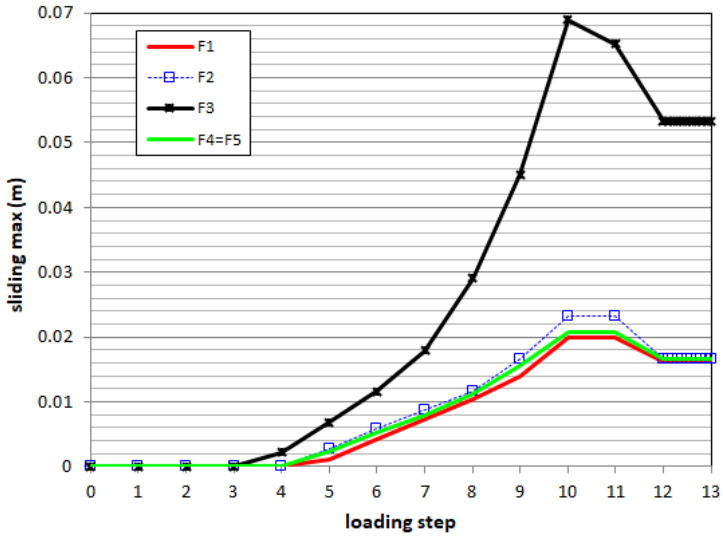


**Figure 68** Combination 1 ($P_f = 0$): Maximum sliding $\delta_{max}$.

The time behaviour of $\delta_{max}$ in the case $P_f = 0$ is shown in Figure 68. Notice that, during cushion gas injection, fault F3 slides in the opposite direction relative to what develops during primary production; therefore $\delta_{max}$ reduces (Figure 68). Figure 69 provides a 3D view of the $\chi_{max}$ distribution at a few significant loading steps for combination 1 ($P_f = 0$).

For completeness, the values of $\chi_{max}$ $t_a$, $t_{80}$, and $t_{50}$ are provided in Annex III for both cases with and without Pf within the faults.

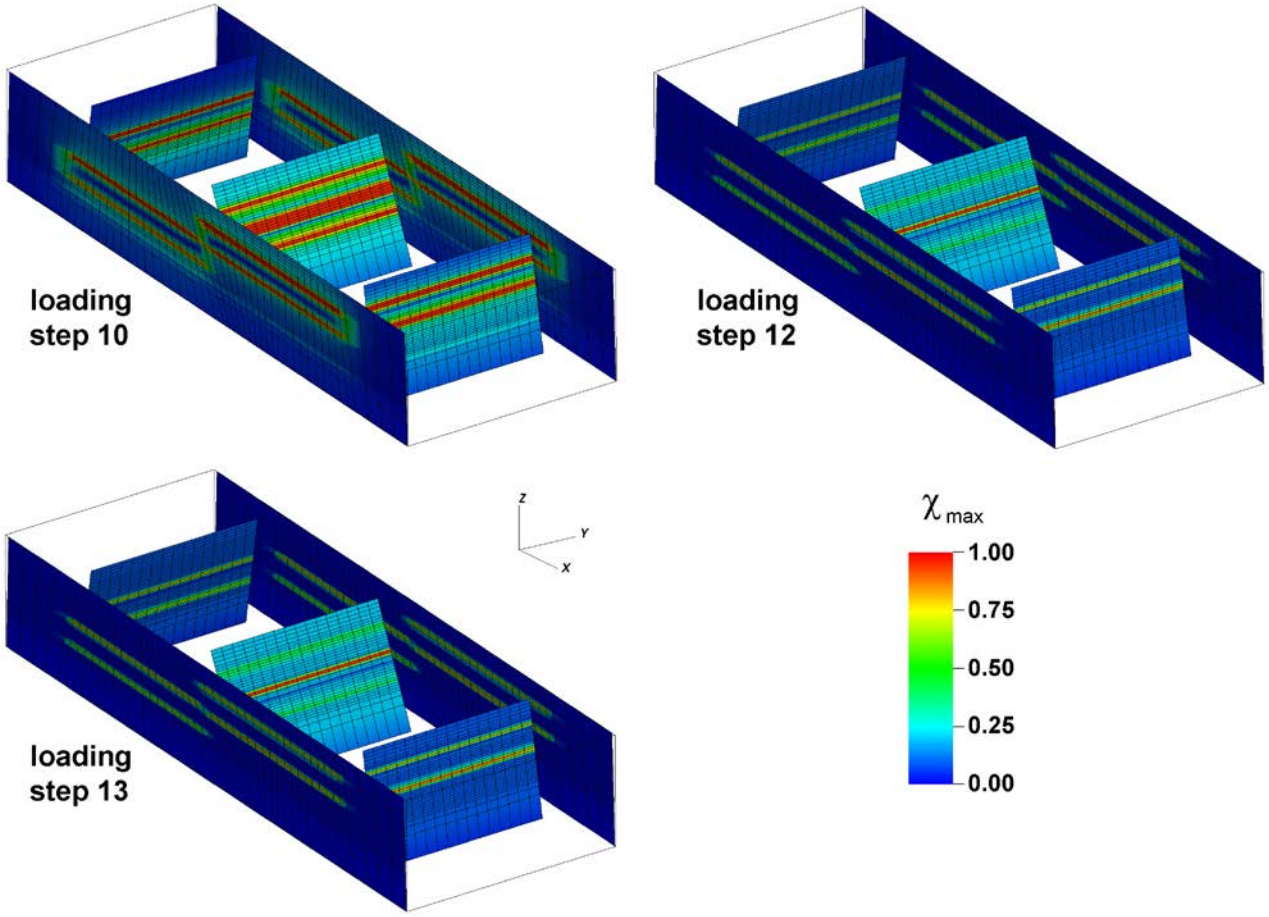


**Figure 69** Combination 1 ($P_f = 0$): $\chi_{max}$ distribution on the fault system at the end of (loading step 10) primary production, (loading step 12) cushion gas injection, and (loading step 13) UGS injection phase for the case investigating a first combination of parameters and mechanisms.

### *9.2 Combination 2*

A second combination is based on the following hypotheses:

- *c* = 20 bar;
- static friction angle = 20°;
- F3 dip angle = +65°;
- salt caprock;
- offset = 200 m.

The difference with respect to combination 1 is the use of a more realistic value of cohesion and the viscous rheology of the reservoir caprock. For the other parameters, the values adopted in reference test case have been used. Moreover, similarly for combination 1, the same simulation has been run by considering a non-null pore pressure $P_f$ within each fault, with a value equal to the average between the pressures at the two sides of the fault.

The simulation outcome in terms of $\chi_{max}$ is shown in Figure 70. The results show that faults F1, F2, F4, F5 behaves identically for both cases (with $P_f = 0$ or $P_f \neq 0$) because of the presence of the viscous Zechstein formation, as pointed out in mechanism 3. Fault F3 is slightly stabilized, mainly during UGS, when $P_f \neq 0$. A zoom of $\chi_{max}$ during UGS cycle is shown in Figure 71. In Figure 72 and Figure 73 the thickness of the active elements and the thickness of the elements with $\chi > 0.8$ are plotted for faults F1-F5. When $P_f \neq 0$, fault F3 activation is delayed during primary production relative to the case with $P_f = 0$; likely due to this, a larger $t_a$ develops with $P_f \neq 0$ at the end of CG injection. Differently, $t_{80}$ with $P_f \neq 0$ is always lower than that observed with $P_f = 0$.

For combination 2 with $P_f = 0$, $\delta_{max}$ is shown in Figure 74. Even if $\delta_{max}$ is smaller for this case than with combination 1 (Figure 68), the comparison between Figure 65 and Figure 70 shows that combination 2 is more prone to fault activation during UGS than combination 1. Salt caprock and friction angle play a significant role. For completeness, the values of $\chi_{max}$ $t_a$, $t_{80}$, and $t_{50}$ are provided in Annex III.

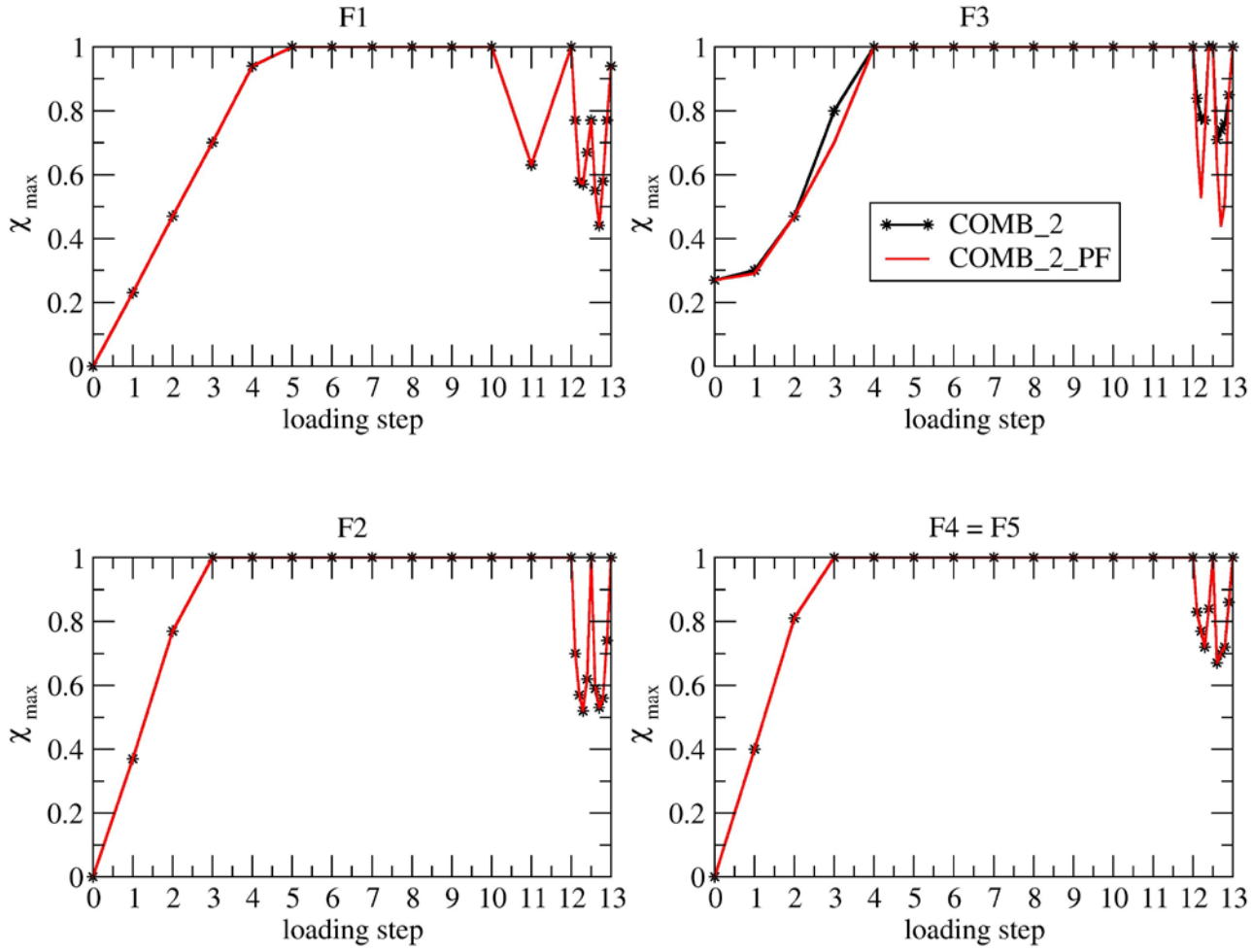


**Figure 70** Combination 2: $\chi_{max}$ versus loading steps for each fault with $P_f = 0$ or $P_f \neq 0$. Note that due to symmetry F4 and F5 behave identically.

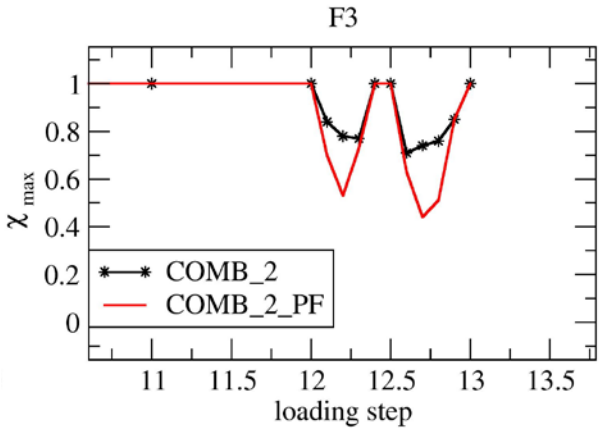


**Figure 71** $\chi_{max}$: zoom of Figure 70 for fault F3 during cushion gas and UGS cycle.

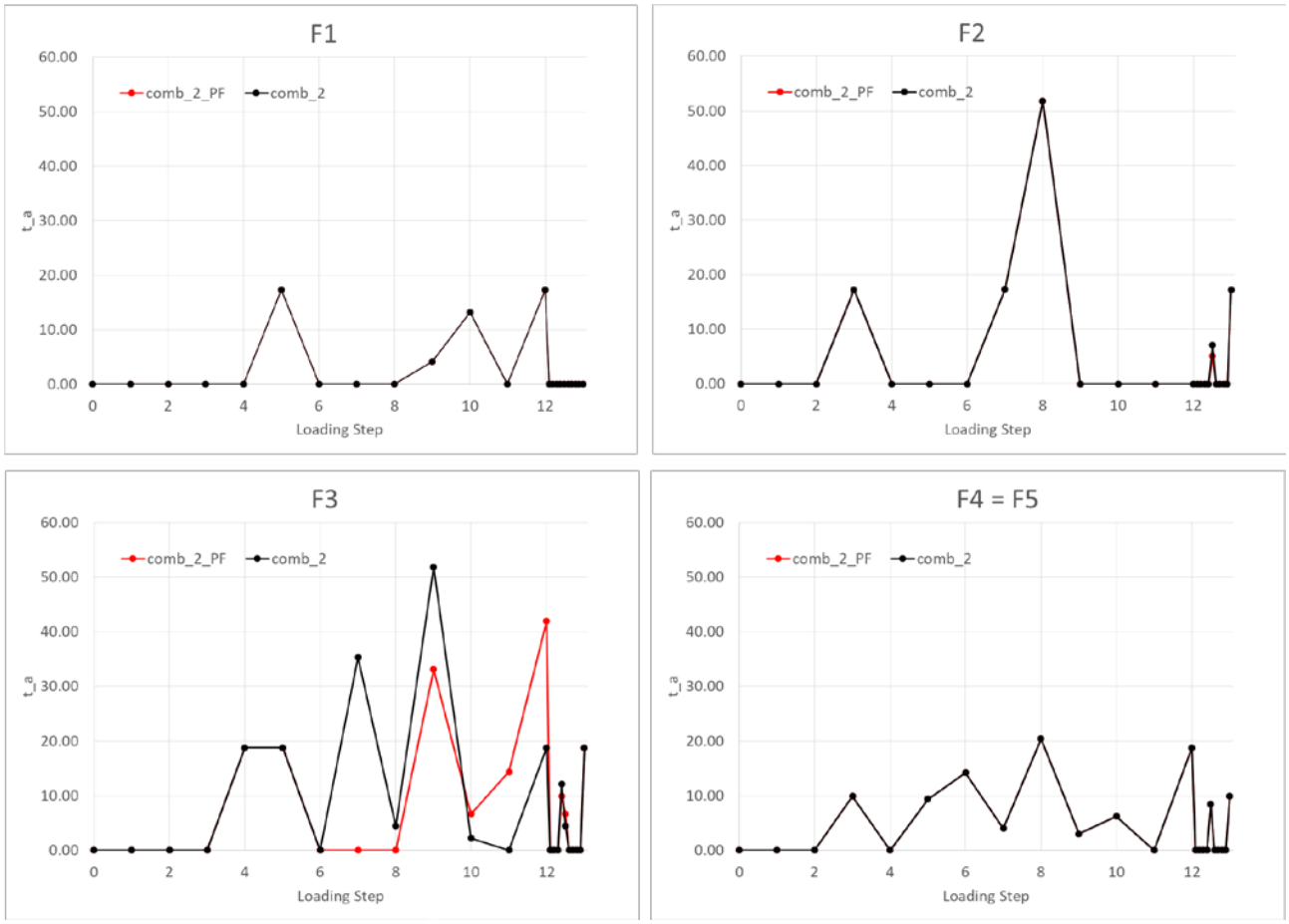


**Figure 72** Thickness of the active elements for faults F1-F5. Combination 2 with $P_f = 0$ or $P_f \neq 0$ are compared.

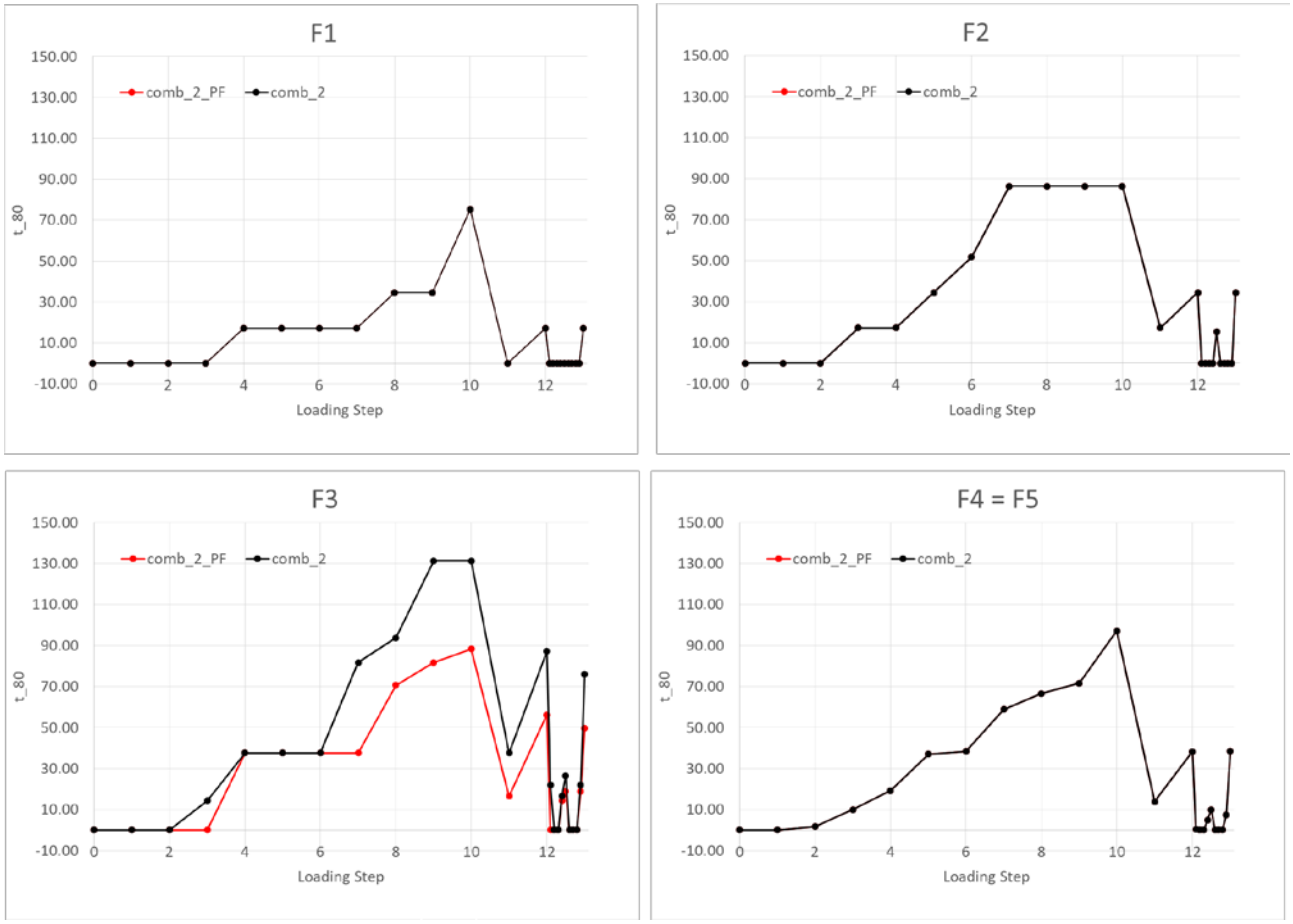


**Figure 73** Thickness $t_{80}$ of the elements with $\chi$>0.8 for faults F1-F5. Combination 2 with $P_f = 0$ or $P_f \neq 0$ are compared

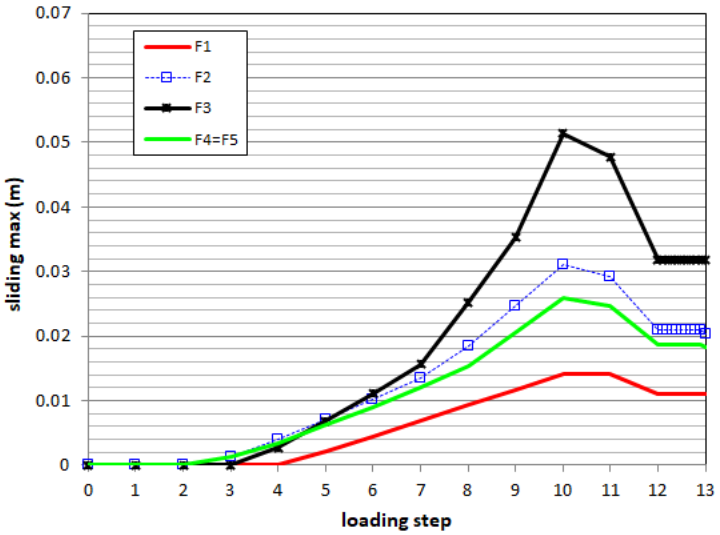


**Figure 74** Combination 2 ($P_f = 0$): Maximum sliding $\delta_{max}$.

## *9.3 Combination 3*

The third combination is based on the following hypotheses:

- $c$ = 20 bar;
- weakening = 30° to 20° in 20 mm;
- F3 dip angle = +65°;
- $E_{II}/E_I$ = 2.5;
- offset = 200 m.

Here, weakening and, secondarily, the different reservoir stiffness in loading / unloading phase are the main effects taken into account. The simulation outcome in terms of $\chi_{max}$ and $\delta_{max}$ are shown in Figure 75 and Figure 76. A certain difference with respect to combination 1 is obtained: 1) faults start sliding one loading step later; 2) during UGS, F3 is characterized by a $\chi_{max}$ ~20% smaller. Therefore, the effect of cohesion seems to be relatively stronger than that of friction angle. For completeness, the values of $\chi_{max}$ $t_a$, $t_{80}$, and $t_{50}$ are provided in Annex III.

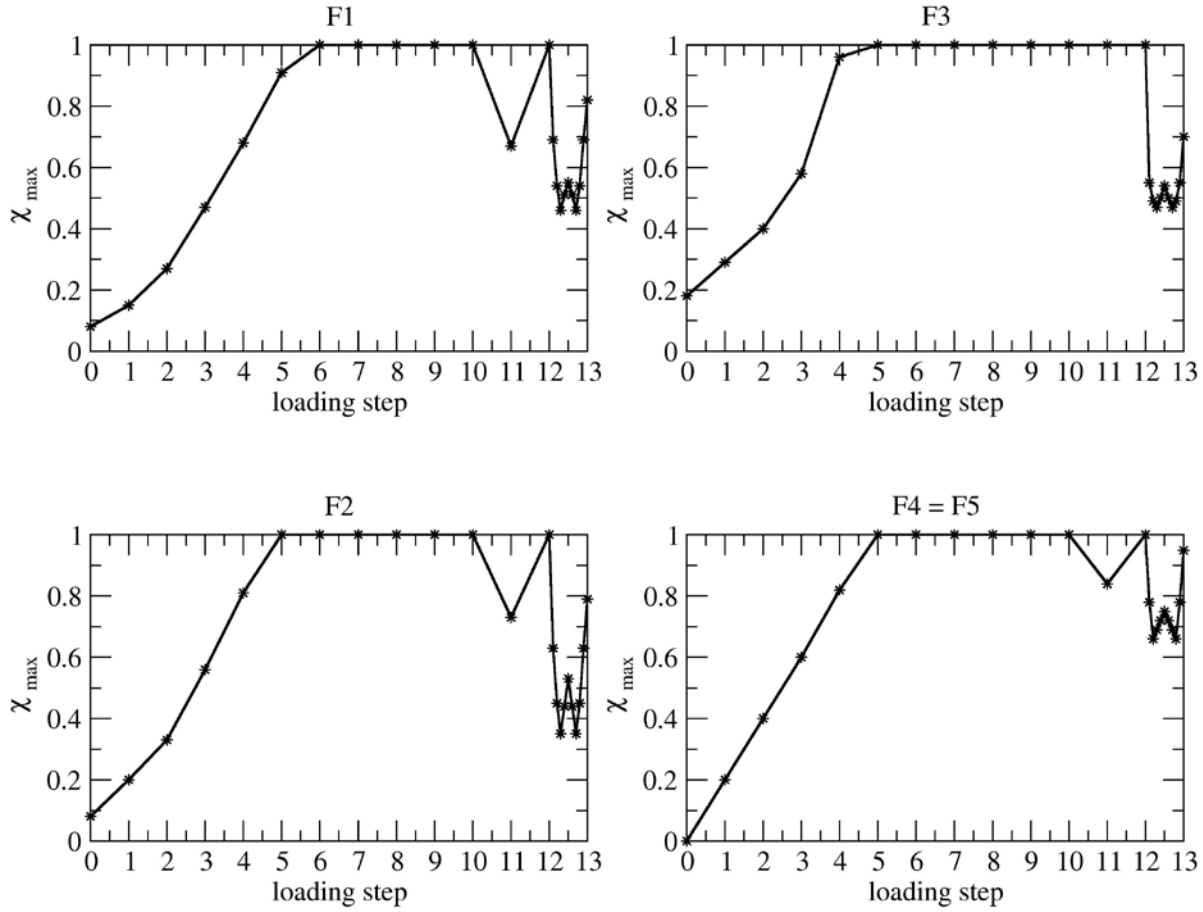


**Figure 75** Combination 3: $\chi_{max}$ versus loading steps. Note that due to symmetry F4 and F5 behave identically.

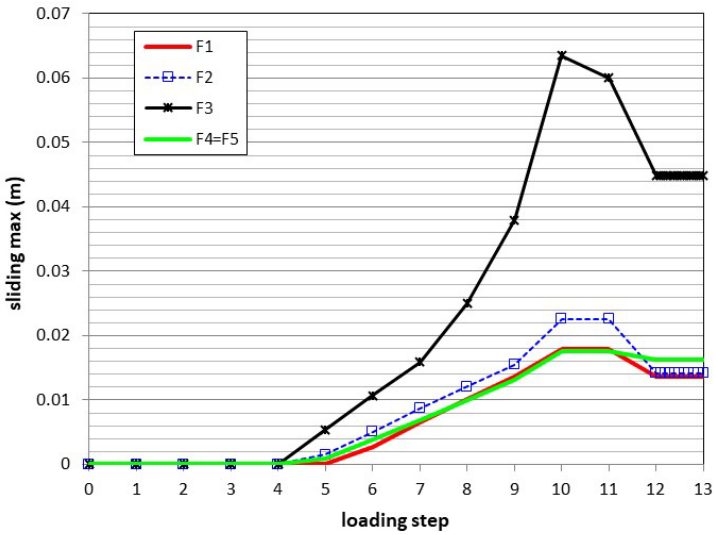


**Figure 76** Combination 3: maximum sliding $\delta_{max}$.

## References

Andrews, D. J. (1985). Dynamic plane-strain shear rupture with a slip-weakening friction law calculated by a boundary integral method, Bulletin of the Seismological Society of America, 75(1), 1-21.

Chierici, G. (1980), Principi di Ingegneria dei Giacimenti Petroliferi, AGIP Ed.

Evans, J. P., C. B. Forster and J. V. Goddard (1997), Permeability of fault-related rocks, and implications for hydraulic structure of fault zones, Journal of Structural Geology, 19(11), 1393-1404.

Fine, R. A. and F. J. Millero (1973), Compressibility of water as a function of temperature and pressure, The Journal of Chemical Physics 59, 5529, doi: 10.1063/1.1679903.

Franceschini, A., M. Ferronato, C. Janna and P. Teatini (2016), A novel Lagrangian approach for a stable numerical simulation of the mechanics of faults, Journal of Computational Physics, 314, 503-521.

Geertsma, J. (1973), Land subsidence above compacting oil and gas reservoir, JPT, 25, 734-744.

Guatteri, M., and P. Spudich (2000), What can strong-motion data tell us about slip-weakening fault-friction laws?, Bulletin of the Seismological Society of America, 90(1), 98-116.

Orlic, B., and B. B. T. Wassing (2013), A study of stress change and fault slip in producing gas reservoirs overlain by elastic and viscoelastic caprocks, Rock Mech. Rock Eng., 46, 421–435.

Schultz, R., R. Wang, Y. J. Gu, K. Haug, and G. Atkinson (2017), A seismological overview of the induced earthquakes in the Duvernay play near Fox Creek, Alberta, J. Geophys. Res. Solid Earth, 122, 492–505.

Vilarrasa, V., R. Y. Makhnenko, and L. Laloui (2017), Potential for fault reactivation due to $CO_2$ injection in a semi-closed saline aquifer, Energy Procedia, 114, 3282 – 3290.

Zbinden, D., A. P. Rinaldi, L. Urpi, and S. Wiemer (2017), On the physics-based processes behind production-induced seismicity in natural gas fields, J. Geophys. Res. Solid Earth, 122, 3792–3812.

# Annex I - $\chi_{max}$

**Table 10 - $\chi_{max}$ – Reference test case**

| reference test case | | | | |
|---|---|---|---|---|
| **Step** | **F1** | **F2** | **F3** | **F4 = F5** |
| 0.00 | 0.08 | 0.08 | 0.00 | 0.00 |
| 1.00 | 0.25 | 0.25 | 0.00 | 0.16 |
| 2.00 | 0.40 | 0.40 | 0.00 | 0.33 |
| 3.00 | 0.54 | 0.54 | 0.00 | 0.50 |
| 4.00 | 0.67 | 0.67 | 0.00 | 0.68 |
| 5.00 | 0.88 | 0.88 | 0.00 | 0.86 |
| 6.00 | 1.00 | 1.00 | 0.00 | 1.00 |
| 7.00 | 1.00 | 1.00 | 0.00 | 1.00 |
| 8.00 | 1.00 | 1.00 | 0.00 | 1.00 |
| 9.00 | 1.00 | 1.00 | 0.00 | 1.00 |
| 10.00 | 1.00 | 1.00 | 0.00 | 1.00 |
| 11.00 | 0.52 | 0.52 | 0.00 | 0.57 |
| 12.00 | 0.89 | 0.89 | 0.00 | 0.79 |
| 12.10 | 0.76 | 0.76 | 0.00 | 0.64 |
| 12.20 | 0.63 | 0.63 | 0.00 | 0.48 |
| 12.30 | 0.48 | 0.48 | 0.00 | 0.48 |
| 12.40 | 0.49 | 0.49 | 0.00 | 0.52 |
| 12.50 | 0.52 | 0.52 | 0.00 | 0.57 |
| 12.60 | 0.49 | 0.49 | 0.00 | 0.52 |
| 12.70 | 0.48 | 0.48 | 0.00 | 0.48 |
| 12.80 | 0.63 | 0.63 | 0.00 | 0.48 |
| 12.90 | 0.76 | 0.76 | 0.00 | 0.64 |
| 13.00 | 0.89 | 0.89 | 0.00 | 0.79 |

**Table 11 - $\chi_{max}$ - Effect of reservoir and fault geometry**

| dip = 65° | | | | |
|---|---|---|---|---|
| **Step** | **F1** | **F2** | **F3** | **F4 = F5** |
| 0.00 | 0.08 | 0.08 | 0.18 | 0.00 |
| 1.00 | 0.25 | 0.25 | 0.22 | 0.16 |
| 2.00 | 0.40 | 0.40 | 0.28 | 0.33 |
| 3.00 | 0.54 | 0.54 | 0.34 | 0.50 |
| 4.00 | 0.67 | 0.67 | 0.41 | 0.68 |
| 5.00 | 0.88 | 0.88 | 0.49 | 0.86 |
| 6.00 | 1.00 | 1.00 | 0.58 | 1.00 |
| 7.00 | 1.00 | 1.00 | 0.68 | 1.00 |
| 8.00 | 1.00 | 1.00 | 0.81 | 1.00 |
| 9.00 | 1.00 | 1.00 | 0.96 | 1.00 |
| 10.00 | 1.00 | 1.00 | 1.00 | 1.00 |
| 11.00 | 0.53 | 0.53 | 0.58 | 0.57 |
| 12.00 | 0.90 | 0.90 | 0.42 | 0.79 |
| 12.10 | 0.77 | 0.77 | 0.45 | 0.64 |
| 12.20 | 0.63 | 0.63 | 0.48 | 0.48 |
| 12.30 | 0.49 | 0.49 | 0.51 | 0.48 |
| 12.40 | 0.50 | 0.50 | 0.55 | 0.52 |
| 12.50 | 0.53 | 0.53 | 0.58 | 0.57 |
| 12.60 | 0.50 | 0.50 | 0.55 | 0.52 |
| 12.70 | 0.49 | 0.49 | 0.51 | 0.48 |
| 12.80 | 0.63 | 0.63 | 0.48 | 0.48 |
| 12.90 | 0.77 | 0.77 | 0.45 | 0.64 |
| 13.00 | 0.90 | 0.90 | 0.42 | 0.79 |

| dip = - 65° | | | | |
|---|---|---|---|---|
| **Step** | **F1** | **F2** | **F3** | **F4 = F5** |
| 0.00 | 0.08 | 0.08 | 0.18 | 0.00 |
| 1.00 | 0.25 | 0.25 | 0.22 | 0.16 |
| 2.00 | 0.40 | 0.40 | 0.28 | 0.33 |
| 3.00 | 0.54 | 0.54 | 0.34 | 0.50 |
| 4.00 | 0.67 | 0.67 | 0.40 | 0.68 |
| 5.00 | 0.88 | 0.89 | 0.48 | 0.86 |
| 6.00 | 1.00 | 1.00 | 0.57 | 1.00 |
| 7.00 | 1.00 | 1.00 | 0.68 | 1.00 |
| 8.00 | 1.00 | 1.00 | 0.80 | 1.00 |
| 9.00 | 1.00 | 1.00 | 0.94 | 1.00 |
| 10.00 | 1.00 | 1.00 | 1.00 | 1.00 |
| 11.00 | 0.53 | 0.53 | 0.56 | 0.58 |
| 12.00 | 0.90 | 0.91 | 0.40 | 0.79 |
| 12.10 | 0.77 | 0.78 | 0.43 | 0.64 |
| 12.20 | 0.63 | 0.64 | 0.46 | 0.48 |
| 12.30 | 0.49 | 0.49 | 0.49 | 0.49 |
| 12.40 | 0.50 | 0.49 | 0.53 | 0.54 |
| 12.50 | 0.53 | 0.53 | 0.56 | 0.58 |
| 12.60 | 0.50 | 0.49 | 0.53 | 0.54 |
| 12.70 | 0.49 | 0.49 | 0.49 | 0.49 |
| 12.80 | 0.63 | 0.64 | 0.46 | 0.48 |
| 12.90 | 0.77 | 0.78 | 0.43 | 0.64 |
| 13.00 | 0.90 | 0.91 | 0.40 | 0.79 |

| dislocation = 100 m | | | | |
|---|---|---|---|---|
| **Step** | **F1** | **F2** | **F3** | **F4 = F5** |
| 0.00 | 0.08 | 0.08 | 0.00 | 0.00 |
| 1.00 | 0.25 | 0.26 | 0.18 | 0.18 |
| 2.00 | 0.40 | 0.42 | 0.38 | 0.35 |
| 3.00 | 0.54 | 0.56 | 0.59 | 0.52 |
| 4.00 | 0.67 | 0.70 | 0.82 | 0.71 |
| 5.00 | 0.87 | 0.92 | 1.00 | 0.90 |
| 6.00 | 1.00 | 1.00 | 1.00 | 1.00 |
| 7.00 | 1.00 | 1.00 | 1.00 | 1.00 |
| 8.00 | 1.00 | 1.00 | 1.00 | 1.00 |
| 9.00 | 1.00 | 1.00 | 1.00 | 1.00 |
| 10.00 | 1.00 | 1.00 | 1.00 | 1.00 |
| 11.00 | 0.52 | 0.57 | 0.63 | 0.63 |
| 12.00 | 0.89 | 0.95 | 1.00 | 0.87 |
| 12.10 | 0.76 | 0.82 | 0.81 | 0.71 |
| 12.20 | 0.63 | 0.68 | 0.68 | 0.55 |
| 12.30 | 0.48 | 0.53 | 0.56 | 0.53 |
| 12.40 | 0.49 | 0.54 | 0.58 | 0.57 |
| 12.50 | 0.52 | 0.57 | 0.63 | 0.63 |
| 12.60 | 0.49 | 0.54 | 0.58 | 0.57 |
| 12.70 | 0.48 | 0.53 | 0.56 | 0.53 |
| 12.80 | 0.63 | 0.68 | 0.68 | 0.55 |
| 12.90 | 0.76 | 0.82 | 0.81 | 0.71 |
| 13.00 | 0.89 | 0.95 | 0.95 | 0.87 |

| dislocation = 200 m | | | | |
|---|---|---|---|---|
| **Step** | **F1** | **F2** | **F3** | **F4 = F5** |
| 0.00 | 0.08 | 0.08 | 0.00 | 0.00 |
| 1.00 | 0.25 | 0.26 | 0.34 | 0.18 |
| 2.00 | 0.40 | 0.43 | 0.68 | 0.36 |
| 3.00 | 0.54 | 0.59 | 1.00 | 0.55 |
| 4.00 | 0.67 | 0.73 | 1.00 | 0.75 |
| 5.00 | 0.87 | 0.96 | 1.00 | 0.95 |
| 6.00 | 1.00 | 1.00 | 1.00 | 1.00 |
| 7.00 | 1.00 | 1.00 | 1.00 | 1.00 |
| 8.00 | 1.00 | 1.00 | 1.00 | 1.00 |
| 9.00 | 1.00 | 1.00 | 1.00 | 1.00 |
| 10.00 | 1.00 | 1.00 | 1.00 | 1.00 |
| 11.00 | 0.52 | 0.63 | 0.72 | 0.65 |
| 12.00 | 0.89 | 1.00 | 1.00 | 0.95 |
| 12.10 | 0.76 | 0.82 | 0.89 | 0.79 |
| 12.20 | 0.63 | 0.67 | 0.86 | 0.63 |
| 12.30 | 0.48 | 0.55 | 0.83 | 0.60 |
| 12.40 | 0.49 | 0.57 | 0.79 | 0.62 |
| 12.50 | 0.52 | 0.59 | 0.79 | 0.65 |
| 12.60 | 0.49 | 0.57 | 0.79 | 0.62 |
| 12.70 | 0.48 | 0.55 | 0.83 | 0.60 |
| 12.80 | 0.63 | 0.67 | 0.86 | 0.63 |
| 12.90 | 0.76 | 0.82 | 0.89 | 0.79 |
| 13.00 | 0.89 | 0.95 | 0.95 | 0.95 |

**Table 12 - $\chi_{max}$ - Effect of initial stress regime**

| θ = 90° | | | | | M_1 = 0.40 ; M_2 = 0.47 | | | | |
|---|---|---|---|---|---|---|---|---|---|
| **Step** | **F1** | **F2** | **F3** | **F4 = F5** | **Step** | **F1** | **F2** | **F3** | **F4 = F5** |
| 0.00 | 0.05 | 0.05 | 0.00 | 0.00 | 0.00 | 0.32 | 0.32 | 0.00 | 0.00 |
| 1.00 | 0.20 | 0.20 | 0.00 | 0.18 | 1.00 | 0.55 | 0.55 | 0.00 | 0.26 |
| 2.00 | 0.34 | 0.34 | 0.00 | 0.36 | 2.00 | 0.77 | 0.77 | 0.00 | 0.53 |
| 3.00 | 0.47 | 0.47 | 0.00 | 0.55 | 3.00 | 0.96 | 0.96 | 0.00 | 0.81 |
| 4.00 | 0.62 | 0.62 | 0.00 | 0.75 | 4.00 | 1.00 | 1.00 | 0.00 | 1.00 |
| 5.00 | 0.82 | 0.82 | 0.00 | 0.95 | 5.00 | 1.00 | 1.00 | 0.00 | 1.00 |
| 6.00 | 1.00 | 1.00 | 0.00 | 1.00 | 6.00 | 1.00 | 1.00 | 0.00 | 1.00 |
| 7.00 | 1.00 | 1.00 | 0.00 | 1.00 | 7.00 | 1.00 | 1.00 | 0.00 | 1.00 |
| 8.00 | 1.00 | 1.00 | 0.00 | 1.00 | 8.00 | 1.00 | 1.00 | 0.00 | 1.00 |
| 9.00 | 1.00 | 1.00 | 0.00 | 1.00 | 9.00 | 1.00 | 1.00 | 1.00 | 1.00 |
| 10.00 | 1.00 | 1.00 | 0.00 | 1.00 | 10.00 | 1.00 | 1.00 | 1.00 | 1.00 |
| 11.00 | 0.47 | 0.47 | 0.00 | 0.65 | 11.00 | 0.91 | 0.91 | 0.00 | 0.84 |
| 12.00 | 0.75 | 0.75 | 0.00 | 0.95 | 12.00 | 1.00 | 1.00 | 0.00 | 1.00 |
| 12.10 | 0.63 | 0.63 | 0.00 | 0.79 | 12.10 | 0.75 | 0.75 | 0.00 | 0.73 |
| 12.20 | 0.50 | 0.50 | 0.00 | 0.63 | 12.20 | 0.78 | 0.78 | 0.00 | 0.60 |
| 12.30 | 0.42 | 0.42 | 0.00 | 0.60 | 12.30 | 0.80 | 0.80 | 0.00 | 0.64 |
| 12.40 | 0.45 | 0.45 | 0.00 | 0.62 | 12.40 | 0.82 | 0.82 | 0.00 | 0.68 |
| 12.50 | 0.47 | 0.47 | 0.00 | 0.65 | 12.50 | 0.84 | 0.84 | 0.00 | 0.71 |
| 12.60 | 0.45 | 0.45 | 0.00 | 0.62 | 12.60 | 0.82 | 0.82 | 0.00 | 0.68 |
| 12.70 | 0.42 | 0.42 | 0.00 | 0.60 | 12.70 | 0.80 | 0.80 | 0.00 | 0.64 |
| 12.80 | 0.50 | 0.50 | 0.00 | 0.63 | 12.80 | 0.78 | 0.78 | 0.00 | 0.60 |
| 12.90 | 0.63 | 0.63 | 0.00 | 0.79 | 12.90 | 0.75 | 0.75 | 0.00 | 0.73 |
| 13.00 | 0.75 | 0.75 | 0.00 | 0.95 | 13.00 | 0.95 | 0.95 | 0.00 | 0.95 |

**Table 13 - $\chi_{max}$ - Effect of Mohr-Coulomb fault parameters**

| c = 0 bar | | | | | c = 100 bar | | | | |
|---|---|---|---|---|---|---|---|---|---|
| **Step** | **F1** | **F2** | **F3** | **F4 = F5** | **Step** | **F1** | **F2** | **F3** | **F4 = F5** |
| 0.00 | 0.10 | 0.10 | 0.00 | 0.00 | 0.00 | 0.05 | 0.05 | 0.00 | 0.00 |
| 1.00 | 0.29 | 0.29 | 0.00 | 0.19 | 1.00 | 0.16 | 0.16 | 0.00 | 0.11 |
| 2.00 | 0.46 | 0.46 | 0.00 | 0.39 | 2.00 | 0.26 | 0.26 | 0.00 | 0.21 |
| 3.00 | 0.62 | 0.62 | 0.00 | 0.59 | 3.00 | 0.35 | 0.35 | 0.00 | 0.31 |
| 4.00 | 0.80 | 0.80 | 0.00 | 0.80 | 4.00 | 0.44 | 0.44 | 0.00 | 0.41 |
| 5.00 | 1.00 | 1.00 | 0.00 | 1.00 | 5.00 | 0.53 | 0.53 | 0.00 | 0.52 |
| 6.00 | 1.00 | 1.00 | 0.00 | 1.00 | 6.00 | 0.62 | 0.62 | 0.00 | 0.63 |
| 7.00 | 1.00 | 1.00 | 0.00 | 1.00 | 7.00 | 0.75 | 0.75 | 0.00 | 0.75 |
| 8.00 | 1.00 | 1.00 | 0.00 | 1.00 | 8.00 | 0.88 | 0.88 | 0.00 | 0.86 |
| 9.00 | 1.00 | 1.00 | 0.00 | 1.00 | 9.00 | 1.00 | 1.00 | 0.00 | 0.98 |
| 10.00 | 1.00 | 1.00 | 0.00 | 1.00 | 10.00 | 1.00 | 1.00 | 0.00 | 1.00 |
| 11.00 | 0.78 | 0.78 | 0.00 | 0.76 | 11.00 | 0.53 | 0.53 | 0.00 | 0.50 |
| 12.00 | 1.00 | 1.00 | 0.00 | 1.00 | 12.00 | 0.22 | 0.22 | 0.00 | 0.14 |
| 12.10 | 0.80 | 0.80 | 0.00 | 0.79 | 12.10 | 0.16 | 0.16 | 0.00 | 0.11 |
| 12.20 | 0.64 | 0.64 | 0.00 | 0.61 | 12.20 | 0.26 | 0.26 | 0.00 | 0.21 |
| 12.30 | 0.65 | 0.65 | 0.00 | 0.64 | 12.30 | 0.35 | 0.35 | 0.00 | 0.31 |
| 12.40 | 0.67 | 0.67 | 0.00 | 0.66 | 12.40 | 0.44 | 0.44 | 0.00 | 0.41 |
| 12.50 | 0.69 | 0.69 | 0.00 | 0.69 | 12.50 | 0.53 | 0.53 | 0.00 | 0.50 |
| 12.60 | 0.67 | 0.67 | 0.00 | 0.66 | 12.60 | 0.44 | 0.44 | 0.00 | 0.41 |
| 12.70 | 0.65 | 0.65 | 0.00 | 0.64 | 12.70 | 0.35 | 0.35 | 0.00 | 0.31 |
| 12.80 | 0.64 | 0.64 | 0.00 | 0.61 | 12.80 | 0.26 | 0.26 | 0.00 | 0.21 |
| 12.90 | 0.80 | 0.80 | 0.00 | 0.79 | 12.90 | 0.16 | 0.16 | 0.00 | 0.11 |
| 13.00 | 0.95 | 0.95 | 0.00 | 0.95 | 13.00 | 0.22 | 0.22 | 0.00 | 0.14 |

| $f_s = 20°$ | | | | | $f_d = 10°$; $d_c = 2$ mm | | | | |
|---|---|---|---|---|---|---|---|---|---|
| **Step** | **F1** | **F2** | **F3** | **F4 = F5** | **Step** | **F1** | **F2** | **F3** | **F4 = F5** |
| 0.00 | 0.12 | 0.12 | 0.00 | 0.00 | 0.00 | 0.08 | 0.08 | 0.00 | 0.00 |
| 1.00 | 0.36 | 0.36 | 0.00 | 0.24 | 1.00 | 0.25 | 0.25 | 0.00 | 0.16 |
| 2.00 | 0.58 | 0.58 | 0.00 | 0.48 | 2.00 | 0.40 | 0.40 | 0.00 | 0.33 |
| 3.00 | 0.79 | 0.79 | 0.00 | 0.72 | 3.00 | 0.54 | 0.54 | 0.00 | 0.50 |
| 4.00 | 0.99 | 0.99 | 0.00 | 0.98 | 4.00 | 0.67 | 0.67 | 0.00 | 0.68 |
| 5.00 | 1.00 | 1.00 | 0.00 | 1.00 | 5.00 | 0.88 | 0.88 | 0.00 | 0.86 |
| 6.00 | 1.00 | 1.00 | 0.00 | 1.00 | 6.00 | 1.00 | 1.00 | 0.00 | 1.00 |
| 7.00 | 1.00 | 1.00 | 0.00 | 1.00 | 7.00 | 1.00 | 1.00 | 0.00 | 1.00 |
| 8.00 | 1.00 | 1.00 | 0.00 | 1.00 | 8.00 | 1.00 | 1.00 | 0.00 | 1.00 |
| 9.00 | 1.00 | 1.00 | 0.00 | 1.00 | 9.00 | 1.00 | 1.00 | 0.00 | 1.00 |
| 10.00 | 1.00 | 1.00 | 0.00 | 1.00 | 10.00 | 1.00 | 1.00 | 0.00 | 1.00 |
| 11.00 | 0.84 | 0.84 | 0.00 | 0.82 | 11.00 | 1.00 | 1.00 | 0.00 | 1.00 |
| 12.00 | 1.00 | 1.00 | 0.00 | 1.00 | 12.00 | 1.00 | 1.00 | 0.00 | 1.00 |
| 12.10 | 0.75 | 0.75 | 0.00 | 0.74 | 12.10 | 1.00 | 1.00 | 0.00 | 0.77 |
| 12.20 | 0.60 | 0.60 | 0.00 | 0.62 | 12.20 | 0.69 | 0.69 | 0.00 | 0.73 |
| 12.30 | 0.63 | 0.63 | 0.00 | 0.64 | 12.30 | 0.71 | 0.71 | 0.00 | 0.69 |
| 12.40 | 0.65 | 0.65 | 0.00 | 0.66 | 12.40 | 0.72 | 0.72 | 0.00 | 0.66 |
| 12.50 | 0.68 | 0.68 | 0.00 | 0.69 | 12.50 | 1.00 | 1.00 | 0.00 | 1.00 |
| 12.60 | 0.65 | 0.65 | 0.00 | 0.66 | 12.60 | 0.72 | 0.72 | 0.00 | 0.61 |
| 12.70 | 0.63 | 0.63 | 0.00 | 0.64 | 12.70 | 0.71 | 0.71 | 0.00 | 0.65 |
| 12.80 | 0.60 | 0.60 | 0.00 | 0.62 | 12.80 | 0.69 | 0.69 | 0.00 | 0.69 |
| 12.90 | 0.75 | 0.75 | 0.00 | 0.74 | 12.90 | 0.95 | 0.95 | 0.00 | 0.73 |
| 13.00 | 0.95 | 0.95 | 0.00 | 0.95 | 13.00 | 1.00 | 1.00 | 0.00 | 1.00 |

| $f_d$= 20°; $d_c$ = 20 mm | | | | |
|---|---|---|---|---|
| **Step** | **F1** | **F2** | **F3** | **F4 = F5** |
| 0.00 | 0.08 | 0.08 | 0.00 | 0.00 |
| 1.00 | 0.25 | 0.25 | 0.00 | 0.16 |
| 2.00 | 0.40 | 0.40 | 0.00 | 0.33 |
| 3.00 | 0.54 | 0.54 | 0.00 | 0.50 |
| 4.00 | 0.67 | 0.67 | 0.00 | 0.68 |
| 5.00 | 0.88 | 0.88 | 0.00 | 0.86 |
| 6.00 | 1.00 | 1.00 | 0.00 | 1.00 |
| 7.00 | 1.00 | 1.00 | 0.00 | 1.00 |
| 8.00 | 1.00 | 1.00 | 0.00 | 1.00 |
| 9.00 | 1.00 | 1.00 | 0.00 | 1.00 |
| 10.00 | 1.00 | 1.00 | 0.00 | 1.00 |
| 11.00 | 0.59 | 0.59 | 0.00 | 0.65 |
| 12.00 | 1.00 | 1.00 | 0.00 | 1.00 |
| 12.10 | 0.76 | 0.76 | 0.00 | 0.80 |
| 12.20 | 0.60 | 0.60 | 0.00 | 0.62 |
| 12.30 | 0.55 | 0.55 | 0.00 | 0.49 |
| 12.40 | 0.57 | 0.57 | 0.00 | 0.53 |
| 12.50 | 0.59 | 0.59 | 0.00 | 0.58 |
| 12.60 | 0.57 | 0.57 | 0.00 | 0.53 |
| 12.70 | 0.55 | 0.55 | 0.00 | 0.49 |
| 12.80 | 0.60 | 0.60 | 0.00 | 0.62 |
| 12.90 | 0.76 | 0.76 | 0.00 | 0.80 |
| 13.00 | 0.92 | 0.92 | 0.00 | 0.98 |

**Table 14 - $\chi_{max}$ - Effect of reservoir stiffness**

| E = 8 GPa | | | | |
|---|---|---|---|---|
| **Step** | **F1** | **F2** | **F3** | **F4 = F5** |
| 0.00 | 0.08 | 0.08 | 0.00 | 0.00 |
| 1.00 | 0.28 | 0.28 | 0.00 | 0.19 |
| 2.00 | 0.45 | 0.45 | 0.00 | 0.38 |
| 3.00 | 0.61 | 0.61 | 0.00 | 0.57 |
| 4.00 | 0.76 | 0.76 | 0.00 | 0.77 |
| 5.00 | 1.00 | 1.00 | 0.00 | 0.97 |
| 6.00 | 1.00 | 1.00 | 0.00 | 1.00 |
| 7.00 | 1.00 | 1.00 | 0.00 | 1.00 |
| 8.00 | 1.00 | 1.00 | 0.00 | 1.00 |
| 9.00 | 1.00 | 1.00 | 0.00 | 1.00 |
| 10.00 | 1.00 | 1.00 | 0.00 | 1.00 |
| 11.00 | 0.73 | 0.73 | 0.00 | 0.72 |
| 12.00 | 1.00 | 1.00 | 0.00 | 1.00 |
| 12.10 | 0.80 | 0.80 | 0.00 | 0.82 |
| 12.20 | 0.64 | 0.64 | 0.00 | 0.64 |
| 12.30 | 0.61 | 0.61 | 0.00 | 0.66 |
| 12.40 | 0.63 | 0.63 | 0.00 | 0.69 |
| 12.50 | 0.64 | 0.64 | 0.00 | 0.72 |
| 12.60 | 0.63 | 0.63 | 0.00 | 0.69 |
| 12.70 | 0.61 | 0.61 | 0.00 | 0.66 |
| 12.80 | 0.64 | 0.64 | 0.00 | 0.64 |
| 12.90 | 0.80 | 0.80 | 0.00 | 0.82 |
| 13.00 | 0.95 | 0.95 | 0.00 | 1.00 |

| E = 20 Gpa | | | | |
|---|---|---|---|---|
| **Step** | **F1** | **F2** | **F3** | **F4 = F5** |
| 0.00 | 0.08 | 0.08 | 0.00 | 0.00 |
| 1.00 | 0.20 | 0.20 | 0.00 | 0.12 |
| 2.00 | 0.31 | 0.31 | 0.00 | 0.24 |
| 3.00 | 0.42 | 0.42 | 0.00 | 0.37 |
| 4.00 | 0.53 | 0.53 | 0.00 | 0.51 |
| 5.00 | 0.63 | 0.63 | 0.00 | 0.65 |
| 6.00 | 0.80 | 0.80 | 0.00 | 0.80 |
| 7.00 | 0.99 | 0.99 | 0.00 | 0.95 |
| 8.00 | 1.00 | 1.00 | 0.00 | 1.00 |
| 9.00 | 1.00 | 1.00 | 0.00 | 1.00 |
| 10.00 | 1.00 | 1.00 | 0.00 | 1.00 |
| 11.00 | 0.47 | 0.47 | 0.00 | 0.42 |
| 12.00 | 0.52 | 0.52 | 0.00 | 0.41 |
| 12.10 | 0.42 | 0.42 | 0.00 | 0.30 |
| 12.20 | 0.32 | 0.32 | 0.00 | 0.27 |
| 12.30 | 0.25 | 0.25 | 0.00 | 0.29 |
| 12.40 | 0.36 | 0.36 | 0.00 | 0.32 |
| 12.50 | 0.47 | 0.47 | 0.00 | 0.42 |
| 12.60 | 0.36 | 0.36 | 0.00 | 0.32 |
| 12.70 | 0.25 | 0.25 | 0.00 | 0.29 |
| 12.80 | 0.32 | 0.32 | 0.00 | 0.27 |
| 12.90 | 0.42 | 0.42 | 0.00 | 0.30 |
| 13.00 | 0.52 | 0.52 | 0.00 | 0.41 |

**Table 15 - $\chi_{max}$ - Effect of differential pore pressure in the reservoir compartments**

| $\Delta P_1$ = -100 bar; $\Delta P_2$ = 0 bar | | | | |
|---|---|---|---|---|
| **Step** | **F1** | **F2** | **F3** | **F4 = F5** |
| 0.00 | 0.08 | 0.08 | 0.00 | 0.00 |
| 1.00 | 0.25 | 0.25 | 0.00 | 0.16 |
| 2.00 | 0.40 | 0.40 | 0.00 | 0.33 |
| 3.00 | 0.54 | 0.54 | 0.00 | 0.50 |
| 4.00 | 0.67 | 0.67 | 0.00 | 0.68 |
| 5.00 | 0.88 | 0.88 | 0.00 | 0.86 |
| 6.00 | 1.00 | 1.00 | 0.00 | 1.00 |
| 7.00 | 1.00 | 1.00 | 0.00 | 1.00 |
| 8.00 | 1.00 | 1.00 | 0.00 | 1.00 |
| 9.00 | 1.00 | 1.00 | 0.00 | 1.00 |
| 10.00 | 1.00 | 1.00 | 0.00 | 1.00 |
| 11.00 | 0.52 | 0.52 | 0.00 | 0.57 |
| 12.00 | 0.89 | 0.89 | 0.00 | 0.79 |
| 12.10 | 0.76 | 0.89 | 0.14 | 0.79 |
| 12.20 | 0.63 | 0.89 | 0.28 | 0.79 |
| 12.30 | 0.48 | 0.89 | 0.43 | 0.79 |
| 12.40 | 0.49 | 0.89 | 0.59 | 0.78 |
| 12.50 | 0.52 | 0.89 | 0.75 | 0.78 |
| 12.60 | 0.49 | 0.89 | 0.59 | 0.78 |
| 12.70 | 0.48 | 0.89 | 0.43 | 0.79 |
| 12.80 | 0.63 | 0.89 | 0.28 | 0.79 |
| 12.90 | 0.76 | 0.89 | 0.14 | 0.79 |
| 13.00 | 0.89 | 0.89 | 0.00 | 0.79 |

| $\Delta P1$ = -100 bar; $\Delta P2$ = -200 bar | | | | |
|---|---|---|---|---|
| **Step** | **F1** | **F2** | **F3** | **F4 = F5** |
| 0.00 | 0.08 | 0.08 | 0.00 | 0.00 |
| 1.00 | 0.25 | 0.25 | 0.00 | 0.16 |
| 2.00 | 0.40 | 0.40 | 0.00 | 0.33 |
| 3.00 | 0.54 | 0.54 | 0.00 | 0.50 |
| 4.00 | 0.67 | 0.67 | 0.00 | 0.68 |
| 5.00 | 0.88 | 0.88 | 0.00 | 0.86 |
| 6.00 | 1.00 | 1.00 | 0.00 | 1.00 |
| 7.00 | 1.00 | 1.00 | 0.00 | 1.00 |
| 8.00 | 1.00 | 1.00 | 0.00 | 1.00 |
| 9.00 | 1.00 | 1.00 | 0.00 | 1.00 |
| 10.00 | 1.00 | 1.00 | 0.00 | 1.00 |
| 11.00 | 0.52 | 0.52 | 0.00 | 0.57 |
| 12.00 | 0.89 | 0.89 | 0.00 | 0.79 |
| 12.10 | 0.76 | 0.63 | 0.14 | 0.64 |
| 12.20 | 0.63 | 0.49 | 0.31 | 0.52 |
| 12.30 | 0.48 | 0.55 | 0.49 | 0.62 |
| 12.40 | 0.49 | 0.74 | 0.69 | 0.73 |
| 12.50 | 0.52 | 0.95 | 0.92 | 0.95 |
| 12.60 | 0.49 | 0.74 | 0.69 | 0.73 |
| 12.70 | 0.48 | 0.55 | 0.49 | 0.62 |
| 12.80 | 0.63 | 0.49 | 0.31 | 0.52 |
| 12.90 | 0.76 | 0.63 | 0.14 | 0.64 |
| 13.00 | 0.89 | 0.89 | 0.00 | 0.79 |

**Table 16 - $\chi_{max}$ - Effect of salt caprock**

| salt caprock | | | | |
|---|---|---|---|---|
| **Step** | **F1** | **F2** | **F3** | **F4 = F5** |
| 0.00 | 0.00 | 0.00 | 0.00 | 0.00 |
| 1.00 | 0.23 | 0.23 | 0.00 | 0.24 |
| 2.00 | 0.47 | 0.47 | 0.00 | 0.48 |
| 3.00 | 0.76 | 0.76 | 0.00 | 0.76 |
| 4.00 | 1.00 | 1.00 | 0.00 | 1.00 |
| 5.00 | 1.00 | 1.00 | 0.00 | 1.00 |
| 6.00 | 1.00 | 1.00 | 0.00 | 1.00 |
| 7.00 | 1.00 | 1.00 | 0.00 | 1.00 |
| 8.00 | 1.00 | 1.00 | 0.00 | 1.00 |
| 9.00 | 1.00 | 1.00 | 0.00 | 1.00 |
| 10.00 | 1.00 | 1.00 | 0.00 | 1.00 |
| 11.00 | 0.67 | 0.67 | 0.00 | 0.84 |
| 12.00 | 1.00 | 1.00 | 0.00 | 1.00 |
| 12.10 | 0.73 | 0.73 | 0.00 | 0.69 |
| 12.20 | 0.52 | 0.52 | 0.00 | 0.45 |
| 12.30 | 0.76 | 0.76 | 0.00 | 0.82 |
| 12.40 | 0.98 | 0.98 | 0.00 | 1.00 |
| 12.50 | 1.00 | 1.00 | 0.00 | 1.00 |
| 12.60 | 0.68 | 0.68 | 0.00 | 0.62 |
| 12.70 | 0.44 | 0.44 | 0.00 | 0.40 |
| 12.80 | 0.54 | 0.54 | 0.00 | 0.48 |
| 12.90 | 0.76 | 0.76 | 0.00 | 0.73 |
| 13.00 | 0.99 | 0.99 | 0.00 | 1.00 |

**Table 17 $\chi_{max}$ – Mechanism 1 (mechanical hysteresis)**

| **Step** | **F1** | **F2** | **F3** | **F4 = F5** |
|---|---|---|---|---|
| 0.00 | 0.08 | 0.08 | 0.00 | 0.00 |
| 1.00 | 0.25 | 0.25 | 0.00 | 0.17 |
| 2.00 | 0.41 | 0.41 | 0.00 | 0.34 |
| 3.00 | 0.55 | 0.55 | 0.00 | 0.51 |
| 4.00 | 0.69 | 0.69 | 0.00 | 0.70 |
| 5.00 | 0.90 | 0.90 | 0.00 | 0.88 |
| 6.00 | 1.00 | 1.00 | 0.00 | 1.00 |
| 7.00 | 1.00 | 1.00 | 0.00 | 1.00 |
| 8.00 | 1.00 | 1.00 | 0.00 | 1.00 |
| 9.00 | 1.00 | 1.00 | 0.00 | 1.00 |
| 10.00 | 1.00 | 1.00 | 0.00 | 1.00 |
| 11.00 | 0.56 | 0.56 | 0.00 | 0.59 |
| 12.00 | 0.93 | 0.93 | 0.00 | 0.83 |
| 12.10 | 0.80 | 0.80 | 0.00 | 0.67 |
| 12.20 | 0.66 | 0.66 | 0.00 | 0.51 |
| 12.30 | 0.51 | 0.51 | 0.00 | 0.51 |
| 12.40 | 0.53 | 0.53 | 0.00 | 0.54 |
| 12.50 | 0.56 | 0.56 | 0.00 | 0.59 |
| 12.60 | 0.53 | 0.53 | 0.00 | 0.54 |
| 12.70 | 0.51 | 0.51 | 0.00 | 0.51 |
| 12.80 | 0.66 | 0.66 | 0.00 | 0.51 |
| 12.90 | 0.80 | 0.80 | 0.00 | 0.67 |
| 13.00 | 0.93 | 0.93 | 0.00 | 0.83 |

**Table 18 - $\chi_{max}$ - Mechanism 2 (pore pressure distribution in the reservoir)**

| Step | F1 | F2 | F3 | F4 = F5 |
|---|---|---|---|---|
| 0.00 | 0.08 | 0.08 | 0.00 | 0.00 |
| 1.00 | 0.25 | 0.25 | 0.00 | 0.16 |
| 2.00 | 0.40 | 0.40 | 0.00 | 0.33 |
| 3.00 | 0.54 | 0.54 | 0.00 | 0.50 |
| 4.00 | 0.67 | 0.67 | 0.00 | 0.68 |
| 5.00 | 0.88 | 0.88 | 0.00 | 0.86 |
| 6.00 | 1.00 | 1.00 | 0.00 | 1.00 |
| 7.00 | 1.00 | 1.00 | 0.00 | 1.00 |
| 8.00 | 1.00 | 1.00 | 0.00 | 1.00 |
| 9.00 | 1.00 | 1.00 | 0.00 | 1.00 |
| 10.00 | 1.00 | 1.00 | 0.00 | 1.00 |
| 11.00 | 0.52 | 0.52 | 0.00 | 0.57 |
| 12.00 | 0.89 | 0.89 | 0.00 | 0.79 |
| 12.10 | 0.86 | 0.86 | 0.01 | 0.75 |
| 12.20 | 0.72 | 0.72 | 0.04 | 0.58 |
| 12.30 | 0.49 | 0.48 | 0.08 | 0.52 |
| 12.40 | 0.52 | 0.52 | 0.03 | 0.56 |
| 12.50 | 0.52 | 0.52 | 0.00 | 0.56 |
| 12.60 | 0.51 | 0.51 | 0.03 | 0.54 |
| 12.70 | 0.48 | 0.48 | 0.04 | 0.49 |
| 12.80 | 0.63 | 0.62 | 0.04 | 0.52 |
| 12.90 | 0.78 | 0.77 | 0.03 | 0.68 |
| 13.00 | 0.86 | 0.86 | 0.01 | 0.76 |

**Table 19 - $\chi_{max}$ - Mechanism 3D (fault lubrification)**

| Mech 3 D | | | | |
|---|---|---|---|---|
| **Step** | **F1** | **F2** | **F3** | **F4 = F5** |
| 12.00 | 0.08 | 0.08 | 0.00 | 0.00 |
| 12.10 | 0.25 | 0.40 | 0.13 | 0.33 |
| 12.20 | 0.40 | 0.67 | 0.25 | 0.68 |
| 12.30 | 0.54 | 1.00 | 0.36 | 1.00 |
| 12.40 | 0.67 | 1.00 | 0.47 | 1.00 |
| 12.50 | 0.88 | 1.00 | 0.57 | 1.00 |
| 12.60 | 0.67 | 0.75 | 0.47 | 0.75 |
| 12.70 | 0.54 | 0.55 | 0.37 | 0.62 |
| 12.80 | 0.40 | 0.49 | 0.26 | 0.52 |
| 12.90 | 0.25 | 0.63 | 0.13 | 0.48 |
| 13.00 | 0.08 | 0.89 | 0.00 | 0.79 |

**Table 20 - $\chi_{max}$ - Reference test case with fault pressure depletion**

| REFERENCE_PF | | | | |
|---|---|---|---|---|
| **Step** | **F1** | **F2** | **F3** | **F4 = F5** |
| 0.00 | 0.08 | 0.08 | 0.00 | 0.00 |
| 1.00 | 0.24 | 0.24 | 0.00 | 0.16 |
| 2.00 | 0.37 | 0.37 | 0.00 | 0.30 |
| 3.00 | 0.48 | 0.48 | 0.00 | 0.44 |
| 4.00 | 0.58 | 0.58 | 0.00 | 0.57 |
| 5.00 | 0.68 | 0.68 | 0.00 | 0.70 |
| 6.00 | 0.83 | 0.83 | 0.00 | 0.82 |
| 7.00 | 0.97 | 0.97 | 0.00 | 0.93 |
| 8.00 | 1.00 | 1.00 | 0.00 | 1.00 |
| 9.00 | 1.00 | 1.00 | 0.00 | 1.00 |
| 10.00 | 1.00 | 1.00 | 0.00 | 1.00 |
| 11.00 | 0.67 | 0.67 | 0.00 | 0.59 |
| 12.00 | 0.51 | 0.51 | 0.00 | 0.37 |
| 12.10 | 0.35 | 0.35 | 0.00 | 0.22 |
| 12.20 | 0.37 | 0.37 | 0.00 | 0.27 |
| 12.30 | 0.48 | 0.48 | 0.00 | 0.38 |
| 12.40 | 0.58 | 0.58 | 0.00 | 0.49 |
| 12.50 | 0.67 | 0.67 | 0.00 | 0.59 |
| 12.60 | 0.58 | 0.58 | 0.00 | 0.49 |
| 12.70 | 0.48 | 0.48 | 0.00 | 0.38 |
| 12.80 | 0.37 | 0.37 | 0.00 | 0.27 |
| 12.90 | 0.35 | 0.35 | 0.00 | 0.22 |
| 13.00 | 0.51 | 0.51 | 0.00 | 0.37 |

**Table 21 $\chi_{max}$ – Mechanism 4 (pore pressure variation versus time)**

| Mech 04 | | | | |
|---|---|---|---|---|
| **Step** | **F1** | **F2** | **F3** | **F4 = F5** |
| 0.00 | 0.08 | 0.08 | 0.00 | 0.00 |
| 1.00 | 0.25 | 0.25 | 0.00 | 0.16 |
| 2.00 | 0.40 | 0.40 | 0.00 | 0.33 |
| 3.00 | 0.54 | 0.54 | 0.00 | 0.50 |
| 4.00 | 0.67 | 0.67 | 0.00 | 0.68 |
| 5.00 | 0.88 | 0.88 | 0.00 | 0.86 |
| 6.00 | 1.00 | 1.00 | 0.00 | 1.00 |
| 7.00 | 1.00 | 1.00 | 0.00 | 1.00 |
| 8.00 | 1.00 | 1.00 | 0.00 | 1.00 |
| 9.00 | 1.00 | 1.00 | 0.00 | 1.00 |
| 10.00 | 1.00 | 1.00 | 0.00 | 1.00 |
| 11.00 | 0.52 | 0.52 | 0.00 | 0.57 |
| 12.00 | 0.89 | 0.89 | 0.00 | 0.79 |
| 12.10 | 0.70 | 0.70 | 0.00 | 0.56 |
| 12.20 | 0.48 | 0.48 | 0.00 | 0.48 |
| 12.30 | 0.51 | 0.51 | 0.00 | 0.54 |
| 12.40 | 0.55 | 0.55 | 0.00 | 0.62 |
| 12.50 | 0.69 | 0.69 | 0.00 | 0.70 |
| 12.60 | 0.55 | 0.55 | 0.00 | 0.62 |
| 12.70 | 0.51 | 0.51 | 0.00 | 0.54 |
| 12.80 | 0.48 | 0.48 | 0.00 | 0.48 |
| 12.90 | 0.70 | 0.70 | 0.00 | 0.56 |
| 13.00 | 0.89 | 0.89 | 0.00 | 0.79 |

## Annex II - $t_a$, $t_{80}$, and $t_{50}$

The critically stressed fault area is normalized over the fault length, thus in the following tables the active thickness $t_a$, the fault thickness with $\chi > 0.8$ ($t_{80}$) and $\chi > 0.5$ ($t_{50}$) are reported for each model simulation, fault and loading step. The IE element in the reservoir is 100m-wide by 20m-thick. Therefore, when a new row of elements is activated, a 20m-thickness is added to the cumulative active thickness $t_a$. Due to fault boundary and fixed normalization factor, the computed thickness at activation of a new row might be slightly lower than 20 m. Note that, in the tables, the notation * indicates that a new row is actually sliding even if $t_a \ll 20$ and ** highlights that on the same row new elements start sliding.

**Table 22 - $t_a$ – Reference test case**

| Reference test case | | | | |
|---|---|---|---|---|
| **Step** | **F1** | **F2** | **F3** | **F4 = F5** |
| 0.00 | 0.00 | 0.00 | 0.00 | 0.00 |
| 1.00 | 0.00 | 0.00 | 0.00 | 0.00 |
| 2.00 | 0.00 | 0.00 | 0.00 | 0.00 |
| 3.00 | 0.00 | 0.00 | 0.00 | 0.00 |
| 4.00 | 0.00 | 0.00 | 0.00 | 0.00 |
| 5.00 | 0.00 | 0.00 | 0.00 | 0.00 |
| 6.00 | 17.27 | 17.27 | 0.00 | 19.34 |
| 7.00 | 13.2* | 13.2* | 0.00 | 16.55* |
| 8.00 | 4.06** | 4.06** | 0.00 | 3.11** |
| 9.00 | 0.00 | 0.00 | 0.00 | 0.00 |
| 10.00 | 0.00 | 0.00 | 0.00 | 0.00 |
| 11.00 | 0.00 | 0.00 | 0.00 | 0.00 |
| 12.00 | 0.00 | 0.00 | 0.00 | 0.00 |
| 12.10 | 0.00 | 0.00 | 0.00 | 0.00 |
| 12.20 | 0.00 | 0.00 | 0.00 | 0.00 |
| 12.30 | 0.00 | 0.00 | 0.00 | 0.00 |
| 12.40 | 0.00 | 0.00 | 0.00 | 0.00 |
| 12.50 | 0.00 | 0.00 | 0.00 | 0.00 |
| 12.60 | 0.00 | 0.00 | 0.00 | 0.00 |
| 12.70 | 0.00 | 0.00 | 0.00 | 0.00 |
| 12.80 | 0.00 | 0.00 | 0.00 | 0.00 |
| 12.90 | 0.00 | 0.00 | 0.00 | 0.00 |
| 13.00 | 0.00 | 0.00 | 0.00 | 0.00 |

**Table 23 – $t_{50}$ – Reference test case**

| Reference test case | | | | |
|---|---|---|---|---|
| **Step** | **F1** | **F2** | **F3** | **F4 = F5** |
| 0.00 | 0.00 | 0.00 | 0.00 | 0.00 |
| 1.00 | 0.00 | 0.00 | 0.00 | 0.00 |
| 2.00 | 0.00 | 0.00 | 0.00 | 0.00 |
| 3.00 | 17.27 | 17.27 | 0.00 | 0.00 |
| 4.00 | 34.53 | 34.53 | 0.00 | 39.00 |
| 5.00 | 34.53 | 34.53 | 0.00 | 39.00 |
| 6.00 | 34.53 | 34.53 | 0.00 | 39.00 |
| 7.00 | 34.53 | 34.53 | 0.00 | 39.00 |
| 8.00 | 34.53 | 34.53 | 0.00 | 57.40 |
| 9.00 | 86.31 | 86.31 | 0.00 | 76.72 |
| 10.00 | 103.58 | 103.58 | 0.00 | 112.31 |
| 11.00 | 23.36 | 23.36 | 0.00 | 37.73 |
| 12.00 | 17.27 | 17.27 | 0.00 | 34.86 |
| 12.10 | 17.27 | 17.27 | 0.00 | 19.34 |
| 12.20 | 17.27 | 17.27 | 0.00 | 0.00 |
| 12.30 | 0.00 | 0.00 | 0.00 | 0.00 |
| 12.40 | 0.00 | 0.00 | 0.00 | 35.80 |
| 12.50 | 23.36 | 23.36 | 0.00 | 37.73 |
| 12.60 | 0.00 | 0.00 | 0.00 | 35.80 |
| 12.70 | 0.00 | 0.00 | 0.00 | 0.00 |
| 12.80 | 17.27 | 17.27 | 0.00 | 0.00 |
| 12.90 | 17.27 | 17.27 | 0.00 | 19.34 |
| 13.00 | 17.27 | 17.27 | 0.00 | 34.86 |

**Table 24 – $t_{80}$ – Reference test case**

| Reference test case | | | | |
|---|---|---|---|---|
| **Step** | **F1** | **F2** | **F3** | **F4 = F5** |
| 0.00 | 0.00 | 0.00 | 0.00 | 0.00 |
| 1.00 | 0.00 | 0.00 | 0.00 | 0.00 |
| 2.00 | 0.00 | 0.00 | 0.00 | 0.00 |
| 3.00 | 0.00 | 0.00 | 0.00 | 0.00 |
| 4.00 | 0.00 | 0.00 | 0.00 | 0.00 |
| 5.00 | 17.27 | 17.27 | 0.00 | 19.34 |
| 6.00 | 34.53 | 34.53 | 0.00 | 39.00 |
| 7.00 | 34.53 | 34.53 | 0.00 | 39.00 |
| 8.00 | 34.53 | 34.53 | 0.00 | 39.00 |
| 9.00 | 34.53 | 34.53 | 0.00 | 39.00 |
| 10.00 | 34.53 | 34.53 | 0.00 | 57.40 |
| 11.00 | 0.00 | 0.00 | 0.00 | 0.00 |
| 12.00 | 17.27 | 17.27 | 0.00 | 0.00 |
| 12.10 | 0.00 | 0.00 | 0.00 | 0.00 |
| 12.20 | 0.00 | 0.00 | 0.00 | 0.00 |
| 12.30 | 0.00 | 0.00 | 0.00 | 0.00 |
| 12.40 | 0.00 | 0.00 | 0.00 | 0.00 |
| 12.50 | 0.00 | 0.00 | 0.00 | 0.00 |
| 12.60 | 0.00 | 0.00 | 0.00 | 0.00 |
| 12.70 | 0.00 | 0.00 | 0.00 | 0.00 |
| 12.80 | 0.00 | 0.00 | 0.00 | 0.00 |
| 12.90 | 0.00 | 0.00 | 0.00 | 0.00 |
| 13.00 | 17.27 | 17.27 | 0.00 | 0.00 |

**Table 25 - $t_a$ - Effect of reservoir and fault geometry**

| dip = 65° | | | | |
|---|---|---|---|---|
| **Step** | **F1** | **F2** | **F3** | **F4 = F5** |
| 0.00 | 0.0 | 0.0 | 0.0 | 0.0 |
| 1.00 | 0.0 | 0.0 | 0.0 | 0.0 |
| 2.00 | 0.0 | 0.0 | 0.0 | 0.0 |
| 3.00 | 0.0 | 0.0 | 0.0 | 0.0 |
| 4.00 | 0.0 | 0.0 | 0.0 | 0.0 |
| 5.00 | 0.0 | 0.0 | 0.0 | 0.0 |
| 6.00 | 17.3 | 17.3 | 0.0 | 19.3 |
| 7.00 | 13.2* | 13.2* | 0.0 | 15.6* |
| 8.00 | 4.1** | 4.1** | 0.0 | 4.1** |
| 9.00 | 0.0 | 0.0 | 0.0 | 0.0 |
| 10.00 | 0.0 | 0.0 | 168.8 | 0.0 |
| 11.00 | 0.0 | 0.0 | 0.0 | 0.0 |
| 12.00 | 0.0 | 0.0 | 0.0 | 0.0 |
| 12.10 | 0.0 | 0.0 | 0.0 | 0.0 |
| 12.20 | 0.0 | 0.0 | 0.0 | 0.0 |
| 12.30 | 0.0 | 0.0 | 0.0 | 0.0 |
| 12.40 | 0.0 | 0.0 | 0.0 | 0.0 |
| 12.50 | 0.0 | 0.0 | 0.0 | 0.0 |
| 12.60 | 0.0 | 0.0 | 0.0 | 0.0 |
| 12.70 | 0.0 | 0.0 | 0.0 | 0.0 |
| 12.80 | 0.0 | 0.0 | 0.0 | 0.0 |
| 12.90 | 0.0 | 0.0 | 0.0 | 0.0 |
| 13.00 | 0.0 | 0.0 | 0.0 | 0.0 |

| dip = - 65° | | | | |
|---|---|---|---|---|
| **Step** | **F1** | **F2** | **F3** | **F4 = F5** |
| 0.00 | 0.00 | 0.00 | 0.00 | 0.00 |
| 1.00 | 0.00 | 0.00 | 0.00 | 0.00 |
| 2.00 | 0.00 | 0.00 | 0.00 | 0.00 |
| 3.00 | 0.00 | 0.00 | 0.00 | 0.00 |
| 4.00 | 0.00 | 0.00 | 0.00 | 0.00 |
| 5.00 | 0.00 | 0.00 | 0.00 | 0.00 |
| 6.00 | 17.27 | 17.27 | 0.00 | 19.33 |
| 7.00 | 13.2* | 13.2* | 0.00 | 15.6* |
| 8.00 | 4.06** | 4.06** | 0.00 | 4.07** |
| 9.00 | 0.00 | 0.00 | 0.00 | 0.00 |
| 10.00 | 0.00 | 0.00 | 168.82 | 0.00 |
| 11.00 | 0.00 | 0.00 | 0.00 | 0.00 |
| 12.00 | 0.00 | 0.00 | 0.00 | 0.00 |
| 12.10 | 0.00 | 0.00 | 0.00 | 0.00 |
| 12.20 | 0.00 | 0.00 | 0.00 | 0.00 |
| 12.30 | 0.00 | 0.00 | 0.00 | 0.00 |
| 12.40 | 0.00 | 0.00 | 0.00 | 0.00 |
| 12.50 | 0.00 | 0.00 | 0.00 | 0.00 |
| 12.60 | 0.00 | 0.00 | 0.00 | 0.00 |
| 12.70 | 0.00 | 0.00 | 0.00 | 0.00 |
| 12.80 | 0.00 | 0.00 | 0.00 | 0.00 |
| 12.90 | 0.00 | 0.00 | 0.00 | 0.00 |
| 13.00 | 0.00 | 0.00 | 0.00 | 0.00 |

| dislocation = 100 m | | | | |
|---|---|---|---|---|
| **Step** | **F1** | **F2** | **F3** | **F4 = F5** |
| 0.00 | 0.00 | 0.00 | 0.00 | 0.00 |
| 1.00 | 0.00 | 0.00 | 0.00 | 0.00 |
| 2.00 | 0.00 | 0.00 | 0.00 | 0.00 |
| 3.00 | 0.00 | 0.00 | 0.00 | 0.00 |
| 4.00 | 0.00 | 0.00 | 0.00 | 0.00 |
| 5.00 | 0.00 | 0.00 | 15.00 | 0.00 |
| 6.00 | 17.27 | 17.27 | 19.00 | 18.76 |
| 7.00 | 13.2* | 17.26 | 29.00 | 16.53* |
| 8.00 | 4.06** | 0.00 | 37.00 | 2.55** |
| 9.00 | 0.00 | 0.00 | 60.00 | 0.00 |
| 10.00 | 0.00 | 0.00 | 25.00 | 0.50 |
| 11.00 | 0.00 | 0.00 | 0.00 | 0.00 |
| 12.00 | 0.00 | 0.00 | 17.00 | 0.00 |
| 12.10 | 0.00 | 0.00 | 0.00 | 0.00 |
| 12.20 | 0.00 | 0.00 | 0.00 | 0.00 |
| 12.30 | 0.00 | 0.00 | 0.00 | 0.00 |
| 12.40 | 0.00 | 0.00 | 0.00 | 0.00 |
| 12.50 | 0.00 | 0.00 | 0.00 | 0.00 |
| 12.60 | 0.00 | 0.00 | 0.00 | 0.00 |
| 12.70 | 0.00 | 0.00 | 0.00 | 0.00 |
| 12.80 | 0.00 | 0.00 | 0.00 | 0.00 |
| 12.90 | 0.00 | 0.00 | 0.00 | 0.00 |
| 13.00 | 0.00 | 0.00 | 0.00 | 0.00 |

| dislocation = 200 m | | | | |
|---|---|---|---|---|
| **Step** | **F1** | **F2** | **F3** | **F4 = F5** |
| 0.00 | 0.00 | 0.00 | 0.00 | 0.00 |
| 1.00 | 0.00 | 0.00 | 0.00 | 0.00 |
| 2.00 | 0.00 | 0.00 | 0.00 | 0.00 |
| 3.00 | 0.00 | 0.00 | 11.00 | 0.00 |
| 4.00 | 0.00 | 0.00 | 6.00 | 0.00 |
| 5.00 | 0.00 | 0.00 | 0.00 | 0.00 |
| 6.00 | 17.27 | 17.26 | 28.00 | 18.18 |
| 7.00 | 13.2* | 17.27 | 55.00 | 16.95* |
| 8.00 | 4.06** | 0.00 | 32.00 | 2.55** |
| 9.00 | 0.00 | 0.00 | 32.00 | 0.00 |
| 10.00 | 0.00 | 15.23* | 32.00 | 8.83 |
| 11.00 | 0.00 | 0.00 | 0.00 | 0.00 |
| 12.00 | 0.00 | 17.26 | 17.00 | 0.00 |
| 12.10 | 0.00 | 0.00 | 0.00 | 0.00 |
| 12.20 | 0.00 | 0.00 | 0.00 | 0.00 |
| 12.30 | 0.00 | 0.00 | 0.00 | 0.00 |
| 12.40 | 0.00 | 0.00 | 0.00 | 0.00 |
| 12.50 | 0.00 | 0.00 | 0.00 | 0.00 |
| 12.60 | 0.00 | 0.00 | 0.00 | 0.00 |
| 12.70 | 0.00 | 0.00 | 0.00 | 0.00 |
| 12.80 | 0.00 | 0.00 | 0.00 | 0.00 |
| 12.90 | 0.00 | 0.00 | 0.00 | 0.00 |
| 13.00 | 0.00 | 0.00 | 0.00 | 0.00 |

**Table 26 – $t_{50}$ - Effect of reservoir and fault geometry**

| dip = 65° | | | | |
|---|---|---|---|---|
| **Step** | **F1** | **F2** | **F3** | **F4 = F5** |
| 0.00 | 0.0 | 0.0 | 0.0 | 0.0 |
| 1.00 | 0.0 | 0.0 | 0.0 | 0.0 |
| 2.00 | 0.0 | 0.0 | 0.0 | 0.0 |
| 3.00 | 17.3 | 17.3 | 0.0 | 0.0 |
| 4.00 | 34.5 | 34.5 | 0.0 | 39.0 |
| 5.00 | 34.5 | 34.5 | 0.0 | 39.0 |
| 6.00 | 34.5 | 34.5 | 168.8 | 39.0 |
| 7.00 | 34.5 | 34.5 | 168.8 | 39.0 |
| 8.00 | 34.5 | 34.5 | 168.8 | 57.4 |
| 9.00 | 86.3 | 86.3 | 168.8 | 76.7 |
| 10.00 | 103.6 | 103.6 | 204.1 | 112.4 |
| 11.00 | 32.5 | 32.5 | 14.3 | 37.7 |
| 12.00 | 17.3 | 17.3 | 0.0 | 34.9 |
| 12.10 | 17.3 | 17.3 | 0.0 | 19.3 |
| 12.20 | 17.3 | 17.3 | 0.0 | 0.0 |
| 12.30 | 0.0 | 0.0 | 7.7 | 0.0 |
| 12.40 | 0.0 | 0.0 | 12.1 | 35.7 |
| 12.50 | 32.5 | 32.5 | 14.3 | 37.7 |
| 12.60 | 0.0 | 0.0 | 12.1 | 35.7 |
| 12.70 | 0.0 | 0.0 | 7.7 | 0.0 |
| 12.80 | 17.3 | 17.3 | 0.0 | 0.0 |
| 12.90 | 17.3 | 17.3 | 0.0 | 19.3 |
| 13.00 | 17.3 | 17.3 | 0.0 | 34.9 |

| dip = - 65° | | | | |
|---|---|---|---|---|
| **Step** | **F1** | **F2** | **F3** | **F4 = F5** |
| 0.00 | 0.00 | 0.00 | 0.00 | 0.00 |
| 1.00 | 0.00 | 0.00 | 0.00 | 0.00 |
| 2.00 | 0.00 | 0.00 | 0.00 | 0.00 |
| 3.00 | 17.27 | 17.27 | 0.00 | 8.21 |
| 4.00 | 34.53 | 34.53 | 0.00 | 39.00 |
| 5.00 | 34.53 | 34.53 | 0.00 | 39.00 |
| 6.00 | 34.53 | 34.53 | 168.82 | 39.00 |
| 7.00 | 34.53 | 34.53 | 168.82 | 39.00 |
| 8.00 | 34.53 | 34.53 | 168.82 | 57.38 |
| 9.00 | 86.31 | 86.31 | 168.82 | 76.20 |
| 10.00 | 103.58 | 103.58 | 204.13 | 112.40 |
| 11.00 | 32.49 | 32.49 | 14.34 | 37.20 |
| 12.00 | 17.27 | 17.27 | 0.00 | 34.93 |
| 12.10 | 17.27 | 17.27 | 0.00 | 19.33 |
| 12.20 | 17.27 | 17.27 | 0.00 | 0.00 |
| 12.30 | 0.00 | 0.00 | 0.00 | 0.00 |
| 12.40 | 0.00 | 0.00 | 9.93 | 27.07 |
| 12.50 | 32.49 | 32.49 | 14.34 | 37.20 |
| 12.60 | 0.00 | 0.00 | 9.93 | 27.07 |
| 12.70 | 0.00 | 0.00 | 0.00 | 0.00 |
| 12.80 | 17.27 | 17.27 | 0.00 | 0.00 |
| 12.90 | 17.27 | 17.27 | 0.00 | 19.33 |
| 13.00 | 17.27 | 17.27 | 0.00 | 34.93 |

| dislocation = 100 m | | | | |
|---|---|---|---|---|
| **Step** | **F1** | **F2** | **F3** | **F4 = F5** |
| 0.00 | 0.00 | 0.00 | 0.00 | 0.00 |
| 1.00 | 0.00 | 0.00 | 0.00 | 0.00 |
| 2.00 | 0.00 | 0.00 | 0.00 | 0.00 |
| 3.00 | 17.27 | 17.26 | 17.00 | 10.34 |
| 4.00 | 34.53 | 34.52 | 68.00 | 37.84 |
| 5.00 | 34.53 | 34.52 | 68.00 | 38.34 |
| 6.00 | 34.53 | 34.52 | 77.00 | 39.34 |
| 7.00 | 34.53 | 34.52 | 119.00 | 39.34 |
| 8.00 | 34.53 | 49.76 | 170.00 | 57.15 |
| 9.00 | 86.31 | 95.45 | 185.00 | 76.39 |
| 10.00 | 103.58 | 103.58 | 221.00 | 112.44 |
| 11.00 | 23.36 | 49.76 | 66.00 | 37.55 |
| 12.00 | 17.27 | 30.46 | 51.00 | 34.77 |
| 12.10 | 17.27 | 17.27 | 41.00 | 18.76 |
| 12.20 | 17.27 | 17.27 | 34.00 | 16.78 |
| 12.30 | 0.00 | 37.57 | 51.00 | 17.75 |
| 12.40 | 0.00 | 43.66 | 45.00 | 34.58 |
| 12.50 | 23.36 | 49.76 | 49.00 | 37.55 |
| 12.60 | 0.00 | 43.66 | 45.00 | 34.58 |
| 12.70 | 0.00 | 37.57 | 51.00 | 17.75 |
| 12.80 | 17.27 | 17.27 | 34.00 | 16.78 |
| 12.90 | 17.27 | 17.27 | 41.00 | 18.76 |
| 13.00 | 17.27 | 30.46 | 51.00 | 34.77 |

| dislocation = 200 m | | | | |
|---|---|---|---|---|
| **Step** | **F1** | **F2** | **F3** | **F4 = F5** |
| 0.00 | 0.00 | 0.00 | 0.00 | 0.00 |
| 1.00 | 0.00 | 0.00 | 0.00 | 0.00 |
| 2.00 | 0.00 | 0.00 | 17.00 | 0.00 |
| 3.00 | 17.27 | 17.27 | 32.00 | 17.72 |
| 4.00 | 34.53 | 34.52 | 66.00 | 37.68 |
| 5.00 | 34.53 | 34.52 | 85.00 | 37.68 |
| 6.00 | 34.53 | 34.52 | 102.00 | 38.18 |
| 7.00 | 34.53 | 34.52 | 126.00 | 38.18 |
| 8.00 | 34.53 | 69.06 | 151.00 | 57.91 |
| 9.00 | 86.31 | 103.58 | 196.00 | 87.56 |
| 10.00 | 103.58 | 103.58 | 255.00 | 112.99 |
| 11.00 | 21.33 | 67.02 | 100.00 | 43.87 |
| 12.00 | 17.27 | 35.54 | 79.00 | 42.91 |
| 12.10 | 17.27 | 28.43 | 51.00 | 32.99 |
| 12.20 | 17.27 | 32.49 | 17.00 | 18.51 |
| 12.30 | 0.00 | 49.75 | 17.00 | 19.60 |
| 12.40 | 0.00 | 36.56 | 62.00 | 39.91 |
| 12.50 | 21.33 | 67.02 | 117.00 | 43.87 |
| 12.60 | 0.00 | 36.56 | 62.00 | 39.91 |
| 12.70 | 0.00 | 49.75 | 17.00 | 19.60 |
| 12.80 | 17.27 | 32.49 | 17.00 | 18.51 |
| 12.90 | 17.27 | 28.43 | 51.00 | 32.99 |
| 13.00 | 17.27 | 35.54 | 79.00 | 42.91 |

**Table 27 – $t_{80}$ - Effect of reservoir and fault geometry**

| dip = 65° | | | | |
|---|---|---|---|---|
| **Step** | **F1** | **F2** | **F3** | **F4 = F5** |
| 0.00 | 0.0 | 0.0 | 0.0 | 0.0 |
| 1.00 | 0.0 | 0.0 | 0.0 | 0.0 |
| 2.00 | 0.0 | 0.0 | 0.0 | 0.0 |
| 3.00 | 0.0 | 0.0 | 0.0 | 0.0 |
| 4.00 | 0.0 | 0.0 | 0.0 | 0.0 |
| 5.00 | 17.3 | 17.3 | 0.0 | 19.3 |
| 6.00 | 34.5 | 34.5 | 0.0 | 39.0 |
| 7.00 | 34.5 | 34.5 | 0.0 | 39.0 |
| 8.00 | 34.5 | 34.5 | 9.9 | 39.0 |
| 9.00 | 34.5 | 34.5 | 168.8 | 39.0 |
| 10.00 | 34.5 | 34.5 | 168.8 | 57.4 |
| 11.00 | 0.0 | 0.0 | 0.0 | 0.0 |
| 12.00 | 17.3 | 17.3 | 0.0 | 0.0 |
| 12.10 | 0.0 | 0.0 | 0.0 | 0.0 |
| 12.20 | 0.0 | 0.0 | 0.0 | 0.0 |
| 12.30 | 0.0 | 0.0 | 0.0 | 0.0 |
| 12.40 | 0.0 | 0.0 | 0.0 | 0.0 |
| 12.50 | 0.0 | 0.0 | 0.0 | 0.0 |
| 12.60 | 0.0 | 0.0 | 0.0 | 0.0 |
| 12.70 | 0.0 | 0.0 | 0.0 | 0.0 |
| 12.80 | 0.0 | 0.0 | 0.0 | 0.0 |
| 12.90 | 0.0 | 0.0 | 0.0 | 0.0 |
| 13.00 | 17.3 | 17.3 | 0.0 | 0.0 |

| dip = - 65° | | | | |
|---|---|---|---|---|
| **Step** | **F1** | **F2** | **F3** | **F4 = F5** |
| 0.00 | 0.00 | 0.00 | 0.00 | 0.00 |
| 1.00 | 0.00 | 0.00 | 0.00 | 0.00 |
| 2.00 | 0.00 | 0.00 | 0.00 | 0.00 |
| 3.00 | 0.00 | 0.00 | 0.00 | 0.00 |
| 4.00 | 0.00 | 0.00 | 0.00 | 0.00 |
| 5.00 | 17.27 | 17.27 | 0.00 | 19.33 |
| 6.00 | 34.53 | 34.53 | 0.00 | 39.00 |
| 7.00 | 34.53 | 34.53 | 0.00 | 39.00 |
| 8.00 | 34.53 | 34.53 | 0.00 | 39.00 |
| 9.00 | 34.53 | 34.53 | 168.82 | 39.00 |
| 10.00 | 34.53 | 36.56 | 168.82 | 57.38 |
| 11.00 | 0.00 | 0.00 | 0.00 | 0.00 |
| 12.00 | 17.27 | 17.27 | 0.00 | 0.00 |
| 12.10 | 0.00 | 0.00 | 0.00 | 0.00 |
| 12.20 | 0.00 | 0.00 | 0.00 | 0.00 |
| 12.30 | 0.00 | 0.00 | 0.00 | 0.00 |
| 12.40 | 0.00 | 0.00 | 0.00 | 0.00 |
| 12.50 | 0.00 | 0.00 | 0.00 | 0.00 |
| 12.60 | 0.00 | 0.00 | 0.00 | 0.00 |
| 12.70 | 0.00 | 0.00 | 0.00 | 0.00 |
| 12.80 | 0.00 | 0.00 | 0.00 | 0.00 |
| 12.90 | 0.00 | 0.00 | 0.00 | 0.00 |
| 13.00 | 17.27 | 17.27 | 0.00 | 0.00 |

| dislocation = 100 m | | | | |
|---|---|---|---|---|
| **Step** | **F1** | **F2** | **F3** | **F4 = F5** |
| 0.00 | 0.00 | 0.00 | 0.00 | 0.00 |
| 1.00 | 0.00 | 0.00 | 0.00 | 0.00 |
| 2.00 | 0.00 | 0.00 | 0.00 | 0.00 |
| 3.00 | 0.00 | 0.00 | 0.00 | 0.00 |
| 4.00 | 0.00 | 0.00 | 11.00 | 0.00 |
| 5.00 | 17.27 | 32.49 | 39.00 | 19.76 |
| 6.00 | 34.53 | 34.52 | 68.00 | 37.84 |
| 7.00 | 34.53 | 34.52 | 68.00 | 37.84 |
| 8.00 | 34.53 | 34.52 | 119.00 | 38.34 |
| 9.00 | 34.53 | 34.52 | 170.00 | 38.34 |
| 10.00 | 34.53 | 52.81 | 196.00 | 57.15 |
| 11.00 | 0.00 | 0.00 | 0.00 | 0.00 |
| 12.00 | 17.27 | 17.27 | 34.00 | 9.34 |
| 12.10 | 0.00 | 17.27 | 6.00 | 0.00 |
| 12.20 | 0.00 | 0.00 | 0.00 | 0.00 |
| 12.30 | 0.00 | 0.00 | 0.00 | 0.00 |
| 12.40 | 0.00 | 0.00 | 0.00 | 0.00 |
| 12.50 | 0.00 | 0.00 | 0.00 | 0.00 |
| 12.60 | 0.00 | 0.00 | 0.00 | 0.00 |
| 12.70 | 0.00 | 0.00 | 0.00 | 0.00 |
| 12.80 | 0.00 | 0.00 | 0.00 | 0.00 |
| 12.90 | 0.00 | 17.27 | 6.00 | 0.00 |
| 13.00 | 17.27 | 17.27 | 34.00 | 9.34 |

| dislocation = 200 m | | | | |
|---|---|---|---|---|
| **Step** | **F1** | **F2** | **F3** | **F4 = F5** |
| 0.00 | 0.00 | 0.00 | 0.00 | 0.00 |
| 1.00 | 0.00 | 0.00 | 0.00 | 0.00 |
| 2.00 | 0.00 | 0.00 | 0.00 | 0.00 |
| 3.00 | 0.00 | 0.00 | 17.00 | 0.00 |
| 4.00 | 0.00 | 0.00 | 17.00 | 0.00 |
| 5.00 | 17.27 | 34.52 | 51.00 | 27.14 |
| 6.00 | 34.53 | 34.52 | 85.00 | 37.68 |
| 7.00 | 34.53 | 34.52 | 102.00 | 37.68 |
| 8.00 | 34.53 | 34.52 | 136.00 | 37.68 |
| 9.00 | 34.53 | 34.52 | 168.00 | 46.01 |
| 10.00 | 34.53 | 69.06 | 200.00 | 55.91 |
| 11.00 | 0.00 | 0.00 | 0.00 | 0.00 |
| 12.00 | 17.27 | 17.26 | 32.00 | 9.26 |
| 12.10 | 0.00 | 17.26 | 15.00 | 0.00 |
| 12.20 | 0.00 | 0.00 | 15.00 | 0.00 |
| 12.30 | 0.00 | 0.00 | 11.00 | 0.00 |
| 12.40 | 0.00 | 0.00 | 0.00 | 0.00 |
| 12.50 | 0.00 | 0.00 | 0.00 | 0.00 |
| 12.60 | 0.00 | 0.00 | 0.00 | 0.00 |
| 12.70 | 0.00 | 0.00 | 11.00 | 0.00 |
| 12.80 | 0.00 | 0.00 | 15.00 | 0.00 |
| 12.90 | 0.00 | 17.26 | 15.00 | 0.00 |
| 13.00 | 17.27 | 17.26 | 32.00 | 9.26 |

**Table 28 – $t_a$ - Effect of initial stress regime**

| θ = 90° | | | | | M_1 = 0.40 ; M_2 = 0.47 | | | | |
|---|---|---|---|---|---|---|---|---|---|
| **Step** | **F1** | **F2** | **F3** | **F4 = F5** | **Step** | **F1** | **F2** | **F3** | **F4 = F5** |
| 0.00 | 0.00 | 0.00 | 0.00 | 0.00 | 0.00 | 0.00 | 0.00 | 0.00 | 0.00 |
| 1.00 | 0.00 | 0.00 | 0.00 | 0.00 | 1.00 | 0.00 | 0.00 | 0.00 | 0.00 |
| 2.00 | 0.00 | 0.00 | 0.00 | 0.00 | 2.00 | 0.00 | 0.00 | 0.00 | 0.00 |
| 3.00 | 0.00 | 0.00 | 0.00 | 0.00 | 3.00 | 0.00 | 0.00 | 0.00 | 0.00 |
| 4.00 | 0.00 | 0.00 | 0.00 | 0.00 | 4.00 | 17.27 | 17.27 | 0.00 | 19.34 |
| 5.00 | 0.00 | 0.00 | 0.00 | 0.00 | 5.00 | 17.27 | 17.27 | 0.00 | 19.66 |
| 6.00 | 17.27 | 17.27 | 0.00 | 19.34 | 6.00 | 17.26 | 17.26 | 0.00 | 0.00 |
| 7.00 | 0.00 | 0.00 | 0.00 | 19.66 | 7.00 | 34.52 | 34.52 | 0.00 | 18.4* |
| 8.00 | 15.23* | 15.23* | 0.00 | 0.00 | 8.00 | 17.27 | 17.27 | 0.00 | 19.32 |
| 9.00 | 2.03** | 2.03** | 0.00 | 0.00 | 9.00 | 67.01 | 67.01 | 0.00 | 54.55 |
| 10.00 | 0.00 | 0.00 | 0.00 | 18.40 | 10.00 | 49.76 | 49.76 | 0.00 | 5.13** |
| 11.00 | 0.00 | 0.00 | 0.00 | 0.00 | 11.00 | 0.00 | 0.00 | 0.00 | 0.00 |
| 12.00 | 0.00 | 0.00 | 0.00 | 0.00 | 12.00 | 34.53 | 34.53 | 0.00 | 39.00 |
| 12.10 | 0.00 | 0.00 | 0.00 | 0.00 | 12.10 | 0.00 | 0.00 | 0.00 | 0.00 |
| 12.20 | 0.00 | 0.00 | 0.00 | 0.00 | 12.20 | 0.00 | 0.00 | 0.00 | 0.00 |
| 12.30 | 0.00 | 0.00 | 0.00 | 0.00 | 12.30 | 0.00 | 0.00 | 0.00 | 0.00 |
| 12.40 | 0.00 | 0.00 | 0.00 | 0.00 | 12.40 | 0.00 | 0.00 | 0.00 | 0.00 |
| 12.50 | 0.00 | 0.00 | 0.00 | 0.00 | 12.50 | 0.00 | 0.00 | 0.00 | 0.00 |
| 12.60 | 0.00 | 0.00 | 0.00 | 0.00 | 12.60 | 0.00 | 0.00 | 0.00 | 0.00 |
| 12.70 | 0.00 | 0.00 | 0.00 | 0.00 | 12.70 | 0.00 | 0.00 | 0.00 | 0.00 |
| 12.80 | 0.00 | 0.00 | 0.00 | 0.00 | 12.80 | 0.00 | 0.00 | 0.00 | 0.00 |
| 12.90 | 0.00 | 0.00 | 0.00 | 0.00 | 12.90 | 0.00 | 0.00 | 0.00 | 0.00 |
| 13.00 | 0.00 | 0.00 | 0.00 | 0.00 | 13.00 | 0.00 | 0.00 | 0.00 | 0.00 |

**Table 29 – $t_{50}$ - Effect of initial stress regime**

| θ = 90° | | | | | M_1 = 0.40 ; M_2 = 0.47 | | | | |
|---|---|---|---|---|---|---|---|---|---|
| **Step** | **F1** | **F2** | **F3** | **F4 = F5** | **Step** | **F1** | **F2** | **F3** | **F4 = F5** |
| 0.00 | 0.00 | 0.00 | 0.00 | 0.00 | 0.00 | 0.00 | 0.00 | 0.00 | 0.00 |
| 1.00 | 0.00 | 0.00 | 0.00 | 0.00 | 1.00 | 17.27 | 17.27 | 0.00 | 0.00 |
| 2.00 | 0.00 | 0.00 | 0.00 | 0.00 | 2.00 | 17.27 | 17.27 | 0.00 | 19.34 |
| 3.00 | 0.00 | 0.00 | 0.00 | 34.86 | 3.00 | 51.79 | 51.79 | 0.00 | 39.00 |
| 4.00 | 34.53 | 34.53 | 0.00 | 39.00 | 4.00 | 101.55 | 101.55 | 0.00 | 39.00 |
| 5.00 | 34.53 | 34.53 | 0.00 | 39.00 | 5.00 | 143.69 | 143.69 | 0.00 | 56.43 |
| 6.00 | 34.53 | 34.53 | 0.00 | 39.00 | 6.00 | 164.00 | 164.00 | 0.00 | 77.68 |
| 7.00 | 34.53 | 34.53 | 0.00 | 39.00 | 7.00 | 188.36 | 188.36 | 0.00 | 120.00 |
| 8.00 | 34.53 | 34.53 | 0.00 | 61.35 | 8.00 | 263.51 | 263.51 | 0.00 | 139.40 |
| 9.00 | 42.65 | 42.65 | 0.00 | 110.24 | 9.00 | 298.29 | 298.29 | 183.00 | 180.26 |
| 10.00 | 86.31 | 86.31 | 0.00 | 120.00 | 10.00 | 326.72 | 326.72 | 187.00 | 227.35 |
| 11.00 | 0.00 | 0.00 | 0.00 | 55.25 | 11.00 | 192.44 | 192.44 | 0.00 | 78.12 |
| 12.00 | 17.27 | 17.27 | 0.00 | 57.35 | 12.00 | 76.16 | 76.16 | 0.00 | 45.47 |
| 12.10 | 17.27 | 17.27 | 0.00 | 38.65 | 12.10 | 82.25 | 82.25 | 0.00 | 58.37 |
| 12.20 | 0.00 | 0.00 | 0.00 | 38.65 | 12.20 | 88.35 | 88.35 | 0.00 | 20.41 |
| 12.30 | 0.00 | 0.00 | 0.00 | 35.75 | 12.30 | 93.42 | 93.42 | 0.00 | 21.45 |
| 12.40 | 0.00 | 0.00 | 0.00 | 53.18 | 12.40 | 110.68 | 110.68 | 0.00 | 25.47 |
| 12.50 | 0.00 | 0.00 | 0.00 | 55.25 | 12.50 | 157.91 | 157.91 | 0.00 | 39.47 |
| 12.60 | 0.00 | 0.00 | 0.00 | 53.18 | 12.60 | 110.68 | 110.68 | 0.00 | 25.47 |
| 12.70 | 0.00 | 0.00 | 0.00 | 35.75 | 12.70 | 93.42 | 93.42 | 0.00 | 21.45 |
| 12.80 | 0.00 | 0.00 | 0.00 | 38.65 | 12.80 | 88.35 | 88.35 | 0.00 | 20.41 |
| 12.90 | 17.27 | 17.27 | 0.00 | 38.65 | 12.90 | 82.25 | 82.25 | 0.00 | 58.37 |
| 13.00 | 17.27 | 17.27 | 0.00 | 57.35 | 13.00 | 76.16 | 76.16 | 0.00 | 45.47 |

**Table 30 – $t_{80}$ - Effect of initial stress regime**

| θ = 90° | | | | |
|---|---|---|---|---|
| **Step** | **F1** | **F2** | **F3** | **F4 = F5** |
| 0.00 | 0.00 | 0.00 | 0.00 | 0.00 |
| 1.00 | 0.00 | 0.00 | 0.00 | 0.00 |
| 2.00 | 0.00 | 0.00 | 0.00 | 0.00 |
| 3.00 | 0.00 | 0.00 | 0.00 | 0.00 |
| 4.00 | 0.00 | 0.00 | 0.00 | 0.00 |
| 5.00 | 17.27 | 17.27 | 0.00 | 35.89 |
| 6.00 | 32.50 | 32.50 | 0.00 | 39.00 |
| 7.00 | 34.53 | 34.53 | 0.00 | 39.00 |
| 8.00 | 34.53 | 34.53 | 0.00 | 39.00 |
| 9.00 | 34.53 | 34.53 | 0.00 | 57.40 |
| 10.00 | 34.53 | 34.53 | 0.00 | 58.37 |
| 11.00 | 0.00 | 0.00 | 0.00 | 0.00 |
| 12.00 | 0.00 | 0.00 | 0.00 | 19.34 |
| 12.10 | 0.00 | 0.00 | 0.00 | 0.00 |
| 12.20 | 0.00 | 0.00 | 0.00 | 0.00 |
| 12.30 | 0.00 | 0.00 | 0.00 | 0.00 |
| 12.40 | 0.00 | 0.00 | 0.00 | 0.00 |
| 12.50 | 0.00 | 0.00 | 0.00 | 0.00 |
| 12.60 | 0.00 | 0.00 | 0.00 | 0.00 |
| 12.70 | 0.00 | 0.00 | 0.00 | 0.00 |
| 12.80 | 0.00 | 0.00 | 0.00 | 0.00 |
| 12.90 | 0.00 | 0.00 | 0.00 | 0.00 |
| 13.00 | 0.00 | 0.00 | 0.00 | 19.34 |

| M_1 = 0.40 ; M_2 = 0.47 | | | | |
|---|---|---|---|---|
| **Step** | **F1** | **F2** | **F3** | **F4 = F5** |
| 0.00 | 0.00 | 0.00 | 0.00 | 0.00 |
| 1.00 | 0.00 | 0.00 | 0.00 | 0.00 |
| 2.00 | 0.00 | 0.00 | 0.00 | 0.00 |
| 3.00 | 0.00 | 0.00 | 0.00 | 0.00 |
| 4.00 | 17.27 | 17.27 | 0.00 | 19.34 |
| 5.00 | 17.27 | 17.27 | 0.00 | 19.66 |
| 6.00 | 17.26 | 17.26 | 0.00 | 0.00 |
| 7.00 | 34.52 | 34.52 | 0.00 | 18.40 |
| 8.00 | 17.27 | 17.27 | 0.00 | 19.32 |
| 9.00 | 67.01 | 67.01 | 0.00 | 54.55 |
| 10.00 | 49.76 | 49.76 | 0.00 | 5.13 |
| 11.00 | 0.00 | 0.00 | 0.00 | 0.00 |
| 12.00 | 34.53 | 34.53 | 0.00 | 39.00 |
| 12.10 | 0.00 | 0.00 | 0.00 | 0.00 |
| 12.20 | 0.00 | 0.00 | 0.00 | 0.00 |
| 12.30 | 0.00 | 0.00 | 0.00 | 0.00 |
| 12.40 | 0.00 | 0.00 | 0.00 | 0.00 |
| 12.50 | 0.00 | 0.00 | 0.00 | 0.00 |
| 12.60 | 0.00 | 0.00 | 0.00 | 0.00 |
| 12.70 | 0.00 | 0.00 | 0.00 | 0.00 |
| 12.80 | 0.00 | 0.00 | 0.00 | 0.00 |
| 12.90 | 0.00 | 0.00 | 0.00 | 0.00 |
| 13.00 | 0.00 | 0.00 | 0.00 | 0.00 |

**Table 31 – $t_a$ - Effect of the Mohr-Coulomb fault parameters**

| c = 0 bar | | | | | c = 100 bar | | | | |
|---|---|---|---|---|---|---|---|---|---|
| **Step** | **F1** | **F2** | **F3** | **F4 = F5** | **Step** | **F1** | **F2** | **F3** | **F4 = F5** |
| 0.00 | 0.00 | 0.00 | 0.00 | 0.00 | 0.00 | 0.00 | 0.00 | 0.00 | 0.00 |
| 1.00 | 0.00 | 0.00 | 0.00 | 0.00 | 1.00 | 0.00 | 0.00 | 0.00 | 0.00 |
| 2.00 | 0.00 | 0.00 | 0.00 | 0.00 | 2.00 | 0.00 | 0.00 | 0.00 | 0.00 |
| 3.00 | 0.00 | 0.00 | 0.00 | 0.00 | 3.00 | 0.00 | 0.00 | 0.00 | 0.00 |
| 4.00 | 0.00 | 0.00 | 0.00 | 0.00 | 4.00 | 0.00 | 0.00 | 0.00 | 0.00 |
| 5.00 | 17.27 | 17.27 | 0.00 | 18.38 | 5.00 | 0.00 | 0.00 | 0.00 | 0.00 |
| 6.00 | 15.23* | 15.23* | 0.00 | 15.46* | 6.00 | 0.00 | 0.00 | 0.00 | 0.00 |
| 7.00 | 2.03** | 2.03** | 0.00 | 5.16** | 7.00 | 0.00 | 0.00 | 0.00 | 0.00 |
| 8.00 | 0.00 | 0.00 | 0.00 | 0.00 | 8.00 | 0.00 | 0.00 | 0.00 | 0.00 |
| 9.00 | 0.00 | 0.00 | 0.00 | 0.00 | 9.00 | 17.27 | 17.27 | 0.00 | 0.00 |
| 10.00 | 28.43* | 28.43* | 0.00 | 19.37 | 10.00 | 0.00 | 0.00 | 0.00 | 19.34 |
| 11.00 | 0.00 | 0.00 | 0.00 | 0.00 | 11.00 | 0.00 | 0.00 | 0.00 | 0.00 |
| 12.00 | 17.27 | 17.27 | 0.00 | 19.34 | 12.00 | 0.00 | 0.00 | 0.00 | 0.00 |
| 12.10 | 0.00 | 0.00 | 0.00 | 0.00 | 12.10 | 0.00 | 0.00 | 0.00 | 0.00 |
| 12.20 | 0.00 | 0.00 | 0.00 | 0.00 | 12.20 | 0.00 | 0.00 | 0.00 | 0.00 |
| 12.30 | 0.00 | 0.00 | 0.00 | 0.00 | 12.30 | 0.00 | 0.00 | 0.00 | 0.00 |
| 12.40 | 0.00 | 0.00 | 0.00 | 0.00 | 12.40 | 0.00 | 0.00 | 0.00 | 0.00 |
| 12.50 | 0.00 | 0.00 | 0.00 | 0.00 | 12.50 | 0.00 | 0.00 | 0.00 | 0.00 |
| 12.60 | 0.00 | 0.00 | 0.00 | 0.00 | 12.60 | 0.00 | 0.00 | 0.00 | 0.00 |
| 12.70 | 0.00 | 0.00 | 0.00 | 0.00 | 12.70 | 0.00 | 0.00 | 0.00 | 0.00 |
| 12.80 | 0.00 | 0.00 | 0.00 | 0.00 | 12.80 | 0.00 | 0.00 | 0.00 | 0.00 |
| 12.90 | 0.00 | 0.00 | 0.00 | 0.00 | 12.90 | 0.00 | 0.00 | 0.00 | 0.00 |
| 13.00 | 0.00 | 0.00 | 0.00 | 0.00 | 13.00 | 0.00 | 0.00 | 0.00 | 0.00 |

| $f_s = 20°$ | | | | |
|---|---|---|---|---|
| **Step** | **F1** | **F2** | **F3** | **F4 = F5** |
| 0.00 | 0.00 | 0.00 | 0.00 | 0.00 |
| 1.00 | 0.00 | 0.00 | 0.00 | 0.00 |
| 2.00 | 0.00 | 0.00 | 0.00 | 0.00 |
| 3.00 | 0.00 | 0.00 | 0.00 | 0.00 |
| 4.00 | 0.00 | 0.00 | 0.00 | 0.00 |
| 5.00 | 34.53 | 34.53 | 0.00 | 39.00 |
| 6.00 | 0.00 | 0.00 | 0.00 | 0.00 |
| 7.00 | 0.00 | 0.00 | 0.00 | 0.00 |
| 8.00 | 0.00 | 0.00 | 0.00 | 0.00 |
| 9.00 | 38.58 | 38.58 | 0.00 | 36.77 |
| 10.00 | 30.46* | 30.46* | 0.00 | 37.11 |
| 11.00 | 0.00 | 0.00 | 0.00 | 0.00 |
| 12.00 | 34.53 | 34.53 | 0.00 | 39.00 |
| 12.10 | 0.00 | 0.00 | 0.00 | 0.00 |
| 12.20 | 0.00 | 0.00 | 0.00 | 0.00 |
| 12.30 | 0.00 | 0.00 | 0.00 | 0.00 |
| 12.40 | 0.00 | 0.00 | 0.00 | 0.00 |
| 12.50 | 0.00 | 0.00 | 0.00 | 0.00 |
| 12.60 | 0.00 | 0.00 | 0.00 | 0.00 |
| 12.70 | 0.00 | 0.00 | 0.00 | 0.00 |
| 12.80 | 0.00 | 0.00 | 0.00 | 0.00 |
| 12.90 | 0.00 | 0.00 | 0.00 | 0.00 |
| 13.00 | 0.00 | 0.00 | 0.00 | 0.00 |

| $f_d = 10°$; $d_c = 2$ mm | | | | |
|---|---|---|---|---|
| **Step** | **F1** | **F2** | **F3** | **F4 = F5** |
| 0.00 | 0.00 | 0.00 | 0.00 | 0.00 |
| 1.00 | 0.00 | 0.00 | 0.00 | 0.00 |
| 2.00 | 0.00 | 0.00 | 0.00 | 0.00 |
| 3.00 | 0.00 | 0.00 | 0.00 | 0.00 |
| 4.00 | 0.00 | 0.00 | 0.00 | 0.00 |
| 5.00 | 0.00 | 0.00 | 0.00 | 0.00 |
| 6.00 | 17.27 | 17.27 | 0.00 | 19.34 |
| 7.00 | 13.2* | 13.2* | 0.00 | 15.52* |
| 8.00 | 2.03** | 2.03** | 0.00 | 4.14** |
| 9.00 | 0.00 | 0.00 | 0.00 | 0.00 |
| 10.00 | 76.15 | 76.15 | 0.00 | 37.73 |
| 11.00 | 0.00 | 0.00 | 0.00 | 0.00 |
| 12.00 | 15.23* | 15.23* | 0.00 | 19.66 |
| 12.10 | 0.00 | 0.00 | 0.00 | 0.00 |
| 12.20 | 0.00 | 0.00 | 0.00 | 0.00 |
| 12.30 | 0.00 | 0.00 | 0.00 | 0.00 |
| 12.40 | 0.00 | 0.00 | 0.00 | 0.00 |
| 12.50 | 17.27 | 17.27 | 0.00 | 33.89 |
| 12.60 | 0.00 | 0.00 | 0.00 | 0.00 |
| 12.70 | 0.00 | 0.00 | 0.00 | 0.00 |
| 12.80 | 0.00 | 0.00 | 0.00 | 0.00 |
| 12.90 | 0.00 | 0.00 | 0.00 | 0.00 |
| 13.00 | 30.47* | 30.47* | 0.00 | 33.89 |

| $f_d = 20°$; $d_c = 20$ mm | | | | |
|---|---|---|---|---|
| **Step** | **F1** | **F2** | **F3** | **F4 = F5** |
| 0.00 | 0.00 | 0.00 | 0.00 | 0.00 |
| 1.00 | 0.00 | 0.00 | 0.00 | 0.00 |
| 2.00 | 0.00 | 0.00 | 0.00 | 0.00 |
| 3.00 | 0.00 | 0.00 | 0.00 | 0.00 |
| 4.00 | 0.00 | 0.00 | 0.00 | 0.00 |
| 5.00 | 0.00 | 0.00 | 0.00 | 0.00 |
| 6.00 | 17.27 | 17.27 | 0.00 | 19.34 |
| 7.00 | 13.2* | 13.2* | 0.00 | 16.55* |
| 8.00 | 4.06** | 4.06** | 0.00 | 3.11** |
| 9.00 | 0.00 | 0.00 | 0.00 | 0.00 |
| 10.00 | 0.00 | 0.00 | 0.00 | 0.00 |
| 11.00 | 0.00 | 0.00 | 0.00 | 0.00 |
| 12.00 | 17.27 | 17.27 | 0.00 | 17.41* |
| 12.10 | 0.00 | 0.00 | 0.00 | 0.00 |
| 12.20 | 0.00 | 0.00 | 0.00 | 0.00 |
| 12.30 | 0.00 | 0.00 | 0.00 | 0.00 |
| 12.40 | 0.00 | 0.00 | 0.00 | 0.00 |
| 12.50 | 0.00 | 0.00 | 0.00 | 0.00 |
| 12.60 | 0.00 | 0.00 | 0.00 | 0.00 |
| 12.70 | 0.00 | 0.00 | 0.00 | 0.00 |
| 12.80 | 0.00 | 0.00 | 0.00 | 0.00 |
| 12.90 | 0.00 | 0.00 | 0.00 | 0.00 |
| 13.00 | 0.00 | 0.00 | 0.00 | 0.00 |

**Table 32 – $t_{50}$ - Effect of the Mohr-Coulomb fault parameters**

| c = 0 bar | | | | | c = 100 bar | | | | |
|---|---|---|---|---|---|---|---|---|---|
| **Step** | **F1** | **F2** | **F3** | **F4 = F5** | **Step** | **F1** | **F2** | **F3** | **F4 = F5** |
| 0.00 | 0.00 | 0.00 | 0.00 | 0.00 | 0.00 | 0.00 | 0.00 | 0.00 | 0.00 |
| 1.00 | 0.00 | 0.00 | 0.00 | 0.00 | 1.00 | 0.00 | 0.00 | 0.00 | 0.00 |
| 2.00 | 0.00 | 0.00 | 0.00 | 0.00 | 2.00 | 0.00 | 0.00 | 0.00 | 0.00 |
| 3.00 | 34.53 | 34.53 | 0.00 | 37.96 | 3.00 | 0.00 | 0.00 | 0.00 | 0.00 |
| 4.00 | 34.53 | 34.53 | 0.00 | 39.00 | 4.00 | 0.00 | 0.00 | 0.00 | 0.00 |
| 5.00 | 34.53 | 34.53 | 0.00 | 39.00 | 5.00 | 17.27 | 17.27 | 0.00 | 30.84 |
| 6.00 | 34.53 | 34.53 | 0.00 | 39.00 | 6.00 | 34.53 | 34.53 | 0.00 | 39.00 |
| 7.00 | 51.79 | 51.79 | 0.00 | 57.40 | 7.00 | 34.53 | 34.53 | 0.00 | 39.00 |
| 8.00 | 101.55 | 101.55 | 0.00 | 77.68 | 8.00 | 34.53 | 34.53 | 0.00 | 39.00 |
| 9.00 | 103.58 | 103.58 | 0.00 | 116.45 | 9.00 | 34.53 | 34.53 | 0.00 | 39.00 |
| 10.00 | 120.84 | 120.84 | 0.00 | 120.00 | 10.00 | 34.53 | 34.53 | 0.00 | 39.00 |
| 11.00 | 69.05 | 69.05 | 0.00 | 57.33 | 11.00 | 17.27 | 17.27 | 0.00 | 11.50 |
| 12.00 | 51.80 | 51.80 | 0.00 | 58.31 | 12.00 | 0.00 | 0.00 | 0.00 | 0.00 |
| 12.10 | 39.61 | 39.61 | 0.00 | 66.74 | 12.10 | 0.00 | 0.00 | 0.00 | 0.00 |
| 12.20 | 49.77 | 49.77 | 0.00 | 55.21 | 12.20 | 0.00 | 0.00 | 0.00 | 0.00 |
| 12.30 | 34.53 | 34.53 | 0.00 | 36.92 | 12.30 | 0.00 | 0.00 | 0.00 | 0.00 |
| 12.40 | 51.79 | 51.79 | 0.00 | 37.96 | 12.40 | 0.00 | 0.00 | 0.00 | 0.00 |
| 12.50 | 51.79 | 51.79 | 0.00 | 39.90 | 12.50 | 17.27 | 17.27 | 0.00 | 11.50 |
| 12.60 | 51.79 | 51.79 | 0.00 | 37.96 | 12.60 | 0.00 | 0.00 | 0.00 | 0.00 |
| 12.70 | 34.53 | 34.53 | 0.00 | 36.92 | 12.70 | 0.00 | 0.00 | 0.00 | 0.00 |
| 12.80 | 49.77 | 49.77 | 0.00 | 55.21 | 12.80 | 0.00 | 0.00 | 0.00 | 0.00 |
| 12.90 | 39.61 | 39.61 | 0.00 | 66.74 | 12.90 | 0.00 | 0.00 | 0.00 | 0.00 |
| 13.00 | 51.80 | 51.80 | 0.00 | 58.31 | 13.00 | 0.00 | 0.00 | 0.00 | 0.00 |

| $f_s = 20°$ | | | | |
|---|---|---|---|---|
| **Step** | **F1** | **F2** | **F3** | **F4 = F5** |
| 0.00 | 0.00 | 0.00 | 0.00 | 0.00 |
| 1.00 | 0.00 | 0.00 | 0.00 | 0.00 |
| 2.00 | 17.27 | 17.27 | 0.00 | 0.00 |
| 3.00 | 34.53 | 34.53 | 0.00 | 39.00 |
| 4.00 | 34.53 | 34.53 | 0.00 | 39.00 |
| 5.00 | 34.53 | 34.53 | 0.00 | 39.00 |
| 6.00 | 69.06 | 69.06 | 0.00 | 57.40 |
| 7.00 | 103.58 | 103.58 | 0.00 | 112.35 |
| 8.00 | 103.58 | 103.58 | 0.00 | 120.00 |
| 9.00 | 129.97 | 129.97 | 0.00 | 120.00 |
| 10.00 | 147.24 | 147.24 | 0.00 | 164.32 |
| 11.00 | 118.80 | 118.80 | 0.00 | 78.00 |
| 12.00 | 38.59 | 38.59 | 0.00 | 41.08 |
| 12.10 | 42.66 | 42.66 | 0.00 | 42.13 |
| 12.20 | 34.53 | 34.53 | 0.00 | 27.57 |
| 12.30 | 35.54 | 35.54 | 0.00 | 19.69 |
| 12.40 | 45.69 | 45.69 | 0.00 | 21.68 |
| 12.50 | 49.75 | 49.75 | 0.00 | 45.13 |
| 12.60 | 45.69 | 45.69 | 0.00 | 21.68 |
| 12.70 | 35.54 | 35.54 | 0.00 | 19.69 |
| 12.80 | 34.53 | 34.53 | 0.00 | 27.57 |
| 12.90 | 42.66 | 42.66 | 0.00 | 42.13 |
| 13.00 | 38.59 | 38.59 | 0.00 | 41.08 |

| $f_d = 10°$; $d_c = 2$ mm | | | | |
|---|---|---|---|---|
| **Step** | **F1** | **F2** | **F3** | **F4 = F5** |
| 0.00 | 0.00 | 0.00 | 0.00 | 0.00 |
| 1.00 | 0.00 | 0.00 | 0.00 | 0.00 |
| 2.00 | 0.00 | 0.00 | 0.00 | 0.00 |
| 3.00 | 17.27 | 17.27 | 0.00 | 0.00 |
| 4.00 | 34.53 | 34.53 | 0.00 | 39.00 |
| 5.00 | 34.53 | 34.53 | 0.00 | 39.00 |
| 6.00 | 34.53 | 34.53 | 0.00 | 57.40 |
| 7.00 | 62.96 | 62.96 | 0.00 | 93.20 |
| 8.00 | 101.55 | 101.55 | 0.00 | 117.00 |
| 9.00 | 103.58 | 103.58 | 0.00 | 117.00 |
| 10.00 | 170.59 | 170.59 | 0.00 | 154.73 |
| 11.00 | 111.70 | 111.70 | 0.00 | 134.38 |
| 12.00 | 75.14 | 75.14 | 0.00 | 76.72 |
| 12.10 | 108.65 | 108.65 | 0.00 | 97.07 |
| 12.20 | 85.29 | 85.29 | 0.00 | 74.48 |
| 12.30 | 67.01 | 67.01 | 0.00 | 73.52 |
| 12.40 | 84.28 | 84.28 | 0.00 | 94.09 |
| 12.50 | 93.42 | 93.42 | 0.00 | 94.15 |
| 12.60 | 80.21 | 80.21 | 0.00 | 93.12 |
| 12.70 | 67.01 | 67.01 | 0.00 | 56.13 |
| 12.80 | 85.29 | 85.29 | 0.00 | 74.48 |
| 12.90 | 108.65 | 108.65 | 0.00 | 97.07 |
| 13.00 | 101.54 | 101.54 | 0.00 | 76.72 |

| $f_d = 20°$; $d_c = 20$ mm | | | | |
|---|---|---|---|---|
| **Step** | **F1** | **F2** | **F3** | **F4 = F5** |
| 0.00 | 0.00 | 0.00 | 0.00 | 0.00 |
| 1.00 | 0.00 | 0.00 | 0.00 | 0.00 |
| 2.00 | 0.00 | 0.00 | 0.00 | 0.00 |
| 3.00 | 17.27 | 17.27 | 0.00 | 0.00 |
| 4.00 | 34.53 | 34.53 | 0.00 | 39.00 |
| 5.00 | 34.53 | 34.53 | 0.00 | 39.00 |
| 6.00 | 34.53 | 34.53 | 0.00 | 39.00 |
| 7.00 | 34.53 | 34.53 | 0.00 | 39.00 |
| 8.00 | 47.73 | 47.73 | 0.00 | 58.37 |
| 9.00 | 103.58 | 103.58 | 0.00 | 77.68 |
| 10.00 | 103.58 | 103.58 | 0.00 | 114.93 |
| 11.00 | 64.99 | 64.99 | 0.00 | 53.18 |
| 12.00 | 34.53 | 34.53 | 0.00 | 39.00 |
| 12.10 | 30.47 | 30.47 | 0.00 | 35.89 |
| 12.20 | 32.50 | 32.50 | 0.00 | 19.34 |
| 12.30 | 17.27 | 17.27 | 0.00 | 0.00 |
| 12.40 | 17.27 | 17.27 | 0.00 | 23.86 |
| 12.50 | 30.46 | 30.46 | 0.00 | 52.23 |
| 12.60 | 17.27 | 17.27 | 0.00 | 23.86 |
| 12.70 | 17.27 | 17.27 | 0.00 | 0.00 |
| 12.80 | 32.50 | 32.50 | 0.00 | 19.34 |
| 12.90 | 30.47 | 30.47 | 0.00 | 35.89 |
| 13.00 | 34.53 | 34.53 | 0.00 | 39.00 |

**Table 33 – $t_{80}$ - Effect of the Mohr-Coulomb fault parameters**

| c = 0 bar | | | | | c = 100 bar | | | | |
|---|---|---|---|---|---|---|---|---|---|
| **Step** | **F1** | **F2** | **F3** | **F4 = F5** | **Step** | **F1** | **F2** | **F3** | **F4 = F5** |
| 0.00 | 0.00 | 0.00 | 0.00 | 0.00 | 0.00 | 0.00 | 0.00 | 0.00 | 0.00 |
| 1.00 | 0.00 | 0.00 | 0.00 | 0.00 | 1.00 | 0.00 | 0.00 | 0.00 | 0.00 |
| 2.00 | 0.00 | 0.00 | 0.00 | 0.00 | 2.00 | 0.00 | 0.00 | 0.00 | 0.00 |
| 3.00 | 0.00 | 0.00 | 0.00 | 0.00 | 3.00 | 0.00 | 0.00 | 0.00 | 0.00 |
| 4.00 | 17.27 | 17.27 | 0.00 | 17.41 | 4.00 | 0.00 | 0.00 | 0.00 | 0.00 |
| 5.00 | 34.53 | 34.53 | 0.00 | 37.96 | 5.00 | 0.00 | 0.00 | 0.00 | 0.00 |
| 6.00 | 34.53 | 34.53 | 0.00 | 39.00 | 6.00 | 0.00 | 0.00 | 0.00 | 0.00 |
| 7.00 | 34.53 | 34.53 | 0.00 | 39.00 | 7.00 | 0.00 | 0.00 | 0.00 | 0.00 |
| 8.00 | 34.53 | 34.53 | 0.00 | 39.00 | 8.00 | 17.27 | 17.27 | 0.00 | 19.34 |
| 9.00 | 67.02 | 67.02 | 0.00 | 58.37 | 9.00 | 34.53 | 34.53 | 0.00 | 37.96 |
| 10.00 | 86.31 | 86.31 | 0.00 | 77.68 | 10.00 | 34.53 | 34.53 | 0.00 | 39.00 |
| 11.00 | 0.00 | 0.00 | 0.00 | 0.00 | 11.00 | 0.00 | 0.00 | 0.00 | 0.00 |
| 12.00 | 17.27 | 17.27 | 0.00 | 19.34 | 12.00 | 0.00 | 0.00 | 0.00 | 0.00 |
| 12.10 | 17.27 | 17.27 | 0.00 | 0.00 | 12.10 | 0.00 | 0.00 | 0.00 | 0.00 |
| 12.20 | 0.00 | 0.00 | 0.00 | 0.00 | 12.20 | 0.00 | 0.00 | 0.00 | 0.00 |
| 12.30 | 0.00 | 0.00 | 0.00 | 0.00 | 12.30 | 0.00 | 0.00 | 0.00 | 0.00 |
| 12.40 | 0.00 | 0.00 | 0.00 | 0.00 | 12.40 | 0.00 | 0.00 | 0.00 | 0.00 |
| 12.50 | 0.00 | 0.00 | 0.00 | 0.00 | 12.50 | 0.00 | 0.00 | 0.00 | 0.00 |
| 12.60 | 0.00 | 0.00 | 0.00 | 0.00 | 12.60 | 0.00 | 0.00 | 0.00 | 0.00 |
| 12.70 | 0.00 | 0.00 | 0.00 | 0.00 | 12.70 | 0.00 | 0.00 | 0.00 | 0.00 |
| 12.80 | 0.00 | 0.00 | 0.00 | 0.00 | 12.80 | 0.00 | 0.00 | 0.00 | 0.00 |
| 12.90 | 17.27 | 17.27 | 0.00 | 0.00 | 12.90 | 0.00 | 0.00 | 0.00 | 0.00 |
| 13.00 | 17.27 | 17.27 | 0.00 | 19.34 | 13.00 | 0.00 | 0.00 | 0.00 | 0.00 |

| $f_s = 20°$ | | | | |
|---|---|---|---|---|
| **Step** | **F1** | **F2** | **F3** | **F4 = F5** |
| 0.00 | 0.00 | 0.00 | 0.00 | 0.00 |
| 1.00 | 0.00 | 0.00 | 0.00 | 0.00 |
| 2.00 | 0.00 | 0.00 | 0.00 | 0.00 |
| 3.00 | 0.00 | 0.00 | 0.00 | 0.00 |
| 4.00 | 34.53 | 34.53 | 0.00 | 39.00 |
| 5.00 | 34.53 | 34.53 | 0.00 | 39.00 |
| 6.00 | 34.53 | 34.53 | 0.00 | 39.00 |
| 7.00 | 34.53 | 34.53 | 0.00 | 39.00 |
| 8.00 | 69.06 | 69.06 | 0.00 | 58.37 |
| 9.00 | 103.58 | 103.58 | 0.00 | 112.87 |
| 10.00 | 120.84 | 120.84 | 0.00 | 117.00 |
| 11.00 | 17.27 | 17.27 | 0.00 | 19.61 |
| 12.00 | 34.53 | 34.53 | 0.00 | 39.00 |
| 12.10 | 0.00 | 0.00 | 0.00 | 0.00 |
| 12.20 | 0.00 | 0.00 | 0.00 | 0.00 |
| 12.30 | 0.00 | 0.00 | 0.00 | 0.00 |
| 12.40 | 0.00 | 0.00 | 0.00 | 0.00 |
| 12.50 | 0.00 | 0.00 | 0.00 | 0.00 |
| 12.60 | 0.00 | 0.00 | 0.00 | 0.00 |
| 12.70 | 0.00 | 0.00 | 0.00 | 0.00 |
| 12.80 | 0.00 | 0.00 | 0.00 | 0.00 |
| 12.90 | 0.00 | 0.00 | 0.00 | 0.00 |
| 13.00 | 34.53 | 34.53 | 0.00 | 39.00 |

| $f_d = 10°$; $d_c = 2$ mm | | | | |
|---|---|---|---|---|
| **Step** | **F1** | **F2** | **F3** | **F4 = F5** |
| 0.00 | 0.00 | 0.00 | 0.00 | 0.00 |
| 1.00 | 0.00 | 0.00 | 0.00 | 0.00 |
| 2.00 | 0.00 | 0.00 | 0.00 | 0.00 |
| 3.00 | 0.00 | 0.00 | 0.00 | 0.00 |
| 4.00 | 0.00 | 0.00 | 0.00 | 0.00 |
| 5.00 | 17.27 | 17.27 | 0.00 | 19.34 |
| 6.00 | 34.53 | 34.53 | 0.00 | 39.00 |
| 7.00 | 34.53 | 34.53 | 0.00 | 39.00 |
| 8.00 | 54.84 | 54.84 | 0.00 | 57.40 |
| 9.00 | 82.25 | 82.25 | 0.00 | 74.94 |
| 10.00 | 146.22 | 146.22 | 0.00 | 132.33 |
| 11.00 | 32.50 | 32.50 | 0.00 | 55.57 |
| 12.00 | 38.59 | 38.59 | 0.00 | 57.40 |
| 12.10 | 13.20 | 13.20 | 0.00 | 0.00 |
| 12.20 | 0.00 | 0.00 | 0.00 | 0.00 |
| 12.30 | 0.00 | 0.00 | 0.00 | 0.00 |
| 12.40 | 0.00 | 0.00 | 0.00 | 0.00 |
| 12.50 | 19.30 | 19.30 | 0.00 | 39.00 |
| 12.60 | 0.00 | 0.00 | 0.00 | 0.00 |
| 12.70 | 0.00 | 0.00 | 0.00 | 0.00 |
| 12.80 | 0.00 | 0.00 | 0.00 | 0.00 |
| 12.90 | 13.20 | 13.20 | 0.00 | 0.00 |
| 13.00 | 51.80 | 51.80 | 0.00 | 57.40 |

| $f_d = 20°$; $d_c = 20$ mm | | | | |
|---|---|---|---|---|
| **Step** | **F1** | **F2** | **F3** | **F4 = F5** |
| 0.00 | 0.00 | 0.00 | 0.00 | 0.00 |
| 1.00 | 0.00 | 0.00 | 0.00 | 0.00 |
| 2.00 | 0.00 | 0.00 | 0.00 | 0.00 |
| 3.00 | 0.00 | 0.00 | 0.00 | 0.00 |
| 4.00 | 0.00 | 0.00 | 0.00 | 0.00 |
| 5.00 | 17.27 | 17.27 | 0.00 | 19.34 |
| 6.00 | 34.53 | 34.53 | 0.00 | 39.00 |
| 7.00 | 34.53 | 34.53 | 0.00 | 39.00 |
| 8.00 | 34.53 | 34.53 | 0.00 | 39.00 |
| 9.00 | 34.53 | 34.53 | 0.00 | 39.00 |
| 10.00 | 62.96 | 62.96 | 0.00 | 58.37 |
| 11.00 | 0.00 | 0.00 | 0.00 | 0.00 |
| 12.00 | 17.27 | 17.27 | 0.00 | 19.34 |
| 12.10 | 0.00 | 0.00 | 0.00 | 0.96 |
| 12.20 | 0.00 | 0.00 | 0.00 | 0.00 |
| 12.30 | 0.00 | 0.00 | 0.00 | 0.00 |
| 12.40 | 0.00 | 0.00 | 0.00 | 0.00 |
| 12.50 | 0.00 | 0.00 | 0.00 | 0.00 |
| 12.60 | 0.00 | 0.00 | 0.00 | 0.00 |
| 12.70 | 0.00 | 0.00 | 0.00 | 0.00 |
| 12.80 | 0.00 | 0.00 | 0.00 | 0.00 |
| 12.90 | 0.00 | 0.00 | 0.00 | 0.96 |
| 13.00 | 17.27 | 17.27 | 0.00 | 19.34 |

**Table 34 – $t_a$ - Effect of the reservoir stiffness**

| E = 8 GPa | | | | | E = 20 Gpa | | | | |
|---|---|---|---|---|---|---|---|---|---|
| **Step** | **F1** | **F2** | **F3** | **F4 = F5** | **Step** | **F1** | **F2** | **F3** | **F4 = F5** |
| 0.00 | 0.00 | 0.00 | 0.00 | 0.00 | 0.00 | 0.00 | 0.00 | 0.00 | 0.00 |
| 1.00 | 0.00 | 0.00 | 0.00 | 0.00 | 1.00 | 0.00 | 0.00 | 0.00 | 0.00 |
| 2.00 | 0.00 | 0.00 | 0.00 | 0.00 | 2.00 | 0.00 | 0.00 | 0.00 | 0.00 |
| 3.00 | 0.00 | 0.00 | 0.00 | 0.00 | 3.00 | 0.00 | 0.00 | 0.00 | 0.00 |
| 4.00 | 0.00 | 0.00 | 0.00 | 0.00 | 4.00 | 0.00 | 0.00 | 0.00 | 0.00 |
| 5.00 | 13.2* | 13.2* | 0.00 | 0.00 | 5.00 | 0.00 | 0.00 | 0.00 | 0.00 |
| 6.00 | 4.06** | 4.06** | 0.00 | 26.84* | 6.00 | 0.00 | 0.00 | 0.00 | 0.00 |
| 7.00 | 17.27 | 17.27 | 0.00 | 12.16** | 7.00 | 0.00 | 0.00 | 0.00 | 0.00 |
| 8.00 | 0.00 | 0.00 | 0.00 | 0.00 | 8.00 | 17.27 | 17.27 | 0.00 | 19.34 |
| 9.00 | 0.00 | 0.00 | 0.00 | 0.00 | 9.00 | 17.27 | 17.27 | 0.00 | 13.5* |
| 10.00 | 0.00 | 0.00 | 0.00 | 18.40 | 10.00 | 0.00 | 0.00 | 0.00 | 6.16** |
| 11.00 | 0.00 | 0.00 | 0.00 | 0.00 | 11.00 | 0.00 | 0.00 | 0.00 | 0.00 |
| 12.00 | 17.27 | 17.27 | 0.00 | 0.00 | 12.00 | 0.00 | 0.00 | 0.00 | 0.00 |
| 12.10 | 0.00 | 0.00 | 0.00 | 0.00 | 12.10 | 0.00 | 0.00 | 0.00 | 0.00 |
| 12.20 | 0.00 | 0.00 | 0.00 | 0.00 | 12.20 | 0.00 | 0.00 | 0.00 | 0.00 |
| 12.30 | 0.00 | 0.00 | 0.00 | 0.00 | 12.30 | 0.00 | 0.00 | 0.00 | 0.00 |
| 12.40 | 0.00 | 0.00 | 0.00 | 0.00 | 12.40 | 0.00 | 0.00 | 0.00 | 0.00 |
| 12.50 | 0.00 | 0.00 | 0.00 | 0.00 | 12.50 | 0.00 | 0.00 | 0.00 | 0.00 |
| 12.60 | 0.00 | 0.00 | 0.00 | 0.00 | 12.60 | 0.00 | 0.00 | 0.00 | 0.00 |
| 12.70 | 0.00 | 0.00 | 0.00 | 0.00 | 12.70 | 0.00 | 0.00 | 0.00 | 0.00 |
| 12.80 | 0.00 | 0.00 | 0.00 | 0.00 | 12.80 | 0.00 | 0.00 | 0.00 | 0.00 |
| 12.90 | 0.00 | 0.00 | 0.00 | 0.00 | 12.90 | 0.00 | 0.00 | 0.00 | 0.00 |
| 13.00 | 0.00 | 0.00 | 0.00 | 0.00 | 13.00 | 0.00 | 0.00 | 0.00 | 0.00 |

**Table 35 – $t_{50}$ - Effect of the reservoir stiffness**

| E = 8 GPa | | | | | E = 20 Gpa | | | | |
|---|---|---|---|---|---|---|---|---|---|
| **Step** | **F1** | **F2** | **F3** | **F4 = F5** | **Step** | **F1** | **F2** | **F3** | **F4 = F5** |
| 0.00 | 0.00 | 0.00 | 0.00 | 0.00 | 0.00 | 0.00 | 0.00 | 0.00 | 0.00 |
| 1.00 | 0.00 | 0.00 | 0.00 | 0.00 | 1.00 | 0.00 | 0.00 | 0.00 | 0.00 |
| 2.00 | 0.00 | 0.00 | 0.00 | 0.00 | 2.00 | 0.00 | 0.00 | 0.00 | 0.00 |
| 3.00 | 34.53 | 34.53 | 0.00 | 37.96 | 3.00 | 0.00 | 0.00 | 0.00 | 0.00 |
| 4.00 | 34.53 | 34.53 | 0.00 | 39.00 | 4.00 | 17.27 | 17.27 | 0.00 | 3.88 |
| 5.00 | 34.53 | 34.53 | 0.00 | 39.00 | 5.00 | 34.53 | 34.53 | 0.00 | 39.00 |
| 6.00 | 34.53 | 34.53 | 0.00 | 39.00 | 6.00 | 34.53 | 34.53 | 0.00 | 39.00 |
| 7.00 | 34.53 | 34.53 | 0.00 | 39.00 | 7.00 | 34.53 | 34.53 | 0.00 | 39.00 |
| 8.00 | 89.36 | 89.36 | 0.00 | 76.72 | 8.00 | 34.53 | 34.53 | 0.00 | 39.00 |
| 9.00 | 103.58 | 103.58 | 0.00 | 105.79 | 9.00 | 34.53 | 34.53 | 0.00 | 39.00 |
| 10.00 | 103.58 | 103.58 | 0.00 | 118.97 | 10.00 | 34.53 | 34.53 | 0.00 | 42.90 |
| 11.00 | 64.99 | 64.99 | 0.00 | 57.33 | 11.00 | 0.00 | 0.00 | 0.00 | 0.00 |
| 12.00 | 49.77 | 49.77 | 0.00 | 65.81 | 12.00 | 17.27 | 17.27 | 0.00 | 0.00 |
| 12.10 | 34.53 | 34.53 | 0.00 | 68.67 | 12.10 | 0.00 | 0.00 | 0.00 | 0.00 |
| 12.20 | 51.80 | 51.80 | 0.00 | 55.21 | 12.20 | 0.00 | 0.00 | 0.00 | 0.00 |
| 12.30 | 34.53 | 34.53 | 0.00 | 36.92 | 12.30 | 0.00 | 0.00 | 0.00 | 0.00 |
| 12.40 | 34.53 | 34.53 | 0.00 | 56.29 | 12.40 | 0.00 | 0.00 | 0.00 | 0.00 |
| 12.50 | 64.99 | 64.99 | 0.00 | 57.33 | 12.50 | 0.00 | 0.00 | 0.00 | 0.00 |
| 12.60 | 34.53 | 34.53 | 0.00 | 56.29 | 12.60 | 0.00 | 0.00 | 0.00 | 0.00 |
| 12.70 | 34.53 | 34.53 | 0.00 | 36.92 | 12.70 | 0.00 | 0.00 | 0.00 | 0.00 |
| 12.80 | 51.80 | 51.80 | 0.00 | 55.21 | 12.80 | 0.00 | 0.00 | 0.00 | 0.00 |
| 12.90 | 34.53 | 34.53 | 0.00 | 68.67 | 12.90 | 0.00 | 0.00 | 0.00 | 0.00 |
| 13.00 | 49.77 | 49.77 | 0.00 | 65.81 | 13.00 | 17.27 | 17.27 | 0.00 | 0.00 |

**Table 36 – $t_{80}$ - Effect of the reservoir stiffness**

| E = 8 GPa | | | | |
|---|---|---|---|---|
| **Step** | **F1** | **F2** | **F3** | **F4 = F5** |
| 0.00 | 0.00 | 0.00 | 0.00 | 0.00 |
| 1.00 | 0.00 | 0.00 | 0.00 | 0.00 |
| 2.00 | 0.00 | 0.00 | 0.00 | 0.00 |
| 3.00 | 0.00 | 0.00 | 0.00 | 0.00 |
| 4.00 | 0.00 | 0.00 | 0.00 | 0.00 |
| 5.00 | 34.53 | 34.53 | 0.00 | 37.96 |
| 6.00 | 34.53 | 34.53 | 0.00 | 39.00 |
| 7.00 | 34.53 | 34.53 | 0.00 | 39.00 |
| 8.00 | 34.53 | 34.53 | 0.00 | 39.00 |
| 9.00 | 34.53 | 34.53 | 0.00 | 57.40 |
| 10.00 | 84.28 | 84.28 | 0.00 | 76.72 |
| 11.00 | 0.00 | 0.00 | 0.00 | 0.00 |
| 12.00 | 17.27 | 17.27 | 0.00 | 19.34 |
| 12.10 | 0.00 | 0.00 | 0.00 | 16.45 |
| 12.20 | 0.00 | 0.00 | 0.00 | 0.00 |
| 12.30 | 0.00 | 0.00 | 0.00 | 0.00 |
| 12.40 | 0.00 | 0.00 | 0.00 | 0.00 |
| 12.50 | 0.00 | 0.00 | 0.00 | 0.00 |
| 12.60 | 0.00 | 0.00 | 0.00 | 0.00 |
| 12.70 | 0.00 | 0.00 | 0.00 | 0.00 |
| 12.80 | 0.00 | 0.00 | 0.00 | 0.00 |
| 12.90 | 0.00 | 0.00 | 0.00 | 16.45 |
| 13.00 | 17.27 | 17.27 | 0.00 | 19.34 |

| E = 20 Gpa | | | | |
|---|---|---|---|---|
| **Step** | **F1** | **F2** | **F3** | **F4 = F5** |
| 0.00 | 0.00 | 0.00 | 0.00 | 0.00 |
| 1.00 | 0.00 | 0.00 | 0.00 | 0.00 |
| 2.00 | 0.00 | 0.00 | 0.00 | 0.00 |
| 3.00 | 0.00 | 0.00 | 0.00 | 0.00 |
| 4.00 | 0.00 | 0.00 | 0.00 | 0.00 |
| 5.00 | 0.00 | 0.00 | 0.00 | 0.00 |
| 6.00 | 0.00 | 0.00 | 0.00 | 0.00 |
| 7.00 | 34.53 | 34.53 | 0.00 | 19.34 |
| 8.00 | 34.53 | 34.53 | 0.00 | 39.00 |
| 9.00 | 34.53 | 34.53 | 0.00 | 39.00 |
| 10.00 | 34.53 | 34.53 | 0.00 | 39.00 |
| 11.00 | 0.00 | 0.00 | 0.00 | 0.00 |
| 12.00 | 0.00 | 0.00 | 0.00 | 0.00 |
| 12.10 | 0.00 | 0.00 | 0.00 | 0.00 |
| 12.20 | 0.00 | 0.00 | 0.00 | 0.00 |
| 12.30 | 0.00 | 0.00 | 0.00 | 0.00 |
| 12.40 | 0.00 | 0.00 | 0.00 | 0.00 |
| 12.50 | 0.00 | 0.00 | 0.00 | 0.00 |
| 12.60 | 0.00 | 0.00 | 0.00 | 0.00 |
| 12.70 | 0.00 | 0.00 | 0.00 | 0.00 |
| 12.80 | 0.00 | 0.00 | 0.00 | 0.00 |
| 12.90 | 0.00 | 0.00 | 0.00 | 0.00 |
| 13.00 | 0.00 | 0.00 | 0.00 | 0.00 |

**Table 37 – $t_a$ - Effect of the differential pore pressure in the reservoir compartments**

| $\Delta P_1$ = -100 bar; $\Delta P_2$ = 0 bar | | | | | $\Delta P1$ = -100 bar; $\Delta P2$ = -200 bar | | | | |
|---|---|---|---|---|---|---|---|---|---|
| **Step** | **F1** | **F2** | **F3** | **F4 = F5** | **Step** | **F1** | **F2** | **F3** | **F4 = F5** |
| 0.00 | 0.00 | 0.00 | 0.00 | 0.00 | 0.00 | 0.00 | 0.00 | 0.00 | 0.00 |
| 1.00 | 0.00 | 0.00 | 0.00 | 0.00 | 1.00 | 0.00 | 0.00 | 0.00 | 0.00 |
| 2.00 | 0.00 | 0.00 | 0.00 | 0.00 | 2.00 | 0.00 | 0.00 | 0.00 | 0.00 |
| 3.00 | 0.00 | 0.00 | 0.00 | 0.00 | 3.00 | 0.00 | 0.00 | 0.00 | 0.00 |
| 4.00 | 0.00 | 0.00 | 0.00 | 0.00 | 4.00 | 0.00 | 0.00 | 0.00 | 0.00 |
| 5.00 | 17.27 | 17.27 | 0.00 | 19.34 | 5.00 | 17.27 | 17.27 | 0.00 | 19.34 |
| 6.00 | 34.53 | 34.53 | 0.00 | 39.00 | 6.00 | 34.53 | 34.53 | 0.00 | 39.00 |
| 7.00 | 34.53 | 34.53 | 0.00 | 39.00 | 7.00 | 34.53 | 34.53 | 0.00 | 39.00 |
| 8.00 | 34.53 | 34.53 | 0.00 | 39.00 | 8.00 | 34.53 | 34.53 | 0.00 | 39.00 |
| 9.00 | 34.53 | 34.53 | 0.00 | 39.00 | 9.00 | 34.53 | 34.53 | 0.00 | 39.00 |
| 10.00 | 34.53 | 34.53 | 0.00 | 57.40 | 10.00 | 34.53 | 34.53 | 0.00 | 57.40 |
| 11.00 | 0.00 | 0.00 | 0.00 | 0.00 | 11.00 | 0.00 | 0.00 | 0.00 | 0.00 |
| 12.00 | 17.27 | 17.27 | 0.00 | 0.00 | 12.00 | 17.27 | 17.27 | 0.00 | 0.00 |
| 12.10 | 0.00 | 17.27 | 0.00 | 0.00 | 12.10 | 0.00 | 0.00 | 0.00 | 0.00 |
| 12.20 | 0.00 | 17.27 | 0.00 | 0.00 | 12.20 | 0.00 | 0.00 | 0.00 | 0.00 |
| 12.30 | 0.00 | 17.27 | 0.00 | 0.00 | 12.30 | 0.00 | 0.00 | 0.00 | 0.00 |
| 12.40 | 0.00 | 17.27 | 0.00 | 0.00 | 12.40 | 0.00 | 0.00 | 0.00 | 0.00 |
| 12.50 | 0.00 | 17.27 | 0.00 | 0.00 | 12.50 | 0.00 | 34.53 | 34.00 | 27.95 |
| 12.60 | 0.00 | 17.27 | 0.00 | 0.00 | 12.60 | 0.00 | 0.00 | 0.00 | 0.00 |
| 12.70 | 0.00 | 17.27 | 0.00 | 0.00 | 12.70 | 0.00 | 0.00 | 0.00 | 0.00 |
| 12.80 | 0.00 | 17.27 | 0.00 | 0.00 | 12.80 | 0.00 | 0.00 | 0.00 | 0.00 |
| 12.90 | 0.00 | 17.27 | 0.00 | 0.00 | 12.90 | 0.00 | 0.00 | 0.00 | 0.00 |
| 13.00 | 17.27 | 17.27 | 0.00 | 0.00 | 13.00 | 17.27 | 17.27 | 0.00 | 0.00 |

**Table 38 – $t_{50}$ - Effect of the differential pore pressure in the reservoir compartments**

| $\Delta P_1$ = -100 bar; $\Delta P_2$ = 0 bar | | | | | $\Delta P1$ = -100 bar; $\Delta P2$ = -200 bar | | | | |
|---|---|---|---|---|---|---|---|---|---|
| **Step** | **F1** | **F2** | **F3** | **F4 = F5** | **Step** | **F1** | **F2** | **F3** | **F4 = F5** |
| 0.00 | 0.00 | 0.00 | 0.00 | 0.00 | 0.00 | 0.00 | 0.00 | 0.00 | 0.00 |
| 1.00 | 0.00 | 0.00 | 0.00 | 0.00 | 1.00 | 0.00 | 0.00 | 0.00 | 0.00 |
| 2.00 | 0.00 | 0.00 | 0.00 | 0.00 | 2.00 | 0.00 | 0.00 | 0.00 | 0.00 |
| 3.00 | 17.27 | 17.27 | 0.00 | 0.00 | 3.00 | 17.27 | 17.27 | 0.00 | 0.00 |
| 4.00 | 34.53 | 34.53 | 0.00 | 39.00 | 4.00 | 34.53 | 34.53 | 0.00 | 39.00 |
| 5.00 | 34.53 | 34.53 | 0.00 | 39.00 | 5.00 | 34.53 | 34.53 | 0.00 | 39.00 |
| 6.00 | 34.53 | 34.53 | 0.00 | 39.00 | 6.00 | 34.53 | 34.53 | 0.00 | 39.00 |
| 7.00 | 34.53 | 34.53 | 0.00 | 39.00 | 7.00 | 34.53 | 34.53 | 0.00 | 39.00 |
| 8.00 | 34.53 | 34.53 | 0.00 | 57.40 | 8.00 | 34.53 | 34.53 | 0.00 | 57.40 |
| 9.00 | 86.31 | 86.31 | 0.00 | 76.72 | 9.00 | 86.31 | 86.31 | 0.00 | 76.72 |
| 10.00 | 103.58 | 103.58 | 0.00 | 112.31 | 10.00 | 103.58 | 103.58 | 0.00 | 112.31 |
| 11.00 | 23.36 | 23.36 | 0.00 | 37.73 | 11.00 | 23.36 | 23.36 | 0.00 | 37.73 |
| 12.00 | 17.27 | 17.27 | 0.00 | 34.86 | 12.00 | 17.27 | 17.27 | 0.00 | 34.86 |
| 12.10 | 17.27 | 17.27 | 0.00 | 26.85 | 12.10 | 17.27 | 17.27 | 0.00 | 9.92 |
| 12.20 | 17.27 | 17.27 | 0.00 | 16.93 | 12.20 | 17.27 | 0.00 | 0.00 | 16.90 |
| 12.30 | 0.00 | 17.27 | 0.00 | 16.93 | 12.30 | 0.00 | 62.96 | 0.00 | 19.84 |
| 12.40 | 0.00 | 17.27 | 34.00 | 32.33 | 12.40 | 0.00 | 84.28 | 34.00 | 56.24 |
| 12.50 | 23.36 | 17.27 | 34.00 | 34.29 | 12.50 | 23.36 | 103.58 | 34.00 | 74.52 |
| 12.60 | 0.00 | 17.27 | 34.00 | 32.33 | 12.60 | 0.00 | 84.28 | 34.00 | 56.24 |
| 12.70 | 0.00 | 17.27 | 0.00 | 16.93 | 12.70 | 0.00 | 62.96 | 0.00 | 19.84 |
| 12.80 | 17.27 | 17.27 | 0.00 | 16.93 | 12.80 | 17.27 | 0.00 | 0.00 | 16.90 |
| 12.90 | 17.27 | 17.27 | 0.00 | 26.85 | 12.90 | 17.27 | 17.27 | 0.00 | 9.92 |
| 13.00 | 17.27 | 17.27 | 0.00 | 34.86 | 13.00 | 17.27 | 17.27 | 0.00 | 34.86 |

**Table 39 – $t_{80}$ - Effect of the differential pore pressure in the reservoir compartments**

| $\Delta P_1$ = -100 bar; $\Delta P_2$ = 0 bar | | | | | $\Delta P1$ = -100 bar; $\Delta P2$ = -200 bar | | | | |
|---|---|---|---|---|---|---|---|---|---|
| **Step** | **F1** | **F2** | **F3** | **F4 = F5** | **Step** | **F1** | **F2** | **F3** | **F4 = F5** |
| 0.00 | 0.00 | 0.00 | 0.00 | 0.00 | 0.00 | 0.00 | 0.00 | 0.00 | 0.00 |
| 1.00 | 0.00 | 0.00 | 0.00 | 0.00 | 1.00 | 0.00 | 0.00 | 0.00 | 0.00 |
| 2.00 | 0.00 | 0.00 | 0.00 | 0.00 | 2.00 | 0.00 | 0.00 | 0.00 | 0.00 |
| 3.00 | 0.00 | 0.00 | 0.00 | 0.00 | 3.00 | 0.00 | 0.00 | 0.00 | 0.00 |
| 4.00 | 0.00 | 0.00 | 0.00 | 0.00 | 4.00 | 0.00 | 0.00 | 0.00 | 0.00 |
| 5.00 | 17.27 | 17.27 | 0.00 | 19.34 | 5.00 | 17.27 | 17.27 | 0.00 | 19.34 |
| 6.00 | 34.53 | 34.53 | 0.00 | 39.00 | 6.00 | 34.53 | 34.53 | 0.00 | 39.00 |
| 7.00 | 34.53 | 34.53 | 0.00 | 39.00 | 7.00 | 34.53 | 34.53 | 0.00 | 39.00 |
| 8.00 | 34.53 | 34.53 | 0.00 | 39.00 | 8.00 | 34.53 | 34.53 | 0.00 | 39.00 |
| 9.00 | 34.53 | 34.53 | 0.00 | 39.00 | 9.00 | 34.53 | 34.53 | 0.00 | 39.00 |
| 10.00 | 34.53 | 34.53 | 0.00 | 57.40 | 10.00 | 34.53 | 34.53 | 0.00 | 57.40 |
| 11.00 | 0.00 | 0.00 | 0.00 | 0.00 | 11.00 | 0.00 | 0.00 | 0.00 | 0.00 |
| 12.00 | 17.27 | 17.27 | 0.00 | 0.00 | 12.00 | 17.27 | 17.27 | 0.00 | 0.00 |
| 12.10 | 0.00 | 17.27 | 0.00 | 0.00 | 12.10 | 0.00 | 0.00 | 0.00 | 0.00 |
| 12.20 | 0.00 | 17.27 | 0.00 | 0.00 | 12.20 | 0.00 | 0.00 | 0.00 | 0.00 |
| 12.30 | 0.00 | 17.27 | 0.00 | 0.00 | 12.30 | 0.00 | 0.00 | 0.00 | 0.00 |
| 12.40 | 0.00 | 17.27 | 0.00 | 0.00 | 12.40 | 0.00 | 0.00 | 0.00 | 0.00 |
| 12.50 | 0.00 | 17.27 | 0.00 | 0.00 | 12.50 | 0.00 | 34.53 | 34.00 | 27.95 |
| 12.60 | 0.00 | 17.27 | 0.00 | 0.00 | 12.60 | 0.00 | 0.00 | 0.00 | 0.00 |
| 12.70 | 0.00 | 17.27 | 0.00 | 0.00 | 12.70 | 0.00 | 0.00 | 0.00 | 0.00 |
| 12.80 | 0.00 | 17.27 | 0.00 | 0.00 | 12.80 | 0.00 | 0.00 | 0.00 | 0.00 |
| 12.90 | 0.00 | 17.27 | 0.00 | 0.00 | 12.90 | 0.00 | 0.00 | 0.00 | 0.00 |
| 13.00 | 17.27 | 17.27 | 0.00 | 0.00 | 13.00 | 17.27 | 17.27 | 0.00 | 0.00 |

**Table 40 – $t_a$ - Effect of salt caprock**

| salt caprock | | | | |
|---|---|---|---|---|
| **Step** | **F1** | **F2** | **F3** | **F4 = F5** |
| 0.00 | 0.00 | 0.00 | 0.00 | 0.00 |
| 1.00 | 0.00 | 0.00 | 0.00 | 0.00 |
| 2.00 | 0.00 | 0.00 | 0.00 | 0.00 |
| 3.00 | 0.00 | 0.00 | 0.00 | 0.00 |
| 4.00 | 17.27 | 17.27 | 0.00 | 18.38 |
| 5.00 | 0.00 | 0.00 | 0.00 | 0.96 |
| 6.00 | 0.00 | 0.00 | 0.00 | 0.00 |
| 7.00 | 0.00 | 0.00 | 0.00 | 4.12 ** |
| 8.00 | 14.22 * | 14.22 * | 0.00 | 15.54 * |
| 9.00 | 3.05 ** | 3.05 ** | 0.00 | 0.00 |
| 10.00 | 0.00 | 0.00 | 0.00 | 0.00 |
| 11.00 | 0.00 | 0.00 | 0.00 | 0.00 |
| 12.00 | 34.53 | 34.53 | 0.00 | 39.00 |
| 12.10 | 0.00 | 0.00 | 0.00 | 0.00 |
| 12.20 | 0.00 | 0.00 | 0.00 | 0.00 |
| 12.30 | 0.00 | 0.00 | 0.00 | 0.00 |
| 12.40 | 0.00 | 0.00 | 0.00 | 12.5 * |
| 12.50 | 11.17 * | 11.17 * | 0.00 | 4.05 ** |
| 12.60 | 0.00 | 0.00 | 0.00 | 0.00 |
| 12.70 | 0.00 | 0.00 | 0.00 | 0.00 |
| 12.80 | 0.00 | 0.00 | 0.00 | 0.00 |
| 12.90 | 0.00 | 0.00 | 0.00 | 0.00 |
| 13.00 | 0.00 | 0.00 | 0.00 | 16.39 |

**Table 41 – $t_{50}$ - Effect of salt caprock**

| Salt caprock | | | | |
|---|---|---|---|---|
| **Step** | **F1** | **F2** | **F3** | **F4 = F5** |
| 0.00 | 0.00 | 0.00 | 0.00 | 0.00 |
| 1.00 | 0.00 | 0.00 | 0.00 | 0.00 |
| 2.00 | 0.00 | 0.00 | 0.00 | 0.00 |
| 3.00 | 17.27 | 17.27 | 0.00 | 19.34 |
| 4.00 | 34.53 | 34.53 | 0.00 | 39.00 |
| 5.00 | 34.53 | 34.53 | 0.00 | 39.00 |
| 6.00 | 34.53 | 34.53 | 0.00 | 39.00 |
| 7.00 | 34.53 | 34.53 | 0.00 | 39.00 |
| 8.00 | 46.72 | 46.72 | 0.00 | 46.90 |
| 9.00 | 69.06 | 69.06 | 0.00 | 68.18 |
| 10.00 | 69.06 | 69.06 | 0.00 | 77.68 |
| 11.00 | 44.68 | 44.68 | 0.00 | 57.17 |
| 12.00 | 34.53 | 34.53 | 0.00 | 39.00 |
| 12.10 | 17.27 | 17.27 | 0.00 | 20.38 |
| 12.20 | 2.03 | 2.03 | 0.00 | 0.00 |
| 12.30 | 15.23 | 15.23 | 0.00 | 16.55 |
| 12.40 | 17.27 | 17.27 | 0.00 | 18.62 |
| 12.50 | 17.27 | 17.27 | 0.00 | 19.66 |
| 12.60 | 17.27 | 17.27 | 0.00 | 18.62 |
| 12.70 | 0.00 | 0.00 | 0.00 | 0.00 |
| 12.80 | 6.09 | 6.09 | 0.00 | 0.00 |
| 12.90 | 17.27 | 17.27 | 0.00 | 34.86 |
| 13.00 | 34.53 | 34.53 | 0.00 | 39.00 |

**Table 42 – $t_{80}$ - Effect of salt caprock**

| Salt caprock | | | | |
|---|---|---|---|---|
| **Step** | **F1** | **F2** | **F3** | **F4 = F5** |
| 0.00 | 0.00 | 0.00 | 0.00 | 0.00 |
| 1.00 | 0.00 | 0.00 | 0.00 | 0.00 |
| 2.00 | 0.00 | 0.00 | 0.00 | 0.00 |
| 3.00 | 0.00 | 0.00 | 0.00 | 0.00 |
| 4.00 | 17.27 | 17.27 | 0.00 | 19.34 |
| 5.00 | 17.27 | 17.27 | 0.00 | 19.34 |
| 6.00 | 17.27 | 17.27 | 0.00 | 39.00 |
| 7.00 | 34.53 | 34.53 | 0.00 | 39.00 |
| 8.00 | 34.53 | 34.53 | 0.00 | 39.00 |
| 9.00 | 34.53 | 34.53 | 0.00 | 39.00 |
| 10.00 | 36.56 | 36.56 | 0.00 | 40.94 |
| 11.00 | 0.00 | 0.00 | 0.00 | 20.00 |
| 12.00 | 34.53 | 34.53 | 0.00 | 39.00 |
| 12.10 | 0.00 | 0.00 | 0.00 | 0.00 |
| 12.20 | 0.00 | 0.00 | 0.00 | 0.00 |
| 12.30 | 0.00 | 0.00 | 0.00 | 7.50 |
| 12.40 | 13.20 | 13.20 | 0.00 | 16.55 |
| 12.50 | 17.27 | 17.27 | 0.00 | 18.62 |
| 12.60 | 0.00 | 0.00 | 0.00 | 0.00 |
| 12.70 | 0.00 | 0.00 | 0.00 | 0.00 |
| 12.80 | 0.00 | 0.00 | 0.00 | 0.00 |
| 12.90 | 0.00 | 0.00 | 0.00 | 0.00 |
| 13.00 | 28.44 | 28.44 | 0.00 | 35.89 |

**Table 43 – $t_a$ – Mechanism 1 (mechanical hysteresis)**

| Step | F1 | F2 | F3 | F4 = F5 |
|---|---|---|---|---|
| 0.00 | 0.00 | 0.00 | 0.00 | 0.00 |
| 1.00 | 0.00 | 0.00 | 0.00 | 0.00 |
| 2.00 | 0.00 | 0.00 | 0.00 | 0.00 |
| 3.00 | 0.00 | 0.00 | 0.00 | 0.00 |
| 4.00 | 0.00 | 0.00 | 0.00 | 0.00 |
| 5.00 | 0.00 | 0.00 | 0.00 | 0.00 |
| 6.00 | 17.27 | 17.27 | 0.00 | 19.34 |
| 7.00 | 17.27 | 17.27 | 0.00 | 17.59 |
| 8.00 | 0.00 | 0.00 | 0.00 | 2.07 |
| 9.00 | 0.00 | 0.00 | 0.00 | 0.00 |
| 10.00 | 0.00 | 0.00 | 0.00 | 0.00 |
| 11.00 | 0.00 | 0.00 | 0.00 | 0.00 |
| 12.00 | 0.00 | 0.00 | 0.00 | 0.00 |
| 12.10 | 0.00 | 0.00 | 0.00 | 0.00 |
| 12.20 | 0.00 | 0.00 | 0.00 | 0.00 |
| 12.30 | 0.00 | 0.00 | 0.00 | 0.00 |
| 12.40 | 0.00 | 0.00 | 0.00 | 0.00 |
| 12.50 | 0.00 | 0.00 | 0.00 | 0.00 |
| 12.60 | 0.00 | 0.00 | 0.00 | 0.00 |
| 12.70 | 0.00 | 0.00 | 0.00 | 0.00 |
| 12.80 | 0.00 | 0.00 | 0.00 | 0.00 |
| 12.90 | 0.00 | 0.00 | 0.00 | 0.00 |
| 13.00 | 0.00 | 0.00 | 0.00 | 0.00 |

**Table 44 – $t_{50}$ - Mechanism 1 (mechanical hysteresis)**

| Step | F1 | F2 | F3 | F4 = F5 |
|---|---|---|---|---|
| 0.00 | 0.00 | 0.00 | 0.00 | 0.00 |
| 1.00 | 0.00 | 0.00 | 0.00 | 0.00 |
| 2.00 | 0.00 | 0.00 | 0.00 | 0.00 |
| 3.00 | 17.27 | 17.27 | 0.00 | 18.38 |
| 4.00 | 34.53 | 34.53 | 0.00 | 39.00 |
| 5.00 | 34.53 | 34.53 | 0.00 | 39.00 |
| 6.00 | 34.53 | 34.53 | 0.00 | 39.00 |
| 7.00 | 34.53 | 34.53 | 0.00 | 39.00 |
| 8.00 | 47.73 | 47.73 | 0.00 | 57.40 |
| 9.00 | 95.45 | 95.45 | 0.00 | 77.68 |
| 10.00 | 103.58 | 103.58 | 0.00 | 115.42 |
| 11.00 | 47.73 | 47.73 | 0.00 | 38.68 |
| 12.00 | 24.38 | 24.38 | 0.00 | 36.93 |
| 12.10 | 17.27 | 17.27 | 0.00 | 19.34 |
| 12.20 | 17.27 | 17.27 | 0.00 | 18.38 |
| 12.30 | 32.50 | 32.50 | 0.00 | 18.35 |
| 12.40 | 26.41 | 26.41 | 0.00 | 36.75 |
| 12.50 | 47.73 | 47.73 | 0.00 | 38.68 |
| 12.60 | 26.41 | 26.41 | 0.00 | 36.75 |
| 12.70 | 32.50 | 32.50 | 0.00 | 18.35 |
| 12.80 | 17.27 | 17.27 | 0.00 | 18.38 |
| 12.90 | 17.27 | 17.27 | 0.00 | 19.34 |
| 13.00 | 24.38 | 24.38 | 0.00 | 36.93 |

**Table 45 – $t_{80}$ - Mechanism 1 (mechanical hysteresis)**

| | | | | |
|---|---|---|---|---|
| 0.00 | 0.00 | 0.00 | 0.00 | 0.00 |
| 1.00 | 0.00 | 0.00 | 0.00 | 0.00 |
| 2.00 | 0.00 | 0.00 | 0.00 | 0.00 |
| 3.00 | 0.00 | 0.00 | 0.00 | 0.00 |
| 4.00 | 0.00 | 0.00 | 0.00 | 0.00 |
| 5.00 | 30.47 | 30.47 | 0.00 | 19.34 |
| 6.00 | 34.53 | 34.53 | 0.00 | 39.00 |
| 7.00 | 34.53 | 34.53 | 0.00 | 39.00 |
| 8.00 | 34.53 | 34.53 | 0.00 | 39.00 |
| 9.00 | 34.53 | 34.53 | 0.00 | 39.00 |
| 10.00 | 51.79 | 51.79 | 0.00 | 58.37 |
| 11.00 | 0.00 | 0.00 | 0.00 | 0.00 |
| 12.00 | 17.27 | 17.27 | 0.00 | 18.38 |
| 12.10 | 6.09 | 6.09 | 0.00 | 0.00 |
| 12.20 | 0.00 | 0.00 | 0.00 | 0.00 |
| 12.30 | 0.00 | 0.00 | 0.00 | 0.00 |
| 12.40 | 0.00 | 0.00 | 0.00 | 0.00 |
| 12.50 | 0.00 | 0.00 | 0.00 | 0.00 |
| 12.60 | 0.00 | 0.00 | 0.00 | 0.00 |
| 12.70 | 0.00 | 0.00 | 0.00 | 0.00 |
| 12.80 | 0.00 | 0.00 | 0.00 | 0.00 |
| 12.90 | 6.09 | 6.09 | 0.00 | 0.00 |
| 13.00 | 17.27 | 17.27 | 0.00 | 18.38 |

**Table 46 – $t_a$ – Mechanism 2 (pore pressure distribution in the reservoir)**

| Mech 2 | | | | |
|---|---|---|---|---|
| **Step** | **F1** | **F2** | **F3** | **F4 = F5** |
| 12.10 | 0.00 | 0.00 | 0.00 | 0.00 |
| 12.20 | 0.00 | 0.00 | 0.00 | 0.00 |
| 12.30 | 0.00 | 0.00 | 0.00 | 0.00 |
| 12.40 | 0.00 | 0.00 | 0.00 | 0.00 |
| 12.50 | 0.00 | 0.00 | 0.00 | 0.00 |
| 12.60 | 0.00 | 0.00 | 0.00 | 0.00 |
| 12.70 | 0.00 | 0.00 | 0.00 | 0.00 |
| 12.80 | 0.00 | 0.00 | 0.00 | 0.00 |
| 12.90 | 0.00 | 0.00 | 0.00 | 0.00 |
| 13.00 | 0.00 | 0.00 | 0.00 | 0.00 |

**Table 47 – $t_{50}$ - Mechanism 2 (pore pressure distribution in the reservoir)**

| Mech 2 | | | | |
|---|---|---|---|---|
| **Step** | **F1** | **F2** | **F3** | **F4 = F5** |
| 12.10 | 17.27 | 17.27 | 0.00 | 19.34 |
| 12.20 | 17.27 | 17.27 | 0.00 | 19.34 |
| 12.30 | 0.00 | 0.00 | 0.00 | 22.42 |
| 12.40 | 17.27 | 17.27 | 0.00 | 37.73 |
| 12.50 | 21.33 | 21.33 | 0.00 | 37.73 |
| 12.60 | 15.23 | 15.23 | 0.00 | 36.75 |
| 12.70 | 0.00 | 0.00 | 0.00 | 0.00 |
| 12.80 | 17.27 | 17.27 | 0.00 | 4.00 |
| 12.90 | 17.27 | 17.27 | 0.00 | 19.34 |
| 13.00 | 17.27 | 17.27 | 0.00 | 19.34 |

**Table 48 – $t_{80}$ - Mechanism 2 (pore pressure distribution in the reservoir)**

| Mech 2 | | | | |
|---|---|---|---|---|
| **Step** | **F1** | **F2** | **F3** | **F4 = F5** |
| 12.10 | 17.27 | 17.27 | 0.00 | 0.00 |
| 12.20 | 0.00 | 0.00 | 0.00 | 0.00 |
| 12.30 | 0.00 | 0.00 | 0.00 | 0.00 |
| 12.40 | 0.00 | 0.00 | 0.00 | 0.00 |
| 12.50 | 0.00 | 0.00 | 0.00 | 0.00 |
| 12.60 | 0.00 | 0.00 | 0.00 | 0.00 |
| 12.70 | 0.00 | 0.00 | 0.00 | 0.00 |
| 12.80 | 0.00 | 0.00 | 0.00 | 0.00 |
| 12.90 | 0.00 | 0.00 | 0.00 | 0.00 |
| 13.00 | 17.27 | 17.27 | 0.00 | 0.00 |

**Table 49 – $t_a$ – Mechanism 3D (fault lubrification)**

| Mech 3 D | | | | |
|---|---|---|---|---|
| **Step** | **F1** | **F2** | **F3** | **F4 = F5** |
| 12.00 | 0.00 | 0.00 | 0.00 | 0.00 |
| 12.10 | 0.00 | 0.00 | 0.00 | 0.00 |
| 12.20 | 0.00 | 0.00 | 0.00 | 0.00 |
| 12.30 | 0.00 | 17.27 | 0.00 | 9.42 |
| 12.40 | 0.00 | 17.27 | 0.00 | 9.58 |
| 12.50 | 0.00 | 0.00 | 0.00 | 1.00 |
| 12.60 | 0.00 | 0.00 | 0.00 | 0.00 |
| 12.70 | 0.00 | 0.00 | 0.00 | 0.00 |
| 12.80 | 0.00 | 0.00 | 0.00 | 0.00 |
| 12.90 | 0.00 | 0.00 | 0.00 | 0.00 |
| 13.00 | 0.00 | 0.00 | 0.00 | 0.00 |

**Table 50 – $t_{50}$ - Mechanism 3D (fault lubrification)**

| Mech 3 D | | | | |
|---|---|---|---|---|
| **Step** | **F1** | **F2** | **F3** | **F4 = F5** |
| 12.00 | 0.00 | 0.00 | 0.00 | 0.00 |
| 12.10 | 0.00 | 0.00 | 0.00 | 0.00 |
| 12.20 | 0.00 | 34.53 | 0.00 | 19.50 |
| 12.30 | 17.27 | 34.53 | 0.00 | 21.50 |
| 12.40 | 34.53 | 34.53 | 0.00 | 47.45 |
| 12.50 | 34.53 | 103.58 | 34.00 | 74.15 |
| 12.60 | 34.53 | 84.28 | 0.00 | 57.84 |
| 12.70 | 17.27 | 67.02 | 0.00 | 19.84 |
| 12.80 | 0.00 | 0.00 | 0.00 | 15.90 |
| 12.90 | 0.00 | 17.27 | 0.00 | 0.00 |
| 13.00 | 0.00 | 17.27 | 0.00 | 15.93 |

**Table 51 – $t_{80}$ - Mechanism 3D (fault lubrification)**

| Mech 3 D | | | | |
|---|---|---|---|---|
| **Step** | **F1** | **F2** | **F3** | **F4 = F5** |
| 12.00 | 0.00 | 0.00 | 0.00 | 0.00 |
| 12.10 | 0.00 | 0.00 | 0.00 | 0.00 |
| 12.20 | 0.00 | 0.00 | 0.00 | 0.00 |
| 12.30 | 0.00 | 34.53 | 0.00 | 19.00 |
| 12.40 | 0.00 | 34.53 | 0.00 | 20.00 |
| 12.50 | 17.27 | 34.53 | 0.00 | 38.87 |
| 12.60 | 0.00 | 0.00 | 0.00 | 0.00 |
| 12.70 | 0.00 | 0.00 | 0.00 | 0.00 |
| 12.80 | 0.00 | 0.00 | 0.00 | 0.00 |
| 12.90 | 0.00 | 0.00 | 0.00 | 0.00 |
| 13.00 | 0.00 | 17.27 | 0.00 | 0.00 |

**Table 52 – $t_a$ - Reference test case with fault pressure depletion**

| REFERENCE_PF | | | | |
|---|---|---|---|---|
| **Step** | **F1** | **F2** | **F3** | **F4 = F5** |
| 0.00 | 0.00 | 0.00 | 0.00 | 0.00 |
| 1.00 | 0.00 | 0.00 | 0.00 | 0.00 |
| 2.00 | 0.00 | 0.00 | 0.00 | 0.00 |
| 3.00 | 0.00 | 0.00 | 0.00 | 0.00 |
| 4.00 | 0.00 | 0.00 | 0.00 | 0.00 |
| 5.00 | 0.00 | 0.00 | 0.00 | 0.00 |
| 6.00 | 0.00 | 0.00 | 0.00 | 0.00 |
| 7.00 | 0.00 | 0.00 | 0.00 | 0.00 |
| 8.00 | 17.27 | 17.27 | 0.00 | 19.34 |
| 9.00 | 0.00 | 0.00 | 0.00 | 0.00 |
| 10.00 | 0.00 | 0.00 | 0.00 | 17.59 |
| 11.00 | 0.00 | 0.00 | 0.00 | 0.00 |
| 12.00 | 0.00 | 0.00 | 0.00 | 0.00 |
| 12.10 | 0.00 | 0.00 | 0.00 | 0.00 |
| 12.20 | 0.00 | 0.00 | 0.00 | 0.00 |
| 12.30 | 0.00 | 0.00 | 0.00 | 0.00 |
| 12.40 | 0.00 | 0.00 | 0.00 | 0.00 |
| 12.50 | 0.00 | 0.00 | 0.00 | 0.00 |
| 12.60 | 0.00 | 0.00 | 0.00 | 0.00 |
| 12.70 | 0.00 | 0.00 | 0.00 | 0.00 |
| 12.80 | 0.00 | 0.00 | 0.00 | 0.00 |
| 12.90 | 0.00 | 0.00 | 0.00 | 0.00 |
| 13.00 | 0.00 | 0.00 | 0.00 | 0.00 |

**Table 53 – $t_{50}$ - Reference test case with fault pressure depletion**

| REFERENCE_PF | | | | |
|---|---|---|---|---|
| **Step** | **F1** | **F2** | **F3** | **F4 = F5** |
| 0.00 | 0.00 | 0.00 | 0.00 | 0.00 |
| 1.00 | 0.00 | 0.00 | 0.00 | 0.00 |
| 2.00 | 0.00 | 0.00 | 0.00 | 0.00 |
| 3.00 | 0.00 | 0.00 | 0.00 | 0.00 |
| 4.00 | 34.53 | 34.53 | 0.00 | 37.96 |
| 5.00 | 34.53 | 34.53 | 0.00 | 39.00 |
| 6.00 | 34.53 | 34.53 | 0.00 | 39.00 |
| 7.00 | 34.53 | 34.53 | 0.00 | 39.00 |
| 8.00 | 34.53 | 34.53 | 0.00 | 39.00 |
| 9.00 | 34.53 | 34.53 | 0.00 | 39.00 |
| 10.00 | 34.53 | 34.53 | 0.00 | 39.00 |
| 11.00 | 17.27 | 17.27 | 0.00 | 19.66 |
| 12.00 | 17.27 | 17.27 | 0.00 | 0.00 |
| 12.10 | 0.00 | 0.00 | 0.00 | 0.00 |
| 12.20 | 0.00 | 0.00 | 0.00 | 0.00 |
| 12.30 | 0.00 | 0.00 | 0.00 | 0.00 |
| 12.40 | 17.27 | 17.27 | 0.00 | 0.00 |
| 12.50 | 17.27 | 17.27 | 0.00 | 19.66 |
| 12.60 | 17.27 | 17.27 | 0.00 | 0.00 |
| 12.70 | 0.00 | 0.00 | 0.00 | 0.00 |
| 12.80 | 0.00 | 0.00 | 0.00 | 0.00 |
| 12.90 | 0.00 | 0.00 | 0.00 | 0.00 |
| 13.00 | 17.27 | 17.27 | 0.00 | 0.00 |

**Table 54 – $t_{80}$ - Reference test case with fault pressure depletion**

| REFERENCE_PF | | | | |
|---|---|---|---|---|
| **Step** | **F1** | **F2** | **F3** | **F4 = F5** |
| 0.00 | 0.00 | 0.00 | 0.00 | 0.00 |
| 1.00 | 0.00 | 0.00 | 0.00 | 0.00 |
| 2.00 | 0.00 | 0.00 | 0.00 | 0.00 |
| 3.00 | 0.00 | 0.00 | 0.00 | 0.00 |
| 4.00 | 0.00 | 0.00 | 0.00 | 0.00 |
| 5.00 | 0.00 | 0.00 | 0.00 | 0.00 |
| 6.00 | 17.27 | 17.27 | 0.00 | 18.38 |
| 7.00 | 32.50 | 32.50 | 0.00 | 35.89 |
| 8.00 | 34.53 | 34.53 | 0.00 | 39.00 |
| 9.00 | 34.53 | 34.53 | 0.00 | 39.00 |
| 10.00 | 34.53 | 34.53 | 0.00 | 39.00 |
| 11.00 | 0.00 | 0.00 | 0.00 | 0.00 |
| 12.00 | 0.00 | 0.00 | 0.00 | 0.00 |
| 12.10 | 0.00 | 0.00 | 0.00 | 0.00 |
| 12.20 | 0.00 | 0.00 | 0.00 | 0.00 |
| 12.30 | 0.00 | 0.00 | 0.00 | 0.00 |
| 12.40 | 0.00 | 0.00 | 0.00 | 0.00 |
| 12.50 | 0.00 | 0.00 | 0.00 | 0.00 |
| 12.60 | 0.00 | 0.00 | 0.00 | 0.00 |
| 12.70 | 0.00 | 0.00 | 0.00 | 0.00 |
| 12.80 | 0.00 | 0.00 | 0.00 | 0.00 |
| 12.90 | 0.00 | 0.00 | 0.00 | 0.00 |
| 13.00 | 0.00 | 0.00 | 0.00 | 0.00 |

**Table 55 – $t_a$ – Mechanism 4 (pore pressure variation versus time)**

| Mech 04 | | | | |
|---|---|---|---|---|
| **Step** | **F1** | **F2** | **F3** | **F4 = F5** |
| 12.10 | 0.00 | 0.00 | 0.00 | 0.00 |
| 12.20 | 0.00 | 0.00 | 0.00 | 0.00 |
| 12.30 | 0.00 | 0.00 | 0.00 | 0.00 |
| 12.40 | 0.00 | 0.00 | 0.00 | 0.00 |
| 12.50 | 0.00 | 0.00 | 0.00 | 0.00 |
| 12.60 | 0.00 | 0.00 | 0.00 | 0.00 |
| 12.70 | 0.00 | 0.00 | 0.00 | 0.00 |
| 12.80 | 0.00 | 0.00 | 0.00 | 0.00 |
| 12.90 | 0.00 | 0.00 | 0.00 | 0.00 |
| 13.00 | 0.00 | 0.00 | 0.00 | 0.00 |

**Table 56 – $t_{50}$ - Mechanism 4 (pore pressure variation versus time)**

| Mech 04 | | | | |
|---|---|---|---|---|
| **Step** | **F1** | **F2** | **F3** | **F4 = F5** |
| 12.10 | 17.27 | 17.27 | 0.00 | 19.34 |
| 12.20 | 0.00 | 0.00 | 0.00 | 0.00 |
| 12.30 | 15.23 | 15.23 | 0.00 | 36.75 |
| 12.40 | 64.99 | 64.99 | 0.00 | 38.68 |
| 12.50 | 84.28 | 84.28 | 0.00 | 58.34 |
| 12.60 | 64.99 | 64.99 | 0.00 | 38.68 |
| 12.70 | 15.23 | 15.23 | 0.00 | 36.75 |
| 12.80 | 0.00 | 0.00 | 0.00 | 0.00 |
| 12.90 | 17.27 | 17.27 | 0.00 | 19.34 |
| 13.00 | 17.27 | 17.27 | 0.00 | 34.86 |

**Table 57 – $t_{80}$ - Mechanism 4 (pore pressure variation versus time)**

| Mech 04 | | | | |
|---|---|---|---|---|
| **Step** | **F1** | **F2** | **F3** | **F4 = F5** |
| 12.10 | 0.00 | 0.00 | 0.00 | 0.00 |
| 12.20 | 0.00 | 0.00 | 0.00 | 0.00 |
| 12.30 | 0.00 | 0.00 | 0.00 | 0.00 |
| 12.40 | 0.00 | 0.00 | 0.00 | 0.00 |
| 12.50 | 0.00 | 0.00 | 0.00 | 0.00 |
| 12.60 | 0.00 | 0.00 | 0.00 | 0.00 |
| 12.70 | 0.00 | 0.00 | 0.00 | 0.00 |
| 12.80 | 0.00 | 0.00 | 0.00 | 0.00 |
| 12.90 | 0.00 | 0.00 | 0.00 | 0.00 |
| 13.00 | 17.27 | 17.27 | 0.00 | 0.00 |

# Annex III - $\chi_{max}$, $t_a$, $t_{80}$, and $t_{50}$ for the "combination scenarios"

**Table 58 – $\chi_{max}$ – Combination 1**

| COMBINATION 1 | | | | |
|---|---|---|---|---|
| **Step** | **F1** | **F2** | **F3** | **F4 = F5** |
| 0.00 | 0.10 | 0.10 | 0.21 | 0.00 |
| 1.00 | 0.17 | 0.23 | 0.34 | 0.22 |
| 2.00 | 0.31 | 0.37 | 0.46 | 0.45 |
| 3.00 | 0.55 | 0.65 | 0.72 | 0.69 |
| 4.00 | 0.80 | 0.95 | 1.00 | 0.94 |
| 5.00 | 1.00 | 1.00 | 1.00 | 1.00 |
| 6.00 | 1.00 | 1.00 | 1.00 | 1.00 |
| 7.00 | 1.00 | 1.00 | 1.00 | 1.00 |
| 8.00 | 1.00 | 1.00 | 1.00 | 1.00 |
| 9.00 | 1.00 | 1.00 | 1.00 | 1.00 |
| 10.00 | 1.00 | 1.00 | 1.00 | 1.00 |
| 11.00 | 0.72 | 0.73 | 1.00 | 0.83 |
| 12.00 | 1.00 | 1.00 | 1.00 | 1.00 |
| 12.10 | 0.80 | 0.78 | 0.81 | 0.81 |
| 12.20 | 0.64 | 0.60 | 0.63 | 0.64 |
| 12.30 | 0.49 | 0.47 | 0.60 | 0.68 |
| 12.40 | 0.53 | 0.52 | 0.60 | 0.71 |
| 12.50 | 0.58 | 0.57 | 0.65 | 0.75 |
| 12.60 | 0.53 | 0.52 | 0.60 | 0.71 |
| 12.70 | 0.49 | 0.47 | 0.60 | 0.68 |
| 12.80 | 0.64 | 0.60 | 0.63 | 0.64 |
| 12.90 | 0.80 | 0.78 | 0.81 | 0.81 |
| 13.00 | 0.95 | 0.95 | 0.95 | 0.98 |

**Table 59 – $t_a$ – Combination 1**

| COMBINATION 1 | | | | |
|---|---|---|---|---|
| **Step** | **F1** | **F2** | **F3** | **F4 = F5** |
| 0.00 | 0.00 | 0.00 | 0.00 | 0.00 |
| 1.00 | 0.00 | 0.00 | 0.00 | 0.00 |
| 2.00 | 0.00 | 0.00 | 0.00 | 0.00 |
| 3.00 | 0.00 | 0.00 | 0.00 | 0.00 |
| 4.00 | 0.00 | 0.00 | 18.76 | 0.00 |
| 5.00 | 17.27 | 17.26 | 0.00 | 13.37 |
| 6.00 | 0.00 | 0.00 | 0.00 | 5.92 |
| 7.00 | 0.00 | 15.23 | 56.27 | 0.00 |
| 8.00 | 0.00 | 25.39 | 0.00 | 17.47 |
| 9.00 | 17.27 | 28.44 | 56.27 | 12.68 |
| 10.00 | 11.17 | 0.00 | 35.31 | 8.79 |
| 11.00 | 0.00 | 0.00 | 0.00 | 0.00 |
| 12.00 | 17.27 | 17.26 | 0.00 | 17.81 |
| 12.10 | 0.00 | 0.00 | 0.00 | 0.00 |
| 12.20 | 0.00 | 0.00 | 0.00 | 0.00 |
| 12.30 | 0.00 | 0.00 | 0.00 | 0.00 |
| 12.40 | 0.00 | 0.00 | 0.00 | 0.00 |
| 12.50 | 0.00 | 0.00 | 0.00 | 0.00 |
| 12.60 | 0.00 | 0.00 | 0.00 | 0.00 |
| 12.70 | 0.00 | 0.00 | 0.00 | 0.00 |
| 12.80 | 0.00 | 0.00 | 0.00 | 0.00 |
| 12.90 | 0.00 | 0.00 | 0.00 | 0.00 |
| 13.00 | 0.00 | 0.00 | 0.00 | 0.00 |

**Table 60 – $t_{50}$ – Combination 1**

| COMBINATION 1 | | | | |
|---|---|---|---|---|
| **Step** | **F1** | **F2** | **F3** | **F4 = F5** |
| 0.00 | 0.00 | 0.00 | 0.00 | 0.00 |
| 1.00 | 0.00 | 0.00 | 0.00 | 0.00 |
| 2.00 | 0.00 | 0.00 | 0.00 | 0.00 |
| 3.00 | 17.27 | 24.37 | 37.51 | 19.29 |
| 4.00 | 17.27 | 51.79 | 37.51 | 28.39 |
| 5.00 | 17.27 | 51.79 | 37.51 | 37.97 |
| 6.00 | 34.53 | 51.79 | 93.79 | 48.39 |
| 7.00 | 64.99 | 86.32 | 112.54 | 75.08 |
| 8.00 | 69.06 | 112.72 | 180.95 | 97.02 |
| 9.00 | 69.06 | 138.10 | 216.26 | 121.26 |
| 10.00 | 86.31 | 189.90 | 262.60 | 154.47 |
| 11.00 | 17.26 | 64.98 | 37.51 | 38.55 |
| 12.00 | 17.27 | 17.26 | 56.27 | 28.59 |
| 12.10 | 17.27 | 17.26 | 44.14 | 29.17 |
| 12.20 | 17.27 | 17.26 | 44.13 | 31.54 |
| 12.30 | 0.00 | 0.00 | 37.51 | 18.60 |
| 12.40 | 10.15 | 13.20 | 37.51 | 21.37 |
| 12.50 | 17.26 | 30.46 | 37.51 | 30.64 |
| 12.60 | 10.15 | 13.20 | 37.51 | 21.37 |
| 12.70 | 0.00 | 0.00 | 37.51 | 18.60 |
| 12.80 | 17.27 | 17.26 | 44.13 | 31.54 |
| 12.90 | 17.27 | 17.26 | 44.14 | 29.17 |
| 13.00 | 17.27 | 17.26 | 56.27 | 28.59 |

**Table 61 – $t_{80}$ – Combination 1**

| COMBINATION 1 | | | | |
|---|---|---|---|---|
| **Step** | **F1** | **F2** | **F3** | **F4 = F5** |
| 0.00 | 0.00 | 0.00 | 0.00 | 0.00 |
| 1.00 | 0.00 | 0.00 | 0.00 | 0.00 |
| 2.00 | 0.00 | 0.00 | 0.00 | 0.00 |
| 3.00 | 0.00 | 0.00 | 0.00 | 0.00 |
| 4.00 | 11.17 | 17.26 | 18.76 | 9.91 |
| 5.00 | 17.27 | 17.26 | 37.51 | 19.29 |
| 6.00 | 17.27 | 49.76 | 37.51 | 19.29 |
| 7.00 | 17.27 | 51.79 | 75.03 | 37.64 |
| 8.00 | 32.50 | 73.12 | 93.79 | 58.02 |
| 9.00 | 56.87 | 86.32 | 150.06 | 69.23 |
| 10.00 | 69.06 | 110.69 | 187.57 | 86.46 |
| 11.00 | 0.00 | 0.00 | 18.76 | 4.19 |
| 12.00 | 17.27 | 17.26 | 18.76 | 19.29 |
| 12.10 | 12.19 | 0.00 | 18.76 | 0.99 |
| 12.20 | 0.00 | 0.00 | 0.00 | 0.00 |
| 12.30 | 0.00 | 0.00 | 0.00 | 0.00 |
| 12.40 | 0.00 | 0.00 | 0.00 | 0.00 |
| 12.50 | 0.00 | 0.00 | 0.00 | 0.00 |
| 12.60 | 0.00 | 0.00 | 0.00 | 0.00 |
| 12.70 | 0.00 | 0.00 | 0.00 | 0.00 |
| 12.80 | 0.00 | 0.00 | 0.00 | 0.00 |
| 12.90 | 12.19 | 0.00 | 18.76 | 0.99 |
| 13.00 | 17.27 | 17.26 | 18.76 | 19.29 |

**Table 62 – $\chi_{max}$ – Combination 1 with fault pore pressure depletion**

| COMB1B_PF | | | | |
|---|---|---|---|---|
| **Step** | **F1** | **F2** | **F3** | **F4 = F5** |
| 0.00 | 0.10 | 0.10 | 0.21 | 0.00 |
| 1.00 | 0.16 | 0.23 | 0.32 | 0.21 |
| 2.00 | 0.28 | 0.37 | 0.41 | 0.40 |
| 3.00 | 0.46 | 0.53 | 0.59 | 0.58 |
| 4.00 | 0.64 | 0.73 | 0.92 | 0.75 |
| 5.00 | 0.81 | 0.92 | 1.00 | 0.91 |
| 6.00 | 0.98 | 1.00 | 1.00 | 1.00 |
| 7.00 | 1.00 | 1.00 | 1.00 | 1.00 |
| 8.00 | 1.00 | 1.00 | 1.00 | 1.00 |
| 9.00 | 1.00 | 1.00 | 1.00 | 1.00 |
| 10.00 | 1.00 | 1.00 | 1.00 | 1.00 |
| 11.00 | 0.40 | 0.62 | 0.73 | 0.64 |
| 12.00 | 0.77 | 0.97 | 1.00 | 0.87 |
| 12.10 | 0.58 | 0.76 | 0.77 | 0.63 |
| 12.20 | 0.39 | 0.55 | 0.58 | 0.53 |
| 12.30 | 0.35 | 0.53 | 0.50 | 0.57 |
| 12.40 | 0.37 | 0.58 | 0.57 | 0.60 |
| 12.50 | 0.40 | 0.62 | 0.64 | 0.64 |
| 12.60 | 0.37 | 0.58 | 0.57 | 0.60 |
| 12.70 | 0.35 | 0.53 | 0.50 | 0.57 |
| 12.80 | 0.39 | 0.55 | 0.58 | 0.53 |
| 12.90 | 0.58 | 0.76 | 0.77 | 0.63 |
| 13.00 | 0.77 | 0.97 | 0.95 | 0.87 |

**Table 63 – $t_a$ – Combination 1 with fault pore pressure depletion**

| COMB1B_PF | | | | |
|---|---|---|---|---|
| **Step** | **F1** | **F2** | **F3** | **F4 = F5** |
| 0.00 | 0.00 | 0.00 | 0.00 | 0.00 |
| 1.00 | 0.00 | 0.00 | 0.00 | 0.00 |
| 2.00 | 0.00 | 0.00 | 0.00 | 0.00 |
| 3.00 | 0.00 | 0.00 | 0.00 | 0.00 |
| 4.00 | 0.00 | 0.00 | 0.00 | 0.00 |
| 5.00 | 0.00 | 0.00 | 18.76 | 0.00 |
| 6.00 | 0.00 | 17.26 | 0.00 | 9.91 |
| 7.00 | 17.27 | 15.23 | 0.00 | 8.89 |
| 8.00 | 0.00 | 2.03 | 0.00 | 9.03 |
| 9.00 | 0.00 | 0.00 | 0.00 | 0.51 |
| 10.00 | 0.00 | 0.00 | 37.51 | 0.51 |
| 11.00 | 0.00 | 0.00 | 0.00 | 0.00 |
| 12.00 | 0.00 | 0.00 | 18.76 | 0.00 |
| 12.10 | 0.00 | 0.00 | 0.00 | 0.00 |
| 12.20 | 0.00 | 0.00 | 0.00 | 0.00 |
| 12.30 | 0.00 | 0.00 | 0.00 | 0.00 |
| 12.40 | 0.00 | 0.00 | 0.00 | 0.00 |
| 12.50 | 0.00 | 0.00 | 0.00 | 0.00 |
| 12.60 | 0.00 | 0.00 | 0.00 | 0.00 |
| 12.70 | 0.00 | 0.00 | 0.00 | 0.00 |
| 12.80 | 0.00 | 0.00 | 0.00 | 0.00 |
| 12.90 | 0.00 | 0.00 | 0.00 | 0.00 |
| 13.00 | 0.00 | 0.00 | 0.00 | 0.00 |

**Table 64 – $t_{50}$ – Combination 1 with fault pore pressure depletion**

| COMB1B_PF | | | | |
|---|---|---|---|---|
| **Step** | **F1** | **F2** | **F3** | **F4 = F5** |
| 0.00 | 0.00 | 0.00 | 0.00 | 0.00 |
| 1.00 | 0.00 | 0.00 | 0.00 | 0.00 |
| 2.00 | 0.00 | 0.00 | 0.00 | 0.00 |
| 3.00 | 0.00 | 24.37 | 18.76 | 15.84 |
| 4.00 | 17.27 | 41.63 | 37.51 | 26.31 |
| 5.00 | 17.27 | 51.79 | 37.51 | 30.42 |
| 6.00 | 17.27 | 51.79 | 37.51 | 37.97 |
| 7.00 | 17.27 | 51.79 | 72.82 | 40.59 |
| 8.00 | 26.41 | 86.31 | 75.03 | 55.58 |
| 9.00 | 34.53 | 86.31 | 84.96 | 78.33 |
| 10.00 | 49.77 | 120.85 | 91.58 | 100.75 |
| 11.00 | 0.00 | 51.79 | 56.27 | 20.45 |
| 12.00 | 17.27 | 17.26 | 18.76 | 18.80 |
| 12.10 | 17.27 | 17.26 | 18.76 | 9.91 |
| 12.20 | 0.00 | 17.26 | 18.76 | 4.60 |
| 12.30 | 0.00 | 17.27 | 0.00 | 9.47 |
| 12.40 | 0.00 | 39.60 | 18.76 | 12.77 |
| 12.50 | 0.00 | 51.79 | 18.76 | 20.45 |
| 12.60 | 0.00 | 39.60 | 18.76 | 12.77 |
| 12.70 | 0.00 | 17.27 | 0.00 | 9.47 |
| 12.80 | 0.00 | 17.26 | 18.76 | 4.60 |
| 12.90 | 17.27 | 17.26 | 18.76 | 9.91 |
| 13.00 | 17.27 | 17.26 | 18.76 | 18.80 |

**Table 65 – $t_{80}$ – Combination 1 with fault pore pressure depletion**

| COMB1B_PF | | | | |
|---|---|---|---|---|
| **Step** | **F1** | **F2** | **F3** | **F4 = F5** |
| 0.00 | 0.00 | 0.00 | 0.00 | 0.00 |
| 1.00 | 0.00 | 0.00 | 0.00 | 0.00 |
| 2.00 | 0.00 | 0.00 | 0.00 | 0.00 |
| 3.00 | 0.00 | 0.00 | 0.00 | 0.00 |
| 4.00 | 0.00 | 0.00 | 18.76 | 0.00 |
| 5.00 | 15.23 | 17.26 | 18.76 | 9.91 |
| 6.00 | 17.27 | 34.52 | 18.76 | 19.29 |
| 7.00 | 17.27 | 34.52 | 18.76 | 28.34 |
| 8.00 | 17.27 | 34.52 | 18.76 | 28.85 |
| 9.00 | 17.27 | 43.66 | 75.03 | 28.85 |
| 10.00 | 17.27 | 82.25 | 75.03 | 36.67 |
| 11.00 | 0.00 | 0.00 | 0.00 | 0.00 |
| 12.00 | 0.00 | 17.26 | 18.76 | 8.97 |
| 12.10 | 0.00 | 0.00 | 0.00 | 0.00 |
| 12.20 | 0.00 | 0.00 | 0.00 | 0.00 |
| 12.30 | 0.00 | 0.00 | 0.00 | 0.00 |
| 12.40 | 0.00 | 0.00 | 0.00 | 0.00 |
| 12.50 | 0.00 | 0.00 | 0.00 | 0.00 |
| 12.60 | 0.00 | 0.00 | 0.00 | 0.00 |
| 12.70 | 0.00 | 0.00 | 0.00 | 0.00 |
| 12.80 | 0.00 | 0.00 | 0.00 | 0.00 |
| 12.90 | 0.00 | 0.00 | 0.00 | 0.00 |
| 13.00 | 0.00 | 17.26 | 18.76 | 8.97 |

**Table 66 – $\chi_{max}$ – Combination 2**

| COMBINATION 2 | | | | |
|---|---|---|---|---|
| **Step** | **F1** | **F2** | **F3** | **F4 = F5** |
| 0.00 | 0.00 | 0.00 | 0.27 | 0.00 |
| 1.00 | 0.23 | 0.37 | 0.30 | 0.40 |
| 2.00 | 0.47 | 0.77 | 0.47 | 0.81 |
| 3.00 | 0.70 | 1.00 | 0.80 | 1.00 |
| 4.00 | 0.94 | 1.00 | 1.00 | 1.00 |
| 5.00 | 1.00 | 1.00 | 1.00 | 1.00 |
| 6.00 | 1.00 | 1.00 | 1.00 | 1.00 |
| 7.00 | 1.00 | 1.00 | 1.00 | 1.00 |
| 8.00 | 1.00 | 1.00 | 1.00 | 1.00 |
| 9.00 | 1.00 | 1.00 | 1.00 | 1.00 |
| 10.00 | 1.00 | 1.00 | 1.00 | 1.00 |
| 11.00 | 0.63 | 1.00 | 1.00 | 1.00 |
| 12.00 | 1.00 | 1.00 | 1.00 | 1.00 |
| 12.10 | 0.77 | 0.70 | 0.84 | 0.83 |
| 12.20 | 0.58 | 0.57 | 0.78 | 0.77 |
| 12.30 | 0.57 | 0.52 | 0.77 | 0.72 |
| 12.40 | 0.67 | 0.62 | 1.00 | 0.84 |
| 12.50 | 0.77 | 1.00 | 1.00 | 1.00 |
| 12.60 | 0.55 | 0.59 | 0.71 | 0.67 |
| 12.70 | 0.44 | 0.53 | 0.74 | 0.70 |
| 12.80 | 0.58 | 0.56 | 0.76 | 0.72 |
| 12.90 | 0.77 | 0.74 | 0.85 | 0.86 |
| 13.00 | 0.94 | 1.00 | 1.00 | 1.00 |

**Table 67 – $t_a$ – Combination 2**

| COMBINATION 2 | | | | |
|---|---|---|---|---|
| **Step** | **F1** | **F2** | **F3** | **F4 = F5** |
| 0.00 | 0.00 | 0.00 | 0.00 | 0.00 |
| 1.00 | 0.00 | 0.00 | 0.00 | 0.00 |
| 2.00 | 0.00 | 0.00 | 0.00 | 0.00 |
| 3.00 | 0.00 | 17.26 | 0.00 | 9.91 |
| 4.00 | 0.00 | 0.00 | 18.76 | 0.00 |
| 5.00 | 17.27 | 0.00 | 18.76 | 9.38 |
| 6.00 | 0.00 | 0.00 | 0.00 | 14.20 |
| 7.00 | 0.00 | 17.27 | 35.31 | 3.98 |
| 8.00 | 0.00 | 51.80 | 4.41 | 20.39 |
| 9.00 | 4.06 | 0.00 | 51.86 | 2.98 |
| 10.00 | 13.20 | 0.00 | 2.21 | 6.20 |
| 11.00 | 0.00 | 0.00 | 0.00 | 0.00 |
| 12.00 | 17.27 | 0.00 | 18.76 | 18.78 |
| 12.10 | 0.00 | 0.00 | 0.00 | 0.00 |
| 12.20 | 0.00 | 0.00 | 0.00 | 0.00 |
| 12.30 | 0.00 | 0.00 | 0.00 | 0.00 |
| 12.40 | 0.00 | 0.00 | 12.14 | 0.00 |
| 12.50 | 0.00 | 7.11 | 4.41 | 8.40 |
| 12.60 | 0.00 | 0.00 | 0.00 | 0.00 |
| 12.70 | 0.00 | 0.00 | 0.00 | 0.00 |
| 12.80 | 0.00 | 0.00 | 0.00 | 0.00 |
| 12.90 | 0.00 | 0.00 | 0.00 | 0.00 |
| 13.00 | 0.00 | 17.26 | 18.76 | 9.91 |

**Table 68 – $t_{50}$ – Combination 2**

| COMBINATION 2 | | | | |
|---|---|---|---|---|
| **Step** | **F1** | **F2** | **F3** | **F4 = F5** |
| 0.00 | 0.00 | 0.00 | 0.00 | 0.00 |
| 1.00 | 0.00 | 0.00 | 0.00 | 0.00 |
| 2.00 | 0.00 | 17.26 | 0.00 | 9.91 |
| 3.00 | 17.27 | 34.52 | 37.51 | 35.47 |
| 4.00 | 17.27 | 51.79 | 56.27 | 38.98 |
| 5.00 | 25.39 | 59.91 | 56.27 | 49.90 |
| 6.00 | 34.53 | 86.32 | 112.54 | 72.84 |
| 7.00 | 69.06 | 86.32 | 112.54 | 83.00 |
| 8.00 | 86.32 | 86.32 | 145.65 | 116.11 |
| 9.00 | 89.37 | 86.32 | 158.89 | 138.42 |
| 10.00 | 92.41 | 120.85 | 219.02 | 173.50 |
| 11.00 | 51.79 | 51.79 | 48.55 | 44.66 |
| 12.00 | 17.27 | 82.26 | 110.34 | 55.78 |
| 12.10 | 17.27 | 69.06 | 84.96 | 44.87 |
| 12.20 | 17.27 | 5.08 | 37.51 | 24.45 |
| 12.30 | 15.23 | 2.03 | 51.86 | 10.02 |
| 12.40 | 17.27 | 17.26 | 56.27 | 14.25 |
| 12.50 | 55.85 | 21.32 | 87.17 | 25.87 |
| 12.60 | 17.27 | 17.26 | 56.27 | 12.60 |
| 12.70 | 0.00 | 4.06 | 37.51 | 7.54 |
| 12.80 | 17.27 | 6.09 | 46.34 | 20.96 |
| 12.90 | 17.27 | 60.93 | 89.37 | 52.79 |
| 13.00 | 17.27 | 84.29 | 93.79 | 55.84 |

**Table 69 – $t_{80}$ – Combination 2**

| COMBINATION 2 | | | | |
|---|---|---|---|---|
| **Step** | **F1** | **F2** | **F3** | **F4 = F5** |
| 0.00 | 0.00 | 0.00 | 0.00 | 0.00 |
| 1.00 | 0.00 | 0.00 | 0.00 | 0.00 |
| 2.00 | 0.00 | 0.00 | 0.00 | 1.71 |
| 3.00 | 0.00 | 17.26 | 14.34 | 9.91 |
| 4.00 | 17.27 | 17.26 | 37.51 | 19.29 |
| 5.00 | 17.27 | 34.52 | 37.51 | 36.98 |
| 6.00 | 17.27 | 51.79 | 37.51 | 38.48 |
| 7.00 | 17.27 | 86.32 | 81.65 | 58.84 |
| 8.00 | 34.53 | 86.32 | 93.79 | 66.52 |
| 9.00 | 34.53 | 86.32 | 131.30 | 71.59 |
| 10.00 | 75.15 | 86.32 | 131.30 | 97.09 |
| 11.00 | 0.00 | 17.26 | 37.51 | 13.84 |
| 12.00 | 17.27 | 34.52 | 87.17 | 38.25 |
| 12.10 | 0.00 | 0.00 | 22.07 | 0.51 |
| 12.20 | 0.00 | 0.00 | 0.00 | 0.00 |
| 12.30 | 0.00 | 0.00 | 0.00 | 0.00 |
| 12.40 | 0.00 | 0.00 | 16.55 | 4.98 |
| 12.50 | 0.00 | 15.23 | 26.48 | 9.91 |
| 12.60 | 0.00 | 0.00 | 0.00 | 0.00 |
| 12.70 | 0.00 | 0.00 | 0.00 | 0.00 |
| 12.80 | 0.00 | 0.00 | 0.00 | 0.00 |
| 12.90 | 0.00 | 0.00 | 22.07 | 7.35 |
| 13.00 | 17.27 | 34.52 | 76.13 | 38.54 |

**Table 70 – $\chi_{max}$ – Combination 2 with fault pore pressure depletion**

| COMB2C_PF | | | | |
|---|---|---|---|---|
| **Step** | **F1** | **F2** | **F3** | **F4 = F5** |
| 0.00 | 0.00 | 0.00 | 0.27 | 0.00 |
| 1.00 | 0.23 | 0.37 | 0.29 | 0.40 |
| 2.00 | 0.47 | 0.77 | 0.47 | 0.81 |
| 3.00 | 0.70 | 1.00 | 0.70 | 1.00 |
| 4.00 | 0.94 | 1.00 | 1.00 | 1.00 |
| 5.00 | 1.00 | 1.00 | 1.00 | 1.00 |
| 6.00 | 1.00 | 1.00 | 1.00 | 1.00 |
| 7.00 | 1.00 | 1.00 | 1.00 | 1.00 |
| 8.00 | 1.00 | 1.00 | 1.00 | 1.00 |
| 9.00 | 1.00 | 1.00 | 1.00 | 1.00 |
| 10.00 | 1.00 | 1.00 | 1.00 | 1.00 |
| 11.00 | 0.63 | 1.00 | 1.00 | 1.00 |
| 12.00 | 1.00 | 1.00 | 1.00 | 1.00 |
| 12.10 | 0.77 | 0.70 | 0.70 | 0.83 |
| 12.20 | 0.58 | 0.57 | 0.53 | 0.77 |
| 12.30 | 0.57 | 0.52 | 0.73 | 0.72 |
| 12.40 | 0.67 | 0.62 | 1.00 | 0.84 |
| 12.50 | 0.77 | 1.00 | 1.00 | 1.00 |
| 12.60 | 0.55 | 0.60 | 0.63 | 0.67 |
| 12.70 | 0.44 | 0.53 | 0.44 | 0.70 |
| 12.80 | 0.58 | 0.56 | 0.51 | 0.72 |
| 12.90 | 0.77 | 0.74 | 0.85 | 0.85 |
| 13.00 | 0.94 | 1.00 | 1.00 | 1.00 |

**Table 71 – $t_a$ – Combination 2 with fault pore pressure depletion**

| COMB2C_PF | | | | |
|---|---|---|---|---|
| **Step** | **F1** | **F2** | **F3** | **F4 = F5** |
| 0.00 | 0.00 | 0.00 | 0.00 | 0.00 |
| 1.00 | 0.00 | 0.00 | 0.00 | 0.00 |
| 2.00 | 0.00 | 0.00 | 0.00 | 0.00 |
| 3.00 | 0.00 | 17.26 | 0.00 | 9.91 |
| 4.00 | 0.00 | 0.00 | 18.76 | 0.00 |
| 5.00 | 17.27 | 0.00 | 18.76 | 9.38 |
| 6.00 | 0.00 | 0.00 | 0.00 | 14.20 |
| 7.00 | 0.00 | 17.27 | 0.00 | 3.98 |
| 8.00 | 0.00 | 51.80 | 0.00 | 20.39 |
| 9.00 | 4.06 | 0.00 | 33.10 | 2.98 |
| 10.00 | 13.20 | 0.00 | 6.62 | 6.20 |
| 11.00 | 0.00 | 0.00 | 14.34 | 0.00 |
| 12.00 | 17.27 | 0.00 | 41.93 | 18.78 |
| 12.10 | 0.00 | 0.00 | 0.00 | 0.00 |
| 12.20 | 0.00 | 0.00 | 0.00 | 0.00 |
| 12.30 | 0.00 | 0.00 | 0.00 | 0.00 |
| 12.40 | 0.00 | 0.00 | 9.93 | 0.00 |
| 12.50 | 0.00 | 5.08 | 6.62 | 8.40 |
| 12.60 | 0.00 | 0.00 | 0.00 | 0.00 |
| 12.70 | 0.00 | 0.00 | 0.00 | 0.00 |
| 12.80 | 0.00 | 0.00 | 0.00 | 0.00 |
| 12.90 | 0.00 | 0.00 | 0.00 | 0.00 |
| 13.00 | 0.00 | 17.26 | 18.76 | 9.91 |

**Table 72 – $t_{50}$ – Combination 2 with fault pore pressure depletion**

| COMB2C_PF | | | | |
|---|---|---|---|---|
| **Step** | **F1** | **F2** | **F3** | **F4 = F5** |
| 0.00 | 0.00 | 0.00 | 0.00 | 0.00 |
| 1.00 | 0.00 | 0.00 | 0.00 | 0.00 |
| 2.00 | 0.00 | 17.26 | 0.00 | 9.91 |
| 3.00 | 17.27 | 34.52 | 37.51 | 35.47 |
| 4.00 | 17.27 | 51.79 | 39.72 | 38.98 |
| 5.00 | 25.39 | 59.91 | 56.27 | 49.90 |
| 6.00 | 34.53 | 86.32 | 56.27 | 72.84 |
| 7.00 | 69.06 | 86.32 | 112.54 | 83.00 |
| 8.00 | 86.32 | 86.32 | 112.54 | 116.11 |
| 9.00 | 89.37 | 86.32 | 121.37 | 138.42 |
| 10.00 | 92.41 | 120.85 | 146.20 | 173.50 |
| 11.00 | 51.79 | 51.79 | 81.65 | 44.66 |
| 12.00 | 17.27 | 82.26 | 75.03 | 55.78 |
| 12.10 | 17.27 | 69.06 | 54.07 | 44.87 |
| 12.20 | 17.27 | 4.06 | 9.93 | 24.45 |
| 12.30 | 15.23 | 2.03 | 14.34 | 10.02 |
| 12.40 | 17.27 | 17.26 | 18.76 | 14.25 |
| 12.50 | 55.85 | 21.32 | 37.51 | 26.37 |
| 12.60 | 17.27 | 17.26 | 18.76 | 12.60 |
| 12.70 | 0.00 | 4.06 | 0.00 | 7.54 |
| 12.80 | 17.27 | 6.09 | 8.83 | 20.96 |
| 12.90 | 17.27 | 62.96 | 47.44 | 52.79 |
| 13.00 | 17.27 | 84.29 | 75.03 | 55.84 |

**Table 73 – $t_{80}$ – Combination 2 with fault pore pressure depletion**

| COMB2C_PF | | | | |
|---|---|---|---|---|
| **Step** | **F1** | **F2** | **F3** | **F4 = F5** |
| 0.00 | 0.00 | 0.00 | 0.00 | 0.00 |
| 1.00 | 0.00 | 0.00 | 0.00 | 0.00 |
| 2.00 | 0.00 | 0.00 | 0.00 | 1.71 |
| 3.00 | 0.00 | 17.26 | 0.00 | 9.91 |
| 4.00 | 17.27 | 17.26 | 37.51 | 19.29 |
| 5.00 | 17.27 | 34.52 | 37.51 | 36.98 |
| 6.00 | 17.27 | 51.79 | 37.51 | 38.48 |
| 7.00 | 17.27 | 86.32 | 37.51 | 58.84 |
| 8.00 | 34.53 | 86.32 | 70.62 | 66.52 |
| 9.00 | 34.53 | 86.32 | 81.65 | 71.59 |
| 10.00 | 75.15 | 86.32 | 88.27 | 97.09 |
| 11.00 | 0.00 | 17.26 | 16.55 | 13.84 |
| 12.00 | 17.27 | 34.52 | 56.27 | 38.25 |
| 12.10 | 0.00 | 0.00 | 0.00 | 0.51 |
| 12.20 | 0.00 | 0.00 | 0.00 | 0.00 |
| 12.30 | 0.00 | 0.00 | 0.00 | 0.00 |
| 12.40 | 0.00 | 0.00 | 14.34 | 4.98 |
| 12.50 | 0.00 | 15.23 | 18.76 | 9.91 |
| 12.60 | 0.00 | 0.00 | 0.00 | 0.00 |
| 12.70 | 0.00 | 0.00 | 0.00 | 0.00 |
| 12.80 | 0.00 | 0.00 | 0.00 | 0.00 |
| 12.90 | 0.00 | 0.00 | 18.76 | 7.35 |
| 13.00 | 17.27 | 34.52 | 49.65 | 38.54 |

**Table 74 – $\chi_{max}$ – Combination 3**

| COMBINATION 3 | | | | |
|---|---|---|---|---|
| **Step** | **F1** | **F2** | **F3** | **F4 = F5** |
| 0.00 | 0.08 | 0.08 | 0.18 | 0.00 |
| 1.00 | 0.15 | 0.20 | 0.29 | 0.20 |
| 2.00 | 0.27 | 0.33 | 0.40 | 0.40 |
| 3.00 | 0.47 | 0.56 | 0.58 | 0.60 |
| 4.00 | 0.68 | 0.81 | 0.96 | 0.82 |
| 5.00 | 0.91 | 1.00 | 1.00 | 1.00 |
| 6.00 | 1.00 | 1.00 | 1.00 | 1.00 |
| 7.00 | 1.00 | 1.00 | 1.00 | 1.00 |
| 8.00 | 1.00 | 1.00 | 1.00 | 1.00 |
| 9.00 | 1.00 | 1.00 | 1.00 | 1.00 |
| 10.00 | 1.00 | 1.00 | 1.00 | 1.00 |
| 11.00 | 0.67 | 0.73 | 1.00 | 0.84 |
| 12.00 | 1.00 | 1.00 | 1.00 | 1.00 |
| 12.10 | 0.69 | 0.63 | 0.55 | 0.78 |
| 12.20 | 0.54 | 0.45 | 0.49 | 0.66 |
| 12.30 | 0.46 | 0.35 | 0.47 | 0.69 |
| 12.40 | 0.51 | 0.44 | 0.50 | 0.72 |
| 12.50 | 0.55 | 0.53 | 0.54 | 0.75 |
| 12.60 | 0.51 | 0.44 | 0.50 | 0.72 |
| 12.70 | 0.46 | 0.35 | 0.47 | 0.69 |
| 12.80 | 0.54 | 0.45 | 0.49 | 0.66 |
| 12.90 | 0.69 | 0.63 | 0.55 | 0.78 |
| 13.00 | 0.82 | 0.79 | 0.70 | 0.95 |

**Table 75 – $t_a$ – Combination 3**

| COMBINATION 3 | | | | |
|---|---|---|---|---|
| **Step** | **F1** | **F2** | **F3** | **F4 = F5** |
| 0.00 | 0.00 | 0.00 | 0.00 | 0.00 |
| 1.00 | 0.00 | 0.00 | 0.00 | 0.00 |
| 2.00 | 0.00 | 0.00 | 0.00 | 0.00 |
| 3.00 | 0.00 | 0.00 | 0.00 | 0.00 |
| 4.00 | 0.00 | 0.00 | 0.00 | 0.00 |
| 5.00 | 0.00 | 17.26 | 18.76 | 9.44 |
| 6.00 | 17.27 | 0.00 | 0.00 | 9.36 |
| 7.00 | 0.00 | 0.00 | 0.00 | 0.49 |
| 8.00 | 0.00 | 0.00 | 37.51 | 0.00 |
| 9.00 | 0.00 | 30.47 | 5.52 | 12.89 |
| 10.00 | 17.27 | 34.53 | 72.82 | 21.63 |
| 11.00 | 0.00 | 0.00 | 0.00 | 0.00 |
| 12.00 | 17.27 | 17.26 | 0.00 | 9.91 |
| 12.10 | 0.00 | 0.00 | 0.00 | 0.00 |
| 12.20 | 0.00 | 0.00 | 0.00 | 0.00 |
| 12.30 | 0.00 | 0.00 | 0.00 | 0.00 |
| 12.40 | 0.00 | 0.00 | 0.00 | 0.00 |
| 12.50 | 0.00 | 0.00 | 0.00 | 0.00 |
| 12.60 | 0.00 | 0.00 | 0.00 | 0.00 |
| 12.70 | 0.00 | 0.00 | 0.00 | 0.00 |
| 12.80 | 0.00 | 0.00 | 0.00 | 0.00 |
| 12.90 | 0.00 | 0.00 | 0.00 | 0.00 |
| 13.00 | 0.00 | 0.00 | 0.00 | 0.00 |

**Table 76 – $t_{50}$ – Combination 3**

| COMBINATION 3 | | | | |
|---|---|---|---|---|
| **Step** | **F1** | **F2** | **F3** | **F4 = F5** |
| 0.00 | 0.00 | 0.00 | 0.00 | 0.00 |
| 1.00 | 0.00 | 0.00 | 0.00 | 0.00 |
| 2.00 | 0.00 | 0.00 | 0.00 | 0.00 |
| 3.00 | 0.00 | 17.26 | 37.51 | 16.83 |
| 4.00 | 17.27 | 51.79 | 37.51 | 19.29 |
| 5.00 | 17.27 | 51.79 | 37.51 | 37.46 |
| 6.00 | 22.34 | 51.79 | 72.82 | 38.98 |
| 7.00 | 34.53 | 64.99 | 93.79 | 48.39 |
| 8.00 | 69.06 | 86.32 | 93.79 | 78.65 |
| 9.00 | 69.06 | 93.43 | 150.06 | 97.04 |
| 10.00 | 69.06 | 132.01 | 218.47 | 116.43 |
| 11.00 | 34.52 | 36.56 | 49.65 | 37.60 |
| 12.00 | 17.27 | 17.26 | 51.86 | 29.23 |
| 12.10 | 17.27 | 17.26 | 35.31 | 29.23 |
| 12.20 | 17.27 | 0.00 | 0.00 | 19.85 |
| 12.30 | 0.00 | 0.00 | 0.00 | 16.82 |
| 12.40 | 15.23 | 0.00 | 0.00 | 26.73 |
| 12.50 | 17.26 | 2.03 | 30.89 | 28.67 |
| 12.60 | 15.23 | 0.00 | 0.00 | 26.73 |
| 12.70 | 0.00 | 0.00 | 0.00 | 16.82 |
| 12.80 | 17.27 | 0.00 | 0.00 | 19.85 |
| 12.90 | 17.27 | 17.26 | 35.31 | 29.23 |
| 13.00 | 17.27 | 17.26 | 51.86 | 29.23 |

**Table 77 – $t_{80}$ – Combination 3**

| COMBINATION 3 | | | | |
|---|---|---|---|---|
| **Step** | **F1** | **F2** | **F3** | **F4 = F5** |
| 0.00 | 0.00 | 0.00 | 0.00 | 0.00 |
| 1.00 | 0.00 | 0.00 | 0.00 | 0.00 |
| 2.00 | 0.00 | 0.00 | 0.00 | 0.00 |
| 3.00 | 0.00 | 0.00 | 0.00 | 0.00 |
| 4.00 | 0.00 | 15.23 | 18.76 | 7.92 |
| 5.00 | 17.27 | 17.26 | 18.76 | 19.29 |
| 6.00 | 17.27 | 17.26 | 37.51 | 19.29 |
| 7.00 | 17.27 | 49.76 | 70.62 | 19.29 |
| 8.00 | 17.27 | 51.79 | 89.37 | 36.47 |
| 9.00 | 34.53 | 86.32 | 129.09 | 55.31 |
| 10.00 | 51.79 | 86.32 | 166.61 | 67.75 |
| 11.00 | 0.00 | 0.00 | 18.76 | 4.60 |
| 12.00 | 17.27 | 17.26 | 18.76 | 9.91 |
| 12.10 | 0.00 | 0.00 | 0.00 | 0.00 |
| 12.20 | 0.00 | 0.00 | 0.00 | 0.00 |
| 12.30 | 0.00 | 0.00 | 0.00 | 0.00 |
| 12.40 | 0.00 | 0.00 | 0.00 | 0.00 |
| 12.50 | 0.00 | 0.00 | 0.00 | 0.00 |
| 12.60 | 0.00 | 0.00 | 0.00 | 0.00 |
| 12.70 | 0.00 | 0.00 | 0.00 | 0.00 |
| 12.80 | 0.00 | 0.00 | 0.00 | 0.00 |
| 12.90 | 0.00 | 0.00 | 0.00 | 0.00 |
| 13.00 | 15.23 | 0.00 | 0.00 | 9.91 |